Experimental Investigation of the Wall Deposition of Food Containing Carbohydrates, in a Pilot Scale Spray Dryer

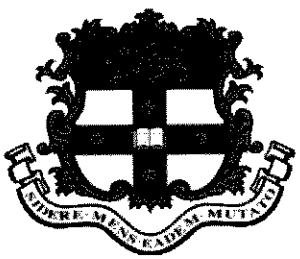

A thesis submitted in fulfillment of the requirements for the

Degree of

MASTER IN ENGINEERING (RESEARCH)

By

Linda Ozmen

Department of Chemical Engineering

The University of Sydney

November 2002

Examiner 2 Comment 1: There should be some further discussion of efficiency and effectiveness when presenting optimum vane angle. It may be that the vane angle of 0° result in the least wall deposition but the drying effectiveness is not satisfactory.

Efficiency and effectiveness are extensively discussed in this thesis on pages 124-126, 163 and 164. It is clear that the drying performance is limited by the equilibrium between gas and solids, so that 0° angle results in the least wall deposition with an insignificant penalty regarding the drying effectiveness. Further discussion seems unwarranted in view of the view of this examiner that the thesis is already very long.

Examiner 2 Comment 2: It is noted that the comparison between glass transition point and sticky point has been made for only one material. One would wonder if these results are able to be extrapolated to all materials.

There is a discussion on page 68 that highlights the applicability of this comparion to other materials containing carbohydrates, hence indicating the ability of these results to be extrapolated.

Examiner 2 Comment 3: Table 3.1 on P58 shows a moisture content 40% higher that actual – not 2.7% inferred in the discussion.

The 2.7% difference is a percentage moisture content, which is an absolute moisture content difference. It is appropriate to present the results as absolute moisture contents because the uncertainties in measurements are also evaluated in absolute terms.

Examiner 2 Comment 4: There is little discussion on P92 as to why there was such a high deviation of mass flow for the background case.

There is considerable discussion on page 93 regarding the discrepancies, which are between 5 and 24%, and a number of explanations are explored and discussed.

Examiner 2 Comment 5: The thesis is very long and difficult to read. The sensitivity analysis on P93-100 could well be put in the Appendix together with some of the propagation of errors material and the sample calculations provided.

The sensitivity analysis on pages 93-100 has been placed in the Appendix, as requested.

The remaining typographical errors identified by the examiner (comment 6) have been corrected.

Declaration

I hereby declare that this thesis is my own work and that, to the best of my knowledge, it contains no material previously published or written by another person nor material which has been accepted for the award of any other degree or diploma at an institute of higher education, except where due acknowledgement is given.

Linda Ozmen

30 November 2002

Abstract

Spray dryers are the core components of a milk powder production plant, where the basic configuration usually features co-current flow of milk powder and air. Spray dryers have to be cleaned frequently due to powder deposit build-up on the walls. Powder deposit build-up gives rise to lower product yields and poses a potential fire risk. If the powder deposits are scorched (from being overheated) they will contaminate, and thus compromise, the quality and consumer safety of the final product, if the powder deposits fall in and mix with it. With milk powder production rates of most industrial spray dryers ranging from 4-28 tonnes of dry powder an hour, these wall deposition problems are significant. This problem is worth investigating because the outcome of reducing or eliminating wall deposition is that a spray dryer could operate for a longer period of time without having to be cleaned. Reduction in downtime due to cleaning would give rise to increased production time and possibly a reduction in the cost of manufacturing the product.

The spray dryer used in this work was a modified short-form co-current Niro unit, fabricated from stainless steel. The spray dryer had an internal diameter of 0.80 m, narrowing down to 0.06 m at the base, and a height of 2 m. A two-fluid nozzle was used to spray the process fluids (water, skim milk and grape skin extract) into the drying chamber. To measure the wall deposition fluxes on the internal walls of the spray dryer, four stainless steel plates (dimensions 110 mm by 120 mm) were inserted in place of the windows that were previously used as sight glasses. A fifth plate (dimensions 110 mm by 120 mm) and a sixth plate (dimensions 110 mm by 110 mm) were also placed on the conical section of the spray dryer at different circumferential locations.

Before this work, no quantitative data on the effects of spray dryer operating conditions on the wall deposition fluxes of food material were available. This work investigated the effect on the spray deposition flux of skim milk powder on the walls of the spray dryer of (i) flow patterns in the spray dryer, by changing the degree of swirl imparted to the incoming air by using three swirl vane angles of 0°, 25° and 30°, and (ii) the stickiness of the product, through first changing the temperature of the incoming air by using three inlet air temperatures of $170^{\circ}C$, $200^{\circ}C$ and $230^{\circ}C$; and then changing the process fluid flowrate by using three flowrates of 1.4 kg hr^{-1}, 1.6 kg hr^{-1} and 1.8 kg hr^{-1}.

Previous researchers have found that the extent to which water droplets spread out in the drying chamber is affected by the amount of swirl in the inlet air. This is likely to affect wall deposition fluxes because the particles will be closer to the walls if the droplets spread out widely. The results of this work have quantitatively confirmed that the spray deposition flux increases at higher swirl vane angles, where the spray deposition flux increased from 7 g m^{-2} hr^{-1} (swirl vane angle 0°) to 12.9 g m^{-2} hr^{-1} (swirl vane angle 30°). When a swirl vane angle of 0° was used, it was observed that the cross-sectional area of the spray cloud did not change very significantly with time. However, when a swirl vane angle of 25° was used, the spray cloud was observed to "flutter", and when the swirl vane angle was increased to 30°, the spray cloud was observed to recirculate rapidly back in the direction of the nozzle. Thus, the chance of the particles being thrown further towards the walls of the chamber is likely to increase at higher swirl vane angles. This result suggests that higher wall deposition arises because more swirl is imparted to the air entering the dryer, which in turn affects the stability of the spray cloud and, therefore, the stability of the flow patterns in the spray dryer.

The stickiness of the skim milk powder is related to the temperature and moisture content of the particles. In the past, the sticky-point curve has been suggested as a semi-quantitative concept in selecting operating conditions for spray drying food material containing carbohydrates, where it has been implied that there is no significant wall deposition below the sticky-point curve. This work has quantified the spray deposition in spray dryers with respect to the sticky-point curve, where the highest spray deposition flux of skim milk powder on the walls was 16 g m^{-2} hr^{-1}, and the operating point corresponding to this spray deposition flux was located at and above the sticky-point curve. Hence, both particle stickiness and flow patterns affect the wall deposition of particles in a spray dryer.

This work also investigated the effect of wall properties, namely a non-stick food grade material (nylon), adhesive tape and stainless steel, on the spray deposition flux of skim milk powder on the walls. The effect of electrostatics on wall deposition was studied by grounding the spray dryer and an anti-static agent was added to the skim milk to investigate if altering the properties of the feed material could reduce wall deposition.

This work has quantitatively confirmed that cohesion occurs at the same rate as adhesion for skim milk powder in this spray dryer, because firstly, decreasing the adhesion tendency of the

wall by using nylon coating had no significant effect on the spray deposition flux compared with a smooth stainless steel wall and a wall covered with a double-sided adhesive tape; and secondly the powder collected on the walls was a linear function of time with and without adhesive on the plates. Furthermore, using a nylon coated wall did not eliminate wall deposition, and the wall deposition flux was found to be the same as when a stainless steel wall was used. This result further supports the finding here that spray deposition on the walls for skim milk powder is controlled by cohesion rather than adhesion.

The spray dryer operating parameters that gave rise to the least spray deposition flux on the walls were a swirl vane angle of 0°, an inlet air temperature of 230°C and a process fluid flowrate of 1.4 kg hr^{-1}. Decreasing the feed flowrate from 1.8 kg hr^{-1} to 1.4 kg hr^{-1} (decrease by 24%), with the inlet air temperature and swirl vane angle held constant, decreased the wall deposition flux by 43% from 7 g m^{-2} hr^{-1} to 4 g m^{-2} hr^{-1}. Since the spray deposition flux on the walls decreased by 43% when the feed flowrate was decreased by 24%, it might be considered that the production process is in favour of a decrease in the feed flowrate to 1.4 kg hr^{-1} in this dryer, and consequently a decrease in the spray deposition flux on the walls per unit production output.

Finally, this work investigated if the outlet moisture content from this small spray dryer used here was equilibrium limited or controlled by drying kinetics. The findings in this work confirmed the product moisture locus concept, which implies that the outlet moisture content of the skim milk particles approaches the equilibrium moisture content (in equilibrium with the outlet gas), and that the outlet moisture content of spray-dried food material containing carbohydrates is probably not limited by particle drying kinetics, even though the spray dryer is smaller (diameter 0.8 m, height 2 m) than those used in the dairy industry, typically with a diameter of 30 m and a height of 10 m.

Acknowledgements

I wish to express my sincere thanks to my supervisor Associate Professor Tim Langrish for his expert supervision and patience, from which I have greatly benefited as a researcher. His timely and conscientious comments at every stage of this thesis writing have been particularly appreciated. I also would like to thank my associate supervisor, Associate Professor David Fletcher for his helpful advice.

I would like to acknowledge the scholarship from the Australian Research Council and the industry partners Mr Graham Nottle and Mr Tim Lang from Food Ingredients Technologies Australia Pty Ltd. Thanks are also due to Messers Dennis Trevaskis and Leigh Couper from the departmental workshop who carried out equipment modifications, and along with Dr Jay Mukhraiya for helping to position the spray dryer lid on to the spray drying chamber on numerous occasions. I would like to acknowledge Mr Trevor Shearing from the Department of Mechanical Engineering, for his assistance with the DSC equipment, and Mr Stuart Allen for his assistance with the stirred fluidised bed. I would also like to thank Dr Ian Kaplin at the Electron Microscopy Unit at the University of Sydney for his help with the Scanning Electron Microscope, Dr Jeffrey Shi for his assistance with the Malvern Particle Size Analyser, and Ms Binh Nguyen at the School of Chemistry with her assistance with the Tenisometer equipment. I would also like to thank BASF Corporation in New York, for sending me a free sample of Larostat Anti-static agent.

I would like to thank Mr Javier Orellana from the departmental Technical Services, Dr David Southwell, the Postgraduates, and Research Staff at the Department of Chemical Engineering for their helpful advice and assistance.

Finally, I would like to thank my parents and brother, John, for their love and support, and for always encouraging me to pursue further studies. Their faith in my abilities have made such a project as this possible.

Publications

Ozmen, L., Langrish, T.A.G., Comparison of Glass Transition Temperature and Sticky-Point Temperature for Skim Milk Powder, In *Drying Technology*, Mujumdar, A.S., Devahastin, S. (eds.), Vol. 20, pp. 1177-1192. (Best paper award in the category of Drying of Food at the 2nd Asian-Oceania Drying Conference, 2001).

Ozmen, L., Langrish, T.A.G., Experimental Investigation of the Wall Deposition of Milk Powder in Spray Dryers, *CHEMECA 2002*, (accepted).

Ozmen, L., Langrish, T.A.G., A Study of the Limitations to Spray Dryer Outlet Performance, *Drying Technology – An International Journal, 2002*, (accepted).

Contents

1 Introduction 1

2 Literature Review 8

2.1 Applications of Spray Dryers to Produce Products for Human Consumption 9

2.1.1 Milk Products 9

2.1.2 Nutraceutical Products 9

2.2 Air Flow Patterns. 13

2.3 Computational Fluid Dynamics 14

2.3.1 Steady-State Axisymmetric CFD Simulations and Experimental Studies 16

2.3.2 Transient CFD Simulations and Experimental Studies 18

2.4 Studies on Particle-Wall Interactions in Process Equipment 22

2.5 Mechanisms Involved in Stickiness 24

2.5.1 Adhesion 25

2.5.2 Cohesion 28

2.6 Sticky-Point Temperature 30

2.7 Glass Transition 32

2.8 Sorption Isotherms 36

2.9 Spray Drying of Sticky Materials – Experimental Studies of Wall Deposition And methods for Reducing It 39

2.9.1 Additives 39

2.9.2 Injecting Cold Air into the Spray Dryer 42

2.9.3 Cooling the Dryer Walls 43

2.9.4 Scraping the Chamber Walls 45

2.9.5 Drying Conditions 45

2.9.6 Dryer Size and Shape. 47

2.9.7 Increasing the Rate of Static Dissipation 48

2.9.8 Internal Chamber Finishes 50

2.10 Conclusions. 50

3 Comparison of Glass Transition Temperature and Sticky-Point Temperature for Skim Powder **52**

3.1 Differential Scanning Calorimetry 53

3.2 Materials and Methods 56

3.2.1 Rehumidification of the Skim Milk Powder to Obtain the Desired Moisture Content 56

3.2.2 Determination of the Glass Transition Temperature of Skim Milk Powder 58

3.3 Glass Transition Temperature of Skim Milk Powder at Various Moisture Contents 59

3.4 The Effect of Heating Rate on Glass Transition Temperature 63

3.5 Denaturation of Milk Proteins 65

3.6 Discussion 66

3.7 Conclusions 68

4 Spray Drying – The Equipment, Experimental Design and Mass and Energy Balances **70**

4.1 Spray Drying Equipment 70

4.1.1 General Description of Spray Dryer used in this Work 71

4.1.2 Nozzle Atomiser 74

4.1.3 Description of Dryer Control 75

4.1.4 Analogue to Digital Converter Card 76

4.1.5 Calibration of Thermocouples 77

4.1.6 Modification to Spray Dryer for Experimentation 78

4.1.7 Conclusions 79

4.2 Experimental Design 80

4.2.1 Choice of Material to be Spray Dried 80

4.2.2 Choice of Inlet Swirl Vane Angle. 81

4.2.3 Choice of Inlet Air Temperature and Process Fluid Flowrate. . 81

4.2.4 Addition of Anti-static Agent to Skim Milk 83

4.2.5 Grounding the Spray Dryer 83

4.2.6 Testing the Effect of Surface Properties and Time on Wall Deposition Flux 84

4.2.7 Increasing the Residence Time of Particles inside the Spray

Dryer 84
4.2.8 Scanning Electron Microscope and Particle Size Analysis 85
4.2.9 The Protocol for Spray Drying Skim Milk 86
4.2.10 Conclusions 87
4.3 Mass and Energy Balances. 88
4.3.1 Experimental Procedure 88
4.3.2 Mass Balance for Air 91
4.3.3 Mass Balance for Water 93
4.3.4 Sensitivity Analysis and Propagation of Error and Uncertainties 94
4.3.5 Energy Balances 95
4.3.6 Overall Discussion 98
4.3.7 Conclusions 99

5 Wall Deposition Fluxes for Skim Milk Powder 101
5.1 Mass and Energy Balances 102
5.1.1 Operating Parameters Varied 102
5.2 The Symmetry of the Wall Deposition Fluxes within the Spray Dryer and an Estimate of the Uncertainty for these Fluxes. 105
5.3 The Effect of the Swirl Vane Angle on the Wall Deposition Fluxes of Skim Milk Powder. 109
5.3.1 Product Moisture Locus 111
5.4 The Effect of Inlet Air Temperature and Feed Flowrate on Wall Deposition Fluxes of Skim Milk Powder 116
5.4.1 Inlet Air Temperature 116
5.4.2 Feed Flowrate and Feed Concentrations 120
5.4.3 Interaction of Spray Dryer Operating Conditions with the Sticky-Point Curve 124
5.4.4 The Effect of the Difference between Particle Temperature and Sticky-Point Temperature on Wall Deposition Fluxes 129
5.4.5 Estimation of Evaporative Capacity for Spray Dryer. 140
5.5 A Preliminary Investigation of the Effect of Electrostatics Charges on the Wall Deposition Flux of Skim Milk Powder 143
5.5.1 Grounding the Spray Dryer. 143

5.6 The Effect of Changing the Wall Properties and Time on the Wall Deposition Fluxes 144
5.7 Overall Discussion and Conclusions 150

6 Spray Drying of Concord Grape Skin Extract 153
6.1 Operating Conditions for Spray Drying Grape Skin Extract. 155
6.1.1 Feed Conditions. 155
6.1.2 Spray Dryer Settings 156
6.1.3 Comparison of Dryer Performance between Kockel and Southwell's (1999) Work and this Work. 156
6.2 Results 157
6.2.1 Experimental Observations 157
6.2.2 Wall Deposition Flux of Grape Powder. 158
6.2.3 Composition of Grape Powder 158
6.2.4 Mass and Energy Balances 158
6.2.5 Moisture Content of Grape Powder 159
6.2.6 Particle Size Analysis 160
6.3 Estimating Particle Size for Two-Fluid Nozzle. 161
6.3.1 Water Droplet 164
6.3.2 Skim Milk Droplet 167
6.3.3 Grape Skin Extract Droplet 169
6.4 The Use of Fibre in Spray Drying Grape Skin Extract 172
6.5 Conclusions 173

7 Conclusions and Recommendations 175
7.1 Conclusions 175
7.2 Recommendations for Future Work 178

References 181
Appendix A 187
Appendix B 193
Appendix C 230
Appendix D 274

List of Figures

Figure 1.1 - Twin Spray Dryer Installation 2

Figure 1.2 - Classes of Spray Dryers 3

Figure 2.1 - Chemical Structure of Catechin 11

Figure 2.2 - Chemical Structure of Flavanones 12

Figure 2.3 - Chemical Structure of Limonoids 12

Figure 2.4 - Velocity Vectors in the Axial-Radial Plane of a Short-form Spray Dryer 17

Figure 2.5 - Schematic Diagram of Sudden Expansion 19

Figure 2.6 - Schematic Diagram of Flows in the Confined Jet Model 20

Figure 2.7 - Van der Waals Adhesive Force 25

Figure 2.8 - Adhesive Force due to a Liquid Film 27

Figure 2.9 - Pendular Liquid Bridge between Solid Particles. 29

Figure 2.10 - Schematic Diagram of Phase Changes in Sugars 32

Figure 2.11 - The Glass Transition Region for Skim Milk Powder 33

Figure 2.12 - Equilibrium Chart with Product Moisture Locus 38

Figure 2.13 - Interaction between Sticky-Point Behaviour and Sorption Isotherms . . 38

Figure 2.14 - Photograph of Skim Milk Powder on a Plate as Observed Under a Scanning Electron Microscope 47

Figure 3.1 - Schematic Diagram of a DSC Cell 54

Figure 3.2 - Characterisation of the Glass Transition Temperature of Lactose by MDSC showing the Separation of Total Heat Flow into Reversing (Heat Capacity) and Non-Reversing (Kinetic) Components 55

Figure 3.3 - Glass Transition Temperatures for Skim Milk Powder with Different Moisture Contents, found in this Study 60

Figure 3.4 - The Glass Transition Temperatures and Sticky-Point Temperatures for Skim Milk Powder as a Function of Moisture Content 61

Figure 3.5 - Comparison of Glass Transition Temperatures for Skim Milk with Those Found by Other Researchers 63

Figure 3.6 - Heat Flow Signal as a Function of Temperature, Showing the Glass Transition Region for Skim Milk Powder for Different Heating Rates 64

Figure 3.7 - Reverse Heat Flow Signal as a Function of Temperature, Showing the Glass Transition Region for Skim Milk Powder for Different Heating Rates 65

Figure 4.1 - Photograph of Spray Dryer at the Department of Chemical Engineering 72
Figure 4.2 - Photograph of Spray Dryer Heater and Fans Cabinet at the Department of Chemical Engineering. 72
Figure 4.3 - Schematic of Dryer Rig 74
Figure 4.4 - Diagram of Delavan GA1 Two-Fluid Nozzle Atomiser 75
Figure 4.5 - Modification to Spray Dryer Showing Location of Plates 1 to 4 in Relation to the Spray Dryer for Measuring the Wall Deposition of Skim Milk Powder 79
Figure 5.1 - Photograph Showing All Plates at the End of a Run. 106
Figure 5.2 - Schematic Diagram Showing the Spray Impaction of Particle on the Conical Section of the Spray Dryer 106
Figure 5.3 - Photograph showing that Wall Deposition Flux is Not Influenced by the Circumferential Location in the Spray Dryer 108
Figure 5.4 - The Average Deposition Flux of Skim Milk Powder and the Average Outlet Moisture Content of the Skim Milk Powder on a Dry Basis, as a Function of the Swirl Vane Angle 109
Figure 5.5 - Product Moisture Locus for Skim Milk Powder and Soy Milk Powder 115
Figure 5.6 - Influence of Reducing the Inlet Air Temperature on Particle Stickiness . 117
Figure 5.7 - The Average Deposition Flux of skim Milk Powder and the Average Outlet Moisture Content of the Skim Milk Powder on a Dry Basis, as a Function of the Inlet Air Temperature 118
Figure 5.8 - Schematic Diagram Showing Particles from the Atomiser Entraining Particles that are Held Up Inside the Recirculation Zones in the Spray Dryer 121
Figure 5.9 - The Average Deposition Flux of skim Milk Powder and the Average Outlet Moisture Content of the Skim Milk Powder on a Dry Basis, as a Function of the Feed Flowrate 122
Figure 5.10 - Operating Conditions and Corresponding Wall Deposition Fluxes on the Sticky-Point Diagram for Skim Milk Powder 125
Figure 5.11 - Wall Deposition Flux as a Function of the Difference Between the Particle Temperature and Sticky-Point Temperature for Different Operating Conditions. 129
Figure 5.12 - Comparison Between Predicted and Experimental Operating Points on

Sticky-Point Diagram for Skim Milk Powder 139
Figure 5.13 - Schematic Diagram Showing Input/Output Streams for the Spray Dryer 141
Figure 5.14 - Photograph of Adhesive on Plates 5 and 6 for Experiments to Test the Effect of Adhesion and Time on Wall Deposition of Skim Milk Powder 145
Figure 5.15 - The Mass of Powder Collected on Plates as a Function of Time For the Cases of No Adhesive and Adhesive on Plates 5 and 6 146
Figure 5.16 - Photograph of Skim Milk Powder Particles Adhering to the Aluminium Sample Plate Placed in the Spray Dryer 147
Figure 5.17 - Photograph of the Skim Milk Powder Particles that Have Left the Spray Dryer 148
Figure 5.18 - Particle Size Distribution for the Skim Milk Powder 149
Figure 6.1 - Particle Size Distribution Chart for Grape Powder 160
Figure 6.2 - An Externally Mixing Two-Fluid Nozzle 163

List of Tables

Table 2.1 - Dimensions of Spray Dryer and Type of Atomiser used by Previous Researchers in Experimental Studies on the Flow Patterns in Spray Dryers 16

Table 2.2 - Glass Transition Temperature of Anhydrous Sugars 36

Table 2.3 - The Use of Carriers to Modify the Stickiness of Dried Foodstuffs in Spray Dryers and Different Spray Dryer Designs used to Combat Wall Deposition 40

Table 2.4 - Influence of the Increase in Temperature of the Product above the Glass Transition Temperature on the Structural Characteristics of the Product 46

Table 3.1 - Operating Conditions for the Stirred Fluidised Bed, Predicted Equilibrium Moisture Contents and Actual Moisture Contents of the Skim Milk Powder 58

Table 3.2 - Denaturation Temperature of Whey Proteins 66

Table 4.1 - Flow Capacity for the Delavan Two-Fluid GA1 Nozzle Atomiser 74

Table 4.2 - The Distance from the Roof of the Spray Dryer to the Centres of the Plates and their Respective Weights 78

Table 4.3 - Pump Settings and Corresponding Feed Flowrates 82

Table 4.4 - Experimental Conditions for the Spray Dryer when used for Assessing Mass and Energy Balances 89

Table 4.5 - Mass Balance for Air over Spray Dryer 91

Table 4.6 - Mass Balance Results for Water over the Spray Dryer 92

Table 4.7 - Energy Balance Results over the Spray Dryer 95

Table 4.8 - The Effect on the Measured Absolute Humidity of the Air, If There Was a Systematic Error of 2°C in the Cold Junction Temperature. . . . 99

Table 4.9 - Effect on Water Balance for Run 2, if there was a Systematic Error of 2°C in the Cold Junction Temperature 99

Table 4.10 - Effect on Energy Balance for Run 2, if there was a Systematic Error of 2°C in the Cold Junction Temperature. 99

Table 5.1 - Operating Parameters for Spray Drying Skim Milk, Testing the Effect of Different Swirl Vane Angles 103

Table 5.2 - Operating Parameters for Spray Drying Skim Milk, Testing the Effect of Different Inlet Air Temperatures 103

Table 5.3 - Operating Parameters for Spray Drying Skim Milk, Testing the Effect of Different Feed Flowrates 103

Table 5.4 - Studying the Influence of Wall Properties and Electrostatics on the Wall Deposition Flux of Skim Milk Powder 104

Table 5.5 - Studying the Influence of Different Surface Material and Residence Time On the Wall Deposition Flux of Skim Milk Powder 105

Table 5.6 - Wall Deposition Fluxes of Skim Milk Powder for Swirl Vane Angle of 30° 108

Table 5.7 - Summary of Statistical Analysis Study of the Difference in the Wall Deposition Fluxes for Skim Milk Powder for Different Swirl Vane Angles 111

Table 5.8 - Comparison of Equilibrium and Measured Outlet Moisture Contents for Skim Milk Powder 113

Table 5.9 - Comparison of Equilibrium Particle Moisture Content (%) with Predicted Moisture Content found using CFD 114

Table 5.10 - Wall Deposition Flux on Plates 1 to 4 with and without Insulation . . 128

Table 5.11 - Comparison of the Predictions of the Outlet Air Temperature and Equilibrium Moisture Content for Different Operating Conditions . . 138

Table 5.12 - Summary of Evaporative Capacity Study for Spray Dryer for Three Different Inlet Air Temperatures 143

Table 5.13 - Densities and Concentration of Components of Skim Milk Powder . . 150

Table 6.1 - Densities and Concentrations of Components in Skim Milk 168

Table 6.2 - Physical Properties, Namely Surface Tension, Viscosity, Density and Solids Concentration of the Process Fluids Studied Here 171

Table 6.3 - Droplet Sizes Predicted using the Lefebvre (1980) Equation and Filkova and Cedik (1982) Correlation for a Two-Fluid Nozzle, and Actual Particle Sizes found using the Malvern 171

Chapter 1

Introduction

Spray drying is a process whereby liquid material is sprayed into hot air entering a drying chamber. The heat from the air evaporates the water from the liquid droplets, forming dried solid particles that are later separated from the air. Masters (1996) has discussed the history of spray drying back to the first recorded patent in 1872 by Percy, who described the spraying of a liquid into hot air to form a powder. The Second World War gave the incentive for drying food material at high throughputs, and spray drying was found to be very suitable for doing this. Spray drying is suitable for drying food material because (1) Rapid drying rates and small residence times for particles reduce the contact time between heat sensitive foods and the heating medium (Gupta, 1978); (2) Commercial spray dryers have high product throughputs (4-28 tonnes per hour of milk powder for most spray dryers in the Australian dairy industry); (3) Spray drying is an efficient and relatively inexpensive process compared with many other drying techniques, such as freeze-drying. The spray drying process can be broken into three steps:

1. The liquid is atomised into a liquid spray by a rotary atomiser, pneumatic nozzle, pressure nozzle or sonic atomiser (Keey, 1992a) and discharged into the drying chamber.
2. The droplet spray is dried by the flow of hot gas, producing a dried solid product.
3. The dried solid product is separated from the hot gas, usually by means of a cyclone separator, possibly followed by a bag filter or electrostatic precipitator (Masters, 1991).

Spray drying is used for commercially drying food materials such as milk, instant coffee, soluble tea and egg products (Masters, 1991). Spray drying is also used in the pharmaceutical industry and in the production of soap, detergents, plastic and ceramic material. Large-scale

spray dryers (height 24 m, diameter 12 m) are used for commercially drying milk (Birch, 1997). Figure 1.1 shows a twin spray dryer installation used in industry. On the other hand, small bench-scale spray dryers are used in the pharmaceutical industry for preparing drugs.

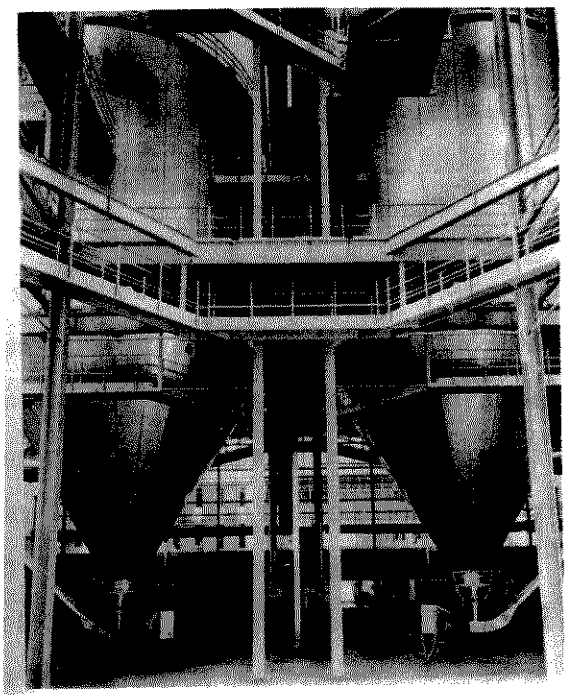

Figure 1.1 – Twin spray dryer installation. Source : Niro Atomisers.

A common spray dryer configuration is a cylinder on an inverted cone with an atomiser, or atomiser manifold, at the top of the cylinder. As shown in Figure 1.2, such dryers are generally divided into two classes, short-form dryers, where the height to diameter aspect ratio is typically of the order of 2:1, and tall-form dryers, where the aspect ratio often exceeds 5:1 (Langrish, 1996). A rotary atomiser gives a wider spray cloud and is often used in short-form dryers, while a nozzle atomiser produces a narrower cone of spray and is often used in tall-form dryers. The atomiser design affects both the process fluid flowrate that can be used and the particle size distribution of the dried product, which governs the product appearance, packing and subsequent processing requirements (Masters, 1991).

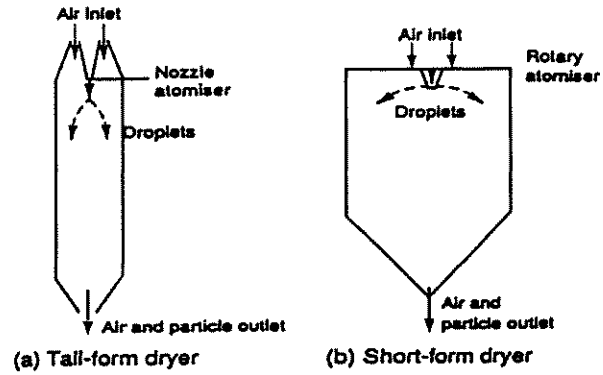

Figure 1.2 - Classes of spray dryers. Source : Langrish (1996).

Spray dryers may also be run with either co-current flow, where the liquid and gas flow into the drying chamber in the same direction, or countercurrent flow, where the liquid and gas flow into the drying chamber in opposite directions. The co-current design is used when handling heat sensitive products like food. The temperature of the product is low during the time that the bulk of the evaporation takes place, and the particles are in contact with much cooler air when they approach their final moisture content. In contrast, the countercurrent design subjects the driest powder to the hottest gas stream, and this design meets the requirements of products like detergents that are not highly heat sensitive.

While spray drying is a successful technique for drying food material such as milk, spray dryers have to be cleaned frequently due to powder deposit build-up on the walls (Bloore, 2001). The build-up of powder deposits in a spray dryer is undesirable for the following reasons.

1. Deposits undergo oxidation (particularly for whole milk powder) and browning or scorching, and will degrade the quality and safety of the final product if they fall off and mix with it (Raemy *et al.*, 1983). For heat sensitive products, wall deposition can lead to overheating of the product, resulting in unpleasant sensory characteristics and degradation (Downton *et al.*, 1982).
2. Wall deposits give rise to lower product yields, since the product sticks to the walls.
3. Wall deposits give rise to increased downtime for cleaning. Reduction in cleaning time is desirable because it will give rise to increased production time and possibly a reduction in the cost of manufacturing the product.

The above problems are preventing some materials, notably fruit juices which contain large amounts of hygroscopic, amorphous sugars, from being successfully dried (Downton *et al.*, 1982).

4. Wall deposits also pose a potential fire risk and are hygiene problems (Abbott, 1990). Spray drying of milk is not considered a highly hazardous process (Beever and Crowhurst, 1989), but product degradation owing to charring and minor fires occur persistently. The first publications on the subject of fire in milk powder plants appeared in the 1960's by Pisecky (1968) and Sapryngin and Kiselejev (1966). Pineau (1984) reported that, of 35 major accidents occuring between 1967 and 1982 in the French dairy industry, 14 involved fire and explosion. Spontaneous combustion (self-ignition) of milk powder deposits are believed to be the most important cause of fires and explosions in milk powders (Pisecky, 1972; Pineau, 1984) due to the exothermic Maillard reaction. Powder deposits on areas exposed directly to the incoming hot air can also cause fires (Pisecky, 1997). The powder layer test described in Abbott (1990) p. 18-20, involves passing heated air over a layer of material 15 mm deep, which is representative of the powder layers that build up in most spray-drying plant, and monitoring the temperature of the material. The ignition temperature of the material (determined when exothermic activity begins) is found by conducting a series of extended isothermal tests which run for about eight hours, because the layers of material can build up on the walls of the dryers and stay there for long periods. The rate of reaction depends on the thickness and porosity of the powder deposit layer, the surrounding air temperature and the composition of the powder, including the moisture content (Pisecky, 1997).

The production rates of most individual spray dryers range from 4-28 tonnes of dry powder per hour, so these wall deposition problems are significant. Spray dryers are the core components of a milk powder production plant, where the basic configuration usually features co-current flow of milk powder and air. Significant requirements in the dairy processing industry include reducing the deposition rate of skim particles on walls and increasing the time period between cleaning cycles, thereby enhancing plant availability. Remedial measures, such as air sweeps around walls and hammers at the wall, are possible and are used to reduce wall deposition (Masters, 1996). However, hammers are not effective away from the hitting zone, and cool air sweeps are only effective up to 1 m from the air sweeps. A 4 tonne per hour (dry basis) dryer

is approximately 30 m in diameter and 10 m high, so it is not practical to install air sweeps everywhere.

There are two main factors that determine whether particles will deposit on the walls, namely whether or not the particles approach the walls and whether or not they stick to the walls when they get there. Regarding whether or not the particles approach the walls, Southwell and Langrish (2001) found evidence that the extent to which particles spread out in a spray dryer was affected by the amount of swirl in the inlet air, which is created by installing a ring of swirl vanes in the air inlet annulus at the top of the dryer. Swirl vane angles between 0° and 45°, in 5° increments, were investigated in a pilot-scale dryer using a complementary combination of flow visualisation and Laser Doppler Velocimetry techniques. They found that the spray cloud showed only minor instability at swirl vane angles up to 20°, but became increasingly unstable thereafter. They found wall deposition of water droplets in the cylindrical section of the spray dryer was unacceptably high for swirl vane angles exceeding 30°. Oakley *et al.* (1988) also found that for a swirl vane angle of 30°, significant on-axis recirculation occurred (unsteady flow) in the spray dryer design that they studied.

The conditions that cause a material containing carbohydrates to become sticky can be measured using the sticky-point test developed by Lazar *et al.* (1956). The sticky-point test assesses the influence of temperature and moisture content of particles on powder cohesion. At a certain temperature, which is a function of the moisture content of the particles, the force required to turn the stirrer embedded in the powder increases sharply, and the current to the stirrer motor increases sharply (Notter *et al.*, 1959). The temperature at which this occurs is usually referred to as the sticky-point temperature. A sticky-point curve (temperature versus moisture content of the material) can be plotted from these data. The sticky-point curve has been used as a semi-quantitative concept in selecting operating conditions for spray drying sticky material, where it has been implied that there is no significant wall deposition below the sticky-point curve (Lazar *et al.*, 1956; Brennan *et al.*, 1971; Gupta, 1978; Genskow, 1988; Yang *et al.*, 2000). It is possible that a key parameter affecting wall deposition is the difference between the particle temperature and sticky-point temperature, and this hypothesis is tested in this work.

Previous researchers have not resolved the problem of the wall deposition of particles in spray dryers. No quantitative data has been produced on the wall deposition rates or fluxes of food material in spray dryers. Only qualitative data was obtained by Brennan *et al.* (1971) and

Gupta (1978), who suggested that controlling the temperature of the spray dryer walls affected whether or not wall deposition occurred. They observed less wall deposits when the temperature of the walls was below the sticky-point temperature of the material. Chen *et al.* (1993) obtained quantitative data on the amount (mass/area) of wall deposition for skim milk and whole milk powder in an industrial spray dryer, but they did not provided any time scale for the wall deposition results, so the wall deposition flux cannot be estimated from their data. In addition, the effect of different operating conditions on the wall deposition flux was not quantified. A more comprehensive review of the literature is given in Chapter 2.

The aim of this work was to quantify the effects of the following parameters on the wall deposition flux:

1. The swirl vane angle, which imparts swirl to the incoming air and affects the stability of the flow patterns and spray cloud in the spray dryer, and
2. The inlet air temperature and liquid feed flowrate, which affect the particle temperatures and moisture contents, with respect to the sticky-point curve, and
3. Wall properties: surface materials, namely non-stick food grade material (nylon), adhesive tape and stainless steel, and
4. Electrostatic effects such as grounding the spray dryer, and
5. Altering the properties of the feed by adding an anti-static agent.
6. A combination of surface material and time, which addressed a fundamental question in the field of spray drying; if cohesion occurs at the same rate as adhesion for skim milk powder in this spray dryer.

Furthermore, the differences between spray drying skim milk and grape extract were also investigated here.

This thesis is organised into six parts. Chapter 2 provides a literature review of the flow patterns inside spray dryers, the mechanisms which are responsible for particle stickiness. It discusses experimental studies carried out by previous researchers in studying the wall deposition problem and the methods they have used for reducing wall deposition. To determine if an alternative test to the sticky-point measurements can be used to characterise the stickiness of skim milk powder, which contains carbohydrates, the glass transition temperature of skim milk powder was measured using Differential Scanning Calorimetry (DSC). The

results of this work are discussed in Chapter 3. Chapter 4 is organised into three parts. Section 4.1 provides a description of the spray dryer, nozzle atomiser, dryer control, and the modifications made to the spray dryer for experimentation. Section 4.2 provides a description of the experimental design used in this work. Section 4.3 discusses the mass and energy balances carried out over the spray dryer. Chapter 5 reports and then interprets the wall deposition flux data for skim milk powder. Finally, Chapter 6 reports and then interprets the wall deposition flux data for spray drying fermented concord grape extract supplied by Food Ingredients Technologies Australia Pty Ltd, and compares the drying performance of concord grape extract with that of skim milk.

Chapter 2

Literature Review

This literature review is organised as follows. The application of spray dryers to produce products for human consumption is discussed first in section 2.1. The two main factors that determine if particles will deposit on the walls of the spray dryer are whether or not the particles approach the walls of the spray dryer, and whether or not the particles stick to the walls when they get there. The flow patterns of particles and gas inside the spray dryer determine if particles will approach the walls of the spray dryer. Sections 2.2 to 2.4 discuss the development of understanding the flow patterns inside spray dryers, which has led to the use of Computational Fluid Dynamics (CFD) to predict the flow patterns inside spray dryers, and experiments which have been carried out by previous workers to validate these predictions. The preliminary experimental work and/or simulations carried out by previous researchers investigating wall deposition of water droplets and food particles is also discussed here. Particle stickiness will determine if the particles stick to the walls of the spray dryer when they get there. Sections 2.5 to 2.8 discuss the mechanisms involved in stickiness and the methods which have been used to measure and predict the stickiness of material. Section 2.9 discusses the work of previous researchers who spray dried food containing carbohydrates (sticky material), and how they addressed the wall deposition problem that occurred from spray drying this material. Section 2.10 draws conclusions from the literature review and highlights where further research is required in studying the problem of wall deposition in spray dryers.

2.1 Applications of Spray Dryers to Produce Products for Human Consumption

2.1.1 Milk Products

Australia produces a range of milk powders, of which skim milk powder is a major one. In 1998, 231 000 tonnes of skim milk powder were produced, which is approximately 7.5% of the world production (Canadian Dairy Information Centre Home Page, accessed April 2002). Skim milk powder is used as an ingredient in confectionary, cakes, biscuits and soup. Thus, the production of skim milk powder is an important sector of the Australian dairy industry. A typical spray drying plant processes skim milk concentrate with 50% (w/w) total solids into a powder containing around 3.5% (w/w) moisture on a mass basis (Shallcross, 2000). This extends the shelf-life of the food (since skim milk is a perishable item), and thus allows the food to be transported long distances and provided out of season. Furthermore, transporting skim milk powder saves transport costs because large amounts of water (present in skim milk) do not have to be moved.

2.1.2 Nutraceutical Products

In Australia, all grape marc, which is the grape skin and seeds that remain from pressing grapes in the wine and fruit processing industry (approximately 80 000 tonnes per year), is collected, and all soluble components are recovered, fermented and distilled, producing approximately 8 million litres of alcohol per year (Private Communication: Lang, 2000). All insoluble materials are used as boiler fuel, like bagasse is used in the sugar industry. 80 million litres of effluent are generated from this process, and the effluent has a Biological Oxygen Demand (BOD) of around 20 000 mg per litre, and thus depletes the water of oxygen and is expensive to treat.

In the major citrus processing countries, such as the United States of America and Brazil, citrus peel is pressed and dried to stock food pellets. This is a revenue neutral activity but requires heavy capital expenditure, which is justified by avoiding large waste treatment costs. Australia processes around 150 000 to 200 000 tonnes of oranges annually, and 450 kg per tonne is discharged as peel. Citrus peel is disposed of locally as stock food. (Private Communication: Lang, 2001).

Food Ingredients Technologies Australia Pty Ltd have developed an agitated washing process for extracting potentially valuable liquid products such as nutraceuticals and natural food colourings, from grape marc and citrus peel. The grape marc and citrus peel would otherwise have a low (or even negative) value due to the costs of effluent treatment and disposal. Nutraceuticals, are compounds that are helpful in the prevention of illness and disease (Belem, 1999). Several drying processes, such as freeze drying and spray drying, could be used to dry the liquid extracts into a more stable solid form to extend the shelf life of these materials and for compact delivery.

The freeze drying process involves sublimation of water from a frozen mass of the juice and is effective in retaining the natural flavour and aroma of the product. However, the disadvantage of using freeze drying is that it requires expensive equipment for creating and maintaining a high vacuum for sublimation. The equipment is costly to operate and a long processing time is required, since sublimation from the solid state is a much slower process than evaporation from the liquid state (Strashun and Talburt, 1954). Furthermore, freeze drying is normally a batch process, while spray drying is a continuous process, and therefore the amount of variability in the products due to processing tends to be less in spray drying than that in a batch process like freeze drying.

Freeze drying a material costs about $30 per kg of dried powder produced, while spray drying costs only $1 per kg of dried powder (Private Communication: Lang, 2001). Aroma compounds are not an important factor for the extracts, and these are commonly degraded when products are spray dried (King, 1990). Since retaining them is not critical, spray drying is worth investigating on the grounds of its low operating costs. The wider use of nutraceuticals is likely to see the price of the product fall, in which case the significance of the processing price advantage in spray drying will become more important. Consultancy work at the University of Sydney in 1999 has shown that a key issue that limits spray drying grape extract is the deposition of particles on the walls of spray dryers. Product losses in the spray drying process must be avoided since the material is valuable.

The nutraceuticals found in grape marc and citrus peel are frequently phenolic compounds (Singleton, 1982; Montanari *et al.*, 1997). Citrus peel also contains nutraceuticals called limonoids (Montanari *et al.*, 1997). Phenolic compounds are compounds that have an aromatic ring bearing a hydroxyl substituent. They are present in many plants and are significant in

citrus fruits and wine. The phenolic compounds which are considered to be important in foods are the phenolic acids, flavonoids (anthocyanins, flavonols, flavones, catechins, and flavanones) and their glycosides. Anthocyanins and flavonols are present as red pigments in a variety of fruits and vegetables. In addition to colour, phenolic compounds also contribute to flavour and other qualities of foods, such as astrigency, which is useful for determining the overall quality of fresh fruits, fruit beverages and wines (Lee, 2000). Limonoids are triterpene derivatives that bear a furan ring and are abundant in citrus fruit, with the highest concentration being in the seeds (Montanari *et al.*, 1997). Some of the therapeutic properties of flavonoids and limonoids will now be described.

The 'French Paradox' is the name given to the phenomenon that the inhabitants of some regions of France have a lower rate of coronary heart disease than that found in the United States of America, despite consumption of fat at comparable levels and less exercise (Holmgren, 1993; Renaud and de Loregenl, 1992). This paradox has been attributed to the routine consumption of wine. The oxidation of human low density lipoproteins has been implicated in coronary heart disease (Ross and Harker, 1976). Hence substances such as catechin (Figure 2.1), which are present in red wine and grape seeds and which can block this oxidation, should slow the progress of this disease (Mangiapane *et al.*, 1992).

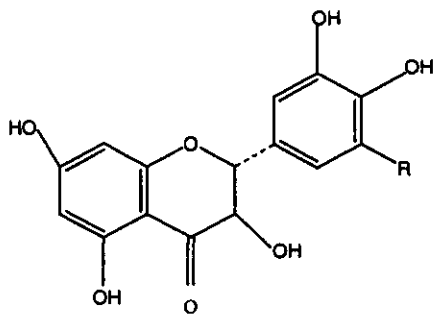

Figure 2.1 - Chemical structure of catechin R=H, (+), and epicatechin R=H, (-). Source : Lee (2000).

In citrus fruit, the predominant flavonoids are hesperidin, narirutin and naringin (Figure 2.2). So *et al.* (1996) found that hesperetin and naringenin are effective in inhibiting the *in vitro* proliferation of human breast cancer cells. Kaul *et al.* (1985) found that hesperetin actively inhibited the replication but not the infectivity of herpes simplex, polio and parainfluenza type viruses.

The limonoids (Figure 2.3) isolated from citrus products possess strong anticancer activity (Lam *et al.*, 1993). The protection afforded by the limonoids seems to follow their ability to induce glutathione S-transferase activity. Natural products like limonoids which contain the furan ring will stimulate the glutathione S-transferase enzyme detoxifying system which inhibits chemically induced carcinogenesis. This system catalyzes the conjugation of glutathione to activated carcinogens, making them more water soluble, less reactive, and easier to excrete (Montanari *et al.*, 1997).

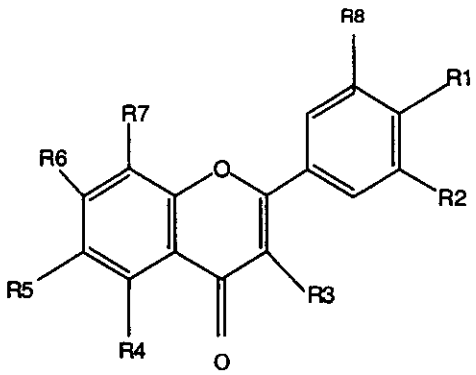

Hesperidin	R1 =OH, R2=OCH_3, R6=O-Rutinose
Hesperetin	R1=OCH_3, R2 R6 R8=OH
Narirutin	R1=OH, R6=O-Rutinose
Naringin	R1=OH, R6=O-Neohesperidose
Naringenin	R1=OH, R2 R6=OH
Note:	Unspecified symbols are hydrogen

Figure 2.2 - Chemical structure of flavanones. Source : Montanari *et al.* (1997).

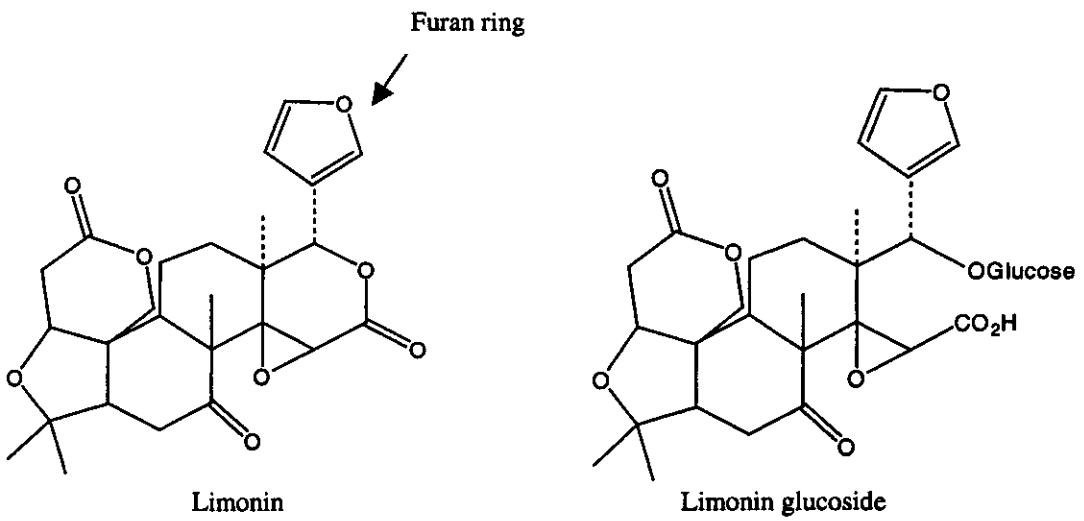

Figure 2.3 - Chemical structure of limonoids. Source : Manners and Hasegawa (1999).

This brief review of the therapeutic properties illustrates that there is some basis for the claims that the grape and citrus extracts obtained by processing grape marc and citrus peel may have some beneficial effect on people.

2.2 Air Flow Patterns

Understanding the flow patterns in a spray dryer is important for predicting whether or not the particles approach the walls of the dryer. Langrish and Fletcher (2001) highlighted developments in understanding the flow patterns inside spray dryers in a recent review. The first stage of understanding the flow patterns in spray dryers was borrowed from reaction engineering and concentrated on fitting somewhat arbitary sequences of well-mixed and plug flow stages, together with bypasses, to residence time distributions from helium-injection tracer measurements (Place *et al.*, 1959; Paris *et al.*, 1971). Place *et al.* (1959) found that the degree of back-mixing in a spray dryer (diameter 7 m, height 15 m) corresponded to about six well-mixed stages in series. Likewise, Paris *et al.* (1971) found the residence time distribution curves of a spray dryer (diameter 6.7 m, height 24 m) could be fitted by five well-mixed stages with complicated bypass connections. Katta and Gauvin (1975) and Keey and Pham (1976) used highly simplified semi-empirical representations of the gas flow pattern in spray dryers. Common features of their work included dividing the drying chamber into two regions characterised by intense mixing in the upper zone (near the atomiser) and essentially plug flow in the lower zone.

Reay (1988) pointed out the weaknesses in the above approaches. These approaches are unsuitable for designing new drying chambers because they are tied to specific geometries in existing dryers, and they require accurate measurements using helium injection and flow visualisation equipment to be performed in existing dryers. A variety of zone sequences (well-mixed, plug flow, bypass) may fit the data equally well, and it is then difficult to decide which is most appropriate. Furthermore, the most appropriate sequence of zones varies with operating conditions. This approach does not enable the effects of varying chamber geometry or operating parameters to be assessed, and both these types of variations are likely to have significant effects on the flow patterns inside spray dryers. In turn, these changes will affect the dryer performance, both in terms of product moisture content and wall deposition rates (Langrish and Fletcher, 2001).

Computational Fluid Dynamics (CFD) has represented the second stage in understanding flow patterns inside spray dryers. This has been made possible by the development of powerful computer workstations at accessible cost. A summary of CFD is given next.

2.3 Computational Fluid Dynamics

CFD allows the solution of conservation equations for mass, momentum and energy to be obtained for many engineering flows in complex geometries, such as spray dryers. One approach to CFD is a finite volume one, involving the division of the flow domain into an array of small control volumes (typically 10 000 or more). Local conditions like the pressure, velocity field and temperature are assumed to be constant over each control volume. The Navier-Stokes equations (Patankar, 1980), which are coupled partial differential equations governing the flow, are integrated over the volume of each cell using Gauss's Theorem to obtain a set of coupled non-linear algebraic equations that must be solved for the entire flow domain. At this stage, boundary conditions at the inlets, exits and walls are also applied. Then, an iterative matrix solver is used to invert this set of coupled, non-linear equations, to provide values for all of the variables, namely the mean velocity components in the axial, radial and tangential directions, and the fluid density, pressure, temperature and static thermodynamic enthalpy, for each volume. These values provide a discrete approximation to the flowfield. These results can then be visualised.

Despite the complexity of turbulent flow, the full Navier-Stokes equations can be time-ensemble averaged to yield the Reynolds Averaged Navier-Stokes equations (RANS). Solving the RANS equations requires less computational resources than solving the full Navier-Stokes equations directly and is used successfully to compute many flows of practical importance. However, the development of turbulence models to predict the Reynolds stresses (which arise from time-ensemble averaging) is an on-going research issue (Wilcox, 1996).

The first worker to apply CFD to spray dryers was Crowe (1980). His work included a common feature of CFD for gas-particle flows, namely the application of the concept known as the Particle-Source-In-Cell (PSI Cell) method (Crowe *et al.*, 1977). This method treats the droplets as sources and sinks of mass, momentum and energy for the gaseous phase and incorporates a two-way coupling technique which includes not only the effect of the gas on the droplets, but also the effect of the droplets on the drying gas. The PSI Cell method is applied by first neglecting the influence of spray on the flow field and calculating the axial, radial and tangential component of the gas velocities, as well as gas temperatures and water mass fractions. A large number of representative droplets are then tracked through the gas inside the chamber. These droplets are chosen to represent the range of droplet sizes leaving the atomiser

so that the sum of the flowrates of each droplet size equals the total liquid flowrate. The droplets act as sources and sinks of momentum, heat and mass for the gas phase, and the velocities, temperatures and mass fractions in the gas phase are recalculated using these sources and sinks from the droplets. This gas-particle coupling process is continued until the flow field does not change significantly with further iteration.

Using a development of the model used by Crowe (1980), Papadakis and King (1988) have shown that the predictions of this CFD technique agree well with measured air temperatures and humidities at various levels below the roof of a co-current spray drying chamber (diameter 0.56 m, height 3.6 m) when water is sprayed through a pressure nozzle. Their work demonstrated clearly the significant effect of the spray on the gas flow patterns in the chamber.

Swirl-induced transient behaviour is sometimes useful in combustion and mixing applications (Dellenback *et al.*, 1988) because a central recirculation zone (which is induced by swirl) may enhance the combustion performance by returning uncombusted fuel and heat towards the base of the flame, but the situation may be different in a spray dryer. In a spray dryer, swirl may also adversely affect the quality of thermally sensitive products like food, if the formation of recirculation zones significantly increases residence times (Oakley *et al.* 1988; Southwell, 2000; Southwell and Langrish, 2001). Furthermore, recirculation of hot dry powder back to the hot air inlet (usually very close to the atomiser) may lead to deposition of particles in this hot zone, and this has been implicated in fires and explosions in milk dryers, since dry milk undergoes a rapid exothermic reaction at the inlet temperatures used in spray dryers (Pisecky, 1997).

Many reported studies have used axisymmetric steady state simulations to model the air flow patterns in a spray dryer, due to the limited computational resources available for these simulations. Their findings with respect to studying the effect of swirl flow in spray dryers are described next.

2.3.1 Steady-State Axisymmetric CFD Simulations and Experimental Studies

The dimensions of the co-current spray dryers and the types of atomiser used by previous researchers in carrying out experimental studies of the flow patterns in spray dryers are given below in Table 2.1.

Table 2.1– Dimensions of spray dryers and type of atomiser used by previous researchers in experimental studies on the flow patterns in spray dryers.

Researcher(s)	Diameter (m)	Length (m)	Atomiser type
Goldberg (1987)	0.76	1.43	Rotary atomiser
Papadakis and King (1988)	0.56	3.6	Pressure nozzle
Langrish and Zbicinski (1994)	0.935	1.69	Two-fluid nozzle
Kieviet and Kerkhof (1995)	2.2	3.7	Pressure nozzle
Stafford *et al.* (1996)	1	1.8	Two-fluid nozzle
Kieviet and Kerkhof (1997)	2.2	3.7	Pressure nozzle
Kieviet *et al.* (1997)	2.2	3.7	No spray in this work.
Godijn *et al.* (1999)	0.8	1.6	Two-fluid nozzle
Southwell and Langrish (2001)	0.8	2	Two-fluid nozzle

Oakley *et al.* (1988) studied the airflow patterns in the same spray dryer used by Goldberg (1987). They predicted the airflow patterns in the spray dryer using the CFD code FLOW3D with the k-ε turbulence model (k = turbulence kinetic energy, ε = turbulence dissipation rate) and compared the CFD predictions with five-hole Pitot tube and Laser Doppler Anemometry measurements. The spray dryer was operating with cold air and no spray was present. The flow in the chamber was assumed to be axisymmetric. The atomiser was seated on a removable ring of swirl vanes which impart swirl flow to the air entering the spray dryer. Measurements were taken without swirl vanes and with swirl vanes inclined at 25° and 30° to the axial direction. Due to the assumption of axial symmetry, measurements were taken over only half the dryer. Where no swirl was introduced at the air inlet, a fast flowing central core surrounded by large recirculation zones was observed. This observation was also reported by Langrish and Zbicinski (1994), Kieviet and Kerkhof (1995), Kieviet *et al.* (1997) and Southwell and Langrish, (2001). Figure 2.4 shows measurements and predictions of flow with swirl vanes of 25° and 30°, respectively, in the form of velocity vector plots. The arrows denote the magnitude and direction of axial and radial velocities. For a swirl vane angle of 25°, both predictions and measurements indicate that the flow resembles that of the no-swirl case except for a greater angle of spread and a higher rate of decay and axial velocity. However,

with a swirl vane angle of 30°, both measurements and predictions indicate that the swirl is sufficient to induce on-axis recirculation. This phenomenon is known as vortex breakdown, where an upward flowing region is formed along the centre-line of the spray dryer (Channaud, 1965).

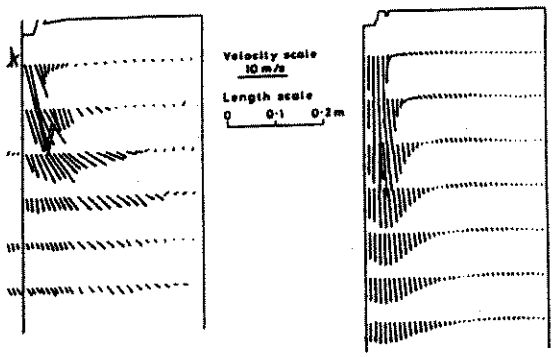

(a) Measurements (b) FLOW3D predictions

25° swirl vanes

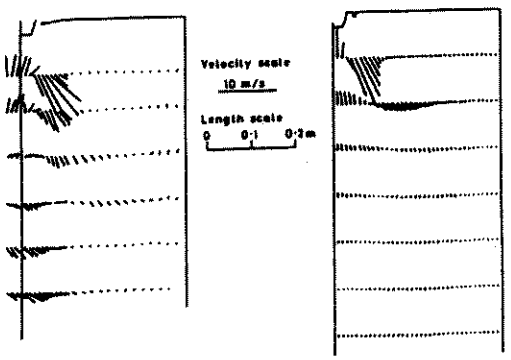

(a) Measurements (b) FLOW3D predictions

30° swirl vanes

Figure 2.4 - Velocity vectors in the axial-radial plane of a short-form spray dryer at an air flowrate through the chamber of 330 m^3hr^{-1}. Source : Oakley *et al.* (1988).

In the high swirl regime (swirl vane angle 30°), the CFD predictions overpredicted the size of the central recirculation zone, and the fast flowing central core near the outlet was not predicted. The predictions of the gas flow were accurate near the inlet and in the top section of the drying chamber but become worse further from the inlet. Oakley *et al.* (1988) explained that the reason for the difference between predictions and measurements of flow for a swirl

vane angle of 30° was the sensitivity of the k and ε values to the inlet conditions for swirling flows. This led Oakley and Bahu (1991) to carry out a preliminary investigation of the effectiveness of the Reynolds stress model as a turbulence model for predicting flow for high swirl flows. They found this model gave more satisfactory results for swirling flows than the k-ε model. However, even though an improvement was noted by using the complex differential Reynolds stress model, it involved substantially greater computational effort than the k-ε model.

Oakley *et al.* (1988) found that convergence rates were slow for higher swirl regimes. A time-dependent calculation showed that, in this case, the code was not predicting a steady-state at all, but an oscillating flow of a low frequency (~1 Hz). They concluded that fluctuations in the experimental data suggest that this is a real effect. Subsequent measurements using a hot-wire anemometer by Langrish *et al.* (1993), on a spray dryer with dimensions not too dissimilar to that used by Oakley *et al.* (1988), have confirmed this feature of the flow. Langrish *et al.* (1993) found the strongest oscillations occur under the conditions predicted by numerical simulations, where significant swirl in the inlet air (swirl vane angle was 30°) is sufficient to cause vortex breakdown and a Precessing Vortex Core. They found good agreement between the measured and predicted time periods of the flow oscillations. A Precessing Vortex Core is associated with highly swirling flows and is caused by the central forced vortex core becoming unstable and precessing about the axis of symmetry. A Precessing Vortex Core may throw particles further towards the side walls of the chamber, increasing the wall deposition rates.

The use of axisymmetric steady state CFD models in spray dryers is limited, since flow patterns in spray dryers exhibit time-dependent asymmetrical behaviour both with and without spray (Southwell and Langrish, 2001) and Precessing Vortex Cores are inherently transient, three-dimensional phenomena. Studies that have used this approach are described next.

2.3.2 Transient CFD Simulations and Experimental Studies

It has been pointed out that the flow patterns in spray dryers are inherently transient, three-dimensional and time-dependent (Kieviet *et al.*, 1997; Godijn *et al.*, 1998; Southwell, 2000; Southwell and Langrish, 2000; Langrish and Fletcher, 2001; LeBarbier *et al.*, 2001; Southwell and Langrish, 2001). The wall deposition patterns and fluxes that result from transient flow patterns (both experimentally and from simulations) are almost certain to be significantly

different from those that are predicted by steady-state simulations. Godijn *et al.* (1999) used video imaging to analyse the flow patterns in a spray dryer (no swirl) and observed that the flow was time-dependent and asymmetrical. Non-axisymmetric recirculation of the air and spray was observed near the walls, exhibiting some similarity to the behaviour noted by Stafford *et al.* (1996), who observed up flowing air and downflowing air along opposite sidewalls, forming an overall circulating motion. Kieviet *et al.* (1997) observed flow instabilities in their spray dryer and were unable to measure stable mean velocities in many areas.

The inlet feature of spray dryers is similar to those found in sudden expansion situations (Figure 2.5). For an expansion ration (D/d) of 2.22, Hallett and Gunther (1984) observed regular motion of the central jet around the axis (precession) under low swirl conditions. Hill *et al.* (1995) and Nathan *et al.* (1998) have demonstrated that swirl in the inlet flow is not necessarily a pre-requisite for precession. They concluded that precession was a three-dimensional analog of the flapping motion often observed in two-dimensional sudden expansion studies. Furthermore, Guo (2001) concluded that the asymmetry and subsequent oscillation observed in axisymmetric sudden expansion are inherently physical phenomena within an expansion flow rather than originating from any possible imperfection of the geometry or asymmetry upstream. Guo *et al.* (1998) suggested that a stable precessing motion may be produced in a sudden expansion for the following basic reasons.

Figure 2.5 - Schematic diagram of sudden expansion. Source : Guo *et al.* (1998).

Any initial displacement of the jet from the centreline causes a negative pressure gradient to form across the jet, as shown in Figure 2.6. The jet moves from the centreline towards the cavity side wall in response to this pressure gradient, but the momentum of the entrained flow on that side of the cavity simultaneously increases. If the transverse component of the jet pressure increases more than the jet momentum as the displacement increases, then a steady asymmetric flow pattern will form permanently. However, if cross flow exists across the jet, the pressure difference can be dampened. Eventually a point can be reached where the jet

momentum exceeds the pressure gradient and the jet movement reverses, which is the fundamental cause of this precession. This cross-flow is necessary for the sustained swinging oscillation (Gerbert *et al.*, 1998). Consequently, the swinging oscillation is produced by a dynamic balance between the pressure difference across the jet and the transverse momentum of the jet. In a three-dimensional situation, it is always possible to have air moving around (effectively across) the jet because the central jet cannot separate recirculation zones.

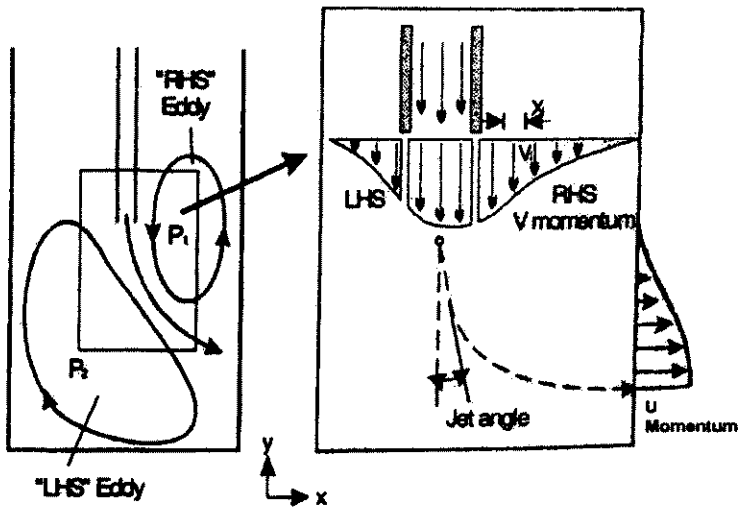

Figure 2.6 – Schematic diagram of flows in the confined jet model, predicted using computational fluid dynamics, where it was found that the jet flow oscillated in response to a dynamic balance between pressure gradient and momentum. Source : Honeyands and Molloy (1995).

Guo *et al.* (2001) used a fully transient, three-dimensional CFD simulation (CFX4), with the k-ε turbulence model and predicted a Precessing Vortex Core in axisymmetric sudden expansion flow as observed experimentally by Hallett and Gunther (1984) for an expansion ratio of 2.22 and Dellenback *et al.* (1988) for an expansion ratio of 1.96. Their computational model was based on axisymmetric geometry with steady boundary conditions, indicating that the Precessing Vortex Core is an inherent characteristic of the swirling flow inside the axisymmetric sudden expansion. They suggested that steady asymmetric flow should not normally be expected in an axisymmetric sudden expansion, and oscillations in the flow patterns are likely. They found that both the swinging and the precessing motion of the jet caused by the instability are predicted for turbulent mean flow, resulting in intense flow oscillation.

The frequencies simulated with an expansion ratio of 1.96 (Guo *et al.*, 2001) agreed with the measured frequencies of Hallet and Gunther (1995) and Dellenback *et al.* (1988). Thus, CFD

can be used to predict the instability characterised by the precessing jet in axisymmetric sudden expansions. In general, however, the spray dryer has complex inlet features that limit the direct application of sudden expansion results to spray drying problems (Southwell and Langrish, 2001), although the same basic processes occur (LeBarbier *et al.*, 2001).

CFD simulations are necessary for a true representation of the flow patterns and the spray-gas interaction. However, despite the increasing evidence for transient, three-dimensional flows in spray dryers, Straatsma *et al.* (1999) still used a two-dimensional axisymmetrical steady state simulation to simulate the gas flow in a spray dryer. The flow in spray dryers is asymmetrical, and any oscillation predictions in an axisymmetric simulation may not fully predict the real behaviour in spray dryers.

Langrish and Southwell (2001) sprayed water into a co-current spray dryer (diameter 0.8 m, height 2 m) to study the effect of varying the amount of inlet air swirl on the stability of the flow patterns in the spray dryer. Swirl vane angles between 0° and 45°, in 5° increments, were investigated using a complementary combination of flow visualisation and Laser Doppler Velocimetry techniques. The found evidence that the extent to which droplets spread out in the drying chamber was affected by the amount of swirl in the inlet air. The spray cloud showed only minor instability at swirl vane angles up to 20°, but became increasingly unstable thereafter. Transient behaviour was visible at a vane angle of 25°, and the spray cloud appeared to precess inside the swirling inlet air immediately below the inlet. At vane angles of 30° and higher, the spray cloud became increasingly dispersed and mixed with the swirling inlet air, so that the cloud did not have a constant cross section and was periodically 'ripped apart'. They found that wall deposition in the cylindrical section of the spray dryer was unacceptably high for vane angles exceeding 30°. Thus, when spray drying feed material containing dissolved solids, the amount of particle spread will almost inevitably affect how many particles are near the walls of the dryer. The effect of dryer size on the flow patterns, with the same design of dryer, does not appear to have been studied yet.

LeBarbier *et al.* (2001) carried out CFD simulations to predict the flow behaviour observed in a hydraulic model (diameter 0.29 m, height 0.5m) of an industrial co-current short-form spray dryer with swirl vane angles of 0°, 25°, and 40°. A conventional video system was used to record the flow patterns in the spray dryer, and characteristic parameters representing the jet precession in the dryer were extracted from the video system as frames. They found that

transient CFD simulations using the k-ε model predicted the same flow behaviour as observed during the experiments, where the flow was strongly time dependent for all swirl vane angles. The central jet of spray expanded more with greater swirl, with the vortex breaking down at a swirl vane angle of 40° (swirl number: 0.42) for both simulations and experiments. This result agrees well with the work of Dellenback *et al.* (1988) on sudden expansion flows, who found that the vortex breakdown is likely to occur for swirl numbers greater than 0.37. The swirl number, which characterises the degree of swirl, is defined as the ratio of the axial flux of angular momentum to the axial flux of axial momentum divided by a characteristic radius. The Strouhal numbers, which characterise the frequencies of precession, predicted using CFD and measured by image analysis were within experimental error for no swirl and swirl vane angle of 40°. The difference at a swirl angle of 25° was only slightly outside the error bounds. The difference in the results between Southwell and Langrish (2001) (30°) and LeBarbier *et al.* (2001) (40°) for vortex breakdown may possibly be explained by the different dryer geometries they used. Previous work in predicting powder deposition on the walls in spray dryers using CFD is now described.

2.4 Studies on Particle-Wall Interactions in Process Equipment

Particle impaction and wall deposition are of importance in many engineering problems. For example, the depositon of ash particles on the heat transfer surfaces of a heat exchanger in a furnace leads to reduced heat transfer and corrosion of the surfaces. However, despite a considerable amount of research on wall deposition, there is no theory available, certainly none that takes particle deformation (sticking) into account, which allows the probability that a particle will stick to a wall to be assessed.

Tu and Fletcher (1995) used CFD simulations, using an Eulerian approach to simulate gas-solid particle flow in 90° bend (pipe) and compared it to the Laser Doppler Velocimetry results for particle distribution and particulate velocity profiles of Kliafas and Holt (1987). In the Eulerian approach, the particulate phase is treated as a continuum, subject to interactions with fluid phase and appropriate particulate boundary conditions. Their prediction of the normalised particulate concentration distribution showed that the outer wall of the pipe was impacted by particles and the inner wall was not, which was consistent with the experimental

findings of Klifas and Holt (1987) who found that the inner wall was erosion free in experimental studies. However, the solid particles used in the experimental work of Klifas and Holt (1987) were non-sticky glass spheres, so stickiness in wall-particle interactions was not accounted for.

Schunh *et al.* (1989), Sommerfeld (1992) and Tu (2000) used CFD simulations, using a Lagrangian approach to particle tracking (the trajectories of individual representative particles are calculated) for gas-solid flows. Schunh *et al.* (1989) predicted the particle fluxes to a tube (used in reheater and coal-fired boilers utilising bed combustors). Similarly, Tu (2000) investigated the effects of reflected particles from walls on the behaviour of incoming particles and on the concentrations of particles near the walls. Sommerfeld (1992) investigated various "irregular bouncing" models based on the impulse equations for a particle-wall collision and compared their findings with experimental results. There was little link, in the work of the above researchers, to conditions inside actual process equipment, because their findings were not related to the concentrations of particles found in such equipment. Furthermore, Sommerfeld (1992) commented that his simulations should be compared with experimental data for particle collision angles less than 10° (which is typical for channel and pipe flows), and the effect of surface roughness on velocity fluctuations of the dispersed phase, and such data is not available. None of the above approaches consider particle deformation (sticking) in any way.

Regarding studies carried out on the wall deposition of particles in spray dryers, Reay (1988) discussed the work of Goldberg (1987), who used CFD with the k-ε turbulence model, to simulate the gas flow patterns, droplet trajectories and temperature contours for a Stork-Bowen laboratory spray dryer with a rotary atomiser (diameter 0.76 m, height 1.43 m). He suggested that powder deposition from a rotary atomiser on the walls is likely to be greatest in an annular area of the roof corresponding to the small recirculation eddy (medium sized droplets) and a region of the side wall that is a little below the atomiser height (large drops). This simulation was consistent with the preliminary practical work of Chen *et al.* (1993), who spray dried skim milk and then whole milk using an industrial dryer (diameter 8 m, height 15 m) with a rotary atomiser. They found that finer particles deposited on the ceilings of the spray dryer, while larger particles deposited on the walls of the spray dryer. They suggested that the smaller particles were entrained in the turbulent mixing zone in the top of the dryer and this led them to be deposited on the ceilings of the spray dryer. They measured the wall deposition (defined in

their work as the mass of powder deposited per unit area covered on the wall surface of the spray dryer) at different locations (ceiling and side walls) after each production run. They found that the deposition of skim milk powder was not uniformly distributed around the walls at the same height. They suggested that this indicated that the air flow distribution and the temperature distribution were not symmetrical. Thus, uniform deposition around the dryer circumference cannot be discounted for spray dryers that have symmetrical inlet air and temperature distribution. Chen *et al.* (1993) did not provide a time scale for these results, so that a wall deposition flux (mass per unit area per unit time) could be calculated, nor did they assess the effect of operating conditions on the wall deposition flux.

Swirl flow has been suggested to stabilise flow patterns in spray dryers and therefore to reduce the possibility of powder deposition on the walls of spray dryers (Southwell, 2000; Southwell and Langrish, 2001). Quantitative data on the effect of swirl on wall deposition rates has not been found in the literature. Experimental studies on wall deposition of food material in spray dryers, where only qualitative data was obtained, are discussed in section 2.9.3. As Southwell (2000), Guo (2001) and Langrish and Fletcher (2001) recommended, there is scope for investigating the usefulness of three-dimensional CFD simulations as a predictive tool for determining particle trajectories and wall deposition in a spray dryer. Particles should be incorporated in the fully transient three-dimensional simulations for a spray dryer to quantify the deposition problems in spray dryers and validate these simulations against data from experimental results. CFD may be able to suggest design modifications to the inlet conditions to improve flow stability in spray dryers and thus reduce wall deposition.

Particle stickiness is important in determining whether or not wall deposition of particles will occur, once the particles are close to the walls (Brennan *et al.*, 1971; Gupta, 1978; Downton *et al.*, 1982; Papadakis and Bahu, 1992; Bhandari *et al.*, 1992; Chen *et al.*, 1993; Pisecky, 1997; Rennie *et al.*, 1999). Therefore, the mechanisms involved in stickiness are discussed next.

2.5 Mechanisms Involved in Stickiness

The mechanisms involved in particle stickiness are adhesion of the particles to surfaces and cohesion of particles to each other (Papadakis and Bahu, 1992). Cohesive and adhesive forces play an important role in powder-handling processes such as transportation through pneumatic-

conveying systems of tubes, and caking and agglomeration of particles in storage (Lemetais, 2000).

2.5.1 Adhesion

Adhesive forces hold particles of powder onto the surface of other materials. The main adhesive forces are the van der Waals force, the electrostatic force and the force arising from the surface tension of adsorbed liquid films (Hinds, 1999).

Van der Waals forces are long-range attractive forces that exist between molecules. These forces are long range in comparison with chemical bond forces, which are called short-range forces. The van der Waals forces arise because random movement of electrons in any material creates momentary areas of concentrated charge called dipoles. At any instant, these dipoles induce complementary dipoles in neighbouring material, which in turn produce attractive forces, as shown in Figure 2.7. Van der Waals forces decrease rapidly with separation distance between surfaces; consequently, their influence extends only a few molecular diameters away from a surface.

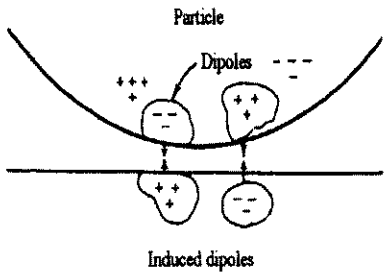

Figure 2.7 - Van der Waals adhesive force. Source : Hinds (1999).

While van der Waal forces arise from the attraction between atomic or molecular dipoles, electrostatic forces result from an overall surplus or deficit of electrons (Clift, 1985). When a charged particle comes into contact with a surface, it will induce an equal and opposite charge in the surface. The charged particle is retained on the surface by the attractive electrostatic force. A material becomes charged when there is a transfer of electrons between atoms or molecules (Jonassen, 1998) and may occur under the following circumstances:

- Triboelectrification - when two identical or different solid materials, contact and possibly rub against each other, with electrons crossing the interface in a preferential direction, giving one material a positive and the other a negative excess charge; or
- When an insulating material flows through a tube; or
- When any kind of liquid is sprayed into droplets.

The atomisation step in spray drying involves breaking up the liquid into droplets, and this gives rise to charging of the droplets known as Lenard's Waterfall Effect. Sprays, which are formed by small particles being separated from the surface of large droplets, lead to the smaller particles acquiring a negative charge, while the larger droplets acquire a positive charge. The effect only applies to liquids of high relative permittivity such as water and not hydrocarbons. Liquid droplets or particles may become charged by mutual contact and friction, or more likely through friction with the inner walls of the spray dryer, so keeping particles away from the dryer walls through modifying the flow patterns may reduce triboelectrification. The electrons in a conductor move freely, but the electrons in an insulator are not mobile, and the phenomenon of static electricity becomes significant. A large amount of frictional charge builds up when insulating powders, such as lactose (present in milk) and glucose (present in fruit juices), are transported pneumatically (Fodor and Forgacs, 1991; Bailey, 1993). Particles of insulating materials at low humidities retain their charge and are held to surfaces by the attractive electrostatic forces. Methods available for dissipating static charge are discussed in section 2.9.

Moisture in the atmosphere tends to produce a layer of adsorbed vapour on the surface of particles (Machowski and Balachandran, 1998). Liquid bridges form with the condensation of atmospheric moisture at relative humidities greater than 65% (Zimon, 1982). An attractive force between a particle and a surface is created by the surface tension of the liquid drawn into the capillary space at the point of contact, as shown in Figure 2.8. Rumpf (1975) showed that liquid bridges and van der Waals forces typically dominate electrostatic forces for close surface contact of 10 μm diameter particles, although electrostatic forces are dominant if particles are more than 1 μm from surfaces. This applies for particles that are not highly charged (Hinds, 1999). The liquid bridge force is likely to be the main adhesive force, as long as a liquid bridge can be formed. Rough surfaces may reduce or even eliminate liquid bridging effects.

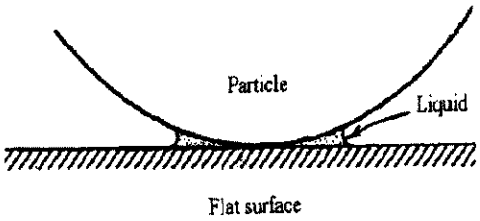

Figure 2.8 - Adhesive force due to a liquid film. Source : Hinds (1999).

Adhesive forces are affected by the properties of the particle, such as the type of material, shape, surface roughness and size, as well as the properties of the contact surface, such as the type of material, roughness and contamination. Temperature, relative humidity, the duration of surface contact and the initial contact velocity also affect adhesion.

Adhesive forces are directly proportional to the diameter of the particle (Hinds, 1999). As the particle size decreases, it becomes more difficult to remove particles from surfaces. The adhesive force on a particle less than 10 μm is much greater than other forces on the particle. For example, the adhesive force is 10^{-6} N, the gravitational force is 5×10^{-12} N, and the air current force (at 10 m/s) is 3×10^{-8} N on a spherical particle with a diameter of 10 μm and standard density (Hinds, 1999). Individual particles less than 10 μm are not likely to be removed by common forces, such as gravity and air currents. However, particles may adhere tightly to each other to form a large agglomerate and this thick layer of particles may be dislodged by blowing them off or shaking them from the surface.

Experimental measurements of adhesive forces have been made by determining the force required to separate a particle from a surface. Rennie *et. al* (1998) used measurements of centrifugal force to study the effect of temperature on the adhesive force of whole milk powder. The powder was exposed to temperatures of 40°C to 60°C, which are typical in the near-wall region in the bottom half of spray dryers. The d_{90} (the upper diameter left behind after each level of centrifuging corresponding to 90% of the cumulative amount of particles) for the 40°C case was 71.5 μm, and that for the 60°C case was 93 μm, which showed that the higher the temperature, the greater the adhesive force. The strength of the adhesive force is influenced by the contact area (Hinds, 1999). Increasing the temperature of the particles gives rise to the deformation of powder particles, possibly through fat liquefaction, and this increases the contact area between the particles and the surface, enhancing the already present adhesive forces.

The initial contact velocity of a particle also influences the adhesive force (Rogers and Reed, 1984). When a particle hits a surface at low velocity, the particle loses its kinetic energy by deforming itself and the surface. Up to a certain point, the greater the velocity of the particle, the greater the deformation and contact area, and the better the adhesion. At high velocities, part of the kinetic energy is dissipated in the deformation process (plastic deformation), and part is converted elastically to kinetic energy of rebound (elastic energy). A particle will bounce away from the surface if the elastic energy is greater than the adhesive energy. However, bouncing does not occur for droplets or easily deformed materials. The harder the particle, or the larger the particle, or the greater its velocity, the more likely bouncing is to occur (Hinds, 1999).

2.5.2 Cohesion

Cohesion is an internal property of the powder, where cohesive forces hold particles to each other. The mechanisms of cohesion and adhesion are similar, but high cohesion is not always associated with high adhesion and vice versa (Papadakis and Bahu, 1992). For example, glass contains many oxygen atoms with a partial negative charge, and these atoms are attracted to the positive end of a polar molecule such as water. Water's adhesive forces towards glass are stronger than its cohesive forces, which is the reason why a concave meniscus of water is formed when it is in a glass tube (Zumdahl, 1989).

Interparticle attraction depends on the physical characteristics of the individual particles and the nature of the physical process by which the particles interact. The main cohesive forces are the van der Waals force, the electrostatic force, the mobile and immobile liquid bridge forces (Rumpf, 1975). The van der Waals force and electrostatic force were considered earlier and will not be discussed here.

Modern adsorption theory holds that water sorbed by hydrophilic substances, such as foods, exist in three different states (Kuprianoff, 1958):

1. Monomolecular layer of water, which refers to water strongly adsorbed on individual polar groups in the substrate.
2. Multilayer water, which refers to additional layers of water hydrogen-bonded to the primary layer.

3. Capillary condensed water, which refers to water condensed in bulk in interstitial pores and capillaries.

As with adhesion, when the relative humidity of the atmosphere is above a critical value between 65% and 80%, moisture in the atmosphere produces a layer of adsorbed water vapour on the surface of particles (Williams, 1990). At humidities above this critical value, a liquid bridge (pendular liquid) is formed between the particles (Figure 2.9), provided that their surfaces are touching or nearly touching. In the pendular state, the void space between the particles is only partially filled with liquid, which forms a bridge between the individual particles. The liquid bridge between particles creates attractive forces between the particles and is due to surface tension and capillary forces (Machowski and Balachandran, 1998). In the capillary state, the void space between the particles is completely filled with liquid, and theoretically, the strength of the agglomerate is approximately three times greater than that in the pendular state (Papadakis and Bahu, 1992). The presence of adsorbed layers of water between particles will increase the van der Waal forces since the average distance between the particles is decreased. This gives rise to a significant reduction in electrostatic forces by providing conducting paths.

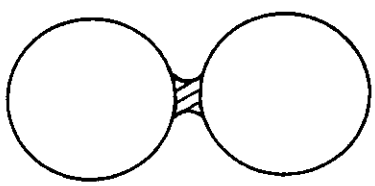

Figure 2.9 - Pendular liquid bridge between solid particles. Source: Clift (1985).

Chen *et al.* (1994) carried out preliminary experiments at room temperature to characterise the deposition of milk powders onto a stainless steel plate, which mimicked the ceiling of an industrial dryer. The amount of deposition increased with an increase in moisture content of powder and fine powder deposited more than coarse powder. They concluded that this was caused by the cohesiveness of the powder, which is related to its moisture content and particle size. Similarily, Rennie *et al.* (1999) found moisture and fat had a significant influence on the cohesion of milk powders, through mechanisms of liquid bridging. They studied cohesion of whole milk and skim milk powders by measuring the unconfined yield stress. Cylindrical plugs from powder being tested were made through consolidation in a mould, and then the powder plug was axially loaded until the sample failed, giving the unconfined yield stress. The

samples were heated to temperatures between 30°C and 70°C, since these are typical of temperatures in industrial spray driers. They found that whole milk powder (26.5% fat) was twice as cohesive as skim milk powder (0.8% fat), indicating the influence of fat in cohesiveness. They suggested that possible reasons were that, as the temperature of the powder increased, the liquid fat formed bridges between the particles, increasing the bonding strength. Alternatively, fat liquefaction may soften the powder, resulting in deformation of powder particles, increasing the contact area between the particles, thus enhancing attractive forces that are already present. They also found that particle size influenced the cohesion of both whole milk powder and skim milk powder, where cohesion increased as the particle size decreased. This is expected, since the smaller the particles, the higher the contact surface area between the particles per unit volume.

Immobile solid bridges are formed between amorphous particles whenever the particles are at temperatures and/or humidities higher than what is called the powder sticky point. These bridges are made of the same material as the particles. In industrial dryers, it is important to know how cohesive and adhesive a powder becomes at the temperatures and humidities encountered in dryers. This knowledge of likely stickiness problems is essential in selecting the most appropriate operating conditions for the dryer. One approach to measuring the cohesiveness of a powder is described next.

2.6 Sticky-Point Behaviour

Sugar-containing foods are known for their hygroscopic nature (they absorb moisture from the surrounding air) and tendency to agglomerate and stick. Milk products and their components (like lactose, a sugar), with the exception of fat, are hygroscopic (Pisecky, 1997). Fruit juices such as grape juice and orange juice have a high content of monosaccharides (fructose and glucose), which are also highly hygroscopic. Hygroscopicity is related to stickiness (Pisecky, 1997) because water affects the attraction between the particles.

The conditions which cause a sugar-containing material to become sticky can be measured using the sticky-point test developed by Lazar *et al.* (1956). The sticky-point test is a thermo-mechanical test that assesses the influence of the temperature and the moisture content of the particles on powder cohesion. At a certain temperature, which is a function of the moisture content of the particles, the force required to turn the stirrer embedded in the powder increases

sharply, and the current to the stirrer motor increases sharply (Notter *et al.*, 1959). The temperature at which this occurs is usually referred to as the sticky-point temperature. Whenever particles are at temperatures and/or moisture contents higher than the 'sticky point', the powder particles deform plastically and cohere to each other.

Many dried foods are amorphous solids because the solid particles are produced from a liquid state by a rapid drying process in such a short time that the molecules do not have enough time to become aligned and form crystals (White and Cakebread, 1966). This situation is particularly found in spray dryers. The amorphous solid is often described as a glass, with typical viscosities being above 10^{12} Pa s (Jones, 1956). Downton *et al.* (1982) found that stickiness can be related to the viscosity of amorphous powders, where as the viscosity of an amorphous powder is decreased below a critical value of 10^{6}-10^{8} Pa s, the powder becomes sticky. The sticky-point test has been used by several researchers including Downton *et al.* (1982) and Wallack and King (1988) and has also been used in the drying industry by Brennan *et al.* (1971) and Genskow (1988).

The sticky-point curve has been used as a semi-quantitative concept in selecting operating conditions for spray drying sticky material, where it has been implied that there is no significant wall deposition below the sticky-point curve (Lazar *et al.*, 1956; Brennan *et al.*, 1971; Gupta, 1978; Genskow, 1988; Roos and Karel, 1990). Data on the sticky-point temperature of skim milk powder as a function of moisture content are available (Hennigs *et al.* 2001). The temperature and relative humidity inside the spray dryer will affect the temperature and moisture content of the material and thus may affect the cohesiveness of the particles. However, the sticky-point test only measures the cohesive nature of particles, whereas wall deposition involves both adhesion and cohesion, so the direct applicability of this test to drying equipment is not obvious from first principles.

Yang *et al.* (2000) used a glass transition temperature curve (glass transition temperature versus moisture content of grain) to explain rice fissuring formation during drying. When drying occurred in the "rubbery region", they found that there was a significant decrease in on the yield (output) of rice. The phenomenon of glass transition, and the glass transition temperature, will be described next.

2.7 Glass Transition

The start of a polymer science approach to the study of glasses (amorphous solid) and glass transition in foods dates back to 1966 with a seminal review by White and Cakebread (1966) on the glassy state and glass transition temperature in sugar-containing food products. When an amorphous solid is heated, it undergoes a second-order phase transition, known as the glass transition. The glass transition occurs over the temperature range at which amorphous solid material is transformed into a more liquid-like "rubbery" structure. The glass will first go through this glassy-to-rubbery phase transition before forming a crystal. Further heating will cause the material to melt. A representative diagram of the changes to the physical structure and form of an amorphous solid is depicted in Figure 2.10 (from Bhandari and Howes, 1999). The glass will melt when heated rapidly. The melted material will become a glass again if it is cooled rapidly.

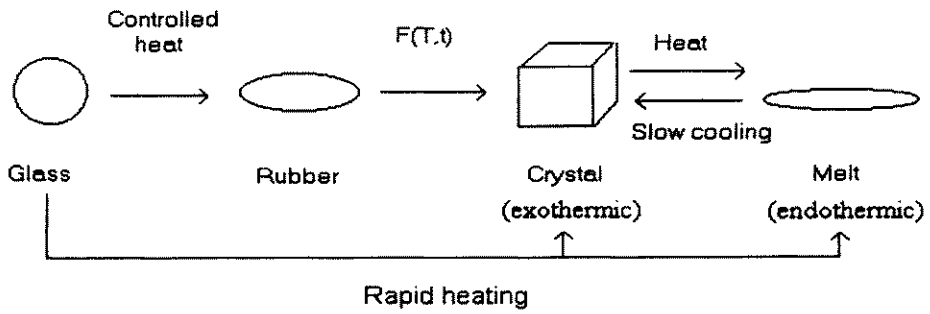

Figure 2.10 - Schematic diagram of phase changes in sugars. Source: Bhandari and Howes (1999).

The glass transition temperature is characterised by an endothermic change in the apparent specific heat capacity that can be detected by using Differential Scanning Calorimetry (DSC) (Turi, 1981; Harwalker and Ma, 1990; Wunderlich, 1990). The glass transition temperature is not a sharp point, since glass transition occurs over a finite temperature range. According to White and Cakebread (1966), the temperature range over which glass transition occurs is 20°C. The glass transition temperature is taken as the midpoint in the endothermic trough, as measured from the extensions of the glass transition curve from the onset and the end temperatures of glass transition. Figure 2.11 is shows the glass transition region of skim milk powder (moisture content 4.4% w/w dry basis). This Figure was obtained from the work discussed in Chapter 3 of this thesis. The onset and end temperature of glass transition are 49.78°C and 53.02°C respectively. The glass transition temperature is 51.40°C.

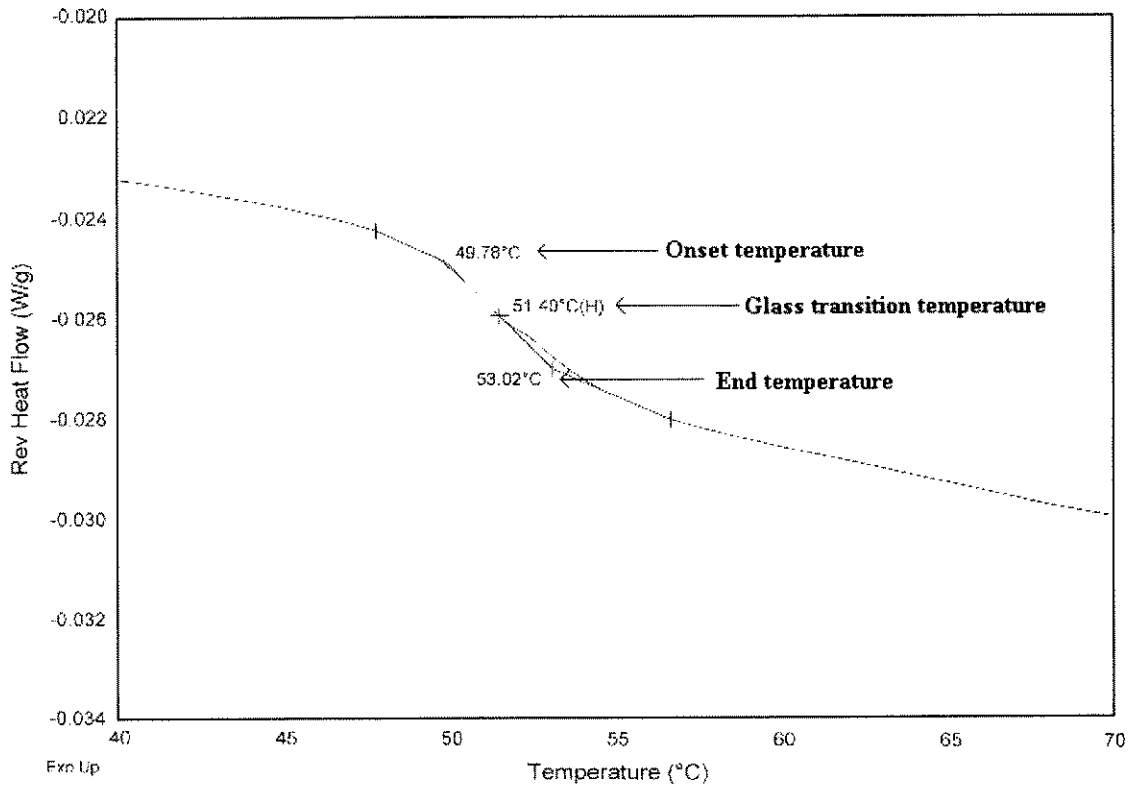

Figure 2.11 – The glass transition region for skim milk powder (moisture content 4.4% on a dry basis), showing the onset and end temperatures and glass transition temperature. Source : Chapter 3 of this thesis.

A description of Differential Scanning Calorimetry is provided in Chapter 3 of this thesis. The prediction of glass transition temperature is described next.

The Gordon-Taylor (1952) equation (equation 2.1) was borrowed from polymer science and can be used to predict the glass transition temperature of food mixtures and pharmaceutical solids as a function of the composition and the glass transition temperature of the individual components that make up the mixture:

$$T_g = \frac{w_1 T_{g1} + k w_2 T_{g2}}{w_1 + k w_2} \tag{2.1}$$

where T_g is the glass transition temperature, w_1 and w_2 are the respective weight fractions of the two components, T_{g1} is the glass transition temperature of one component, T_{g2} is the glass transition temperature of the other component and k is a curvature constant which can be determined empirically. This equation is based the assumption of perfect volume additivity, that is, the liquids mix without any change in volume and there is no specific interaction between the components of the mixture. This equation can be expanded to include mixtures with more than two components (Arvanitoyannis *et al.*, 1993), and has been used by many

workers to predict that glass transition decreases with increasing moisture content. The glass transition temperature is affected by the nature and composition of the components (Roos and Karel, 1990; Roos and Karel, 1991a; Hancock and Zografi, 1994; Jouppila and Roos, 1994).

The Gordon-Taylor equation has been expanded by Couchmann and Karaz (1978) (equation 2.2), who derived the equation independently by starting from the thermodynamic assumptions of entropy (second law of thermodynamics):

$$T_{gm} = \frac{w_1 T_{g1} + \left(\frac{\Delta C_{p2}}{\Delta C_{p1}}\right) w_2 T_{g2}}{w_1 + \left(\frac{\Delta C_{p2}}{\Delta C_{p1}}\right) w_2} \qquad (2.2)$$

where ΔC_{p1} and ΔC_{p2} are the changes in heat capacity of the first and second component over the glass transition range, respectively. The glass transition temperature can be accurately predicted from the glass transition temperature of the individual components when the ratio of the heat capacities is determined empirically (Roos and Karel, 1991e).

Roos and Karel (1991c) have linked the sticky-point temperatures of amorphous sugars to the glass transition temperatures determined by Differential Scanning Calorimetry (DSC). Likewise, Ozmen and Langrish (2001) have found that the measured glass transition temperatures of skim milk powder with various moisture contents were close to the sticky-point temperatures measured by Hennigs *et al.* (2001). Like the sticky-point temperature, the glass transition temperature also decreases with increasing moisture content for amorphous food material (Roos and Karel, 1990; Roos and Karel, 1991a, 1991b, 1991c, 1991d; Ozmen and Langrish, 2001). Further details of the work carried out by Ozmen and Langrish (2001) are provided in Chapter 3 of this thesis. The similarity between the sticky-point temperature and the glass transition temperature suggests that, in future, testing programs for food containing mainly carbohydrate-type material that are more valuable than skim milk powder may be simplified. The glass transition temperature may be used as a guide for selecting operating conditions in a spray dryer to minimise key problems such as wall deposition by keeping the particle temperature below the glass transition temperature. The situation is not so clear for fatty materials, which do not display solid-phase transitions such as the glass-rubber transition. Jouppila and Roos (1994) measured the glass transition temperature of skim milk powder (0% fat) and whole milk powder (32.4% fat). The glass transition temperatures of the two samples at zero moisture content were the same at 92°C, but the wall deposition amounts

measured by Chen *et al.* (1993), were significantly different for skim milk powder and whole milk powder. Thus, while the presence of fat does influence cohesion of particles, it does not have a glass transition temperature and only melts when it is heated.

The Gordon-Taylor equation illustrates that the stickiness of a product can be reduced by changing the composition of the product. The components that contribute most to the stickiness of the mixture can be either destroyed or removed. Sugars with a low glass transition temperature such as fructose and glucose (Table 2.2) can depress the glass transition temperature very significantly in sugar rich foods (Slade and Levine, 1991). This has led to the use of carriers such as maltodextrins, which have a high glass transition temperature, as a means of diluting the sugar rich material, increasing its glass transition temperature and therefore reducing its stickiness. If the glass transition temperature of individual components are measured using Differential Scanning Calorimetery, a mixture can be formulated using by using the Gordon-Taylor equation, with the mixtures having the desired physical properties required in processing and storage of food. For example, a boiled sweet becomes sticky at room temperature because of either (i) a low content of glucose syrup which has a relatively high glass transition temperature, or (ii) a high residual moisture content, which plasticises the sweet causing the viscosity of the boiled sweet to drop, which in turn causes its glass transition temperature to drop below room temperature (White and Cakebread, 1966). According to the Gordon-Taylor equation, this problem can be solved by adding a higher content of glucose syrup or removing the residual water, to raise the glass transition temperature of the sweet above room temperature. When the glass transition temperature is exceeded in spray drying, deposition on drier surfaces may result (Jouppila and Roos, 1994). Reducing the stickiness of the material can promote drying because particles are less likely to stick to the walls of the dryer when they get there and reduce the tendency of the powder to cake during storage. The use of drying aids will be discussed in more detail in section 2.9.1. The concept of sorption isotherms and their importance in drying materials is discussed next.

Table 2.2 - Glass transition temperature of anhydrous sugars. (Source: Roos, 1993; Labuza, 1995; Roos and Karel, 1991d).

Food material	Molecular weight (MW)	Glass transition temperature (°C)
Fructose	180	5
Glucose	180	31
Sucrose	342	62
Maltose	342	87
Lactose	342	101
Maltodextrins		
DE[a] 36	500	100
DE 25	720	121
DE 20	900	141
DE 10	1800	160
DE 5	3600	188

[a] Dextrose Equivalent (DE). The higher the DE, the greater the content of monosaccharides and dextrose.

2.8 Sorption Isotherms

When a solid is exposed to a gas of constant temperature and humidity, it will either gain or lose moisture until equilibrium is established (Papadakis *et al.*, 1993). The equilibrium moisture content of the solid is a function of the relative humidity of the gas, the temperature of the gas and the nature of the solid and the liquid. The variation of the equilibrium moisture content with relative humidity at a constant temperature is called a sorption isotherm.

Data for sorption isotherms are typically obtained by exposing a sample of material to an environment maintained at a known relative humidity and constant temperature until the sample reaches a steady weight (Keey, 1992b). An adsorption isotherm is made by placing a completely dry material into various atmospheres of increasing relative humidity and measuring the weight gain caused by water adsorption (Labuza, 1968). On the other hand, a desportion isotherm is found by placing the initially wet material under the same relative humidities as for the adsorption isotherm, but in this case measuring the loss of weight caused by water evaporation. For a higher temperature, the equilibrium moisture content of the solid will decrease for a fixed relative humidity (Labuza *et al.*, 1985). For drying studies, the equilibrium moisture content is the lower limit of moisture content that can be achieved on drying for the given conditions of gas temperature and humidity, typically approached by desorption from a very wet material. Thus, a desorption isotherm is used to characterise the material being dried.

Sorption isotherms can be correlated by using equations such as the one proposed by Papadakis *et al.* (1993):

$$X_{eq} = A\exp\left[-BT\ln\left(\frac{1}{\psi}\right)\right] \tag{2.3}$$

where X_{eq} is the equilibrium moisture content on a dry basis (in kg water/kg dry material), T is the temperature of the gas (in K), and ψ is the relative humidity of the gas (a fraction from 0 to 1). A and B are empirical constants with units of kg kg^{-1} and K^{-1}, respectively. The amount of moisture held by a solid depends not only on temperature, but is also influenced by the total pressure. The latter effect is small over the range of pressures encountered in normal drying practice (Keey, 1992b).

If equilibrium is attained rapidly in a dryer, then it is likely that the outlet moisture content of the material will be in equilibrium with the outlet air temperature and humidity. According to Bahu (1992), the concept of a product moisture locus applies for many spray dryers and implies that the solids leaving the dryer closely approach their equilibrium moisture contents, as given by the sorption isotherm (Figure 2.12). The work per unit quantity of substance (in J mol^{-1}) in driving off moisture can be expressed, in terms of the relative humidity for an isothermal, reversible process without change in composition, by equation 2.4 (Gibbs Free Energy) (from Keey, 1978) (y-axis on Figure 2.12):

$$G = RT\ln\left(\frac{1}{\psi}\right) \tag{2.4}$$

where G, is the Gibbs Free Energy, T is the temperature, ψ is the relative humidity of the air and R is the Universal gas constant. The Gibbs Free Energy is related to the desorption isotherm as follows. Depending on the temperature and relative humidity of the gas surrounding a solid, moisture is lost to the atmosphere from the solid until the remaining moisture is that with a minimum bond energy to the material given by the Gibbs Free Energy, and the moisture content of the solid is equivalent to its equilibrium moisture content. In other words, if the relative humidity increases, the moisture content of the solid will increase, while the Gibbs Free Energy decreases. In addition, the particle temperatures and moisture contents

determine how likely the particles are to stick to the dryer walls through their influence on the sticky-point temperature. Hence, combining the sticky-point curve and the sorption isotherm may be useful for minimising wall deposition in dryers where the outlet conditions are equilibrium limited. For example, increasing the inlet gas temperature is likely to increase the outlet gas temperature and hence the outlet particle temperature. However, it is also likely that increasing the temperature will decrease the outlet moisture content (through the sorption isotherm). The sticky-point temperature also increases as the moisture content decreases. Hence, depending on the sorption isotherm, increasing the inlet gas temperatures may (material A in Figure 2.13) or may not (material B) move the outlet conditions of a dryer from the sticky to the 'non-sticky region'.

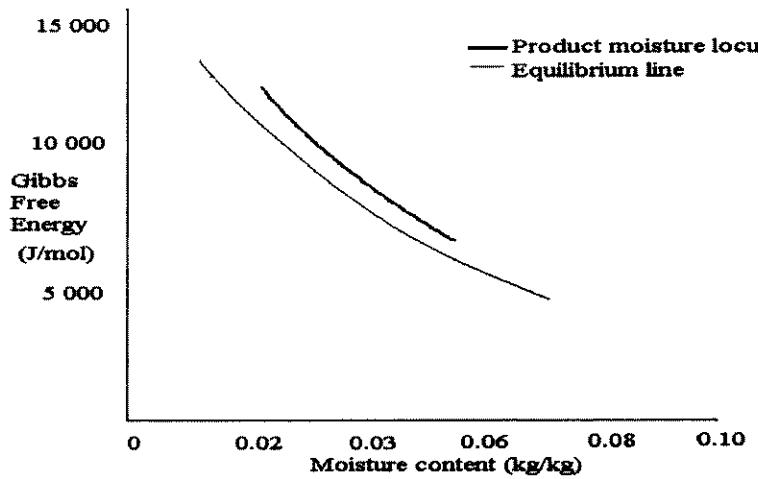

Figure 2.12 - Equilibrium chart with product moisture locus. Source: Bahu (1992).

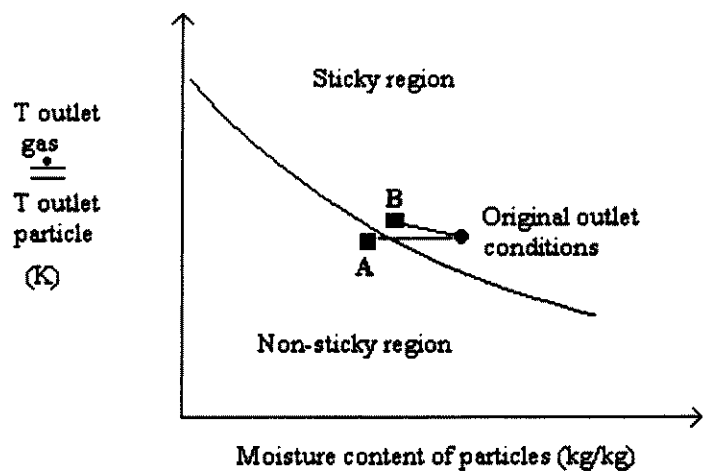

Figure 2.13 - Interaction between sticky-point behaviour and sorption isotherms.

2.9 Spray Drying of Sticky Materials – Experimental Studies of Wall Deposition and Methods for Reducing It

Previous researchers have used "carriers" to modify the stickiness of food materials before drying to improve the drying performance of the material by decreasing wall deposition and consequently increasing the yield and quality of the product. Other researcher have designed spray dryers to spray dry fruit and vegetable juices, with the aim of decreasing the product temperature to reduce particle stickiness, and thus reduce wall deposition. Mechanical removal of the powder from the walls of spray dryers has also been tried. The outcome from drying various sticky food materials with and without a carrier is discussed first. A discussion of the different dryer designs that have been used to reduce wall deposition of fruit and vegetable powders will then follow.

2.9.1 Additives

Dried solid products that have a high sugar content, and/or contain materials which exist in the liquid state at normal drying temperatures (for example, fats), have a considerable tendency to stick on the walls of spray dryers (Coulter and Breene, 1966). As explained in section 2.6 and 2.7 sugars are hygroscopic and have a low glass transition temperature. Thus, liquid bridges consisting of the same material as the particles are formed whenever the particles are at temperatures and/or humidities higher than their glass transition temperature. Also, fats often exist in the liquid state at room temperature and are likely to increase the tendency for liquid bridging, and particle stickiness.

Drying sugar-rich material such as orange juice in a spray dryer gave rise to high wall deposition fluxes (Brennan *et al.*, 1971). The orange juice powder was difficult to remove from the dryer walls, even by cleaning. Various researchers (Table 2.3) have added drying aids to sugar rich material to reduce the stickiness of the material and improve the drying performance of the material by decreasing wall deposition. Orange juice has been spray dried with drying aids to reduce the hygroscopicity of the dried material, which decreases the tendency of the powder to cake during storage (Strashun and Talburt, 1954). However, some of the drying aids used in the previous work introduced "foreign" flavours, or they were used in such large amounts that they altered the nature of the product. "Foreign" flavours may be

undesirable because consumer perception is that they are unnatural, so the value of products with such "foreign" flavours may be decreased.

Table 2.3 : The use of carriers to modify the stickiness of dried foodstuffs in spray dryers and different spray dryer designs used to combat wall deposition.

Researcher (s)	Composition of feed material to be spray dried	Spray dryer design/operating conditions
Bohmn and Bornegg (1931)	Lemon juice with gum acacia	
Campell et al. (1944)	20% lemon-juice solids and 80% corn syrup solids	
Eddy (1950)	Grape fruit juice, orange juice, orange pulp each spray dried with methyl cellulose, concentration 0.1% to 4% of citrus solids	
Strashun (1951)	Orange juice solids with 1% glycerol monostearate	
Lazar *et al.* (1956)	29% tomato solid, 2% sodium chloride, 200 ppm sulfur dioxide	Ambient air introduced tangentially in controlled amounts at different levels of the spray dryer. Cold air injected into lower parts of spray dryer.
Coulter and Breene (1966)	Grape juice or apple juice with skim milk (ratio 50:50) Tomato juice with skim milk (ratio 60:40)	
Breene and Coulter (1967)	Vegetable purees with skim milk (ratio 50:50) Fruit purees with skim milk (ratio 55:45)	Low inlet air temperature used.
Robe *et al.* (1968)	Tomato paste (32% solids, 68% water)	Jacketted spray dryer used. Low inlet air temperature used.
Brennan *et al.* (1971)	Orange juice Orange juice (40%) and sodium carboxymethyl cellulose (1.5%) Orange juice (32.25%) and gum acacia (2.25%) Orange juice (29.85%) and glucose DE 34-43 (23.65%)	Low inlet air temperature used.
Gupta (1978)	Orange juice (50 -85%) and maltodextrin DE 9-15 (15-50%)	Low inlet air temperature used.
Main *et al.* (1978)	Cranberry, concord grapes and roselle calyces with maltodextrin DE 10-13	Low inlet air temperature used.
Lafuente and Welt (1984)	D-limonene with maltodextrin DE 38-46 (10-40%)	Mechanical sweeping device used to scrape off wall deposits.
Karatas and Esin (1990)	Tomato paste with carboxymethylcellulose, sodium chloride and corn starch	Mechanical sweeping device used to scrape off wall deposits. Cold air injected into lower parts of chamber. Low inlet air temperature used.
Bhandari *et al.* (1992)	Citral and linalyl acetate with gum arabic and maltodextrin DE 17	Spray dryer walls and atomiser thermostated at 70°C. Low inlet air temperature used.
Boskovic *et al.* (1992)	Citrus oil with carbohydrate matrix (maltose, maltodextrin DE 5-15, gum arabic)	Low inlet air temperature used.
Bhandari *et al.* (1993)	Fruit juice with maltodextrin DE 6-19 (ratio of juice to additive: blackcurrant 65:35; apricot 60:40, raspberry 55:45)	Low inlet air temperature used. Cold air injected into lower parts of the drying chamber.

During World War II, a spray-dried lemonade powder, containing 20% lemon juice solids and 80% corn-syrup solids (Table 2.3), was developed for military use (Campbell, 1944). Holzcker (1943) prepared an orangeade powder by spray drying which contained 25% orange juice solids and 75% corn syrup solids. While methyl cellulose (Eddy, 1950) and glycerol monostearate (Strashun, 1951) in concentrations as low as 1% on a total solids basis proved to be good drying aids for spray drying orange juice (free-flowing powder obtained), low yields, flavour changes during drying and reconstitution difficulties were not resolved.

Maltodextrins, which are high molecular weight carbohydrates and have a high glass transition temperature (Table 2.3), have been added to sticky material prior to drying, in order to successfully produce free flowing powder. They gave very good results with respect to minimising wall deposition (Stern and Storrs, 1969; Brennan *et al.*, 1971; Gupta, 1978; Main *et al.*, 1978; Bhandari *et al.*, 1993). Thus, high molecular weight carbohydrates are more suitable as carriers, but at least 15% of drying aid had to be added to prevent the product from sticking to the walls, even for the best drying conditions (Gupta, 1978). This finding is supported by the work of Bhandari *et al.* (1993), who found that more wall deposition occurred when the ratio of fruit juice to maltodextrin increased due to increased stickiness during drying. The acceptable range of fruit juice to maltodextrin ratio could be increased by decreasing the inlet air temperature and/or by using a higher molecular weight maltodextrin. The product yield is affected by the nature of the sugars and acids present in the liquid feed. Comparing apricot and blackcurrant juice with the same total sugars content, better drying yield was observed for apricot because it has a lower content of fructose (which has a very low glass transition temperature) and acids (Bhandari *et al.*, 1993) and is likely to have a higher sticky-point temperature, according to the Gordon-Taylor equation, assuming that there is a link between the sticky-point temperature and the glass transition temperature. There is a limit to the extent to which the total solids content can be increased, due to the difficulties in pumping and atomising concentrated liquid pastes.

Turning to the use of pulp as a carrier, when pulp as a fine colloid is present in vegetable and fruit juice, less carrier is required to produce non-hygroscopic powdered fruit concentrate using a drum dryer under vacuum (Perech, 1946). The taste and odour of fibre should not be objectionable any more than is the natural cellulose content in untreated juice. Bhandari *et al.* (1993) also suggested that fibre from fruit may be used as a carrier of fruit juices for spray drying but did not test the idea.

Particle deposits on the walls of spray dryers can sometimes be dislodged by using hammers, rotating scrapers and rotating air brooms (Masters, 1996). However, the effects of using these devices are often very localised (i.e. just near the hammer), so the overall effectiveness of the devices is often limited. Other measures have been used to deal with the problem of drying sticky material, including designing spray dryers to reduce wall deposition. A discussion of these designs is given next.

2.9.2 Injecting Cold Air into the Spray Dryer

Lazar *et al.* (1956) introduced ambient air tangentially in controlled amounts at one or more of three different levels of a large co-current spray dryer (diameter, 23 m, height, 62 m). Their goal was to chill the particles to form a non-sticky shell and thus prevent wall deposits. They found that the drying zone was chilled by the ambient air entering the dryer and the particles did not dry. This led them to introduce ambient air only in the lower parts of the chamber where they believed the particles would be at the desired moisture content. However, this method did not resolve the wall deposition problem. Ambient air introduced into the drying chamber cooled the air inside the dryer and increased the relative humidity of the air. The particles in the spray dryer picked up moisture or were insufficiently dried, and this caused the particles to stick to the walls of the dryer.

Karatas and Esin (1990) and Bhandri *et al.* (1993) also tried the method used by Lazar *et al.* (1956), in an attempt to reduce wall deposition of tomato powder and fruit powder, respectively. Karatas and Esin (1990) fabricated a cast iron chromium lined spray drying chamber with the same dimensions as the common pharmaceutical dryer called the Buchi 190 (diameter, 0.105 m, height 0.52 m), with stainless steel wall scrapers. Like Lazar *et al.* (1956), Karatas and Esin (1990) found that admitting ambient air from the bottom of the spray dryer decreased the chamber outlet temperature and this caused a reduction in the yield of the product (where yield is defined as the percentage of the maximum possible output that can actually be obtained). Bhandari *et al.* (1993) used a laboratory scale Niro spray dryer and a Leaflash spray dryer. The Leaflash technique involves drying hot air flowing at very high velocity in the converging section of the dryer, where it atomises and simultaneously dries the resultant atomised droplets (Prudhon, 1979; Gardais, 1986), while a Niro spray dryer involves atomising the process fluid with an atomising gas and then drying the droplets using hot air. Bhandari *et al.* (1993) found that for the Leaflash dryer, trace heating the walls of the drying

chamber and the rapid cooling of the powder at the outlet (obtained by introducing cold air to the outlet) improved the powder recovery. They observed the dried powder (obtained using the Leaflash spray dryer) under a scanning electron microscope and found that the particles were agglomerated. On the other hand. the dried powder (obtained using the Niro spray dryer) was not agglomerated. They suggested that the agglomeration of the powder obtained by the Leaflash spray dryer was caused by higher humidity at the outlet because cold air was introduced.

According to Lazar *et al.* (1956) the sorption isotherm data and sticky point data for the tomato juice suggested that tomato powder of approximately 2% moisture content cannot be exposed to conditions where the temperature is greater than 60°C and a relative humidity of 7% (absolute humidity 0.009 kg kg^{-1}) without becoming sticky. They stated that, since ambient air has an absolute humidity which is frequently 0.009 kg kg^{-1} or higher, it should not be used to cool the particles. However, this explanation is unclear, because the issue is not just the humidity of the ambient air, since when it is injected into the dryer, it mixes with air inside the dryer. The humidity of the mixed air depends on how much ambient air is injected, as well as the ambient air and dryer air humidities, so injecting only a small quantity of ambient air will have no significant effect on the humidity, temperature or stickiness of most of the particles and hence may not have any detrimental effect on wall deposition.

2.9.3 Cooling the Dryer Walls

Robe *et al.* (1968) used a jacketted industrial spray dryer to control the temperature of the drying chamber walls, when spray drying tomato paste. Ambient air was drawn through the jacket with the aim of cooling the dryer walls. They did not provide enough detail on how using this technology influenced the wall deposition problem. Bhandari *et al.* (1992) also used a jacketted spray dryer to spray dry citral and linaly acetate, where the spray dryer walls and atomiser were trace heated to 70°C. The spray dryer utilised the Leaflash technique. Bhandari *et al.* (1992) believed that controlling the temperature of the walls would stop the temperature of the particles from increasing when they contacted with the walls of the dryer and thus prevent the particles from sticking to the walls. However, this did not resolve the problem of wall deposition. They explained that the reason that the wall deposition problem was not resolved using this method was similar to that of introducing cold air into the chamber. The cold chamber wall will also cool the air inside the drying chamber, increasing the relative

humidity of the air and thus increasing the moisture content of the particles, making them more sticky. In addition, cooling the chamber walls may give rise to condensation inside the dryer and the particles may adhere to the walls by liquid bridging forces.

Brennan *et al.* (1971) spray dried orange juice and indicated that the inability to control the temperature of the dryer wall resulted in wall deposition of the orange juice powder produced. They found that even when adding maltodextrin as a carrier to orange juice, wall deposition amounted to 10% to 60% of the total product yield, and concluded that the temperature of the drying chamber walls influenced this result. They fitted a water cooled plate to the drying chamber and attached a thermocouple to its surface. They observed that when the temperature was less than the sticky-point temperature (40.5°C for a moisture content of 2%), little or no wall deposition occurred, while if the temperature was in excess of the sticky-point temperature by only 9°C, wall deposition occurred, giving rise to low yields. Bhandari *et al.* (1997) suggested that cooling the walls of the spray dryer will allow the outer surface for the thermoplastic particles coming into contact with the wall to harden forming solid outer surface. This would increase the viscosity of the sample, which is related to stickiness (section 2.6), and thus may stop the material from sticking onto the walls of the spray dryer, because its sticky-point temperature would have increased.

Gupta's (1978) work is consistent with the work of Brennan *et al.* (1997). He found that wall deposition occurred with insulated dryer walls and inlet air temperatures of 163°C. Powder deposition on the walls decreased when the insulation was removed because the temperature of the wall decreased, provided that the inlet air temperature was not increased (maintained at 104°C to 149°C) and the temperature of the walls was not above the sticky-point temperature of the orange juice powder produced (57°C). On the other hand, Chen *et al.* (1993) found that after insulating one of the inspection window of an industrial spray dryer used for producing milk powders, the window was almost free from deposition. They believed the insulation increased the temperature close to the window, preventing both vapour condensation and the particles becoming too sticky. Low wall temperatures may mean condensation on the walls, and particles may stick to these wet walls because of liquid bridging forces. While cooling the temperature of the walls below the sticky-point temperature of the product may eliminate wall deposition, no account has been taken of the effect of such cooling on the moisture-removal performance of the dryer (Brennan *et al.*, 1971).

The inlet air temperature and insulation around the spray dryer will influence whether or not the particles (which approach the walls) will become sticky and adhere to the walls of the drying chamber. If low inlet air temperatures are used, it is possible that the product could remain undried, producing a sticky product that may deposit on the dryer walls. Food particles with a higher moisture content may encourage bacterial growth and the product will then be unsuitable for human consumption (Chen *et al.*, 1993). On the other hand, if high inlet air temperatures are used, it is possible that the temperature of the product will be high, and this could cause the product to become rubbery and also deposit on the dryer walls.

2.9.4 Scraping the Chamber Walls

Karatas and Esin (1990) developed an experimental spray dryer with a mechanical sweeping device to remove wall deposits of tomato powder from the spray dryer walls. They obtained a yield of 77% (where yield is defined as the percentage of the maximum possible output that can actually be obtained) for an inlet air temperature of 115°C and outlet air temperature of 65°C. Bhandari *et al.* (1997) suggested that the yield Karatas and Esin (1990) obtained using low inlet air temperatures is unusual in a spray drying process. Laufente and Welti (1984) also used a mechanical sweeping device to remove wall deposits of orange powder from the spray dryer. However, scraping the chamber walls of the spray dryer does not resolve the problem of wall deposition occurring for a start, and moving parts inside the spray dryer will result to higher maintenance costs and and an increase in production costs.

2.9.5 Drying Conditions

A large number of researchers (Table 2.3) have dried heat-sensitive hygroscopic products, using drying conditions where the inlet temperature was low and ranged from 100°C to 180°C and the outlet air temperatures ranged from 63°C to 100°C. Low inlet air temperatures were used to take into account the thermoplasticity of the product and prevent it from becoming sticky inside the drying chamber. Drying conditions such as the inlet air temperature and liquid feed rate affect the temperature and humidity inside the spray dryer, which in turn will affect the temperature and moisture content of the particles in the dryer. This may affect the cohesiveness of the particles, which is related to the stickiness of the material.

Furthermore, when the temperatures of the particles exceed their sticky-point temperature, Bhandari *et al.* (1997) suggest that the particles will stick to the chamber walls on impact. The problem of stickiness may be avoided by using spray drying conditions where the product temperature does not exceed its sticky-point temperature. The powder should then be cooled immediately to temperatures less than the sticky-point temperature to avoid caking in a collection device. Table 2.4 suggests that when the temperature of the particles is about 20°C higher than the glass transition temperature, the particles will stick to each other.

Table 2.4 – The influence of the increase in temperature of the product above the glass transition temperature on the structural characteristics of the product (Labuza, 1995).

Temperature above the glass transition temperature (°C)	Physical characteristics
10	Begins to show adhesion
20	Shows stickiness
30-50	Crystallisation at room temperature
>50	Shows total collapse and flow

Chen *et al.* (1993) observed that heavier deposits of whole milk powder occurred when whole milk was spray dried using an industrial spray dryer, in comparison to skim milk powder deposits produced using the same spray dryer. The work of Mahony (2001) is consistent with these results. She used the same pilot scale spray dryer Southwell and Langrish (2001), to spray dry skim milk and whole milk, and found that the wall deposition of skim milk and whole milk powders on the spray dryer walls was influenced by both operating conditions and material properties. The wall deposition flux of whole milk powder was higher than skim milk powder, possibly due to the presence of fat in the whole milk, which liquifies at air temperatures inside the spray dryer, making the whole milk particles more sticky and thereby more likely to stick to the chamber walls. For both materials, there was a strong correlation between the feed flowrate and the wall deposition flux. However, she suggested that this increase in wall deposition could have been due to more particles being present in the spray dryer. Since increasing the feed flowrate, with the same particle residence time, will result in more particles being in the dryer, it is more likely that particles will be close to the walls of the dryer. She recommended that more tests are required around the sticky region to determine whether or not the rate of wall deposition increased significantly at operating conditions above the sticky- point curve. Furthermore, recommendations were given to determine whether or not electrostatic forces are likely to play an important role in wall deposition.

2.9.6 Dryer Size and Shape

Regarding dryer shape, Mahony (2001) found that the highest wall deposition fluxes occurred in the conical section of the spray dryer because of spray impaction. According to Masters (1991), if the particles in a spray dryer have a relatively high velocity, then they are more likely to hit the walls of the spray dryer. The velocity of the particles is partly controlled by the pressure of the atomising gas. The higher the compressed air pressure, the higher the velocity of the particles and thus the higher the chance of the particles hitting the dryer walls. Thus, spray impaction may be important in small spray dryers. Gupta (1978) recommended that the spray cone angle and the size of the drying chamber should be selected in conjunction with the atomising gas pressure to minimise wall deposition, by keeping the walls outside the path of the spray. The spray cone angle should be narrow relative to the dryer diameter, to decrease the chance of wall impingement, but not too narrow to interfere with good air and feed contact and drying. The type of atomiser used should also be chosen in conjunction with the dryer size, to reduce the chance of wall deposition, where a short-form spray dryer is often equipped with a rotary atomiser, and a tall-form spray dryer is often equipped with a two-fluid nozzle.

Hennigs (2000) placed a small aluminium plate into an industrial spray dryer used for drying milk, to collect particles and observe them under a Scanning Electron Microscope. Little detail was provided about the location of this sample plate with respect to the spray dryer. The skim milk particles closest to the surface of the plate were found to be deformed, and he suggested that the reason for this was that the particles impacted on the plate (Figure 2.14). He also observed that particles cohered to other particles. However, Hennigs' (2000) finding does not eliminate the possibility that electrostatic forces play a role in wall deposition of particles, and possible methods that could be used to increase the rate of static dissipation and reduce wall deposition in spray dryers are discussed next.

Figure 2.14 – Photograph of skim milk powder on a plate as observed under a Scanning Electron Microscope. Source: Hennigs (2000).

2.9.7 Increasing the Rate of Static Dissipation

Chen *et al.* (1993) suggested that electrostatic forces or van der Waals forces may be responsible for wall deposition of milk in spray dryers. They observed that, even at room temperature (e.g. 19°C), very fine milk powder particles adhered to the stainless steel surface of the ceiling of a spray dryer, suggesting that electrostatic forces might be important. However, further experimental work by Chen *et al.* (1994) found that earthing or charging the plates which were used for a preliminary deposition study of milk powders had no effect on the deposition rate (defined as the amount of deposit build up per area of plate) of milk powder on the plates.

In processes such as spray drying, dry particles are being transported through a drying chamber, a system of tubes and a hydrocyclone. The particles may become charged by friction with the walls of the equipment. This kind of charging may take place particularly if the particles are insulators like lactose (found in skim milk) or glucose (Jonassen, 1998). When an electric charge is placed on an insulator, the charge may stay on the surface of the insulator, where it was originally placed. Charged particles may then adhere to the walls of the spray dryer by electrostatic forces. However, according to Beever (1985), milk powders are not very susceptible to static build-up and are not readily ignited by an electrical spray. A spray dryer and its associated equipment is normally grounded as a matter of good practice. Grounding the spray dryer may reduce the effects of static charge build-up and could possibly reduce wall deposition. Grounding involves connecting the conducting objects to earth by using a conductor (usually copper). According to AS/NZS 1020 (1995), a total resistance between the object and earth not exceeding 1 MΩ is sufficient to prevent significant charge accumulation. It is also important to discharge conductive systems, because energetic spark discharges can be produced by insulated charged conductors like some process equipment and individual particles.

According to Jonassen (1998), page 42, "if a charge is located on an insulator, there is in principle no way by which the charge may ever be removed". However, if the charged insulating particle is surrounded with ionised air, the charge may be neutralised by opposite polarity ions being attracted to the insulator. Ionised air is produced by knocking an electron off an oxygen or nitrogen molecule and forming a positive ion. Air ionization devices are commercially available. However, there are limitations in using this method to control electrostatic effects. If the drying air at the inlet to the spray dryer is ionised, it may only

provide charge neutralisation within a limited zone. Subsequent generation of static charge on the particles may occur at the lower parts of the spray dryer away from the ionizing zone. Static may also be dissipated by increasing the conductivity of the insulator.

According to AS/NZS 1020 (1995), the surface of an insulator may be rendered conductive by the adsorption of water vapour from the surrounding air. Water is a relatively conductive material, and can improve electrical contact and reduce triboelectrification by aiding the recombination of charges generated during frictional contact (Clift, 1985). The required conductivity may generally be achieved by maintaining the ambient air at a relative humidity of 70% or higher, provided that the surface of the insulator is at ambient temperature, not hydrophobic or covered by a hydrophobic film like fat. However, a relative humidity of 70% may reduce drying rates unacceptably. An anti-static agent does not retain static charges, so it may be added to the particles to reduce build up of static on the particle surfaces.

Zhang *et al.* (1996) added Larostat 519, an anti-static agent (60% soyadimethylethyl-ammonium and 40% ethasulfate/amorphous silica), to cohesive shale particles and found it significantly reduced the electrostatic forces between particles and between particles and walls in a particle flow system. The molecule of a cationic surfactant like Larostat 519 (quaternary ammonium nitrate) is composed of a positively charged polar hydrophilic portion and a nonpolar hydrophobic portion. The hydrophilic portion of the surfactant at the surface attracts the moisture from the atmosphere; and it is this moisture that has the static dissipative effect. This process increases the moisture content of the powder, not the drying air. Increasing the moisture content of the surface of particles may be acceptable if the average moisture content of the particles is still reasonable. However, it is undesirable to add anti-static agents to products that are for human consumption and, furthermore, care must be taken that any additive does not react adversely with the product (Gupta, 1978).

Thus, the main practical methods for increasing the rate of static dissipation are grounding, air ionisation and the addition of moisture or an anti-static agent to the powder. However, the only method which appears to be generally suitable for spray drying food material is the grounding of the spray dryer. Modifying the airflow patterns may also have an influence on electrostatics, because these flow patterns affect the rate at which particles hit the walls and thereby become tribocharged. The use of different internal chamber finishes in spray dryers to reduce wall deposition will be discussed next.

2.9.8 Internal Chamber Finishes

Particles must first adhere to the walls of the spray dryer before cohesion can take place, and adhesive forces are affected by the properties of the contact surface, for example, the type of material and its roughness. Zimon (1969) found that the adhesion of extremely tenacious soils, such as those of the Hawaiian Islands, to surfaces, can be reduced by covering the surface with a thin plastic film such as teflon or a teflon derivative. Papadakis and Bahu (1992) stated that the above method of reducing adhesion in drying equipment has been rarely applied. Masters (1996) pointed out that internal chamber finishes are used for spray dryers in the pharmaceutical industry to obtain specified deposition levels, but few details were given by him.

2.10 Conclusions

Previous researchers have not resolved the problem of the wall deposition of particles in spray dryers. No quantitiative data has been produced on the wall deposition rates or fluxes of food material. This problem is worth investigating because the outcome of reducing or eliminating wall deposition is that a spray dryer could operate for a longer period of time without having to be cleaned. Adverse effects on powder quality or safety would be minimised. Fire hazards would also be reduced or eliminated. Thus, further progress in this area of research would lead to improvement in the commercial production of spray dried food. To achieve such a goal requires consideration of the factors which are responsible for the formation of wall deposition.

Southwell and Langrish (2001) found evidence that the extent to which particles spread out in a spray dryer was affected by the amount of swirl in the inlet air, and suggested that the wall deposition rates are also likely to be affected by the swirl angle (section 2.3.2). In section 5.3 of Chapter 5 in this thesis, the influence of the swirl vane angle on wall deposition fluxes of skim milk powder has been tested and discussed.

It is possible that a key parameter in determining whether or not particles stick to the walls of spray dryers is the difference between the particle temperature and its sticky-point temperature. The use of the sticky point curve in selecting operating conditions for spray drying sticky material has been recommended (Lazar *et al.*, 1956; Brennan *et al.*, 1971; Gupta, 1978; Genskow, 1988; Yang, 2000) (section 2.6). The inlet air temperature and liquid feed flowrate

will influence the temperature and relative humidity inside the spray dryer, which will affect the temperature and moisture content of the material containing carbohydrates, and thus may affect the cohesiveness of the particles. The influence of the inlet air temperature and feed flowrate on wall deposition fluxes of skim milk powder is discussed in section 5.4 of Chapter 5 in this thesis. The usefulness of using the sticky point curve as a criterion for deciding on the operating conditions of the dryer is also discussed in this section.

The sticky point test only measures the cohesive nature of particles, whereas wall deposition involves both adhesion and cohesion. Since particles must adhere to the walls of the chamber before cohesion takes place, electrostatic forces and wall properties may be important in the wall deposition problem. The influence of electrostatics (section 2.9.7) on wall deposition fluxes is discussed in section 5.5 and the influence of wall properties and time on wall deposition fluxes (section 2.9.8) is discussed in section 5.6.

Finally, the concept of the product moisture locus (section 2.8), which according to Bahu (1992) implies that the solids leaving the dryer closely approach their equilibrium moisture contents, as given by the desorption isotherm. This aspect is discussed in section 5.3.1.

The next chapter will report the results of comparing the sticky-point temperature of skim milk powder (which contains the carbohydrate lactose) with its glass transition temperature. The outcome of this work will be to find out whether or not the glass transition test, which is an easier test than the sticky-point test, can be used to characterise the stickiness of a food material containing carbohydrates, and hence be used as guide for selecting operating conditions for a spray dryer to minimise wall deposition.

Chapter 3

Comparison of Glass Transition Temperature and Sticky Point Temperature for Skim Milk Powder

As discussed in sections 2.6 and 2.7 of Chapter 2 in this thesis, the sticky-point curve has been used as a semi-quantitative concept in selecting operating conditions for spray drying sticky material, where it has been implied that there is no significant wall deposition below the sticky-point curve. Roos and Karel (1991c) have linked the sticky-point temperatures of amorphous sugars to the glass transition temperatures determined by Differential Scanning Calorimetry (DSC). DSC will be discussed in section 3.1 of this chapter. This suggests that the glass transition temperature of the amorphous material that arises from spray drying may be used to guide the selection of operating conditions that may minimise wall deposition (Jouppilla and Roos, 1994).

The purpose of this chapter is to demonstrate explicitly that the glass transition temperature measured for skim milk powder at various moisture contents is close to the sticky-point measurements conducted by Hennigs *et al.* (2001) for skim milk powder with moisture contents ranging from 1 % to 10 % (dry basis). All moisture contents of a solid specified in this thesis are given on a dry solid basis unless otherwise specified. Refer to Appendix C6 for Hennigs *et al.*'s (2001) sticky-point data for skim milk powder found using sticky-point apparatus. The significance of showing the agreement between the sticky-point and glass transition temperatures is that the testing program for drying more valuable carbohydrate-based food material than skim milk may be considerably simplified because first, less material is required for the glass transition test and second, the glass transition test takes a quarter of the time required for the sticky-point test.

3.1 Differential Scanning Calorimetry

As described in section 2.7 of Chapter 2 in this thesis, when an amorphous solid is heated, its heat capacity, C_p, defined as the heat required to raise the temperature of a unit mass $(\partial H / \partial T)_P$ (equation 3.1), increases due to an increase in molecular motion. The source of equation 3.1 is Keey (1978), who shows that for a constant pressure process, the heat capacity of a material is the sum of the internal energy change (∂U) and work done against pressure ($P \partial V$), when the material is heated.

$$C_p = \left(\frac{\partial H}{\partial T}\right)_p = \left(\frac{\partial U}{\partial T}\right)_P + P\left(\frac{\partial V}{\partial T}\right)_P \tag{3.1}$$

The increase in heat capacity of the solid, which is measured using DSC, causes it to transform from a glass into a rubber. The glassy-to-rubbery phase transition is known as the glass transition, which occurs over a temperature range of approximately 20°C (White and Cakebread, 1966).

DSC is a thermal analysis technique which measures the temperature and heat flows associated with transitions in materials as a function of time and temperature (Sauerbrunn *et al.*, 1992). As shown in Figure 3.1, the sample material and reference material are each contained in a hermatically sealed pan and sit on raised platforms formed in a thermoelectric disk, which serves as the primary means of heat transfer to the sample and reference from a temperature-programmed furnace (heating block). The temperature of the furnace is raised in a linear fashion, while the temperature difference between the sample and reference is monitored by area thermocouples fixed to the underside of the disk platforms. The differential heat flow is then calculated using the thermal equivalent of Ohm's law, by dividing the temperature difference measured between the sample and reference by the thermal resistance of the cell (equation 3.2).

$$dQ = \frac{dT}{R} \tag{3.2}$$

where dQ is the differential heat flow between the sample and reference, dT is the temperature difference measured between the sample and reference, and R is the thermal resistance of the cell.

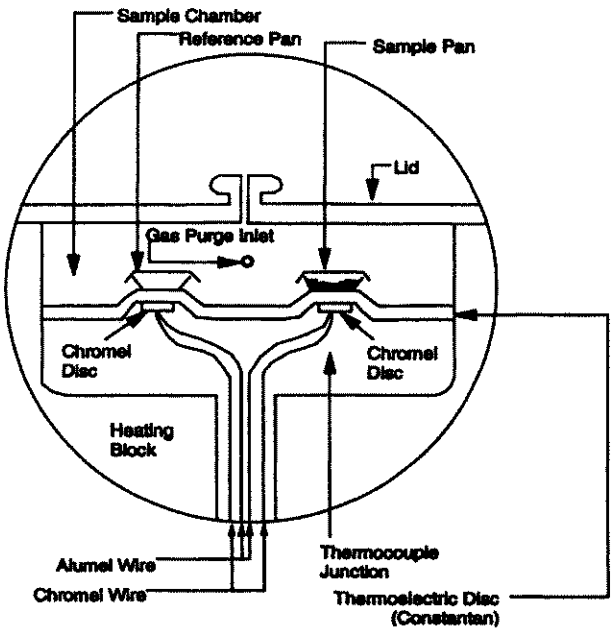

Figure 3.1 - Schematic diagram of a DSC cell. Source: http://www.tainst.com/support/TA211.PDF (accessed August 2000).

Modulated DSC (MDSC) is an extension of DSC and has the advantage of disentangling overlapping phenomena, improving resolution and enhancing sensitivity (Reading *et al.*, 1994). The same cell arrangement is used as for DSC. However, the usually linear temperature programme is modulated by a small perturbation, in this case a sine wave (specified by amplitude and frequency), and a discrete Fourier transformation is applied to the resultant data (total heat flow signal) to deconvolute the sample response to the perturbation from its response to the underlying heating programme. By doing this, the reversible and irreversible nature of a thermal event can be probed. In MDSC, the heat flow is represented by equation 3.3:

$$\frac{dQ}{dt} = \frac{dT}{dt} \times \left[(C_p + f'(t,T) \right] + f(t,T) \tag{3.3}$$

where $\frac{dQ}{dt}$ is the heat flow, $\frac{dT}{dt} \times \left[(C_p + f'(t,T) \right]$ is the heating-rate-dependent transition, which is a reversible event, and $f(t,T)$ is the absolute-temperature-dependent transition, which is an irreversible event. The reversible portion of the heat flow signal can be cycled by alternating the heating and cooling. However, the non-reversing portion of the heat flow signal cannot be reversed by cyclic heating and cooling. As shown in Figure 3.2, the glass transition

temperature appears only in the reversing portion of the MDSC result. Crystallisation associated with rearrangement of the less stable amorphous internal structure to a more stable crystalline structure appears in the irreversible portion of the MDSC result. The materials and methods used to find the glass transition temperature of skim milk powder with various moisture contents in this work are discussed next.

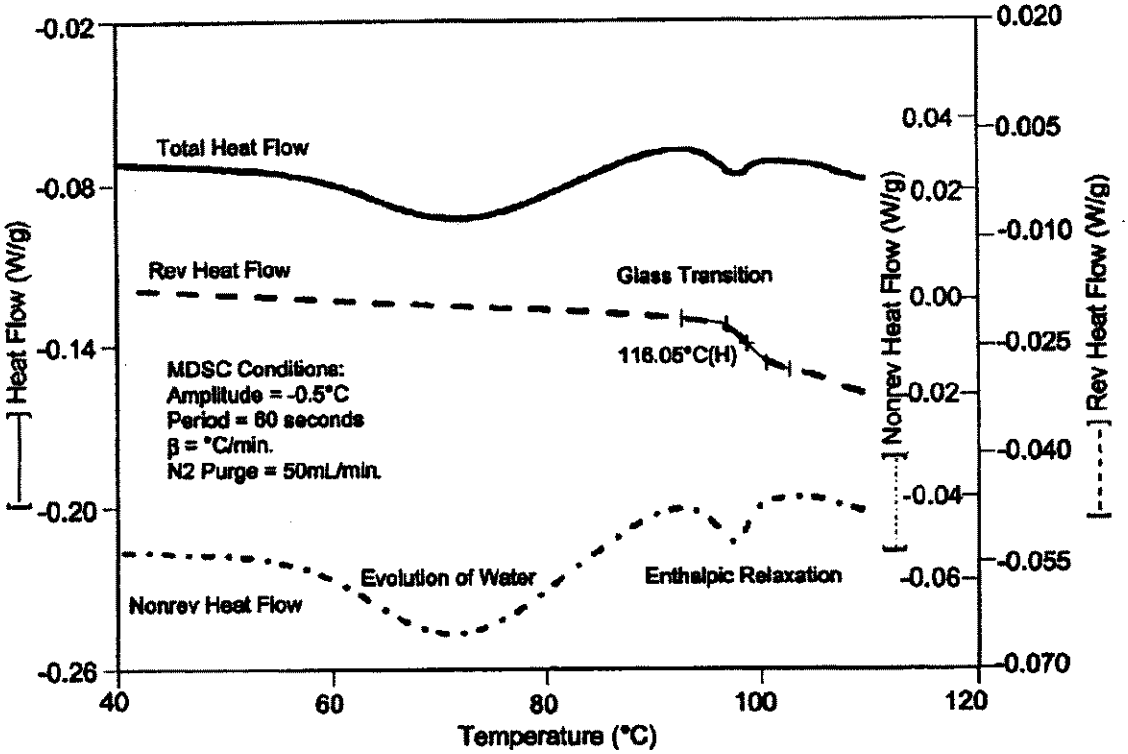

Figure 3.2 – Characterisation of the glass transition temperature of lactose by MDSC showing separation of total heat flow into reversing (heat capacity) and non-reversing (kinetic) components.
Source : http://www.tainst.com/support/TS43.PDF (accessed August 2000).

3.2 Materials and Methods

3.2.1 Rehumidification of the Skim Milk Powder to Obtain the Desired Moisture Content

The model food material used was skim milk powder with an initial moisture content of 4.39%, supplied by Bonlac Foods Ltd, Australia. Kockel *et al.* (2002) used a stirred fluidised bed to re-humidify skim milk powder, as part of an experimental study on the equilibrium moisture contents of skim milk powder at elevated temperatures. Their experimental method was repeated here to obtain skim milk powder at three moisture contents for subsequent DSC tests. The stirred fluidised bed was operated as follows. An air stream from a pressurised grid with a flowrate of 10 L min^{-1} was degreased and throttled to a pressure of 100 kPa and then passed through a heated water bath. The dew point temperature of the air was the temperature of the water in the water bath (approximately 20°C). The air was then heated using a 640 W heating coil. The heated air was passed through a fine mesh and into a 5 L glass cylinder which was used as a fluidised bed. The temperature to which the air could be heated was controlled. All the tubes and vessels downstream of the air heater were trace-heated electrically to prevent heat loss to the environment and condensation on the inner walls of the equipment. A stirrer with sigmoidally-shaped brush impellers was inserted into the fluidised bed for stirring the powder so that a homogenous mixture could be obtained. The stirrer speed was adjusted to 70-120 rpm, to ensure incipient fluidisation.

Kockel *et al.* (2002) found the correlation proposed by Papadakis *et al.* (1993) (equation 3.4) gave the best fit for their experimental results regarding the equilibrium moisture content of skim milk powder at temperatures between 55°C and 90°C (r^2=0.992) and relative humidities in the range 3.3% and 21.4%.

$$X_{eq} = A\exp\left[-BT\ln\left(\frac{1}{\Psi}\right)\right] \tag{3.4}$$

where the symbols were defined in section 2.8. Kockel *et al.* (2002) fitted the empirical constants A and B to their experimental data for skim milk powder and found the values were 0.1499 kg kg^{-1} and 2.306 × 10^{-3} K^{-1}, respectively. Equation 3.4 was used in this study to

estimate the temperature to which the air should be heated to obtain skim milk powder with a desired moisture content. However, for relative humidities greater than 21%, the Guggenheim-Anderson-Deboer equation, which has been used extensively for foodstuffs and has a wider range of applicability (Lomauro *et al.*, 1985) was used to calculate the equilibrium moisture content of the skim milk powder (equation 3.5).

$$X_{eq} = \frac{K_1 K_2 K_3 a_w}{(1 - K_2 a_w)(1 - K_2 a_w + K_2 K_3 a_w)} \tag{3.5}$$

where K_1 = 0.19662. K_2 = 0.26244 and K_3 = 4.6167 (parameters fitted by Kockel *et al.*, 2002) and a_w is the water activity (0 to 1). The measure of the affinity of the moisture to its host material is called the water activity. The water activity is sometimes referred to as the relative humidity, because the solid will be in moisture equilibrium with the surrounding gas having a moisture-vapour content corresponding to a particular relative humidity.

Table 3.1 shows the operating conditions for the stirred fluidised bed, the equilibrium moisture content predicted for these operating conditions and the actual moisture contents of the skim milk powder. Before re-humidifying the skim milk powder, the fluidised bed was run for one hour without skim milk powder, until the temperature of the heated air and water bath stabilised. Then, 300 g of skim milk powder with a moisture content of 4.39 % was added to the fluidised bed. During the run, the temperature and relative humidity of the air upstream of the heater and the temperature of the fluidised bed were monitored using thermocouples connected to heater controllers. A sample of 80 g was removed from the fluidised bed after three hours, which according to Kockel *et al.* (2002) is sufficient time for equilibrium to be obtained under these dynamic (fluidised) conditions. The moisture content of the skim milk powder was determined by weighing three 20 g samples of skim milk powder into a clean glass petrie dish. The samples were then transferred to a drying oven and dried at 85°C for 48 hours. The skim milk was dried at a temperature of 85°C as suggested by German Standard DIN 10321 instead of 102°C as suggested by International Dairy Federation (IDF) Standard 26A:1993, because Kockel *et al.* (2002) observed that skim milk powder thermally degraded when dried at 102°C.

Table 3.1- Operating conditons for the stirred fluidised bed, predicted equilibrium moisture contents and actual moisture contents of the skim milk powder.

Sample	Water bath temperature (°C)	Heated air temperature (°C)	Relative humidity of air (%)	Predicted equilibrium moisture content (%)	Actual moisture content (%)
1	20	76.3	5.7	1.5	1.7
2	20	63.6	10.0	2.5	2.7
3	25	52.1	23.1	7.2	4.5

The moisture contents of the samples were obtained from the decreases in mass on oven drying. The measured moisture contents of the skim milk were adjusted by adding 0.371% (w/w) to the moisture content determined by a decrease in weight to compare with moisture contents of material dried at 102°C, as recommended by de Knegt and van den Brink (1998). Table 3.1 shows there is a difference of 2.7% between the predicted moisture content and actual moisture content for the third sample, where the predicted moisture content is higher. This result was expected because the third sample involved re-wetting to a higher moisture content than the moisture content of the initial sample, and equations 3.4 and 3.5 are used to calculate the equilibrium moisture content when water is removed from the solid (desorption) and not for re-wetting the solid (adsorption). Furthermore, according to Keey (1978), the desorption isotherm always shows a larger equilibrium moisture content at a given relative humidity when compared with the adsorption isotherm.

3.2.2 Determination of the Glass Transition Temperature of Skim Milk Powder

DSC was used to determine the glass transition temperature of the skim milk powder at four different moisture contents. The moisture content of the samples used are given in Table 3.1. The skim milk powder with a moisture content of 4.39% (supplied by Bonlac Foods Ltd, Australia) was also tested. The Differential Scanning Calorimeter used was a TA Instruments DSC 2920 with Universal Analysis software. The software can be used so that both total heat flow (DSC) and reverse heat flow (MDSC) results as a function of temperature can be displayed. Hermetically sealable aluminium sample pans were used in all measurements, with an empty aluminium pan as the reference sample. The reason that hermatically sealable pans were used was to prevent moisture in the skim milk powder from escaping. Then, the effect of moisture content on the glass transition temperature of the skim milk powder could be determined. The method for preparing the skim milk powder samples for the DSC test was as follows. An aluminium sample pan and lid were weighed on an analytical scale [Mettler

AE166 (± 0.0001 g)]. The scale was tared and a small amount of skim milk powder (18-25 mg) was placed in the pan, which was then covered with the lid. The pan was hermatically sealed and reweighed to determine how much skim milk powder was in the pan.

The operating conditions used to characterise the glass transition temperature of the skim milk powder using MDSC were identical to the operating conditions used to characterise the glass transition temperature of lactose by MDSC (http://www.tainst.com/support/TS45.PDF, accessed September 2000). The samples were normally scanned at a rate of 2°C min^{-1} from 0°C to 120°C. The sample was modulated at ± 0.5 °C every 60 seconds. Nitrogen gas with a flow of 50 ml min^{-1} was used to purge the sample head to avoid condensation of moisture. According to the TA Instruments DSC 2920 Manual (1995), in order to get proper separation of the heat flow during a transition, a minimum of four cycles is required. Therefore, if the transition is 10°C wide, the heating rate should not be greater than 2.5°C min^{-1}. Subsequent experiments were performed to assess the impact of different scanning rates, namely, 2°C min^{-1}, 5°C min^{-1} and 10°C min^{-1} on the behaviour of skim milk powder with a moisture content of 4.77%. At least one replicate run was used for each scanning rate. The thermographs obtained were typical of amorphous materials and were analysed for the glass transition temperature. At least one replicate run was used for each moisture content. The uncertainty in the temperatures is ± 0.1°C (TA Instruments, 1995).

3.3 Glass Transition Temperature of Skim Milk Powder at Various Moisture Contents

Figure 3.3 shows the temperature range over which the glass transition occurs for skim milk powder, which is characterised by a trough representing an endothermic process. The point on these curves is known as the glass transition temperature; this is not a sharply located point but defines the centre of a small region over which the glass transition takes place.

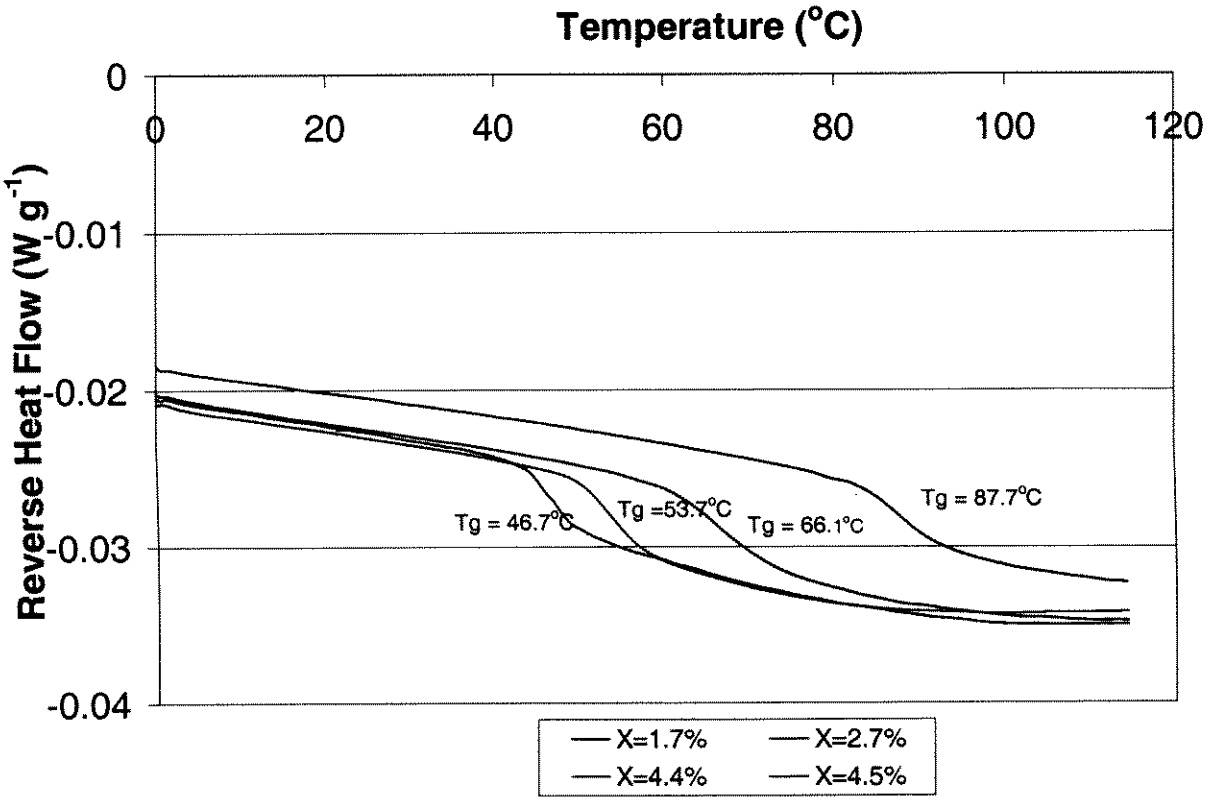

Figure 3.3 - Glass transition temperatures for skim milk with different moisture contents (X), found in this study.

As expected, the glass transition temperature of skim milk powder was found to be affected by water, which acted as a plasticiser. The glass transition temperature decreased as the moisture content increased. For a low moisture content of 1.7 %, the glass transition temperature was 87.7°C; for a high moisture content of 4.5%, the glass transition temperature was 46.7°C.

The sticky-point curve, predicted glass transition curve and measured glass transition temperatures using MDSC and DSC for skim milk powder are shown in Figure 3.4. A trendline for the MDSC results is also shown in Figure 3.4.

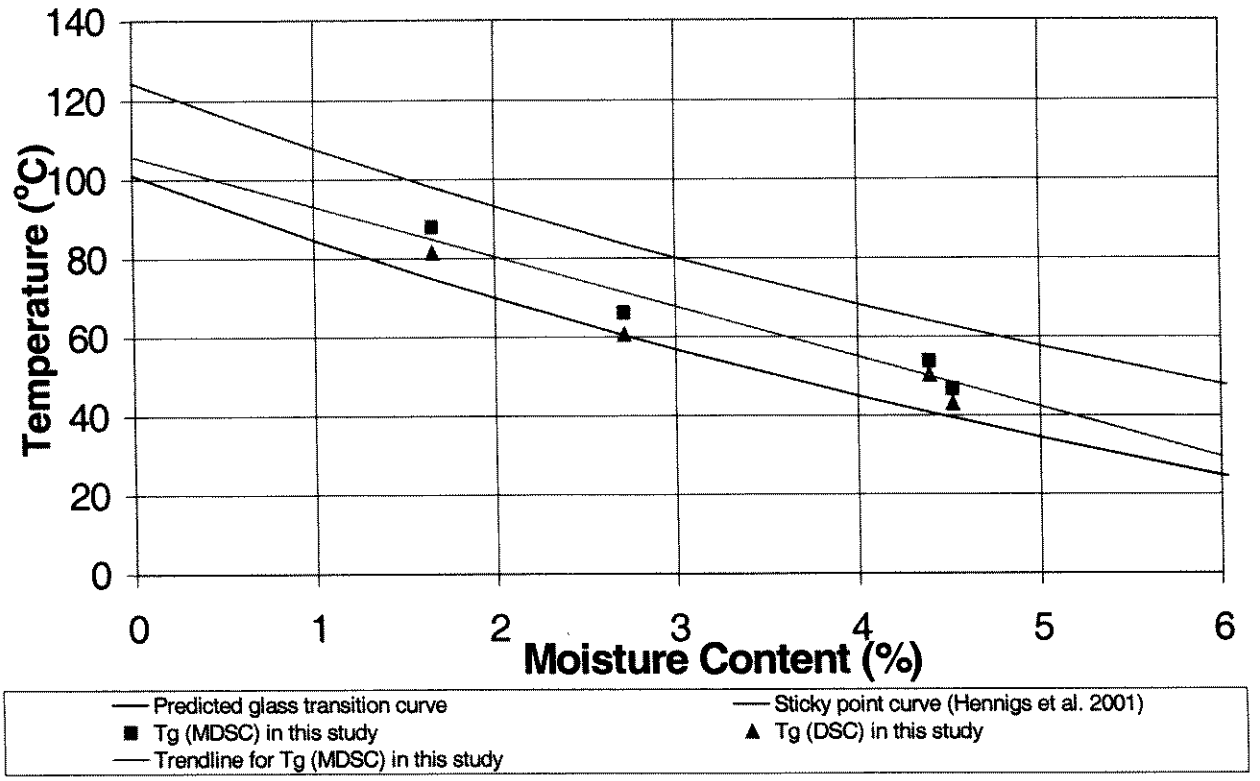

Figure 3.4 - The glass transition temperatures and sticky-point temperatures for skim milk powder as a function of moisture content.

The predicted glass transition curve was obtained by using the Gordon-Taylor (1952) equation (equation 3.6).

$$T_g = \frac{(w_1 T_{g1} + k w_2 T_{g2})}{(w_1 + k w_2)} \tag{3.6}$$

where the symbols are defined in section 2.6. Skim milk was assumed to be a binary mixture of amorphous lactose and water. The glass transition temperature of amorphous lactose (T_{g1}) was taken as 101°C (Roos and Karel, 1991c), and the glass transition temperature of water (T_{g2}) was taken as –137°C (Johari *et al.*, 1987). The value of k for lactose is 7.40 and was obtained empirically by Roos (1993) and Hennigs *et al.* (2001). Values from 0 to 0.06 were used for the weight fractions of water in the skim milk, which was in the range used in this work. An example of using equation 3.6 to find the glass transition temperature of skim milk powder with a moisture content of 3% is given next.

$$T_g = \frac{(0.97 \times 101°C + 7.4 \times 0.03 \times -137°C)}{(0.97 + 7.4 \times 0.03)}$$

$$= 56°C$$

The sticky-point curve was obtained by Hennigs *et al.* (2001). Figure 3.4 shows that there is an offset of about 14 to 22°C between the experimental glass transition temperatures and the sticky-point temperatures. The glass transition temperature was taken as the mid-point in the endothermic trough, as measured from the extensions from the onset and the end temperatures of glass transition. The difference between the onset and end temperatures of glass transition was around 10°C. Furthermore, White and Cakebread (1966) proposed that the glass transition occurs over a temperature range of about 20°C, so the difference between the glass transition temperatures and sticky-point temperatures observed here may be due to this uncertainty in the glass transition temperature. This finding is consistent with the work of Labuza (1984), who found that a material starts to become sticky when its temperature is 20°C above its glass transition temperature. The experimental glass transition temperatures were 2 – 10°C higher than the predicted ones. This difference may also be due to the presence of protein in the skim milk, in addition to lactose and water, and this will be discussed further in section 3.5.

Figure 3.5 shows the glass transition temperature results obtained by Jouppila and Roos (1994) who used DSC testing on freeze-dried skim milk powder with different moisture contents. The sticky-point curve and glass transition curve (predicted using the Gordon-Taylor equation) in this Figure (3.5) were obtained from Figure 3.4. The results of Jouppilla and Roos (1994) are very similar to DSC results found in this study. The differences between the DSC and MDSC results for the glass transition temperature were 3 – 7°C in this study. The glass transition temperatures obtained using MDSC are more accurate than DSC alone, as discussed before in section 3.1. The effect of heating rate used in the DSC test on the glass transition behaviour will be discussed next.

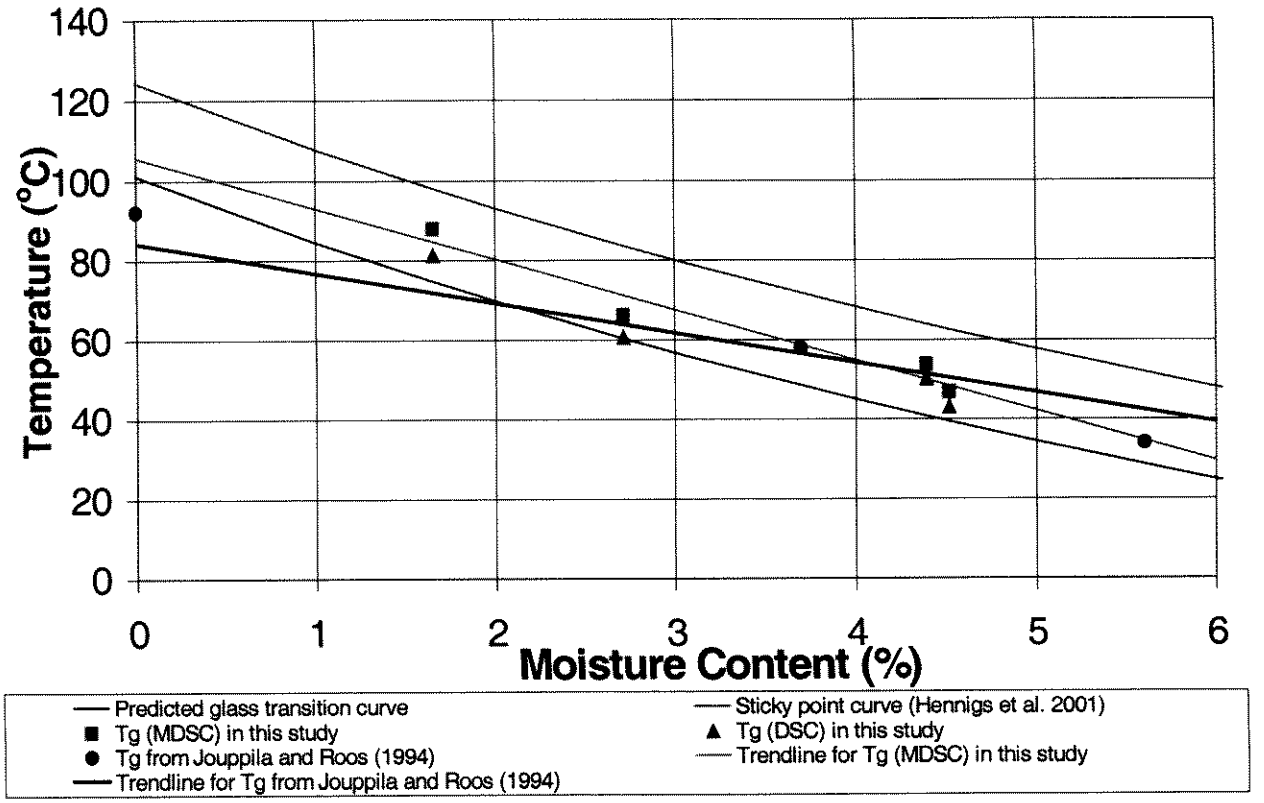

Figure 3.5 - Comparison of glass transition temperatures for skim milk with those found by other researchers.

3.4 The Effect of Heating Rate on Glass Transition Temperature

Figure 3.6 shows a plot of the heat input as a function of temperature, which compares the effect of the rate of heating on the glass transition behaviour (overall heat signal) of skim milk powder having a moisture content of 4.77%. The data were recorded using three heating rates, namely 2°C min^{-1}, 5°C min^{-1} and 10°C min^{-1}. The apparent glass transition temperature decreased significantly by 4.1°C from 50.3°C to 46.2°C when the scanning rate was reduced from 10°C min^{-1} to 2°C min^{-1}.

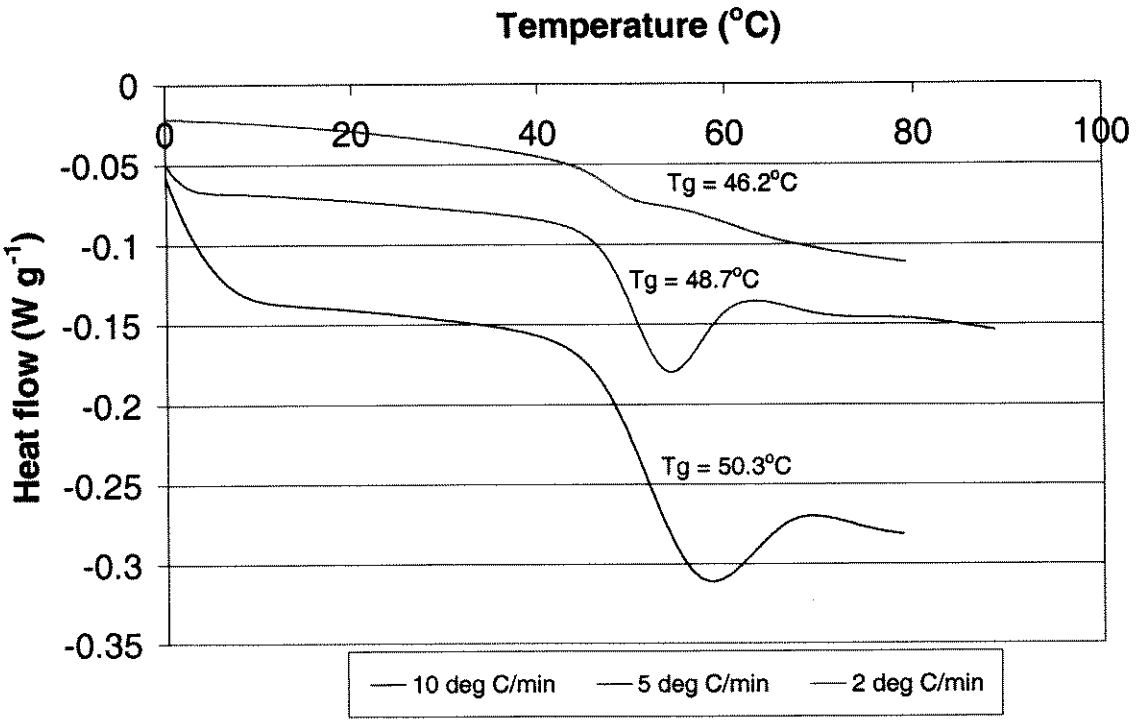

Figure 3.6 – Heat flow signal as a function of temperature, showing the glass transition region for skim milk powder (moisture content of 4.77%) at heating rates of 2°C min^{-1}, 5°C min^{-1}, and 10°C min^{-1}.

In contrast, Figure 3.7 shows a plot of reverse heat signal as a function of temperature, which compares the effect of the heating rate on the glass transition behaviour (reverse heat flow signal) of skim milk powder also having a moisture content of 4.77%. The reverse heat flow signal is obtained from the heat flow signal, by deconvoluting the sample data using discrete Fourier transformations. The data were recorded using three heating rates, namely 2°C min^{-1}, 5°C min^{-1} and 10°C min^{-1}. The glass transition temperature did not change when the heating rate was decreased from 10°C min^{-1} to 5°C min^{-1} but increased slightly by 1.6°C when the heating rate was decreased from 5°C min^{-1} to 2°C min^{-1}. Figure 3.7 is preferred to Figure 3.6 because it shows the glass transition temperature found using MDSC. MDSC disentangles overlapping phenomenon such as crystallisation, as discussed before in section 3.1.

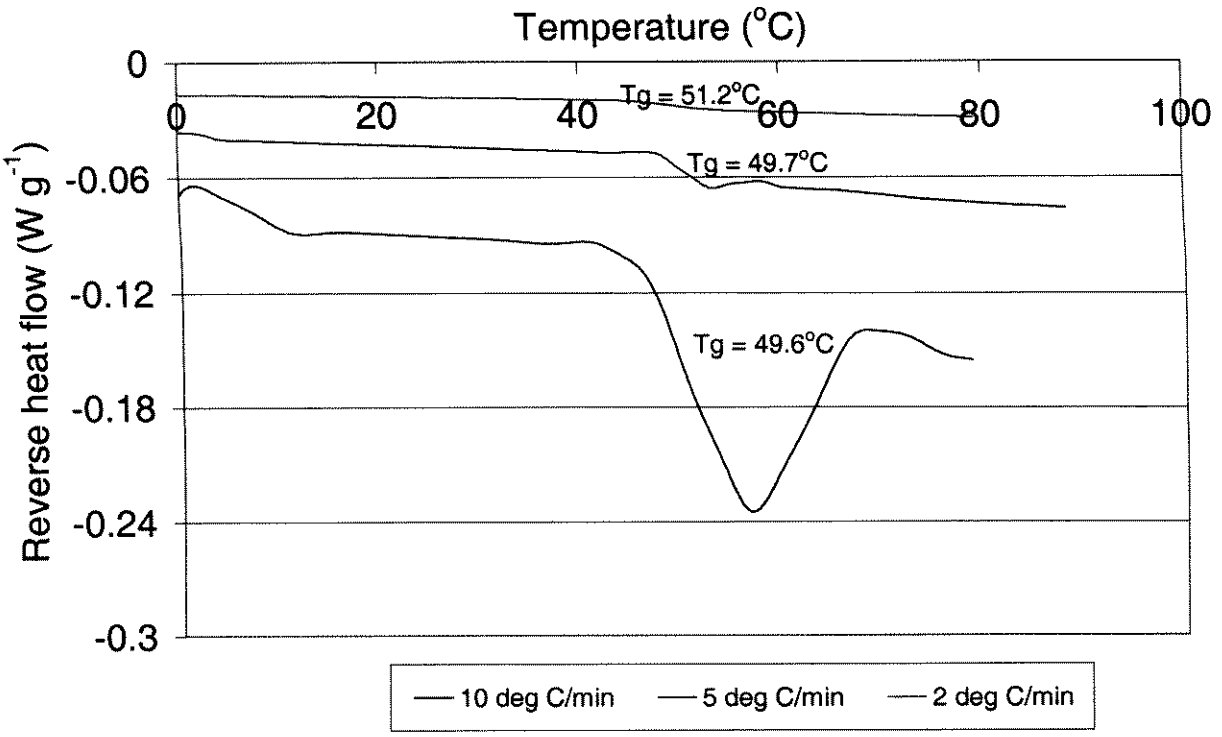

Figure 3.7 - Reverse heat flow signal as a function of temperature, showing the glass transition region for skim milk powder (moisture content of 4.77%) at heating rates of 2°C min^{-1}, 5°C min^{-1} and 10°C min^{-1}.

3.5 Denaturation of Milk Proteins

When the glass transition temperature of skim milk powder was estimated using the Gordon-Taylor equation, it was assumed that the proteins in the skim milk are inert and will therefore not affect the glass transition temperature significantly. However, when proteins are heated, they undergo thermal degradation, and this may affect the glass transition temperature of the skim milk powder. Ruegg *et al.* (1977) used DSC to study the denaturation temperature of whey proteins, which are proteins also found in milk, namely α-lactalbumin, β-lactoglobulin, γ-globulin and serum albumin. The denaturation temperature of these proteins and casein, which is also a protein present in milk, are given in Table 3.2.

Table 3.2 – Denaturation temperature of whey proteins . Source :Kirchmeier (1962) and Ruegg *et al.* (1977).

Protein	Denaturation temperature (°C)
α-lactalbumin	65
β-lactoglobulin	73
γ-globulin	73
Serum albumin	62
Casein	200

According to Grappin and Ribadeau-Dumas (1992), casein make up approximately 79% of the proteins found in milk. Therefore, since casein has a high denaturation temperature of 200°C, and makes up most of the proteins present in skim milk powder, the predicted glass transition temperature will be affected if the presence of proteins is taken into account. The effect of including proteins in the prediction of the glass transition temperature of skim milk powder will be discussed in the next section.

3.6 Discussion

The glass transition temperature of the skim milk powder decreased as the water content increased, as shown in Figures 3.3 and 3.4, which is typical of various amorphous foods (Roos and Karel, 1990; Roos and Karel, 1991b; Jouppilla and Roos, 1994). The sticky-point temperature and the glass transition temperature predicted using the Gordon-Taylor equation, also both decrease with an increase in moisture content. The difference between the glass transition temperature found using MDSC and the sticky-point measurements found by Hennigs *et al.* (2000) for skim milk is 14-22°C. However, the glass transition was estimated to be 10°C wide here, while previous workers have suggested that the glass transition is about 20°C wide. Thus, the glass transition temperature might be considered to be close to the sticky-point temperature, because of the 10-20°C uncertainty in the glass transition temperature. The remaining difference between these values may be due to doing a mechanical test for viscosity (sticky-point) and a phase transition measurement (DSC).

The Gordon-Taylor equation can be used to successfully predict the trend of the glass transition temperature as a function of moisture content (Figure 3.4). The difference between the experimental glass transition temperature and the predicted glass transition temperature was 2 – 10°C. In addition to the reasons just given for the difference in the sticky-point and measured glass transition temperatures, the difference in the experimental and predicted glass transition

temperatures may be due to the presence of protein in skim milk, which was not accounted for in the predicted glass transition temperature. The phase change behaviours of proteins and fats are different to those of carbohydrates such as lactose; rather than the glass transition behaviour of carbohydrates, fats melt, while proteins denature. As pointed out in section 3.5, proteins in milk denature at certain temperatures and this can be a type of phase transition that may affect the glass transition temperature of skim milk powder. Casein makes up approximately 79% of the total protein content in milk and has a high denaturation temperature of 200°C. Thus, if the presence of casein was included in predicting the glass transition temperature of skim milk powder using the Gordon-Taylor equation (equation 3.6), the predicted glass transition temperature might be higher than what was predicted here. Hence, the difference in the predicted and measured glass transition temperature of skim milk powder might decrease.

The glass transition temperature for skim milk found using the total heat flow signal (DSC) (Figure 3.5) is less than the glass transition temperature for skim milk found using the reverse heat flow signal (MDSC) by 3 – 7 °C. The glass transition temperature (DSC) may have been depressed by crystallisation associated with rearrangement of less stable amorphous internal structures to more stable crystalline structures. The total heat flow signal picks up both reversible (glass transition) and irreversible (crystallisation) transitions.

Jouppilla and Roos (1994) carried out DSC testing for freeze-dried skim milk powder. Their results for the glass transition temperature, shown in Figure 3.5, are very similar to the DSC results found in this study. The difference between the glass transition temperatures in this study, found using MDSC, and those found by Jouppilla and Roos (1994) is 4 - 10°C. The difference between the glass transition temperatures decreased as the moisture content increased (low moisture content 1 %, difference is 10°C; high moisture content 3 %, difference is 4°C). Once again, the reason for this difference may be due to crystallisation in Jouppilla and Roos' (1994) results depressing the glass transition temperature.

As shown in Figure 3.6, the glass transition temperature for skim milk powder with a moisture content of 4.77% was found to be generally lower at lower scanning rates, when the total heat flow input as a function of temperature (DSC) data is used to find the glass transition temperature. This was also reported by Noel *et al.* (1991) who measured the glass transition temperature of maltose-water mixtures and Chuy and Labuza (1994), who measured the glass transition temperature for infant formula powders. However, no significant difference was

found between the glass transition temperatures found at different heating rates when the reverse heat flow signal as a function of temperature (MDSC) was used (Figure 3.7). MDSC results from the reverse heat flow signal were not significantly dependent on the scanning rate. Thus, the reversible heat flow signal was used in all other analyses in this work. MDSC results are more accurate, since MDSC has the advantage of disentangling overlapping phenomena, improving resolution and enhancing sensitivity (Readings *et al.*, 1994). The results found in this thesis are most useful for estimating the glass transition temperatures of skim milk powder at various moisture contents.

3.7 Conclusions

The glass transition temperature of skim milk powder determined using DSC decreased as the moisture content increased, as expected. Glass transition occurs over a temperature range of 10°C to 20°C and is not a sharply located point. Hence, if this uncertainty in the glass transition temperature is taken into account, the glass transition temperatures are close to the sticky-point temperatures. Thus, the glass transition temperature may be used as a quick guide for selecting operating conditions for food materials containing carbohydrates that may minimise wall deposition. In future, testing programs for drying food materials containing carbohydrates, which are more valuable than skim milk powder can be simplified because, first, the DSC method requires smaller sized samples (20 mg) than sticky-point equipment (70 –75 g) and second, the glass transition test takes a quarter of the time required for the sticky-point test. The value of using the sticky-point temperature of skim milk powder for deciding on the operating conditions for the spray dryer to minimise wall deposition has been quantified in section 5.4 of Chapter 5 in this thesis. The impact of reducing the inlet air temperature on the productivity of the spray dryer (if this is necessary to reduce the stickiness of the particles) is also given in section 5.4.

The Gordon-Taylor equation was also found to be adequate in predicting the glass transition temperature of a mixture if the composition and glass transition temperature of the pure components present in the mixture are known.

The next chapter, Chapter 4, is divided into three parts. The first section (4.1) provides a description of the spray dryer, particulary how it was operated and modified for this work. The

second section (4.2) describes the experiments designed in this work for determining the effect of spray dryer operating conditions on the wall deposition flux of skim milk powder on the interior walls of the spray dryer. Finally, the third section (4.3) reports and then interprets the mass and energy balances conducted over the spray dryer for assessing the reliability of the humidity and temperature measurements, which in turn influence the reliability of the wall deposition flux data.

Chapter 4

Spray Drying – The Equipment, Experimental Design and Mass and Energy Balances

4.1 Spray Drying Equipment

This section provides a description of the spray dryer, particularly how it was operated and modified for this work. A physical description of the spray dryer is given in section 4.1.1. A description of the nozzle used for spraying water, skim milk and then grape extract into the drying chamber of the spray dryer is given in section 4.1.2. The temperatures in the spray dryer were controlled and recorded using a program developed by Southwell (2000), who used 16 Bit Visual Basic 4.0 operating under the Windows 3.1 operating system. Descriptions of the dryer control is given in section 4.1.3. An analogue-digital conversion card was fitted to the computer for data collection and control of the temperatures in the dryer. A description of how this card and thermocouples (used for measuring the temperatures in the spray dryer) were calibrated are provided in sections 4.1.4 and 4.1.5, respectively. Finally a description of the modifications carried out to the spray dryer for this work is given in section 4.1.6, and the conclusions are given in section 4.1.7.

4.1.1 General Description of Spray Dryer used in this Work

The spray dryer present in The Department of Chemical Engineering at the University of Sydney is a modified co-current Niro unit, fabricated from stainless steel (Figure 4.1). The spray dryer has an internal diameter of 0.80 m, narrowing down to 0.06 m at the base, and a height of 2 m. This height includes a "spacer" (length 0.30 m) incorporating twelve toughed glass panes, allowing observation of the flow inside the dryer. The upper cylindrical portion of the unit is 1.3 m in height, and the lower conical section has a height of 0.63 m. The plenum chamber is located in the dryer lid, and consists of the nozzle, hot air inlet port and the inlet swirl vanes. The swirl vanes are connected by way of levers and a ring, so that all the vanes turn simultaneously between 0° and 45°. Baffles are located inside the plenum chamber to distribute air evenly into the drying chamber. The spray dryer is symmetrical about its axis.

The spray dryer, cyclone and the pipes entering and leaving the spray dryer and cyclone are insulated to reduce heat losses to the environment. In addition to insulation, trace heating tapes are wound around the exit pipes and the cyclone and are connected to heater controllers. The purpose of the trace heating tapes is to heat the outer walls of the pipes and cyclone to a temperature above the dew point temperature of the air inside the pipes and cyclone for the spray drying conditions used here, and thus prevent condensation inside the pipes and cyclone. The sight-glasses and glass panes located in the "spacer" are not insulated.

Air entering the spray dryer is heated by a three-phase, 415 V electric heater, maximum 5 kW per phase, giving a maximum amount of 15 kW heat input. Two of the phases are controlled manually and one is controlled automatically by using a software program developed by Southwell (2000) called CEDRIER (see section 4.1.3). The dryer also uses inlet and exhaust fans (or blowers) which blow air into the dryer and suck air out of the dryer, respectively. Consequently, the dryer is under slightly positive pressure with respect to atmospheric pressure. Figure 4.2 shows the cabinet which contains the fans, heater and airflow meter. The maximum heater outlet temperature, using all three phases and both fans, is approximately 300°C.

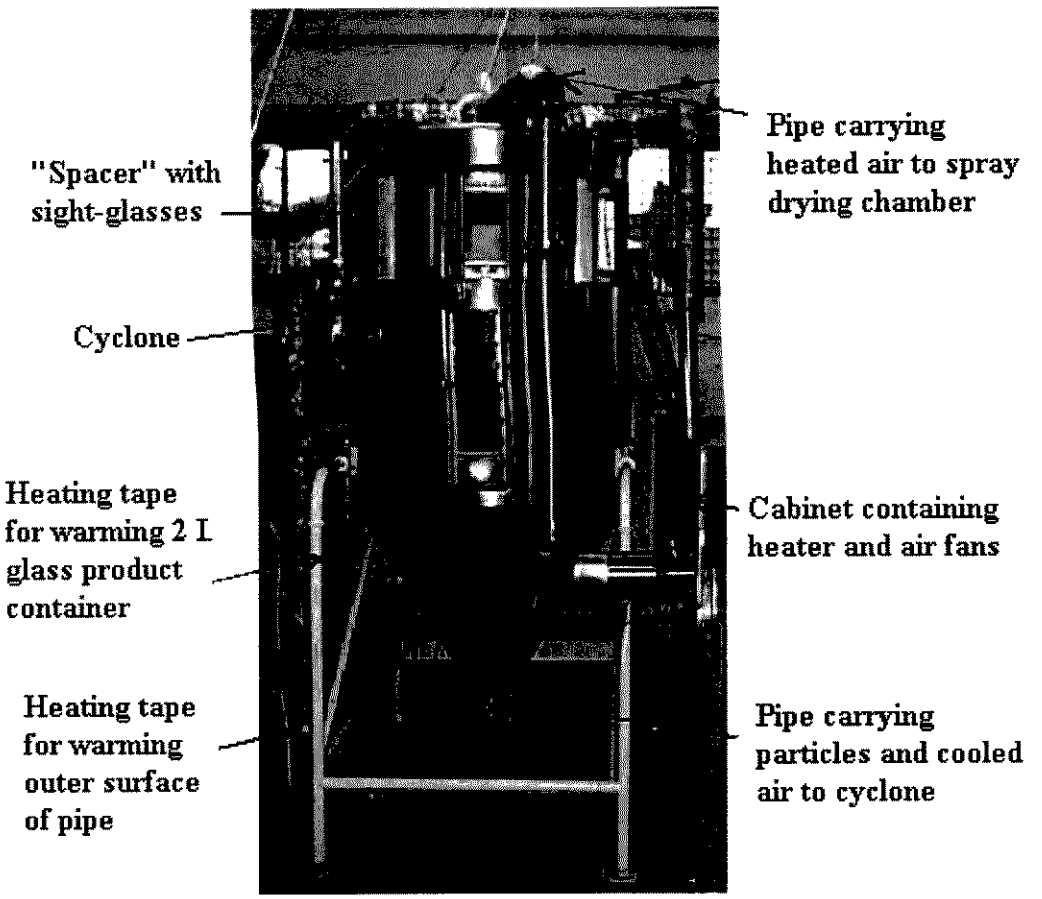

Figure 4.1 – Photograph of Spray Dryer at the Department of Chemical Engineering.

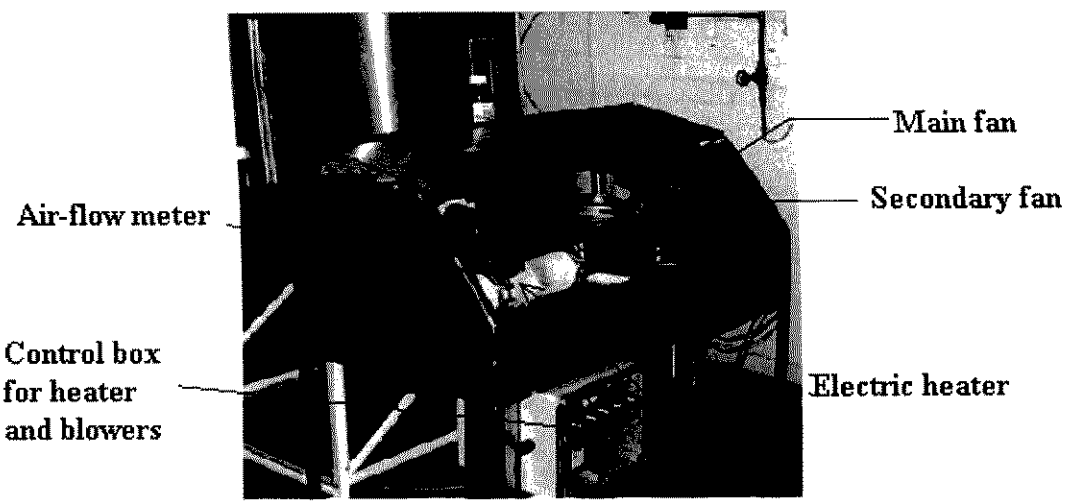

Figure 4.2 – Photograph of spray dryer heater and fans cabinet at the Department of Chemical Engineering. Source : Southwell (2000).

A schematic diagram, showing the key components and instrument locations, is shown in Figure 4.3. Seven thermocouples, denoted T, are located around the dryer to measure the temperature of the air, while wet and dry-bulb thermocouples, denoted Tw and Td, respectively, are located at both the inlet and outlet to allow measurements of air humidity. An air-flow meter, denoted F, is located downstream of the heater. According to Southwell (2000), the flowmeter reflects the true value of the airflow at ambient temperature. However, the flowmeter over-predicts the mass flowrate of air when the heater temperature is increased because it does not compensate for air density variations over the range of temperatures possible for the spray dryer. Hence, the mass flowrate of the air was calculated using traverse air velocity readings, measured using a hot-wire anemometer, type Solomat MPM 500e (U.K.) and the reason for doing this is explained in section 4.3. A peristaltic pump, type Ismatec mp-ge II 50 Hz (Switzerland), was used to control the process fluid flowrate to the atomizer. The pump had six heads, giving a flow with very small pulsations (less than 10%) The procedure used to calibrate the peristaltic pump is given in Appendix B1. Figure 4.3 shows the location of the stainless steel plates that were used to measure the wall deposition flux of skim milk powder, as well as the location of the swirl vanes that were used to impart swirl to the air entering the spray drying chamber.

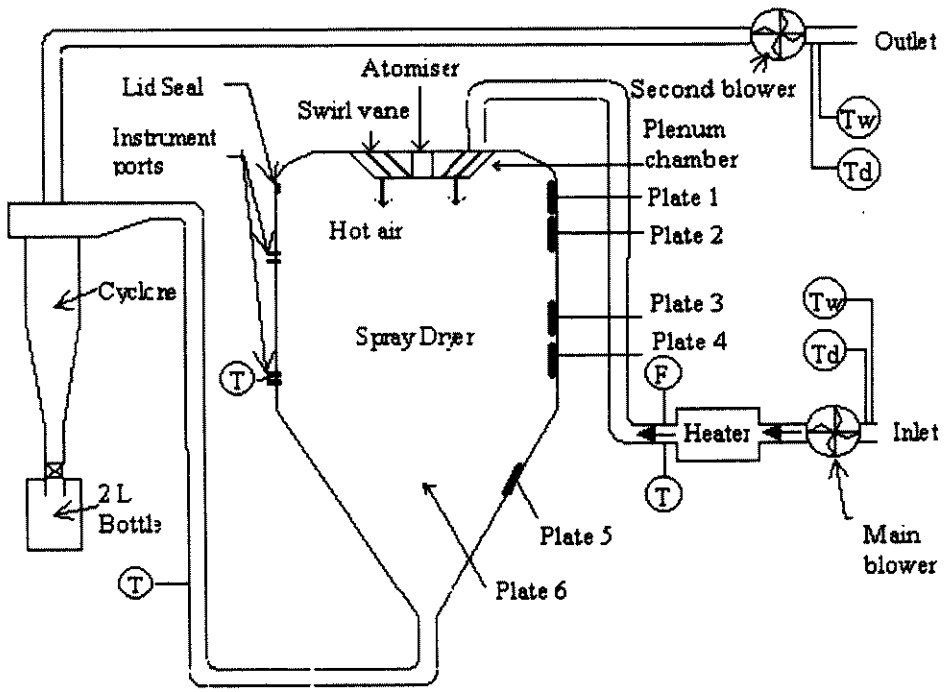

Figure 4.3 –Schematic of dryer rig – not to scale.

4.1.2 Nozzle Atomiser

A Delavan GA1 two-fluid nozzle atomizer was used in this work (Figure 4.4). The main characteristics of this nozzle are that it uses compressed air for atomizing the liquid feed, external mixing of gas and liquid phases takes place, and a full cone spray pattern is obtained (Southwell, 2000). The manufacturer's flow capacity specifications are given in Table 4.1.

Table 4.1 - Flow capacity for the Delavan GA1 two-fluid nozzle atomiser. Source : Delavan Industrial Nozzles and Accessories Manual (2001).

Air pressure (Bar)	0.35	0.70	1.00	1.40	1.70	2.10	2.80	4.20	5.50	6.90
Water ($lt.hr^{-1}$)	0.82	1.90	2.30	2.70	3.20	3.30	3.70	3.80	3.90	4.10
Air ($m^3.min^{-1}$)	0.010	0.016	0.019	0.021	0.023	0.025	0.027	0.033	0.037	0.039
Angle A	40°	35°	30°	28°	25°	22°	22°	18°	18°	18°
Dimension B (m)	1.8	1.8	1.8	1.8	1.8	1.8	2.1	2.1	2.1	2.7

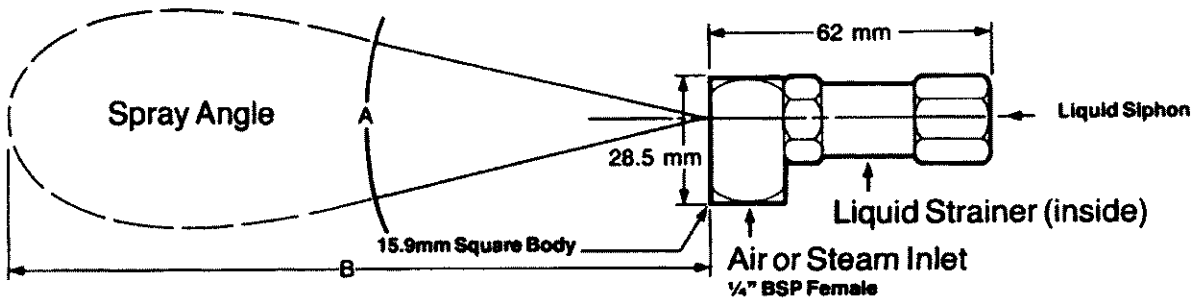

Figure 4.4 – Diagram of Delavan GA1 nozzle atomiser. Source: Delavan Industrial Nozzles and Accessories Manual (2001).

4.1.3 Description of Dryer Control

The CEDRIER software program uses 16 Bit Visual Basic 4.0 and operates under the Windows 3.1 operating system. This program allows the temperatures to be controlled. Once the CEDRIER program has been set up, the equipment can be started up and allowed to reach steady state. Steady state can be determined by observing the temperature readings from the thermocouples, which are displayed on the computer screen. A more detailed description of the dryer control and data logging software is contained in section 4.4 of Southwell (2000). A general description on how the spray dryer was programmed in this work is presented next.

Creating and Executing a Programmed Sequence of Events

A programmed sequence of events can be defined in the program to perform a timed sequence of events. For example, the temperature of the air entering the spray dryer can be set and allowed to remain at that temperature for the desired length of time. This would be accomplished by specifying the heater set-point and then allowing the heater controller to determine when to switch the automatic heater on or off, so that the temperature of the air remains at the set-point temperature. A controlled change of the set-point for the inlet air temperature can also be defined. This controlled change is known as a step. Steps may be grouped into a sequence of events and included in a Process Run List. Once a Process Run List has been specified, the settings must be saved to a unique file prior to running time. Before the spray dryer is ready for an experimental run, a file must be opened to begin the control action. In this work, the file was called loz1.dat.

Observations of the Operating Conditions throughout the Rig

The fans must be turned on manually and one heater must be turned on automatic. A "Mimic" window can be displayed on the computer screen which shows a schematic diagram of the spray dryer and displays the temperature measured by the thermocouples on the diagram. Three diagrams of the dryer system may be displayed including the heater section, dryer section or the whole plant. The control actions can also be monitored on a separate window called "Sequencing" (under Windows in the Menu Bar), which tracks the active file. The operating regime cannot be changed when the program is running. Execution of a process can be suspended any time, but the control action will continue indefinitely and the execution process can be resumed anytime following suspension. The thin bar below the menu bar changes colour constantly, indicating that control action is still occurring. The control action can be ceased by selecting "Shutdown" on the Menu Bar

Logging Data

When the program is running, four files are used to report control actions and for logging temperature measurements at specified intervals, usually every 5 seconds. A normal log file, which reports the temperature measurements, is created as both a binary file (.bnl) and ASCII file (.tnl). A session file, which reports all the changes made by programmed steps and the control actions taken, is also created as both a binary (.bse) and ASCII file (.tse). An ASCII file can be opened in Excel, to read the temperature data, while the binary files can only be read using the control software, as their format is unique. Setting the time interval for data logging (either fast or normal) can be specified at any time as a step in a process when the program is running.

4.1.4 Analogue to Digital Convertor Card

An Analogue to Digital Converter card (PC-74) is fitted to the computer for temperature data collection and control of the dryer inlet air temperature. In this work, the D/A jumpers and fixed jumper settings were set such that the digital output range 0-4095 corresponded to the analogue output range of − 5 V to + 5 V. This analogue output range allowed the thermocouples to measure temperatures below ambient ones, which is important because the wet-bulb temperature of the air (prior to heating) is less than the ambient dry-bulb temperature.

All the thermocouples are connected to the screw terminal board (PC-77) which is connected to the Analogue to Digital Converter card via a ribbon cable. Thus, the screw terminal board provides direct access to all input/output lines to the Analogue to Digital Converter card.

The procedure for calibrating the Analogue to Digital Converter card is given explicitly in the User Manual for the PC-74 card, pages 7-1 to 7-3. The experimental set-up for calibrating the Analogue to Digital Converter card is given in Appendix A1. Southwell (2000) prepared some connections (set of resistors) between the card and precision low-voltage supply to permit calibration of the card. The reference voltage is supplied to the channel and then potentiometers are trimmed as instructed in the manual until the appropriate hexadecimal code is returned by the Analogue to Digital conversion electronics. The hexademical code can be viewed on the computer screen by going to Window, Parameter, Variables and using Channel 0.

The procedure used for specifying values for the conversion between digital and analogue values for the seven thermocouples located around the spray dryer is given in Appendix A2. The procedure for calibrating the thermocouples is described next.

4.1.5 Calibration of Thermocouples

The dry-bulb and wet-bulb thermocouples were calibrated carefully, because the water balance over the spray dryer is sensitive to these measurements. The thermocouples were placed in a temperature controlled water bath. The temperature in the water bath was raised from 15°C to 40°C in 5 degree increments. For readings at 15°C, ice was added to the water bath. When the temperature of the water had stabilised (did not change by more than ±0.5°C), data logging was initiated for approximately 1 minute. The temperature measured by the thermocouples was logged every 5 seconds and stored in a file in the C: drive in a folder called TESTDRY. The files were retrieved and the time average of thermocouple readings was taken for each thermocouple at each water bath temperature. The measurements were repeated, but this time the water was cooled from 40°C to 15°C in 5°C increments by adding ice and stirring the water bath. The wet-bulb thermocouples were also calibrated at 0°C. The average indicated measurements of the temperature for the initial and repeat experiments were taken for each thermocouple.

The three other thermocouples located around the dryer (downstream of the heater, inside the spray dryer and downstream of the spray dryer) were calibrated at 0°C , by placing them in an ice-water bath; and at 100°C, by placing them in a boiling water bath and logging the temperature measurements as described above. The calibration graphs for the thermocouples are given in Appendix A3.

4.1.6 Modification to Spray Dryer for Experimentation

Several modifications were made to the existng spray dryer to enable the wall deposition flux to be estimated. After the "spacer" was installed, silicone was used to seal the windows in the spacer to reduce air leaks. In place of windows that were previously used as sight-glasses, four stainless steel plates were inserted, of dimensions 110 mm by 120 mm, which were held in place by either wing nuts (the upper two plates) or screws (the lower two plates). The location of these plates with respect to the dryer are shown in Figures 4.3 and 4.5. A fifth plate (plate 5) with dimensions 110 mm by 120 mm and a sixth plate (plate 6) with dimensions 110 mm by 110 mm were placed in the conical section of the spray dryer, but at different circumferential locations. The distance from the roof of the spray dryer to the centres of the plates is given in Table 4.2. All the plates were weighed using an analytical balance Mettler AE166 (± 0.0001 g), so that the mass of powder deposited on these plates could be determined. These data are also included in Table 4.2.

Table 4.2 – The distance from the roof of the spray dryer to the centres of the plates and their respective weights.

Plate number	Distance (cm)	Weight (g)
1	22.5	154.608
2	33.5	156.825
3	70.5	148.718
4	81.5	161.940
5	133	153.460
6	142	81.208

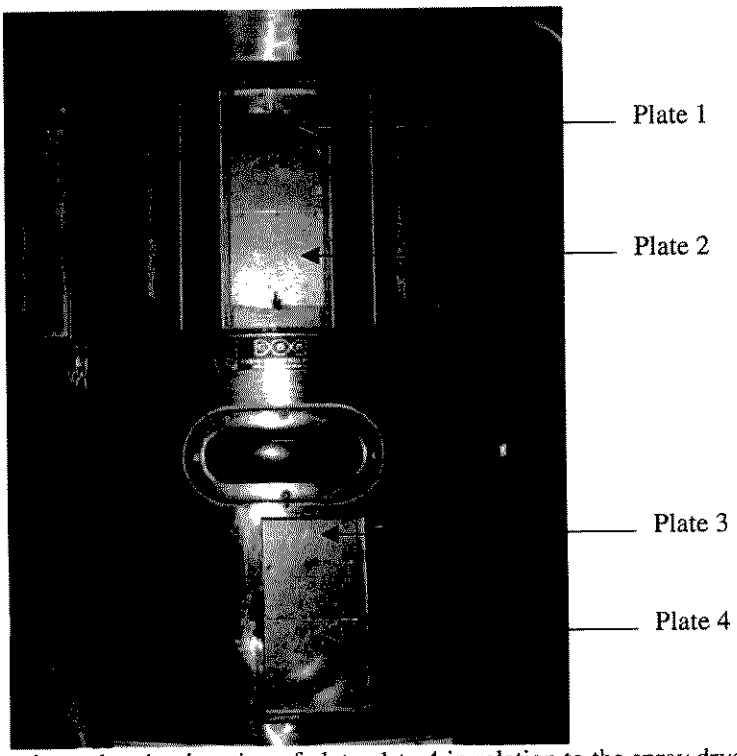

Figure 4.5 – Modifications to spray dryer showing location of plates 1 to 4 in relation to the spray dryer for measuring the wall deposition flux of skim milk powder.

4.1.7 Conclusions

In this section, a general description of the spray dryer, nozzle atomiser and dryer control system used in this work has been provided. The modification to the spray dryer for experimentation has also been described. The next section (4.2) will describe the experimental design used in this work.

4.2 Experimental Design

Experiments were designed in this work with the aim of determining the effect of spray dryer operating parameters on the wall deposition flux of skim milk powder on the interior walls of a spray dryer. In designing the most effective experiments, several factors were considered. These included the choice of material (section 4.2.1) and the spray dryer operating parameters which would be altered and those which would be held constant. First, the swirl vane angle (section 4.2.2), inlet air temperature and liquid feed flowrate (section 4.2.3) were varied in this work, respectively. Second, the effect of surface properties and time on the wall deposition flux was studied (sections 4.2.4 to 4.2.8). Finally, this work tested whether the drying of skim milk powder was limited by particle drying kinetics or equilibrium with the gas (section 4.2.9). The work of previous researchers in the applicability and success of their experiments is also discussed briefly in each of these sections. The protocol for spray drying skim milk and determining the wall deposition flux and moisture content of the resultant skim milk powder is described in section 4.2.10.

4.2.1 Choice of Material to be Spray Dried

As discussed in section 2.1, the production of skim milk powder is an important sector of the Australian dairy industry. Significant requirements in the production of skim milk powder include reducing both the deposition rate of particles on walls and the time period between cleaning cycles. Consequently, skim milk was spray dried in this work. As pointed out by Mahony (2001), skim milk has several advantages when used for experimental purposes. First, skim milk is inexpensive, a significant factor when the product is only being used for research purposes. Secondly, the spray drying of skim milk can be adapted for the relatively small spray dryer available for this research. Thirdly, there are no unmanageable health or safety issues associated with the use of skim milk as a process fluid, as it is not corrosive or otherwise harmful to human health. In addition, skim milk has been characterised, where its sticky-point temperature at various moisture contents was determined by Hennigs *et al.*, (2001) and its glass transition temperature has been determined by Ozmen and Langrish (2002) and reported in Chapter 3 of this thesis. In this work, the brand of skim milk used was Dairy Farmers, produced in Australia. According to Keey (1992), the viscosity of milk concentrates increase on storage, due to the slow denaturing of whey proteins. Thus, it was very important that the skim milk purchased was fresh, prior to spray drying, to eliminate any variability in the

viscosity of the skim milk, which may affect the experimental results through changing the viscosity of the process fluid.

4.2.2 Choice of Inlet Swirl Vane Angle

Southwell and Langrish (2001) found that the extent to which water spray spread out in the drying chamber is affected by the amount of swirl in the inlet air and that this is likely to affect wall deposition fluxes because the water droplets will be closer to the walls if the water spray spreads out widely. The decision to use three swirl vane angles, namely, 0°, 25° and 30° in this work was based on their results. A swirl vane angle of 0° would impart no swirl on the air entering the drying chamber. They found that no single swirl vane angle resulted in behaviour that was clearly steady throughout the dryer, but a swirl vane angle of 25° resulted in good-air spray mixing without excessive spreading of the spray cloud. They also observed that wall deposition of water droplets in the cylindrical section of the spray dryer was unacceptably high for swirl vane angles exceeding 30°.

4.2.3 Choice of Inlet Air Temperature and Process Fluid Flowrate

Drying operating parameters, such as the inlet air temperature, affect the temperature and humidity inside the dryer, which in turn affect the moisture content and temperature of the particles. The stickiness of a material is related to both its temperature and moisture content. As previously described in section 2.6, the sticky-point curve has been used as a semi-quantitative concept in selecting operating conditions for spray drying sticky material.

The temperature of the air entering the drying chamber was the first manipulated variable used. Three inlet air temperatures were used to spray dry skim milk, including 170°C, 200°C and 230°C. Skim milk with a solids content of 50% (weight basis) is typically spray dried using hot air at temperatures of up to 215°C in industry (Shallcross, 2000). The solids content in the skim milk used in this work was approximately 10%, so a slightly higher temperature of 230°C was used as the upper limit for spray drying the skim milk, since the initial moisture content was higher. Considering that the aim of the experiments is to provide an indication of the impact of temperature on the wall deposition flux of skim milk powder, this temperature range of 170°C to 230°C avoids operating problems such as fire hazards.

For these experiments, the inlet air temperature was controlled by the CEDRIER program using the file loz1.dat. For temperatures up to 200°C, only one heater was required to be set on manual, while one heater was set on automatic. For temperatures up to 230°C, a second heater was set on manual to provide enough heat for the temperature of the air to reach the desired set point. The variation in the inlet air temperature was within ± 4°C of the set point. While this degree of variability in control might be considered to be somewhat crude, this range is sometimes seen in commercial operation.

Regarding the effect of the air and liquid flowrates, the spray dryer is equipped with fans that can be set at one speed only, making it simpler to change the liquid feed flowrate rather than the air flowrate. The ratio of liquid to air flowrate is the most important parameter in changing the air and product temperatures (from an energy balance), rather than the actual flowrates themselves, thus it was only necessary to change the liquid flowrate while keeping the air flowrate constant. The liquid feed flowrate could be easily changed by changing the speed of the peristaltic pump, and so was used as the second manipulated variable in the experiments (after the inlet air temperature). The liquid flowrates used in this work and the corresponding pump settings are given in Table 4.3.

Table 4.3 – Pump settings and corresponding feed flowrates.

Pump setting	Feed flowrate (kg hr^{-1})
1	1.4
1.5	1.6
2	1.8

Southwell (2000) estimated that the maximum evaporative capacity of the spray dyer was around 5 kg hr^{-1} during preliminary experiments, with any greater feed rate flooding the bottom pipe and stopping the flow of air from the dryer. Southwell (2000) used water flowrates of 2 to 3 kg hr^{-1} (giving complete evaporation) with the same spray dryer, so the flowrates of skim milk used here were set to be within the evaporative capacity of the unit.

Another variable in the operation of the spray dryer is the temperature of the process fluid. The process fluid temperature is not as important as the inlet air temperature and the ratio of liquid to air flowrates, due to the majority of the enthalpy in the dryer coming from the hot inlet air, and as such the liquid was usually fed at room temperature.

Finally, the compressed air pressure that is used to atomise the liquid feed using the two-fluid nozzle was set. The compressed air flow to the nozzle is supplied from the mains line via a control valve and pressure regulator. The pressure regulator is calibrated in units of pounds per square inch, and can be set with an accuracy of approximately ± 2 psi. The aim is to adjust the air flowrate to give a visible full cone spray pattern, with no liquid feed dripping from the nozzle and causing blockages. Mahony (2001) found that when a compressed air pressure of 40 psi (275 kPa) was used to spray dry skim milk using the same spray dryer, the velocity of the particles was very high and insufficient mixing with the air inside the dryer occurred. However, when she used a compressed air pressure of 20 psi (140 kPa), nozzle blockages were encountered. Thus, a constant compressed air pressure of 30 psi (200 kPa) was used for all the experiments here, since it was half-way between 20 psi and 40 psi.

The base case conditions were a swirl vane angle of 0°, an inlet air temperature of 230°C, and a liquid feed flowrate of 1.8 kg hr^{-1}. The compressed air pressure was held constant at 200 kPa (30 psi) for all the experiments.

4.2.4 Addition of Anti-static agent to Skim Milk

As discussed in section 2.9.7, an anti-static agent Larostat 519 was added to cohesive shale particles, which significantly reduced the electrostatic forces between the particles and between the particles and the walls in a particle flow system. To test the hypothesis that adding an anti-static agent to skim milk would reduce the wall deposition of skim milk powder, a sample of Larostat 519 was obtained from BASF Corporation, Performance Chemicals (New York). 10 g of Larostat 519 was added to 990 g of skim milk, to make a mixture with a concentration of 1% Larostat 519. The Material Safety Data Sheet for Larostat 519 is given in Appendix B1.1.

4.2.5 Grounding the Spray Dryer

To make a preliminary assessment of whether or not electrostatic forces have an influence on the wall deposition flux in the spray dryer, the spray dryer was earthed by connecting the dryer to earth (a water pipe) using conducting car booster cables. Prior to earthing the spray dryer, the resistance between the earth and the dryer was measured to be 0.5 Ω, so the equipment was virtually earthed. When two pairs of car booster cables were connected to the spray dryer from

the water pipe, the resistance dropped to 0.1 Ω. The spray drying conditions used was an inlet air temperature of 170°C, the feed flowrate was 1.84 kg hr, the compressed air flowrate was 30 psi and the swirl vane angle was set to 0°.

4.2.6 Testing the Effect of Surface Properties and Time on Wall Deposition Flux

To test the effect of surface properties and time on the wall deposition flux of skim milk powder, double-backed adhesive tape was placed on plates 5 and 6 and the spray dryer was left to run for 0.5, 1 and 2 hours. These experiments were repeated with the adhesive tape removed, and the plates were cleaned first before being placed back into the spray dryer. The purpose of these experiments was to determine if cohesion or adhesion is likely to be the controlling process in wall deposition in spray dryers, since it was expected that adding an adhesive would increase the chance of particles adhering to the surface. In the final experiments, plates 5 and 6 were coated with a non-stick food grade nylon by PLASDIP COATINGS (Granville, Australia) to determine the effect of changing the wall material of the spray dryer (decreasing the adhesion tendency) on the wall deposition flux.

4.2.7 Increasing the Residence Time of Particles inside the Spray Dryer

It was expected that decreasing the air flowrate of the hot air entering the dryer would increase the residence time of the particles, and this was expected to increase the likelihood of particles impinging on the walls of the spray dryer. Furthermore, if the particles in the spray dryer reach their equilibrium moisture content, then it was expected that increasing the residence time of the particles inside the spray dryer would not influence the equilibrium moisture content of the particles because the dryer is not limited by drying kinetics. To test these two hypotheses, the air mass flowrate was reduced from 0.016 kg s^{-1} to 0.013 kg s^{-1}, by turning the secondary blower off. The base conditions were used to spray dry the skim milk, that is, an inlet air temperature of 230°C, a liquid flowrate of 1.8 kg hr^{-1}, a compressed air pressure of 30 psi and a swirl vane angle of 0°.

4.2.8 Scanning Electron Microscope and Particle Size Analysis

To make a preliminary assessment if agglomeration of particles occurs at the walls of the spray dryer, and thus whether or not cohesion is the controlling process in wall deposition, five small aluminium strips (sample plates) with dimensions 0.4 cm × 2 cm were connected to the wire holding plate 5 onto plate 6. These aluminium strips were left in the dryer for 1 hour to allow skim milk powder to collect on their surface. The base condition for operating the spray dryer was used in this experiment. Two of the sample plates were then coated with platinum and examined under a Philips XL30CP Scanning Electron Microscope (SEM) operating at 10 kV, magnified × 1000.

To investigate further if agglomeration occurs before or during wall deposition, a sample of skim milk powder was taken from the product container and shaken onto a stub covered with a double sided conducting tape. The surface of the stub was coated with platinum and examined under the Scanning Electron Microscope using the same operating settings described above.

The size of the particles leaving the spray dryer was also tested using a Malvern Particle Size Analyser. The Malvern Particle Size Analyser consists of a computer system and an optical unit. The purpose of the optical unit is to collect the information from the scattered light when a laser is passed through the sample. The particle size of the sample that created the scattering pattern of the laser light can then be predicted. First a background measurement was made using iso-propanol (the dispersant). Isopropanol was recommended as a dispersant for skim milk by Pisecky (1997), p. 207. Isopropanol was also recommended as a dispersant by Southwell and Kockel in 1999 when they conducted particle size analysis of grape powder, because they observed that the particles were suspended in the dispersant and that no dissolution occurred. This background measurement is then subtracted from the scattering pattern, with the sample present, to leave only the information from the particles. A small sample of skim milk powder (approximately 10 mg) was suspended in iso-propanol. The Mastersizer estimates the concentration of the sample by measuring the amount of laser light that has been lost by passing through the sample. This is known as the "obscuration" and is given as a percentage. The "obscuration" in the measurement carried out here was 49%, that is 49% of the laser light is lost when it passes through the sample. Samples are usable when the obscuration ranges between 30% and 50% (Malvern User Manual, 1997). The scattering pattern was then measured and the measurement data was analysed by using the "Polydisperse" analysis model which makes no assumptions about the shape of the particle size distribution.

The result was viewed in the form of a histogram and table to provide a final size distribution of the particles.

4.2.9 The Protocol for Spray Drying Skim Milk

As discussed in section 4.1.6, six plates in total were used to measure the wall deposition flux of skim milk powder. Four of these plates (1-4) replaced parts of the dryer walls, while two of these plates (5-6) were supported so that they lay on the conical section of the spray dryer. The protocol for spray drying skim milk is given below:

1. The spray dryer was run for 1.5 hours with just hot air.
2. Water was sprayed for 0.5 hours to be certain the nozzle is operating cleanly.
3. Skim milk was sprayed for 1 hour and then the heater, blowers and peristaltic pump were turned off.
4. The plates were removed from the spray dryer.
5. The plates using an analytical balance Mettler AE166 (± 0.0001 g) to find the mass of skim milk powder deposited on them. The wall deposition flux of the powder was calculated for each plate (in g m^{-2} hr^{-1}) by dividing the mass of powder deposited on the plate by the area of the plate and duration of the experiment.
6. The skim milk powder collected in the product container was weighed into three trays using an analytical balance [Mettler AE166 (± 0.0001 g)], and then the trays containing the powder were placed in the oven for two days at 85°C to determine the moisture content of the sample for that run. The moisture content of the sample was obtained from a decrease in mass. In this work, the drying oven temperature was set to 85°C (as suggested by German Standard DIN) instead of the more common 102°C (International Dairy Federation) because significant browning of skim milk powder was observed at 102°C by Kockel *et al.* (2002). A correction factor of 0.371% w/w was added to the moisture contents measured at 85°C to compare with moisture contents at 102°C, as recommended by de Knegt and van den Brink (1998).
7. The inside of the spray dryer was cleaned before experimenting with new spray drying conditions.

This procedure was repeated for all the operating conditions here.

4.2.10 Conclusions

This section has described the rationale for the experimental operating conditions, with the variable parameters being the inlet air temperatures ranging from 170°C to 230°C, the liquid flowrates of 1.4 kg hr^{-1} to 1.8 kg hr^{-1}, and the swirl vane angles of 0°, 25° and 30°. This section has also presented the method used to determine the effects of surface properties and time on the wall deposition flux of skim milk powder, and whether agglomeration occurs at the walls of the spray dryer or before the particles deposit at the walls. The protocols for spray drying skim milk and determining the wall deposition fluxes and moisture contents of the skim milk powder were also explained.

The following section (4.3) reports the results of using these conditions to perform mass and energy balances across the spray dryer, which assist in establishing the reliability of the experimental measurements in Chapter 5.

4.3 Mass and Energy Balances

Mass and energy balances were conducted over the spray dryer to assess the reliability of the humidity and temperature measurements, by allowing the magnitude of any mass and energy losses to be estimated, compared with expectations, and accounted for in subsequent experiments. The mass balances include both an overall balance (air balance) and a water balance. Initially, only water was sprayed into the air, removing the complication of having to introduce the moisture content of the skim milk into the balances. However, mass and energy balances have also been carried out for the skim milk drying experiments and fermented concord grape skin extract experiments, and these will be reported in Chapter 5 and Chapter 6 of this thesis, respectively.

This chapter initially explains the specific experimental procedures followed when conducting the experiments for the assessment of the mass and energy balances over the spray dryer (section 4.3.1). The results of the mass balance for air (section 4.3.2) and mass balance for water (section 4.3.3) are then discussed. This is followed by a sensitivity analysis (section 4.3.4), which examines the experimental uncertainties, and a propagation of error analysis (section 4.3.5), which examines the impact of random errors on the heat and mass balances. A sensitivity analysis and propagation of error analysis has been conducted for two cases: (i) no water was sprayed into the drying chamber and the drying air was not heated, (ii) water was sprayed into the drying chamber and the drying air was heated. The results of the energy balances (section 4.3.6) are discussed and this is followed by an overall discussion (section 4.3.7). Finally, the conclusions are drawn in section 4.3.8 regarding the accuracy of the mass and energy balances over the spray dryer.

4.3.1 Experimental Procedure

Experimental Conditions

The experimental conditions for the six runs used to calculate the mass and energy balances for the dryer are given in Table 4.4.

Table 4.4- Experimental conditions for the spray dryer when used for assessing mass and energy balances.

Run	Water flowrate (kg s^{-1})	Inlet air temperature (°C)
1	0	Ambient
2	3.9×10^{-4}	170
3	3.9×10^{-4}	200
4	3.9×10^{-4}	230
5	4.4×10^{-4}	230
6	5.1×10^{-4}	230

The rationale for selecting the experimental conditions for run 1 was to test the expectation that the absolute humidities of the air entering and leaving the dryer are equal, and the energy contents of the air entering and leaving the dryer are equal. The rationale for selecting the experimental conditions for runs 2 to 6 was to choose a range of inlet air temperatures used in milk drying because these experimental conditions have also been used to spray dry skim milk by previous workers. The inlet air temperatures and process fluid flowrates used to spray water are specified in section 4.2.3. These conditions were chosen because it is desirable for simplicity in performing mass and energy balances to evaporate all the water in the liquid feed, to prevent complications in these balances due to water collecting on the dryer walls. The compressed air pressure used for the spray nozzle in all the runs here was 140 kPa (20 psi).

Outline of Mass and Energy Balances

The mass balance for air is given by equation 4.1:

$$\text{Mass air in } (m_{a\,in}) = \text{mass air out } (m_{a\,out}) \tag{4.1}$$

The mass flowrate of the air entering and leaving the spray dryer was found in the following way. The velocity of the air entering and leaving the dryer was measured using a hand-held Solomat MPM 500e single hot-wire probe (with temperature compensation), by placing the probe perpendicular to the flow. The velocity of the air was then used to calculate the mass flowrate of the air. Measurements were taken at five separate points across the inlet and outlet ducts of the spray dryer. This allowed the volumetric flowrate to be calculated by integrating the velocity readings across the cross-sectional area of the pipe. The density of the air was calculated using the temperature readings of the air entering and leaving the dryer. The mass flowrate of air entering and leaving the dryer was then calculated by multiplying the density by the volumetric flowrate of the air.

The mass balance for water is given by equation 4.2:

$$\text{Mass water in } (m_{w\ in}) = \text{mass water out } (m_{w\ out}) \tag{4.2}$$

where,

$$\begin{aligned}\text{Mass water in } (m_{w\ in}) = {} & \text{mass flowrate of water sprayed } (m_{w\ s\ pray}) + \\ & \text{mass flowrate of water entering with air } (m_{w\ air\ in}) + \\ & \text{mass flowrate of water entering with compressed air } (m_{w\ comp\ air})\end{aligned} \tag{4.3}$$

For complete evaporation, the mass of water leaving the dryer is:

$$\text{Mass water out } (m_{w\ out}) = \text{mass flowrate of water leaving spray dryer with air } (m_{w\ air\ out}) \tag{4.4}$$

The mass flowrates and absolute humidities of the air entering and leaving the dryer are required to find the mass flowrate of water entering and leaving with the air. The absolute humidity of the air is found using a psychometric chart after measuring the dry-bulb and wet-bulb temperature of the air. The flowrate of water fed into the spray nozzle was obtained from Table 4.2. The absolute humidity of the compressed air was taken to be the same as the absolute humidity of the air entering the dryer. The Delavan Industrial Nozzles and Accessories Manual (2001) suggested that the mass flowrate of the compressed air is 0.0004 kg s^{-1}. Therefore, the mass flowrate of water entering with the compressed air can be found by taking the product of the mass flowrate of compressed air and the absolute humidity of the air.

The energy balance is given by equation 4.5:

$$\text{Energy entering dryer } (H_{in}) = \text{energy leaving dryer } (H_{out} + H_{loss}) \tag{4.5}$$

The energy entering the dryer is given by equation 4.6:

$$\begin{aligned}\text{Energy entering the dryer} = {} & \text{energy entering with air } (H_{in\ air}) + \\ & \text{energy entering with water } (H_{in\ water}) + \\ & \text{energy entering with compressed air } (H_{in\ comp\ air})\end{aligned} \tag{4.6}$$

The energy leaving the dryer is given by equation 4.7:

$$\text{Energy leaving the dryer} = \text{energy leaving the dryer with the air } (H_{out\ air}) + \text{energy losses } (H_{loss}) \quad (4.7)$$

The temperature and absolute humidity of the air entering the drying chamber is required to calculate the energy of the air and water vapour (present in the air) entering the dryer. The mass flowrate and temperature of the process fluid, in this case water, pumped to the spray nozzle is required to calculate the energy of the water entering the spray dryer. If skim milk is sprayed, the composition of the skim milk is required, to calculate the mass flowrate of milk solids and water and then the energy of skim milk entering the dryer can be calculated. The outlet dry-bulb temperature and humidity are used to calculate the energy of the air leaving the dryer.

4.3.2 Mass Balance for Air

The air velocity was measured for runs 1, 3 and 5. Appendix B2 provides the air velocity readings for these runs. The mass balances for the air flowrate are shown in Table 4.5.

Table 4.5 – Mass balance for air over spray dryer.

Run	$m_{a\ in}$ (kg s^{-1})	Standard deviation for $m_{a\ in}$ (kg s^{-1})	$m_{a\ out}$ (kg s^{-1})	Standard deviation for $m_{a\ out}$ (kg s^{-1})	Discrepancy (kg s^{-1})	Discrepancy (%)
1	0.0150	0.0004	0.0250	0.0005	0.0095 ± 0.0007	67
3	0.0160	0.0004	0.0130	0.0006	-0.0030± 0.0007	-19
5	0.0160	0.0004	0.0130	0.0006	-0.0030± 0.0007	-19

Table 4.5 shows that the greatest discrepancy between the calculated inlet and outlet air flowrates was 67% for run 1. The maximum standard deviation in the air flowrate was 0.0006 kg s^{-1} (5%). The inlet air flowrates measured for runs 3 and 5 are identical ($m_{a\ in}$ = 0.016 kg s^{-1}) and may represent the true air flowrates entering and leaving the dryer system, since this value for the mass flowrate was reproducible. The value for the mass flowrate of the air entering the dryer was used as the mass flowrate of the air leaving the dryer when calculating

the outlet water flowrate for the water balance and the outlet energy flowrate for the energy balance. There are four reasons for doing this:

1. The velocity profile at the outlet was much more non-uniform than that at the inlet, so the integration of the outlet velocity profile has a much higher uncertainty.
2. High turbulence intensities (as at the outlet) reduce the accuracy of velocity measurements using a single hot-wire probe (Goldstein, 1996). The air velocity fluctuated by ± 0.5 m s^{-1} due to air turbulence. An uncertainty of 1% (BEP Engineering Products, Australia) of the full scale of the instrument (30 m s^{-1}) which is 0.3 m s^{-1}, is also possible in the air velocity.
3. The velocity measurements in a converging section (here, the inlet) are much more reliable than those at a diverging section (here, the outlet) (Goldstein, 1996).
4. Air is likely to be leaking out of the dryer from small holes and connecting pipework around the dryer, because the dryer is under a slight positive pressure. If the discrepancy between inlet and outlet air mass flowrates is due to air leaking out of the dryer, the practice of using the inlet mass flowrate for the water mass balance is justified because the properties of the leakage air (i.e. temperature and humidity) will be close to those of the outlet air. The true outlet mass flowrate of air should be equated to the inlet mass flowrate because what is measured at the outlet is only the flowrate through the pipe and not the flowrate of leakage air.

Thus, the inlet air mass flowrate will be used in calculations from here onwards because it has a higher degree of accuracy and less uncertainty than the outlet measurements.

4.3.3 Mass Balance for Water

The data used to calculate the water balances is given in Appendix B2-B4. The results for the mass balance for water are shown in Table 4.6.

Table 4.6 - Mass balance results for water over the spray dryer.

Run	$m_{w\ air\ in}$ (kg s^{-1})	$m_{w\ spray}$ (kg s^{-1})	$m_{w\ in}$ (kg s^{-1})	$m_{w\ out}$ (kg s^{-1})	Discrepancy (kg s^{-1})	Discrepancy (%)
1	1.7×10^{-4}	0	1.7×10^{-4}	1.8×10^{-4}	7.9×10^{-6}	5
2	1.7×10^{-4}	3.9×10^{-4}	5.6×10^{-4}	5.0×10^{-4}	-6.1×10^{-5}	-11
3	1.7×10^{-4}	4.4×10^{-4}	6.1×10^{-4}	4.7×10^{-4}	-1.3×10^{-4}	-22
4	1.4×10^{-4}	5.1×10^{-4}	6.5×10^{-4}	5.1×10^{-4}	-1.4×10^{-4}	-21
5	1.5×10^{-4}	4.4×10^{-4}	5.9×10^{-4}	4.7×10^{-4}	-1.2×10^{-4}	-20
6	1.4×10^{-4}	5.1×10^{-4}	6.5×10^{-4}	5.0×10^{-4}	-1.6×10^{-4}	-24

All results are based upon the inlet air mass flowrate measurements, as these are considered more accurate than the outlet readings, although there is still some uncertainty in the measurement. The water mass balances were, on average, 14% worse when using both the measured inlet and the measured outlet air mass flowrates. This result also suggests that the practice here of using the inlet mass flowrate is reasonable.

Table 4.6 shows that for all the runs, except for run 1, the discrepancy in the water balance ranged from –11% to –24%. Run 1 appears to be considerably more accurate, with a discrepancy of 5% or 7.9×10^{-6} kg s^{-1}, which corresponds to the absence of water spraying, which contributes additional uncertainty to the analysis of runs 2-6. In real terms, the mass losses from all the runs, apart from runs 1 and 2, are of the order of 10^{-4} kg s^{-1}. The discrepancies may be due to several reasons:

1. Mass losses can occur through parts of the dryer that are not completely sealed, such as the cavity in which the spray nozzle sits, which might account for the different apparent water flowrates leaving the spray dryer compared with the water flowrates entering the spray dryer.
2. Unevaporated water would need to be accounted for in the balances, however at temperatures of 170°C and above (as used in this work), it is extremely unlikely, and droplets of water inside the spray dryer were not observed for any run.
3. Condensation in the pipes could cause a discrepancy, however, this is unlikely due to the pipes being trace heated to 50°C (above the dew-point temperature of the outlet gas).
4. The dry-bulb and/or wet-bulb thermocouples may be inaccurate and/or variable, causing errors and uncertainties in the measurements, but the calibration procedure for the thermocouples is likely to have minimised any systematic errors in the measurements.

In order to establish whether the uncertainties in the dry-bulb and wet-bulb thermocouples could have led to the discrepancies in the water balance, an analysis of the uncertainties is conducted next.

4.3.4 Sensitivity Analysis and Propagation of Error and Uncertainties

Uncertainties in the thermocouple measurements will propagate through to uncertainties in the humidity of the air entering and leaving the dryer. To eliminate systematic error from offset uncertainty, the thermocouples have been calibrated, but a random uncertainty of ± 0.6°C is inevitable due to the resolution of the analogue to digital converter. The digital output range of 0 to 4095 corresponds to an analogue range of –5 V to + 5V (10 V). The thermocouple output range is also amplified by a factor of ten. Since the analogue output range corresponds to a temperature range of 0°C to 250°C, the normal amount of uncertainty in the temperature reading is $\frac{10\times(250-0)}{4096} = 0.6^{\circ}\mathrm{C}$.

An analysis of the sensitivity of the absolute humidity of the air entering the dryer (Y_i) and leaving the dryer (Y_o) to the dry bulb and wet bulb temperature readings using experimental values from run 1 and 2 is provided in Appendix B5. The sensitivity analysis shows that the calculation of the absolute humidity of the air is more sensitive to the wet-bulb temperatures than to the dry-bulb temperatures. The sensitivity analysis demonstrates the importance of correct wet-bulb temperature measuremens for accurate results. Even with a random uncertainty in the wet-bulb temperature of ±0.6 K, the uncertainty of Y_i is:

$$\frac{\partial Y_i}{\partial T_{w\,out}} \times \partial T_{w\,out} = 0.0010\ \mathrm{kg\ kg^{-1}\ K^{-1}} \times 0.6\ \mathrm{K}$$

$$= 0.0006\ \mathrm{kg\ water/kg\ dry\ air}$$

Thus, even if systematic error is eliminated and considering that the outlet humidity is 0.011 kg water/kg dry air, an uncertainty of 5% will still exist for Y_i under these conditions. Since the absolute humidity is used to calculate further results for mass and energy balances, it is important to take several wet-bulb temperatures and to average them in order to reduce the random uncertainty in the results. The propagation of errors in the water balances from random uncertainty in the experimental measurements for run 1 and 2 is given in Appendix B5 and the results are summarised next.

For run 1, the uncertainty in the water balance discrepancy (3.0×10^{-5} kg water s^{-1}) is greater than the discrepancy itself (1.0×10^{-5} kg water s^{-1}). Thus, the discrepancy could possibly be zero within the uncertainties in the measurements. This result supports the expectation that the absolute humidity of the air should not change when no water is sprayed into the drying chamber.

For run 2, the uncertainty in the water balance discrepancy is 4×10^{-5} kg water s^{-1}. The uncertainty in the discrepancy accounts for 67% of the discrepancy. A number of temperature readings were recorded for each thermocouple per run, and these readings were averaged to reduce the uncertainty from random error. The results for the energy balances are discussed next.

4.3.5 Energy Balances

Results

Appendix B3 and B6 provides the data for calculating the energy balances over the spray dryer. Table 4.7 shows the energy balances over the spray dryer.

Table 4.7 - Energy balance results over the spray dryer.

Run	Heat in (kW)	Heat out (kW)	Heat loss (kW)
1	0.81	0.84	-0.03
2	3.26	2.14	1.12
3	3.72	2.21	1.52
4	4.26	2.46	1.81
5	4.30	2.32	1.97
6	4.28	2.33	1.95

Note that no heating was used for run 1. The inlet heat value of 0.8 kW reflects the use of 273 K (0°C) as a reference temperature.

Discussion of Energy Balances

The increase in energy for run 1 is 30W. In Appendix B5, a propagation of errors analysis is provided for run 1 to determine if the discrepancy in the heat balance for this run could possibly be zero within the uncertainties of the measurements.

In summary, the discrepancy in the heat balance is = 0.03 ± 0.08 kW. Since the uncertainty in the discrepancy is greater than the discrepancy itself, the discrepancy could possibly be zero within the uncertainties in the measurements. Thus, there may well be no real increase in energy across the spray dryer when the air is not heated.

A propagation of errors analysis was also carried out for run 2 in Appendix B5, which was the case where water was sprayed and the air entering the dryer was heated. The results are summarised below.

The inlet enthalpy from equation 4.6 is:

$$H_{in} = H_{in\,air} + H_{in\,water} + H_{in\,comp\,air} \tag{4.8}$$

$$\begin{aligned} H_{in} = {} & m_a C_{pa,i}(T_{hot\,air} - T_{ref}) + m_a Y_i[\lambda + C_{pw,v_{in}}(T_{hot\,air} - T_{ref})] + m_w C_{pw}(T_{water} - T_{ref}) + \\ & m_{ca} C_{pca,i}(T_{ca} - T_{ref}) + m_{ca} Y_i[\lambda + C_{pw,v_{in}}(T_{ca} - T_{ref})] \end{aligned} \tag{4.9}$$

where $C_{pca,i}$ and C_{pw} are the heat capacities of the compressed air entering the dryer and the water sprayed into the dryer, respectively (in kJ kg^{-1} K^{-1}), m_w is the mass flowrate of the water sprayed into the dryer (in kg s^{-1}), T_{water} is the temperature of the water (in K) and T_{ca} is the temperature of the compressed air (in K), which were both taken as ambient, and m_{ca} is the mass flowrate of compressed air entering the dryer (in kg s^{-1}).

The heat loss is given by equation 4.10:

$$\begin{aligned} H_{loss} &= H_{in} - H_{out} \\ &= 1.1 \pm 0.1\,\text{kW} \end{aligned} \tag{4.10}$$

The uncertainty in the discrepancy in the energy entering and leaving the dryer accounts for 18% of the discrepancy. The most likely cause of the difference between the inlet and outlet energy is heat losses from the spray dryer and connecting pipework, as will now be demonstrated.

Heat loss is a function of the heat transfer coefficient from the dryer walls to the ambient environment, as well as the area for heat transfer and the temperature driving force between the outside of the dryer and the ambient air. These are related by the following equation:

$$Q_{loss} = \sum UA\Delta T \tag{4.11}$$

The heat transfer to the ambient air, which occurs largely due to natural convection, is likely to be the rate limiting step for heat loss from the dryer walls. Typical values for the heat transfer coefficient are U=10-20 W m^{-2} K^{-1} (Welty, 1978).

The area over which the heat loss from the spray dryer occurs will now be calculated. The dryer has an external diameter of 0.9 m, and has approximate heights of 1.3 m in the cylindrical section (including the spacer), and 0.63 m in the conical section. The approximate area of the dryer for heat loss is therefore:

$$\begin{aligned} A_{dryer} &= \pi DL + \pi rs \\ &= \pi \times 0.9 \times 1.3 + \pi \times 0.45 \times 0.77 \\ &= 4.76\ \text{m}^2 \end{aligned} \tag{4.12}$$

Heat losses also occur to the external environment from the connecting pipework of the spray dryer. The connecting pipework has a diameter of 0.1 m, and is approximately 5 m in length. Thus, the area over which heat loss occurs from the pipework is:

$$\begin{aligned} A_{pipe} &= \pi DL \\ &= 1.57\ \text{m}^2 \end{aligned}$$

Thus, the total area over which the heat transfer occurs is approximately 6.3 m^2. The external walls of the dryer were at temperatures up to 45°C, especially for the latter runs, therefore a

temperature gradient between the dryer walls and the external air of 25 K is possible. The estimated heat loss is:

$$Q_{loss} \approx (10 - 20)\ \text{W.m}^{-2}\ \text{K}^{-1} \times 6.3\ \text{m}^2 \times 25\ \text{K}$$

$$Q_{loss} \approx 1.5 - 3.1\ \text{kW}$$

This estimated heat loss is very close to that measured for runs 2-6, where the heat loss values were between 1.1 kW and 2.0 kW, suggesting that the discrepancy in the energy balance can be largely explained by heat losses.

4.3.6 Overall Discussion

Several factors can affect the reliability and comparability of the mass and energy balances, such as systematic and random errors.

Systematic and Random Errors

The thermocouples were calibrated to eliminate systematic error. Another type of systematic error that could occur from taking temperature measurements is that the wet-bulb wick could partly dry out, and the indicated temperature would be higher than the true value. The relative humidity of the air entering the spray dryer was 65%, while the relative humidity of the air leaving the spray dryer was 20%. The outlet wet-bulb thermcouple wick is most likely to dry out when the relative humidity is low. To eliminate this possible systematic error, the wick of the outlet wet-bulb thermocouple was wetted with water, and once the indicated temperature (measured by the thermocouple) stabilised, a reading was taken. Furthermore, the propagation of error analysis in section 4.3.5 revealed that all but 33% of the discrepancy found in the water balance can be attributed to random error.

If there was a systematic error in the cold junction temperature, then all the temperatures measured by the thermocouples would be systematically in error by the same amount. If there was a systematic error of 2°C, the effect on the measured absolute humidity of the air entering and leaving the spray dryer and the mass and energy balances for run 2 would be as given in Table 4.8 to 4.10.

Table 4.8 – The effect on the measured absolute humidity of the air, if there was a systematic error of 2°C in the cold junction temperature.

Run	Y_i (kg kg^{-1})	Y_o (kg kg^{-1})
2	0.0110	0.0315
2 (systematic error)	0.0125	0.0370

Table 4.9 – The effect on water balance for run 2, if there was a systematic error of 2°C in the cold junction temperature.

Run	Water in (kg s^{-1})	Water out (kg s^{-1})	Discrepancy (kg s^{-1})	Discrepancy (%)
2	5.59×10^{-4}	4.98×10^{-4}	-6.14×10^{-5}	-11.0
2 (systematic error)	5.83×10^{-4}	5.85×10^{-4}	1.83×10^{-6}	0.3

Table 4.10 – The effect on energy balance for run 2, if there was a systematic error of 2°C in the cold junction temperature.

Run	Heat in (kW)	Heat out (kW)	Discrepancy (kW)
2	3.26	2.14	-1.12
2 (systematic error)	3.34	2.43	-0.91

Table 4.8 shows that the measured absolute humidity of the air increased by 12-15% if there was an error of 2°C in the cold junction temperature. Table 4.9 and 4.10 show that a systematic error of 2°C in the cold junction temperature explains most of the discrepancy in the water balance, while it does not have a large effect on the energy balance.

4.3.7 Conclusions

This chapter has presented the results of the mass and energy balances across the spray dryer for air and water under the conditions given in Table 4.4. The mass balances for air resulted in errors up to 67%, which were identified as being due to less accurate velocity measurements obtained from the outlet of the spray dryer. Since the more accurate readings were obtained from the inlet conditions, these inlet air mass flowrates were used for subsequent calculations.

The mass balances for water contained discrepancies of up to 24%. All but 33% of the discrepancy can be attributed to random error. A systematic error of 2°C in the cold junction temperature can explain most of the discrepancy in the water balance. The energy balance for run 1 (no water spraying and no inlet air heating) was accurate within the uncertainties of the measurements, however, there were discrepancies of 1-2 kW for runs 2-6 (water spraying and

inlet air heating). These discrepancies are probably due to heat losses from the walls and pipes of the spray dryer. Overall, the mass and energy balances given in this chapter establish the uncertainties that can be expected in measurements in this spray dryer. The following chapter (5) uses similar operating conditions to produce skim milk powder, and to determine the wall deposition flux for this material.

Chapter 5

Wall Deposition Fluxes for Skim Milk Powder

The aim of the work reported in this chapter was to quantify the effect of the following parameters on the wall deposition flux of skim milk powder on the interior walls of a pilot-scale short-form spray dryer of a modified Niro design:

1. The swirl vane angle, which imparts swirl to the incoming air and affects the stability of the flow patterns and spray cloud in the spray dryer, and
2. The inlet air temperature and process fluid flowrate, which affect the particle temperatures and moisture contents, with respect to the sticky-point curve, and
3. Wall properties: surface material, namely non-stick food grade material (nylon), adhesive tape and stainless steel, and
4. Electrostatic effects such as grounding the spray dryer; and
5. Altering the properties of the process fluid by adding an anti-static agent, and
6. A combination of surface material and time, which addresses a fundamental question in the field of spray drying; if cohesion occurs at the same rate as adhesion for skim milk powder in this spray dryer.

This work has also addressed another fundamental question in the field of spray drying; whether the outlet particle moisture content and temperature are equilibrium limited or controlled by drying kinetics for this equipment.

This chapter is organised as follows. Section 5.1 reports and then discusses the mass and energy balances for spray drying skim milk. Section 5.2 discusses the symmetry of the wall deposition fluxes within the dryer and reports the estimate of the uncertainty for these fluxes. Section 5.3 reports and then interprets the effect of the swirl vane angle on the wall deposition

fluxes. Section 5.4 reports the effect of the inlet air temperature and process fluid flowrate on the wall deposition fluxes. This section also discusses the interaction of the particle temperature and moisture content (which are related to the spray dryer operating conditions) with the sticky-point curve of skim milk power. A sample calculation of an iterative procedure to predict the effect of inlet air temperature and process fluid flowrates on particle temperature and moisture contents relative to the sticky-point curve is given in this section. A sample calculation showing the impact of reducing the inlet air temperature on the productivity of the spray dryer (if this is necessary to reduce the stickiness of the particles) is also given in this section. Section 5.5 reports the effect of electrostatics, more specifically, the effects of adding an anti-static agent to the skim milk prior to spray drying and grounding the spray dryer on the wall deposition fluxes. Section 5.6 reports the effect of changing the wall properties of the spray dryer and time on the wall deposition fluxes. Finally, section 5.7 provides the overall discussion and conclusions for the work reported in this chapter.

5.1 Mass and Energy Balances

5.1.1 Operating Parameters Varied

A total of 34 experiments were carried out for this work. Tables 5.1 to 5.3 provide a list of the spray dryer operating parameters used for each run, in the order that the experiments were carried out to spray dry the skim milk. The aim of these experiments was to determine the effect of three operating parameters, namely, the swirl vane angle, inlet air temperature and process fluid flowrate, which from here onwards will be called the feed flowrate, on the wall deposition fluxes and to find conditions which give rise to the lowest wall deposition fluxes. Three swirl vane angles were used in this work, including 0^{o}, 25^{o} and 30^{o}, three inlet air temperatures, including 170°C, 200°C, and 230°C, and three feed flowrates, including 1.4 kg hr^{-1}, 1.6 kg hr^{-1}, and 1.8 kg hr^{-1}. The compressed air pressure was held constant at 200 kPa for all the runs. The base case conditions were a swirl vane angle of 0^{o}, an inlet air temperature of 230°C, and a liquid feed flowrate of 1.8 kg hr^{-1}, and a spray dryer running time of 1 hour. For the first set of experiments (runs 1-9), the swirl vane angle was varied while the feed flowrate and inlet air temperature were held constant (Table 5.1). For the second set of experiments (runs 10-15), the inlet air temperature was varied while the feed flowrate and swirl vane angle

were held constant (Table 5.2). For the third set of experiments (runs 16-21), the feed flowrate was varied while the inlet air temperature and swirl vane angle were held constant (Table 5.3).

Table 5.1- Operating parameters for spray drying skim milk, testing the effect of different swirl vane angles at a single feed flowrate (1.8 kg hr^{-1}), inlet air temperature (230°C) and compressed air pressure (200 kPa).

Run	Date experiment done	Swirl vane angle
1	4/09/01	0°
2	4/09/01	0°
3	6/09/01	25°
4	6/09/01	25°
5	12/09/01	0°
6	13/09/01	25°
7	8/10/01	30°
8	9/10/01	30°
9	9/10/01	30°

Table 5.2 - Operating parameters for spray drying skim milk, testing the effect of different inlet air temperatures at a single feed flowrate (1.8 kg hr^{-1}), swirl vane angle (0°) and compressed air pressure (200kPa).

Run	Date experiment done	Inlet air temperature (°C)
10	21/11/01	170
11	22/11/01	170
12	22/11/01	170
13	22/11/01	200
14	23/11/01	200
15	23/11/01	200

Table 5.3 - Operating parameters for spray drying skim milk, testing the effect of different feed flowrates at a single swirl vane angle (0°), inlet air temperature (230°C) and compressed air pressure (200 kPa).

Run	Date experiment done	Feed flowrate (kg hr^{-1})
16	27/11/01	1.6
17	28/11/01	1.6
18	28/11/01	1.6
19	28/11/01	1.4
20	29/11/01	1.4
21	29/11/01	1.4

The operating conditions from run 10, where the inlet air temperature was 170°C, the feed flowrate was 1.8 kg hr^{-1}, the swirl vane angle was 0° and the compressed air pressure was 200 kPa, were used to determine the influence of wall properties on the wall deposition flux (Table 5.4).

Table 5.4 - Studying the influence of wall properties and electrostatic effects on the wall deposition flux of skim milk powder.

Run	Date experiment done	Spray dryer grounded	Adhesive on plate 5 and 6	Duration of experiment (hours)
22	4/12/01	✔		1
23	6/12/01	✔		1
24	6/12/01	✔		1
25	10/12/01	✔		1
26	10/12/01		✔	1
27	12/12/01			0.5
28	12/12/01			1
29	12/12/01			2
30	13/12/01		✔	0.5
31	13/12/01		✔	2

The spray dryer was grounded for the fourth set of experiments (runs 22-25). For the fifth set of experiments (runs 26, 30 and 31), double-sided adhesive tape was placed on plates 5 and 6, and the spray dryer was allowed to run for 0.5 hour, 1 hour and 2 hours, respectively. These experiments were repeated for the sixth set of experiments (runs 27-29), but this time no adhesive was placed on plates 5 and 6. Using the base case conditions, one experiment (run 32) was carried out to determine the effect of changing the wall material of the spray dryer on the wall deposition flux, where plates 5 and 6 were coated with non-stick food grade nylon (Table 5.5). Thermal insulation was also placed behind plates 1 to 4 (which were initially uninsulated) for this run only to determine if insulation has a significant effect on the wall deposition fluxes. Two experiments (runs 33-34) were also carried out to determine if increasing the residence time of particles in the spray dryer by decreasing the air flowrate increases the wall deposition flux. It was expected that when the particles are in the dryer for a longer period of time, they might be more likely to impact on the dryer walls and thus increase the wall deposition flux significantly. Furthermore, the measured moisture content of the skim milk powder from these two experiments may indicate if there are any significant kinetic limitations in drying skim milk powder. If there is no change in the difference between the product moisture content and the equilibrium moisture content of the skim milk powder, then it is possible that there may not be any significant kinetic limitations in drying skim milk. The full wall deposition flux and particle moisture content data for each of the above runs are given in Appendix C1 and the full mass and energy balances data for spray drying skim milk are given in Appendix C2.

Table 5.5 - Studying the influence of different surface material and residence time on the wall deposition flux of skim milk powder.

Run	Date experiment done	Nylon coated plates used	Inlet air flowrate decreased	Feed flowrate (kg hr^{-1})
32	20/2/02	✔		1.4
33	15/2/02		✔	1.8
34	1/3/02		✔	1.8

As shown in Appendix C2, the discrepancies in the water balance for the conditions in Tables 5.1 to 5.5 ranged from –38% to –2%. Also, as shown in Appendix C2, the discrepancies in the energy balance for the conditions in these tables ranged from –1.0 kW to –2.6 kW. From section 4.3 of Chapter 4 of this thesis, the discrepancies in the water balance when spraying just water ranged from -24% to 5%; the discrepancy in the energy balance from spray drying just water ranged from 0.03 kW to –2.0 kW. Thus, the water and energy balance discrepancies when spray drying skim milk appear to be reasonable, because they are consistent with the results for spraying water alone.

5.2 The Symmetry of the Wall Deposition Fluxes within the Spray Dryer and an Estimate of the Uncertainty for these Fluxes

The wall deposition flux was calculated by dividing the mass of powder by the area of the plate and the duration of the experiment. Figure 5.1 shows the plates after a typical experiment. Plates 5 and 6, located in the conical section of the dryer, had a higher wall deposition flux of skim milk powder (by 97% to 98%) compared with the other plates (1-4). The conical section of the spray dryer was most directly subject to spray impaction of particles due to the spray cone angle and the shape of the dryer (Figure 5.2).

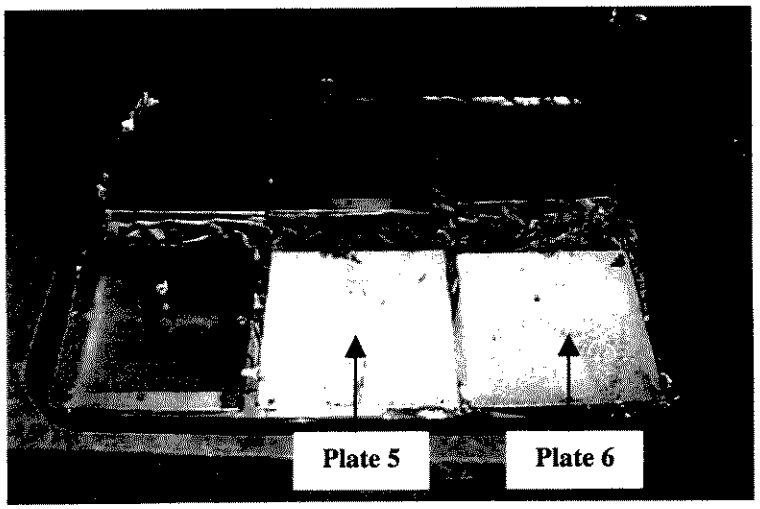

Figure 5.1 - Photographs showing all plates at the end of a run. Plates 5 and 6 are covered with a larger quantity of skim milk powder compared with the other plates.

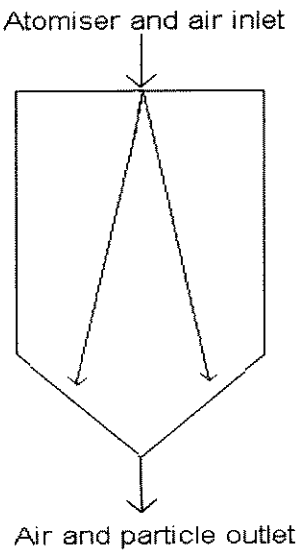

Figure 5.2 - Schematic diagram showing the spray impaction of particles on the conical section of the spray dryer.

The first four plates were inserted in place of the dryer windows and were not insulated as were the other spray dryer walls. Chen *et al.* (1993) noted that when an inspection window was insulated, the window site was almost free from deposition. They concluded that the effect of insulation was to decrease wall deposition by increasing the temperature close to the window, preventing both vapour condensation and the particles being too moist. Therefore, it is possible that the lack of insulation on the plates may affect the amount of wall deposition compared with the actual insulated dryer walls. Accepting the arguments presented by Chen *et al.* (1993), this would suggest that the rate of particle deposition on the first four plates is likely to exceed the rate of deposition on the actual spray dryer walls. However, the fact that the deposition fluxes on these plates (1-4) is so much lower than those on plates 5 and 6 (which

were resting on insulated walls) may make the question of whether the deposition flux on these plates (1-4) is significantly affected by insulation (or not) a less critical issue. The wall deposition fluxes for plates 1 to 4 are also reported in Appendix C1. Another relevant aspect here is that industrial spray dryer walls are typically insulated, so the results from plates 5 and 6, which were effectively insulated in the same way as a typical spray dryer in industry, are probably relevant to those in industrial practice. Due to the fact that plates 5 and 6 were subject to some degree of spray impaction from the nozzle, and spray impaction is unusual in industrial dryers, the quantitative deposition rates measured here may be different to those in industry. However, the outlet moisture contents of the skim milk powder were within 0.4% of the equilibrium values, suggesting that it is possible that the particles impacting on the plates were close to being in equilibrium with the gas. Therefore, it is unlikely that semi-solid particles impacted on these plates.

Table 5.6 shows the wall deposition flux of skim milk powder on plates 5 and 6. The maximum deposition flux was sometimes calculated to be the highest for plate 5 and at other times for plate 6. The two plates were at similar heights in the cone, but at different circumferential positions. The centre of plate 5 was 1.33 m below the roof of the dryer, while the centre of plate 6 was 1.42 m below the roof of the dryer. There was no apparent trend of a particular plate always having the highest wall deposition flux. The deposition fluxes are similar on both plates, suggesting that there is no particular influence of an angle effect from the spray nozzle over the time scale in these experiments. Furthermore, this result suggests that uniform deposition around the dryer circumference cannot be discounted, so any time-dependency in the flow patterns is likely to be on a much shorter time scale than the duration of these experiments (one hour). This finding is consistent with the work of Southwell and Langrish (2001), which suggests that the main oscillations in the flow patterns occur over time scales of less than 10 seconds. Therefore, the time-dependent wall deposition fluxes resulting from such flow oscillations appear to average out over time scales of one hour. Given the absence of any systematic trend between plates 5 and 6, the average of the wall deposition flux on plate 5 and 6 was taken because taking an average reduces the effect of the measurement uncertainty in the wall deposition flux. Figure 5.3 is a photograph taken using a hand-held pocket camera, showing the wall deposits of skim milk powder on the interior walls of the spray dryer after the spray dryer had been run for about four times. The six plates used for measuring the wall deposition fluxes of skim milk powder were cleaned between runs, but the walls and toughened fibre glass windows of the spray dryer were not cleaned between runs. Figure 5.3 shows that there is little apparent difference between the amounts of milk deposited

as a function of circumferential location. Therefore, for a symmetrical spray dryer such as this one, at least, the wall deposition does not appear to be influenced by the circumferential location in the spray dryer.

Figure 5.3 – Photograph showing that wall deposition is not influenced by the circumferential location in the spray dryer because the skim milk powder is evenly spread out.

Table 5.6 - Wall deposition fluxes of skim milk powder for swirl vane angle of 30°, feed flowrate of 1.8 kg hr^{-1}, inlet air temperature 230 °C, and compressed air pressure 200 kPa.

Runs	Deposition flux on plate 5 (g m^{-2} hr^{-1})	Deposition flux on plate 6 (g m^{-2} hr^{-1})
7	11.5	10.9
8	15.2	16.1
9	11.7	12.3
Average	12.8	13.1
Standard deviation	2.4	3.0

Considering the difference between the measured deposition fluxes on each plate in Table 5.6, these differences are between 0.6 and 0.9 g m^{-2} hr^{-1}, with no systematic trend. These differences suggest that there is a random uncertainty in the measurement method of around 1 g m^{-2} hr^{-1} in each individual experiment. For the same experimental inlet conditions, the standard deviation of the deposition fluxes for these runs is around 3 g m^{-2} hr^{-1}, so it is possible that the uncertainty is higher than estimated from the plate-to-plate comparison, so there may be an uncertainty of ± 3 g m^{-2} hr^{-1}. However, three significant figures are given in this table because the deposition fluxes are averaged over 3 experiments, so the uncertainty in such an average is $\pm\frac{3}{\sqrt{3}} \cong 1.7\,\mathrm{g\,m^{-2}\,hr^{-1}}$, since the uncertainty in an average of three measurements is reduced by a factor of $\sqrt{3}$ (Kirkup, 1994). The results from studying the effect of swirl vane

angle, and thus the stability of flow patterns in the spray dryer on the wall deposition fluxes, will be discussed next.

5.3 The Effect of the Swirl Vane Angle on the Wall Deposition Fluxes of Skim Milk Powder

The swirl vane angle was varied to determine the influence of swirl in the inlet air on the wall deposition flux of skim milk powder. A single inlet air temperature (230°C), compressed air pressure (200 kPa) and skim milk feed flowrate (1.8 kg hr^{-1}) were used. Figure 5.4 shows the average wall deposition fluxes for skim milk powder and the average outlet moisture content of the powder on a dry basis, when the swirl vane angles were 0°, 25° and 30°. The maximum wall deposition flux was 13 g m^{-2} hr^{-1} when the swirl vane angle was 30°, while the minimum wall deposition flux was 7 g m^{-2} hr^{-1} when the swirl vane angle was 0°, so increasing the swirl vane angle from 0° to 30° increased the wall deposition flux by 44%. Figure 5.4 also shows that there was a steep rise in the wall deposition flux when the swirl vane angle was changed by only 5° from 25° to 30°, which is consistent with the work by Southwell (2000) in the same dryer. Southwell (2000) sprayed water only, and found a substantial increase in wall deposition (qualitatively) when the swirl vane angle was increased from 25° to 30°.

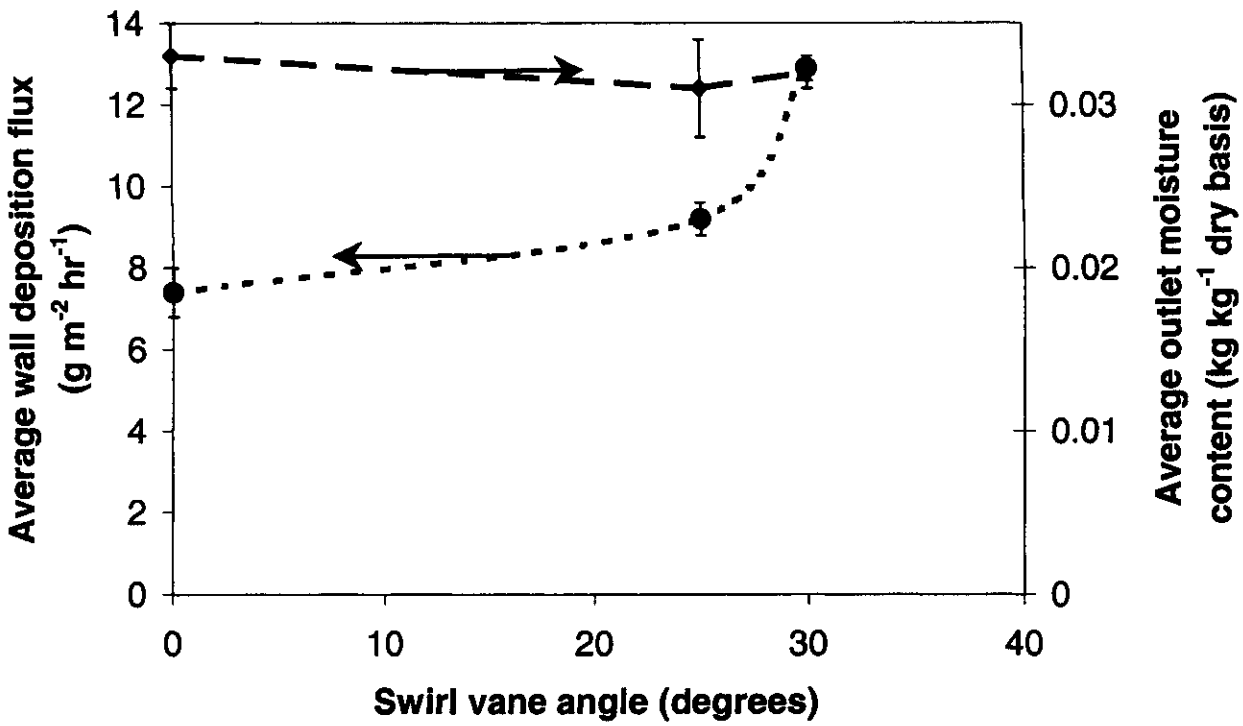

Figure 5.4 - The average deposition flux of skim milk powder and the average outlet moisture content of the skim milk powder on a dry basis, as a function of the swirl vane angle at a single inlet air temperature (230°C), feed flowrate (1.84 kg h^{-1}) and compressed air pressure (200 kPa).

The t statistic test has been used to assess whether or not there is a significant difference between the two sample means (Freund and Simon, 1992). Here, the null hypothesis (H_o) is that there is no difference between the mean wall deposition fluxes of skim milk powder for the various swirl vane angles. The alternative hypothesis (H_A) is that there is a difference between the wall deposition fluxes of skim milk powder for the various swirl vane angles. The degrees of freedom can be calculated using n_1+n_2-2, where n_1 and n_2 are the sample sizes for the first and second samples, respectively. The null hypothesis for swirl vane angles 0° and 25° can be tested as follows:

1. H_o: $\delta = 0$

   H_A: $\delta \neq 0$
2. $\alpha = 0.01$ (level of significance)

3. The mean and the variance of the two samples is $\overline{x_1}$ =7.4 g m^{-2} hr^{-1} (0°), $\overline{x_2}$ =9.2 g m^{-2} hr^{-1} (25°), s_1 =0.6 g m^{-2} hr^{-1} and s_2 = 0.4 g m^{-2} hr^{-1}, respectively, and n_1=n_2=3. Since there are 3+3-2 = 4 degrees of freedom, the value of t at 0.01 level of significance and 4 degrees of freedom ($t_{0.01,\ 4}$) is 3.747, so the null hypothesis can be rejected if t < - 3.747 or $t \geq 3.747$ (page 525, Freund and Simon, 1992). t is calculated by using equation 5.1.

$$t = \frac{\overline{x_1} - \overline{x_2} - \delta}{\sqrt{\frac{(n_1-1)s_1^2 + (n_2-1)s_2^2}{n_1+n_2-2} \times \left(\frac{1}{n_1} + \frac{1}{n_2}\right)}} \qquad (5.1)$$

4. Using equation 5.1 gives:

$$t = \frac{7.4 - 9.2}{\sqrt{\frac{(2)0.6^2 + (2)0.4^2}{4} \times \left(\frac{1}{3} + \frac{1}{3}\right)}}$$

$$= -4.32$$

5. Since t is less than - 3.747, the null hypothesis should be rejected with 99% confidence. In other words, it is possible to conclude that the difference between the wall deposition fluxes for swirl vane angles of 0° and 25° is significant. Table 5.7 summarises the statistical analysis study on the difference in the wall deposition fluxes for swirl vane angles 0° and 30°, and 25° and 30° (Appendix C3).

Table 5.7 – Summary of statistical analysis study on the difference in the wall deposition fluxes for skim milk powder for different swirl vane angles.

Swirl vane angle 1	Swirl vane angle 2	t	Confidence level	t confidence level	Accept or Reject H_o
0°	30°	-14.2	99.5%	-4.6	Reject
25°	30°	-12.8	99.5	-4.6	Reject

Hence, the results in Table 5.7 suggests that the swirl vane angle has a significant effect on wall deposition fluxes for swirl vane angles in this dryer.

The moisture contents of skim milk powder obtained from varying the swirl vane angle were similar, but the wall deposition fluxes changed. The outlet moisture contents appear not to depend on the air and particle flow patterns, suggesting that the drying kinetics are not important in determining the final moisture content. This deduction leads to a consideration of a concept known as the product moisture locus.

5.3.1 Product Moisture Locus

Table 5.8 shows the comparison of the equilibrium moisture content of the skim milk powder and the measured final (outlet) moisture content for the first 21 runs in this work, where the swirl vane angle, inlet air temperature and feed flowrate were varied, respectively. The equilibrium moisture content was calculated using the Separation Processes Service (SPS) Papadakis *et al.* (1993) equation (equation 5.2):

$$X_{eq} = A\exp\left[-BT\ln\left(\frac{1}{\Psi}\right)\right] \tag{5.2}$$

where the symbols were defined in section 2.8 of Chapter 2 in this thesis, and the values of the parameters A and B for skim milk powder, which were empirically determined by Kockel *et al.* (2002), are given in section 3.2 of Chapter 3 in this thesis. The Papadakis *et al.* (1993) equation was only fitted up to relative humidities of 21.4% and is only valid up to this fitted point. Milk is a colloidal material containing fat, lactose and proteins. At a relative humidity of 100%, the Papadakis *et al.* (1993) equation predicts an equilibrium moisture content of $X_{eq} = A = 0.1499$ kg kg^{-1}, which is not found for colloidal materials such as milk. On the other hand, the Guggenheim-Anderson-Deboer equation (equation 5.3), which has been used extensively

for foodstuffs (Lomauro *et al.*, 1985), has a much wider range of applicability and was used to calculate the equilibrium moisture content when the relative humidity was higher than 21.4%:

$$X_{eq} = \frac{K_1 K_2 K_3 a_w}{(1 - K_2 a_w)(1 - K_2 a_w + K_2 K_3 a_w)} \tag{5.3}$$

where symbols, and the values of K_1 , K_2, and K_3, which were determined empirically by Kockel *et al.* (2002), are given in section 3.2.1 of Chapter 3 in this thesis.

The measured moisture content of the skim milk powder was determined by measuring the moisture loss of the sample after it was dried in an oven at 85°C for 48 hours according to the German standard DIN 10321. Table 5.8 show that the product moisture locus (Bahu, 1992), which implies that the solids leaving the dryer closely approach their equilibrium moisture content as given by the desorption isotherm, holds extremely closely. The fact that some measured moisture contents are slightly less than the predicted equilibrium values is most probably due to small experimental errors. The rapid attainment of equilibrium is also consistent with the findings of Langrish and Kockel (2001). They used a CFD simulation to predict that spray-dried particles of 80 μm diameter (larger than those used here, 90% of which were found to have diameters less than 6 μm using a Malvern Particle Size Analyser, Model 2600) typically take less than one second to come within 1% of the equilibrium moisture content.

Table 5.8 - Comparison of equilibrium and measured outlet moisture contents for skim milk powder.

Run	Temperature (°C)	Relative humidity (%)	Measured outlet moisture content (kg water/ kg dry powder)	Equilibrium moisture content X_{eq} (kg water/kg dry powder)
1	68	14	0.037	0.032
2	68	14	0.031	0.032
3	69	19	0.026	0.040
4	69	19	0.034	0.040
5	67	16	0.031	0.036
6	70	15	0.033	0.033
7	68	14	0.030	0.032
8	68	15	0.033	0.034
9	68	15	0.033	0.034
10	52	37	0.068	0.072
11	51	30	0.055	0.060
12	52	31	0.055	0.062
13	59	24	0.044	0.050
14	58	27	0.043	0.055
15	60	23	0.042	0.048
16	66	14	0.033	0.032
17	68	14	0.029	0.032
18	68	14	0.026	0.032
19	71	11	0.025	0.026
20	71	12	0.027	0.028
21	72	12	0.029	0.028

This work is further supported by the findings of Harvie *et al.* (2002), who carried out two phase (solids particles and air) simulations using CFX4.3 for a tall form Delaval skim milk spray dryer (diameter of drying chamber: 2.16 m, diameter of cone section: 2.76 and height: 8.27 m; hollow cone nozzle). They found that the moisture content of the particles predicted using the simulations were similar to the equilibrium moisture contents calculated using the Papadakis *et al.* (1993) equation (equation 5.3). Table 5.9 gives further details of cases they studied, and the equilibrium moisture contents and predicted (simulated) moisture contents of the skim milk powder.

Table 5.9 – Comparison of equilibrium particle moisture content (%) with predicted (simulated) moisture content found using CFD. Source: Harvie et al. (2002)

Case	Outlet air temperature (°C)	Mass fraction of water vapour in outlet	Relative humidity (%)	Equilibrium particle moisture content (%)	Predicted particle moisture content (%)
a	97.1	0.0538	9.31	2.0	2.20
b	97.3	0.0538	9.24	2.0	2.04
c	97.3	0.0536	9.21	2.0	2.13
d	89.8	0.0531	12.06	2.6	3.17
e	97.3	0.0539	9.26	2.0	2.02

Figure 5.5 shows the Product Moisture Locus for skim milk powder (as found in this work) and soy milk powder (Boonyai, 2000), where as expected (Bahu, 1992) and outlined in section 2.9, the Gibbs Free Energy decreases as the moisture content of the sample increases. This figure was prepared by Cheng (2002). Keey (1992b) also pointed out increasing the moisture content of a powder decreases the strength, and thus the Gibbs Free Energy, with which the moisture is bound to the powder. The first layers of moisture are bound more strongly to the material than subsequent layers, so adding moisture adds more layers, which are less tightly bound to the material. Since both soy milk powder and skim milk powder appear to lie on a similar curve, a single smooth curve of best fit was drawn for the data for both materials in Figure 5.5. The significance of this is that, since the Gibbs Free Energy is related to the sorption isotherm (section 2.8), it suggests that the desorption equilibrium behaviour is similar for soy milk powder and skim milk powder. This outcome suggests that the presence of carbohydrates (lactose in skim milk powder; sucrose, raffinose and stachyose in soy milk powder) dominates the desorption isotherm.

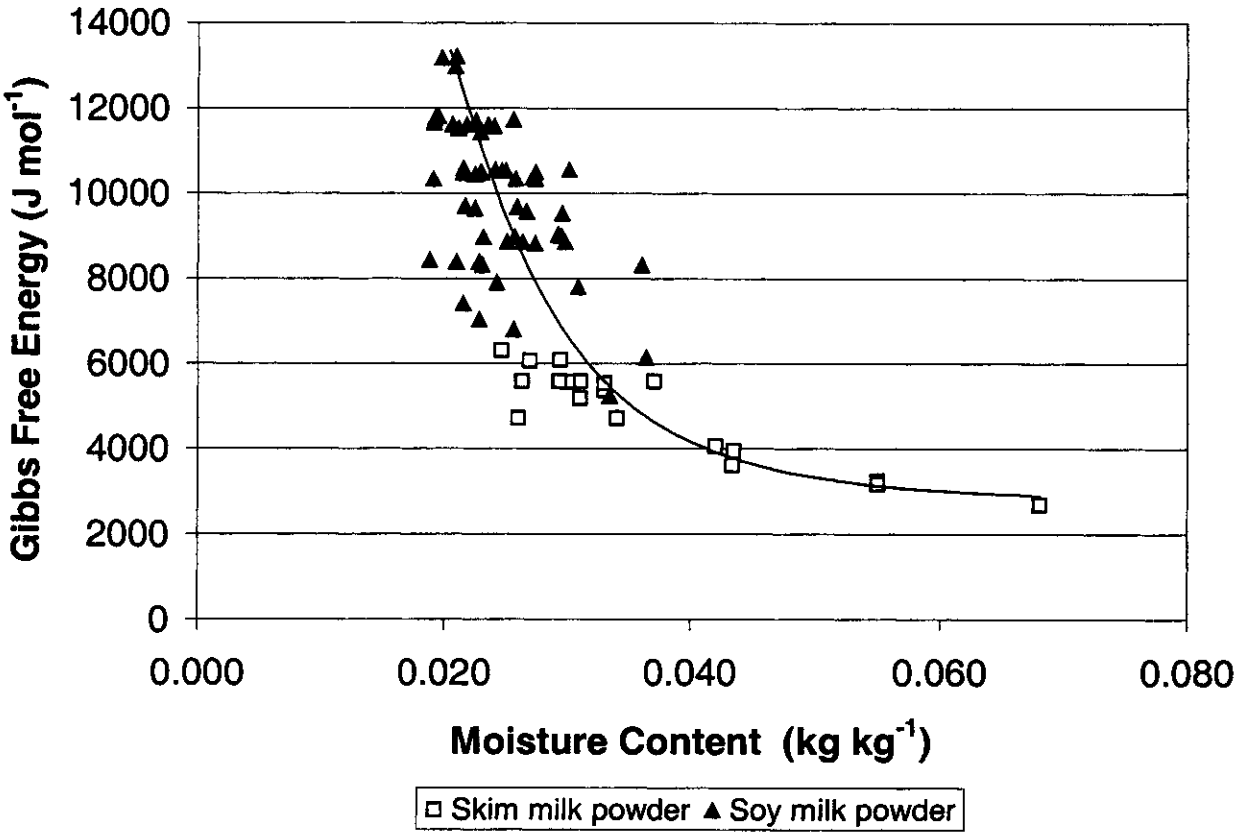

Figure 5.5– Product moisture locus for skim milk powder and soy milk powder, showing that the Gibbs Free Energy decreases as the moisture content of the powder increases. Source : Cheng (2002).

Discussion

Previous researchers have found that the swirl vane angle affects the flow patterns in spray dryers (Oakley *et al.*, 1988; Southwell, 2000; Southwell and Langrish, 2001). Southwell and Langrish (2001) found that the extent to which particles spread out in the drying chamber is affected by the amount of swirl in the inlet air and that this is likely to affect wall deposition fluxes because the particles will be closer to the walls. They found the spray cloud only showed minor instability at swirl vane angles up to 20°. When the swirl vane angle was increased to 25°, they observed transient behaviour, and the spray cloud appeared to precess inside the swirling inlet air immediately below the inlet. This behaviour was also observed in this work, where the spray cloud appeared to "flutter" significantly around the axis of the spray dryer, immediately below the inlet when the swirl vane angle was 25°. This instability in the flow patterns may have been responsible for the increase in the wall deposition flux by 20% when the swirl vane angle was increased from 0° to 25°.

Southwell and Langrish (2001) also observed that when the swirl vane angle was 30° and higher, the spray cloud became increasingly dispersed and mixed with the swirling inlet air, so that the cloud did not have a constant cross section and was periodically ripped apart. They suggested that this type of rapid spray dispersal and instability may be desirable if it results in better mixing and air-spray contact, because it might increase the evaporation rate of water. However, it might be a problem if it gave increased wall deposition fluxes.

In this work, the spray was observed to recirculate rapidly back in the direction of the nozzle at a swirl vane angle of 30°, and the inside of the chamber looked cloudy, as though considerable mixing was taking place. At a 30° swirl vane angle, significant swirl in the inlet air may be sufficient to cause vortex breakdown; a Precessing Vortex Core may occur (Oakley *et al.*, 1988). A Precessing Vortex Core may throw particles further towards the walls of the chamber and increase the wall deposition fluxes. This work confirms that the wall deposition flux increases at higher swirl vane angles, and it suggests that this arises because more swirl is imparted to the air entering the dryer, which in turn affects the stability of the flow patterns in the dryer. The chance of the particles being thrown further towards the walls of the chamber is likely to increase because of the instability in the flow patterns. Further work will be required using CFD to be more certain if vortex breakdown and Precessing Vortex Core has occurred in this dryer (as opposed to the slightly different design used by Oakley *et al.*, 1988) at a swirl vane angle of 30° when particles are present in the spray dryer. It is important to note that the increased wall deposition fluxes at higher swirl vane angles are unlikely to have resulted from increased particle stickiness, since the inlet conditions of air temperature, feed flowrate and compressed air pressure were all the same.

5.4 The Effect of Inlet Air Temperature and Feed Flowrate on Wall Deposition Fluxes of Skim Milk Powder

5.4.1 Inlet Air Temperature

Dryer operating parameters, such as the inlet air temperature, affect the temperature and humidity inside the dryer, which in turn affect the moisture content and temperature of the particles. The stickiness of a material is related to both its temperature and moisture content, and the sticky-point temperature decreases as the moisture content increases. If the air entering

the dryer has a lower temperature, the outlet moisture content of the particles is likely to be higher, and the outlet temperature of the particles will be lower. Hence, from the sticky-point diagram (Figure 5.6), both the particle outlet temperature and the sticky-point temperature corresponding to the new higher particle moisture content are likely to decrease as the inlet air temperature is reduced. If the sticky-point temperature decreases more with lower inlet air temperatures than the particle outlet temperature, then reducing the inlet temperature is likely to increase the stickiness problem, since doing this puts particle temperatures further above the sticky-point temperature and hence in the sticky region of the sticky-point diagram.

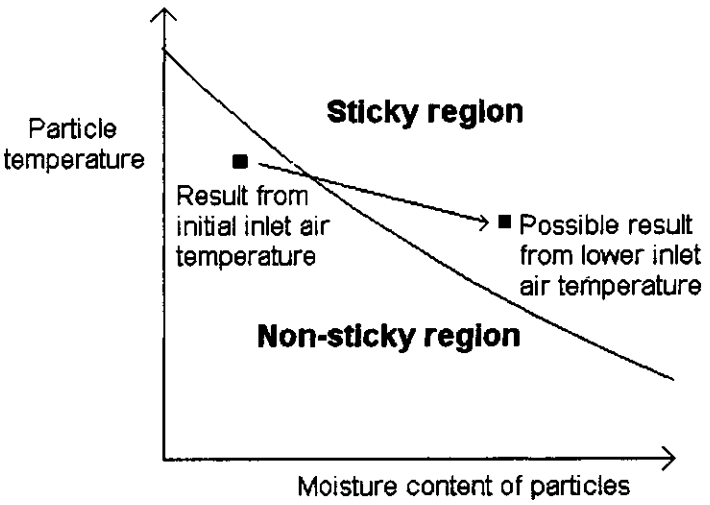

Figure 5.6- Influence of reducing the inlet air temperature on particle stickiness.

Which effect (reduced particle temperature or reduced sticky-point temperature) dominates is likely to depend on the stickiness behaviour of the material (sticky-point diagram) and the way in which the dryer is operated (to give the particle temperature). Resolving which effect is dominant is one reason for quantifying sticky behaviour in a sticky-point diagram. No quantitative data exist on the effect of inlet air temperature on wall deposition. The only data available are that low inlet air temperatures less than 200°C have been used to spray dry fruit juices by Breene and Coulter (1967), Robe *et al.* (1968), Brennan *et al.* (1971), Gupta (1978), Main *et al.* (1978), Karatas and Esin (1990), Bhandari *et al.* (1992), Boskovic *et al.* (1992), and Bhandari *et al.* (1993), because the materials are inherently thermoplastic and heat-sensitive.

Inlet air temperatures of 170°C, 200°C, and 230°C were used here to determine what influence the inlet air temperature has on wall deposition fluxes of skim milk powder. The swirl vane angle was set to 0° because it was previously found to give rise to the least wall deposition (of all the swirl vane angles tested), and one of the aims of this work is to determine which spray

dryer operating parameters minimise wall deposition fluxes. More valuable material than skim milk (such as grape extract) can then be spray dried at the optimal operating parameters. The compressed air pressure (200 kPa) and the skim milk flowrate (1.8 kg hr^{-1}) were held constant here.

Figure 5.7 shows the average wall deposition fluxes for skim milk powder and the average outlet moisture contents of the powder on a dry basis when the inlet air temperatures were 170°C, 200°C and 230°C, respectively. Changing the inlet air temperature has a significant effect on the wall deposition flux. The maximum wall deposition flux was 15 g m^{-2} hr^{-1} when the inlet air temperature was 170°C, while the minimum wall deposition flux was 7 g m^{-2} hr^{-1} when the inlet air temperature was 230°C. Increasing the inlet air temperature by 60°C decreased the wall deposition flux by 53%. Thus, increasing the inlet air temperature decreases the wall deposition fluxes for skim milk powder in this dryer, where (in this dryer), the sticky-point temperature increases more than the particle chamber temperature as the moisture content decreases, raising the sticky-point temperature above the particle temperature and reducing the deposition fluxes.

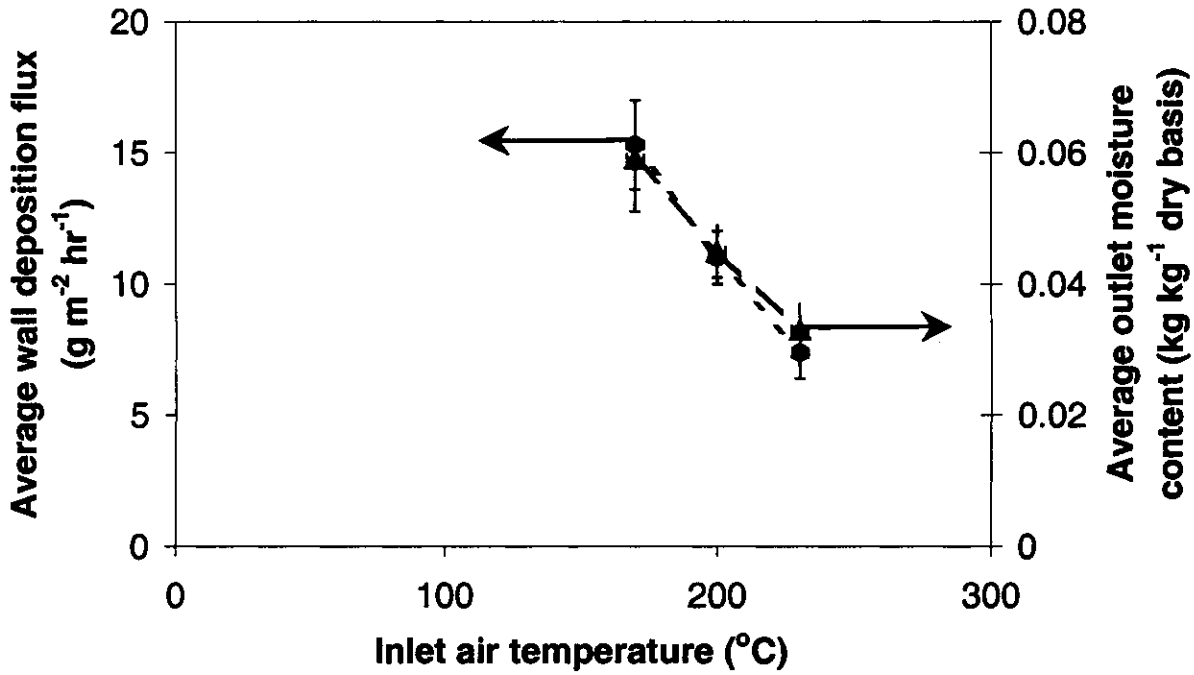

Figure 5.7 - The average deposition flux of skim milk powder and the average moisture content of the skim milk powder on a dry basis, as a function of the inlet air temperature at a single feed flowrate (1.84 kg hr^{-1}), compressed air pressure (200 kPa) and swirl vane angle (0°).

Figure 5.7 also shows that changing the inlet air temperature also has a significant effect on product moisture content. If the inlet air temperature increases, then the equilibrium moisture content will decrease (from the desorption isotherm) if the relative humidity of the air is similar. Hence, decreasing the equilibrium moisture content by increasing the inlet air temperature decreases the product moisture content significantly, as well as the wall deposition fluxes.

Care needs to be taken in recommending higher inlet air temperatures. The finding that this decreases the outlet moisture content is general. However, the result that the sticky-point temperature increases more than the chamber temperatures is specific to this dryer, particularly to the heat losses. Lower heat losses (relative to the amount of drying), which correspond to larger spray dryers, may give higher chamber and particle temperatures and hence particle temperatures that may be above the sticky-point temperature, so stickiness may increase if the inlet temperature is increased in other dryers with lower heat losses.

When drying heat sensitive and high quality products, care must also be taken that the inlet air temperature is not too high, because it would give rise to high outlet air temperatures and therefore high particle temperatures. Active material such as proteins may denature. In addition, high air inlet temperatures mean high wall temperatures, which mean that any particles that deposit on the walls will eventually dry out and are likely to thermally degrade more quickly than if the wall (and inlet air) temperatures are lower. Wall temperatures may or may not affect the wall deposition flux, but they are still important from the viewpoint of affecting the rate at which any deposits on the walls thermally degrade, which is important (for example) for milk powder.

Statistical analysis in Appendix C3 shows that there was a significant difference between the wall deposition fluxes and outlet moisture contents when the inlet air temperatures were 170°C and 200°C, with 99% confidence and 99.5% confidence, respectively. In addition, statistical analysis in Appendix C3 shows that there is a significant difference between the wall deposition fluxes when the inlet air temperatures are 200°C and 230°C, with 99% confidence, and between the moisture contents of the particles, with 99.5% confidence. Hence the changes discussed here are significant relative to the measurement uncertainties.

5.4.2 Feed Flowrate and Feed Concentrations

Like the inlet air temperature, the feed flowrate is an operating parameter that can affect the temperature and humidity inside the dryer, which in turn can affect the moisture content and temperature of the particles inside the dryer and therefore affect the stickiness of the product. High feed flowrates have at least three effects.

First, in a small-sized spray dryer, high feed flowrates may mean high nozzle exit velocities and hence a high likelihood of particles depositing directly on walls, because of spray impaction. This may be particularly true for the conical region (where plates 5 and 6 were located) in the dryer used here, due to the geometry of the chamber and the atomiser spray pattern.

Second, relatively higher feed flowrates may mean a higher total evaporation rate, higher air humidities and a higher particle moisture content (sorption isotherm) since the total evaporation rate is increased. For example, if the initial moisture content of the feed is 9 kg of water per kg of dry solids, a feed flowrate of 1.4 kg hr^{-1} (total) and an outlet particle moisture content of 0.027 kg kg^{-1} (dry basis) (the result from run 20) gives a total evaporation rate of 1.3 kg water per hour. In comparison, a higher feed flowrate of 1.8 kg hr^{-1} (total) and an outlet particle moisture content of 0.033 kg kg^{-1} (dry basis) (the result from run 6) gives a higher total evaporation rate of 1.6 kg water per hour:

$$\text{Evaporation rate} = 1.4\,\text{kg hr}^{-1}(\text{total}) \times \frac{1\,\text{kg(drysolids)}}{9\,\text{kg(water)} + 1\,\text{kg(drysolids)}} \times (9 - 0.027)\frac{\text{kg(water)}}{\text{kg(drysolids)}}$$

$$= 1.3\frac{\text{kg water evaporated}}{\text{hr}}$$

$$\text{Evaporation rate} = 1.8\,\text{kg hr}^{-1}(\text{total}) \times \frac{1\,\text{kg(drysolids)}}{9\,\text{kg(water)} + 1\,\text{kg(drysolids)}} \times (9 - 0.033)\frac{\text{kg(water)}}{\text{kg(drysolids)}}$$

$$= 1.6\frac{\text{kg water evaporated}}{\text{hr}}$$

The reason for the higher particle moisture content (0.033 kg kg^{-1} rather than 0.027 kg kg^{-1}) at the higher feed flowrate (1.8 kg hr^{-1} rather than 1.4 kg hr^{-1}) is that the higher feed flowrate results in more humidification of the air, since the evaporation rate (1.6 kg hr^{-1}) is higher at the higher feed flowrate and the air flowrate is constant. The relative humidity was higher for run

6 at 15% (higher evaporation rate) compared with the relative humidity for run 20 at 12%. Now, while it is realised that the moisture content is not the only factor in stickiness, since particle temperature must be considered as well, higher particle moisture contents, with all other things being equal, are more likely to give high stickiness.

Third, as suggested by Mahony (2001), increasing the feed flowrate will mean more particles residing in the drying chamber, if the particle residence times are the same (which is possible if increasing the feed flowrate does not change the air and particle flow patterns too greatly). More particles residing in the chamber may mean a higher likelihood of particles impinging on the walls. Particles that are dragged to the wall by the spray (Figure 5.8) from the nozzle may increase this impingement effect. Furthermore, particles inside the recirculation zones may give reasonably well-mixed gas conditions, so the particles from the nozzle may entrain the particles that are held up inside the recirculation zones in the dryer. Hence, these particles from the recirculation zones, which are likely to be close to the average temperature and moisture content inside the dryer, may be dragged down to the cone.

There was no clear indication from previous work regarding which of these three reasons is most important. Only overall information is available, such as the observation of Brennan *et al.* (1971) that increasing the feed flowrate gave more wall deposits for an orange juice and maltodextrin mixture when it was spray dried.

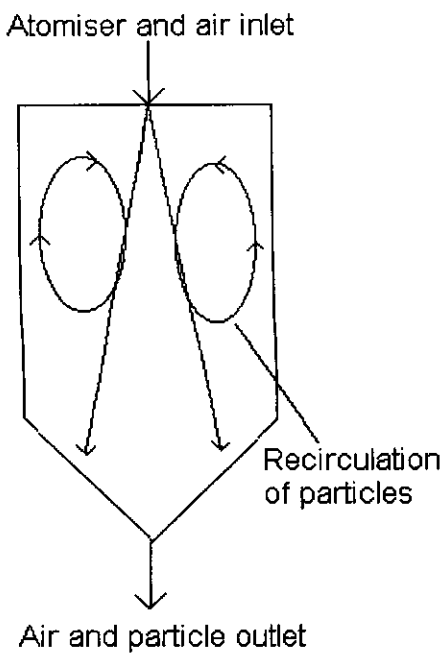

Figure 5.8 - Schematic diagram showing particles from the atomiser entraining particles that are held up inside the recirculation zones in the dryer.

Feed flowrates of 1.4 kg hr^{-1}, 1.6 kg hr^{-1} and 1.8 kg hr^{-1} were used to quantify the effect that feed flowrate has on wall deposition fluxes of skim milk powder. A single inlet air temperature (230°C), swirl vane angle (0°) and compressed air pressure (200 kPa) were used for this test.

Figure 5.9 shows the average wall deposition fluxes for skim milk powder and the average outlet moisture content of the powder on a dry basis when the feed flowrates were 1.4 kg hr^{-1}, 1.6 kg hr^{-1} and 1.8 kg hr^{-1}. Decreasing the feed flowrate from 1.8 kg hr^{-1} to 1.4 kg hr^{-1} (24%) decreased the wall deposition flux from 7 g m^{-2} hr^{-1} to 4 g m^{-2} hr^{-1} (43%). Thus, decreasing the feed flowrate decreases the wall deposition fluxes for skim milk powder. A higher feed flowrate means higher powder production but also higher wall deposition. Since the wall deposition flux decreased by 43% when the feed flowrate was decreased by 24%, it might be considered that the production process is in favour of a decrease in feed flowrate to 1.4 kg hr^{-1} in this dryer, and consequently a decrease in wall deposition flux per unit production output.

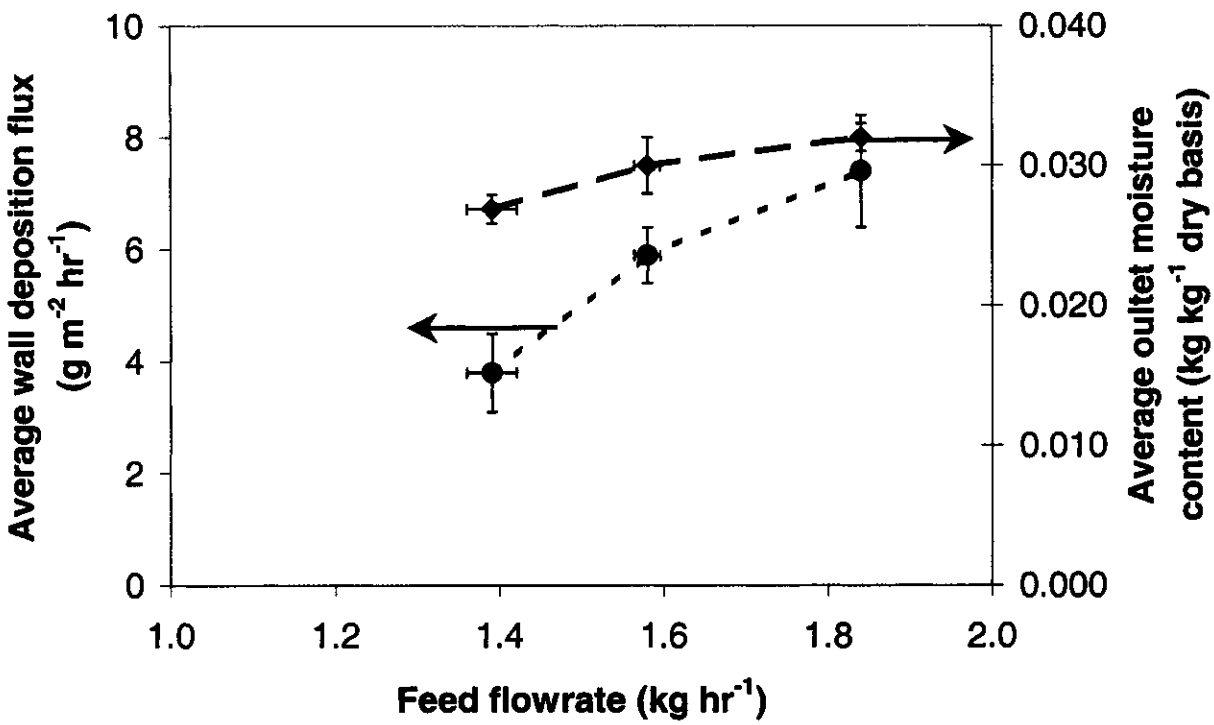

Figure 5.9 - The average deposition flux of skim milk powder and the average moisture content of the skim milk powder on a dry basis (X), as a function of the feed flowrate, at a single inlet air temperature (230°C), compressed air pressure (200 kPa) and swirl vane angle (0°).

Statistical analysis in Appendix C3 confirms that there is a significant difference between the wall deposition fluxes when the feed flowrates are 1.4 kg hr^{-1} and 1.6 kg hr^{-1}, with 99% confidence. In addition, statistical analysis in Appendix C3 shows that there is a significant difference between the wall deposition fluxes when the feed flowrates are 1.6 kg hr^{-1} and

1.8 kg hr^{-1} with 95% confidence. Figure 5.9 shows that there is a slight increase in the final (average) moisture content from 2.7% to 3.0% to 3.2% as the feed flowrate is increased from 1.4 kg hr^{-1} to 1.6 kg hr^{-1} and then 1.8 kg hr^{-1}. The difference between the moisture content of skim milk powder is only slightly statistically significant when the feed flowrates are 1.6 kg hr^{-1} and 1.8 kg hr^{-1} with 60% confidence (as shown in Appendix C3). The difference between the moisture contents of skim milk powder is statistically significant when the feed flowrates are 1.6 kg hr^{-1} and 1.4 kg hr^{-1} with 95% confidence. This statistical analysis thus suggests that the differences discussed here are significant relative to the measurement uncertainties.

The air flowrate was decreased by 19% from 0.016 kg s^{-1} to 0.013 kg s^{-1} by turning the secondary blower off. This was done to test if decreasing the air flowrate will affect the wall deposition flux of skim milk powder, since the particles will be in the spray dryer for a longer period of time. Decreasing the air flowrate increased the wall deposition flux by 40% from 7 g m^{-2} hr^{-1} to 12 g m^{-2} hr^{-1}. Thus, decreasing the air flowrate increases the residence time of the particles in the spray dryer and this increases the likelihood of the particles impinging on the walls, giving rise to higher wall deposition fluxes. Hence the residence time, which will affect the rate of contact between particles and the wall, appears to affect the wall deposition flux significantly, as suggested in the third explanation before.

As expected, decreasing the air flowrate increased the moisture content of the particles from 3.3% to 7.4% (dry basis) because the relative humidity of the air inside the dryer increases from an average of 16% to an average of 34% and less thermal energy enters the dryer to dry the skim milk. Statistical analysis in Appendix C3 confirms that there is a significant difference between the wall deposition fluxes with 99.5% confidence, and that there is a significant difference between the moisture content of the skim milk powder when the air flowrate is decreased, with 99.95% confidence. The equilibrium moisture content was calculated to be 7.3%, which is very close to the measured moisture content, 7.5%, once again supporting the concept of the product moisture locus. However, it is possible that the reason the wall deposition flux was higher was because of both increased particle moisture content and increased residence time of the particles. Thus, which effect (moisture content or particle residence time) dominates here is unclear. In any case, even decreasing the air flowrate still means that the drying performance is equilibrium controlled, for skim milk at least, in this

particular dryer. It is possible that, with a smaller dryer, the performance may be kinetically controlled because the residence time of the particles (for drying) will be less in a small dryer.

At this point, it is worthwhile to consider the implications for spray drying other materials (apart from skim milk). At room temperature, a saturated calcium chloride solution has a low relative humidity (or water activity) of 30% (Young, 1967). As given by equation 5.4, the relative humidity at the surface of a droplet of calcium chloride ($\psi_{droplet}$) is equal to the vapour pressure at the surface of the calcium droplet ($P_{vdroplet}$) divided by the saturated vapour pressure of water at the droplet temperature {P_{vsat}}.

$$\psi_{droplet} = \frac{P_{v\,droplet}}{P_{v\,sat}} \tag{5.4}$$

As the temperature is increased to 45°C, the relative humidity at the surface of the calcium chloride droplet is decreased to a minimum of 17%. The driving force for water to evaporate from the calcium droplet is the difference between the water vapour concentration at the surface of the calcium chloride droplet and that of the bulk gas. If calcium chloride is to be spray dried and the relative humidity of the air in the spray dryer is 30%, the droplets of calcium chloride will not dry out because the driving force for drying would be very small given that the air and particle temperatures are likely to be close if the drying behaviour is equilibrium limited. In this case, the relative humidity of the air should be less than 30% for drying to occur. Thus, the relative humidity at the surface of a droplet (which contains suspended or dissolved solids) is very important for drying. It is more probable that kinetic limitations will be present in spray drying material such as calcium chloride, and it is more likely that semi-solid particles may then impact on the dryer walls, increasing the wall deposition flux.

5.4.3 Interaction of Spray Dryer Operating Conditions with the Sticky-Point Curve

Figure 5.10 shows the temperature of the air in the drying chamber as a function of the moisture content of the skim milk powder particles for five different cases, where the inlet air temperature and feed flowrate were varied. The swirl vane angle was kept constant at 0°. The sticky-point curve for skim milk powder (Hennigs *et al.*, 2001) is also included in the figure.

Since the moisture content of the particles was found to be within 0.4% of the equilibrium moisture content, this suggests that the particles were in equilibrium with the air and that no further drying of the particles can be expected to occur. Thus, assuming the spray dryer is well mixed (Bahu, 1992), the temperature of the air in the drying chamber is close to that of the particles. Hence, the temperatures and moisture contents of the particles correspond to the dryer operating conditions. The points on the sticky-point curve move further to the right and towards the sticky region as the temperature is decreased from 230°C to 170°C, since the particle temperature decreases and the particle moisture content increases. The sticky-point temperature and particle temperature both decrease as the inlet air temperature is reduced. However, here the sticky-point temperature decreases more than the particle temperature as the inlet air temperature is reduced to 170°C, so placing the dryer operating conditions closer to the sticky region. Figure 5.10 also shows the wall deposition fluxes plotted on the sticky-point curve for the different dryer operating conditions. The points lie below the sticky-point curve for all conditions except when the inlet air temperature was 170°C. At this condition, the average wall deposition flux was the highest at 16 g m^{-2} hr^{-1}, and the points lie at or above the sticky-point curve in the "sticky region".

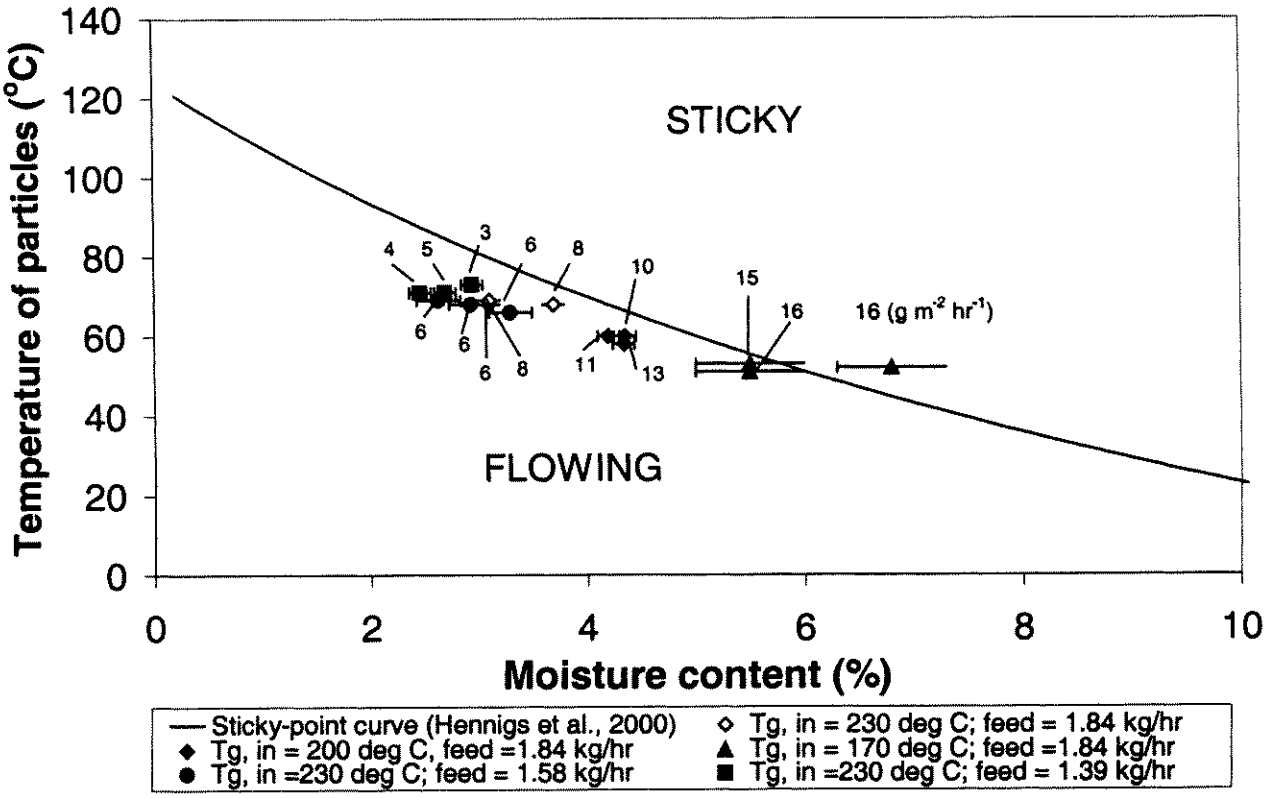

Figure 5.10 - Operating conditions and corresponding wall deposition fluxes (g m^{-2} hr^{-1}) on the sticky-point diagram for skim milk powder.

Figure 5.10 also shows that as the feed flowrate is increased from 1.4 kg hr^{-1} to 1.8 kg hr^{-1}, the moisture content of the particles increases and the operating point on the figure moves further towards the "sticky region". Like the inlet air temperature, the feed flowrate is an operating parameter that can affect the temperature and humidity inside the dryer, which in turn can affect the moisture content and temperature of the particles inside the dryer and therefore the stickiness of the product. As a higher feed flowrate is used, the total evaporation rate in the dryer also increases, as discussed previously in section 4.5.2. Greater total evaporation rates, with a constant air flowrate, will mean higher air humidities in the dryer, higher equilibrium moisture contents and higher product moisture contents if the concept of a product moisture locus is true. There is already some evidence for this concept (Table 5.2). As previously mentioned in section 5.4.2, the experimental evidence here is that there is a slight increase in the final (average) moisture content from 2.7% to 3.0% to 3.2% as the feed flowrate is increased from 1.4 kg hr^{-1} to 1.6 kg hr^{-1} and then 1.8 kg hr^{-1}, even though the increase in moisture content is only slightly statistically significant. This increase in product moisture content is consistent with the increase in product equilibrium moisture content, due to the increase in air humidity arising from the greater feed flowrate and consequently the higher amount of evaporation in the dryer. Since the experimental evidence is that higher product moisture contents result from higher feed flowrates, the concept of a product moisture locus is further supported, as shown in Table 5.2.

Previous researchers have found that the temperatures of the walls affect the deposition of the particles. Brennan *et al.* (1971) and Gupta (1978) found that when the walls were too hot, more deposition was observed and vice versa. One reason why previous researchers have found that wall temperature is important in determining wall deposition fluxes may be that cooled walls (which they observed to give lower amounts of deposition) may have resulted in cooler air near the walls and hence lower particle temperatures. These lower particle temperatures may then have fallen below the sticky-point curve. Care does need to be taken to avoid condensation on the dryer walls, because this effect is likely to give higher wall deposition fluxes (compared with no condensation), not because of altered particle stickiness, but because particles hitting the wall will fall onto a liquid film. This situation might also explain Chen *et al.* (1993)'s recommendation that insulation can reduce wall deposition fluxes depending on the temperature to which the walls are increased, which may prevent both vapour condensation and the particles becoming sticky.

This work has shown that the higher the temperature of the air, the lower the moisture content of the particles, the less sticky the particles will be, resulting in a lower wall deposition flux. When higher inlet air temperatures are used, the wall temperatures are higher. When the inlet air temperature is 230°C, the wall temperature was measured to be 52°C, while when the inlet temperature is 170°C, the wall temperature was measured to be 10°C lower, at 42°C. Having a lower wall temperature did not appear to reduce the wall deposition flux directly here for changed inlet air conditions.

For these experiments, the sticky-point curve appears to be a better indication of the tendency for wall deposition to occur than the wall temperature on its own. It is also possible that the sticky-point curve may explain the findings of previous workers such as Brennan *et al.* (1971) and Gupta (1978), who found that delibrately reducing the wall temperature reduced the deposition of fruit juice particles on the walls, since cooled walls might have cooled the air next to the walls and hence the particles in this region of the dryer (in their case), making them less sticky. In this case, the plates on which the maximum deposition fluxes were found (plates 5 and 6) were placed on the walls of the conical section of the dryer, which was insulated and were at the same temperature as the walls. Hence plates 5 and 6 were effectively insulated from the ambient environment, so this reduces the possibility that the increase in wall deposition flux on plates 5 and 6 could be due to the plates being cooler than the actual dryer walls.

Further experimental work was carried out to determine if insulating plates 1 to 4 would increase the wall deposition flux. The results are shown in Table 5.10 for the base case operating conditions. Placing insulation behind plates 1 to 4 had some effect on the wall deposition fluxes on these plates but did not increase the fluxes to the levels seen on plates 5 and 6. The fluxes on plates 1 to 4 were still an order of magnitude lower than those on plates 5 and 6, possibly due to different air and particle flow patterns in these regions of the dryer. These flow patterns may have brought more particles closer to the walls in the conical section of the dryer (where plates 5 and 6 were located), compared with the top cylindrical section of the dryer (where plates 1-4 were located). The higher wall deposition fluxes with insulation (higher wall temperatures) are consistent with the findings of Brennan *et al.* (1971) and Gupta (1978), since the higher wall temperatures might increase the air and hence particle temperatures near the wall, moving the local particle conditions towards the sticky-region for the same inlet air conditions.

Table 5.10 - Wall deposition flux on plates 1 to 4 with and without insulation.

Plate	Wall deposition flux without insulation on plates ($g\ m^{-2}\ h^{-1}$)	Wall deposition flux with insulation on plates ($g\ m^{-2}\ h^{-1}$)
1	0.0	0.4
2	0.1	0.7
3	0.1	0.2
4	0.2	0.5

Drawing this discussion together about the effect of wall temperature on the wall deposition flux, a lower wall temperature due to a lower inlet air temperature actually led to a higher deposition flux; the higher flux is consistent with the closer approach of the particle conditions to the sticky-point curve. However, a lower wall temperature due to uninsulated plates did give lower deposition fluxes. These two findings (higher flux with lower wall temperature at lower air temperature and lower flux with cooled uninsulated walls) suggest that the wall temperature on its own is not sufficient to fully predict wall deposition fluxes. The effect of the insulation does mean that the sticky-point curve is not fully sufficient either, since the deposition flux is affected even though the point on the sticky-point curve is not affected by the wall insulation of the plates, since the total heat loss from the dryer is only slightly affected by the insulation on these plates (these plates only cover a small part of the wall). Nevertheless, the wall deposition flux does appear to be affected by the approach of the particle temperature to the sticky-point one, as will be shown in the next sub-section.

It is also possible that the two differing effects of wall temperature (as just described) may be due to differing wall particle interactions. The results in Figure 5.10, where increasing the wall temperature decreased the flux, occurred for plates where spray impaction was more important. Spray impaction is likely to be important for small dryers, as here. The effects of turbulence on particles travelling parallel to the wall are likely to be greater for plates 1-4 (Table 5.10), where the plates were away from the spray impaction region and where higher wall temperatures (due to insulation) gave higher fluxes. No trend was evident in the wall deposition fluxes for plate 1 to 4, when the operating conditions of the spray dryer (swirl vane angle, inlet air temperature, feed flowrate) were changed. The fluxes on these plates were less then 2 $g\ m^{-2}\ hr^{-1}$. Hence, the differing effects of wall temperatures may be due to different wall-particle interaction processes, due in part to different air and particle flow patterns.

5.4.4 The Effect of the Difference between Particle Temperature and Sticky-Point Temperature on Wall Deposition Fluxes

Figure 5.11 shows the wall deposition flux as a function of the difference between the particle temperature and sticky point temperature for the cases where the swirl vane angle, inlet air temperature and feed flowrate were changed for the plates in the bottom (conical) section of the dryer, where spray impaction was more likely. This figure suggests that a higher wall deposition flux tends to occur when the particle temperature is higher than the sticky-point temperature, and this occurs when the inlet air temperature is the lowest at 170°C. The wall deposition flux is also high when the swirl vane angle is the highest at 30°, even though the particle temperature is below the sticky-point temperature. Thus, while the stickiness of the material is important in quantifying the wall deposition in spray dryers, the flow patterns in the spray dryer are also important.

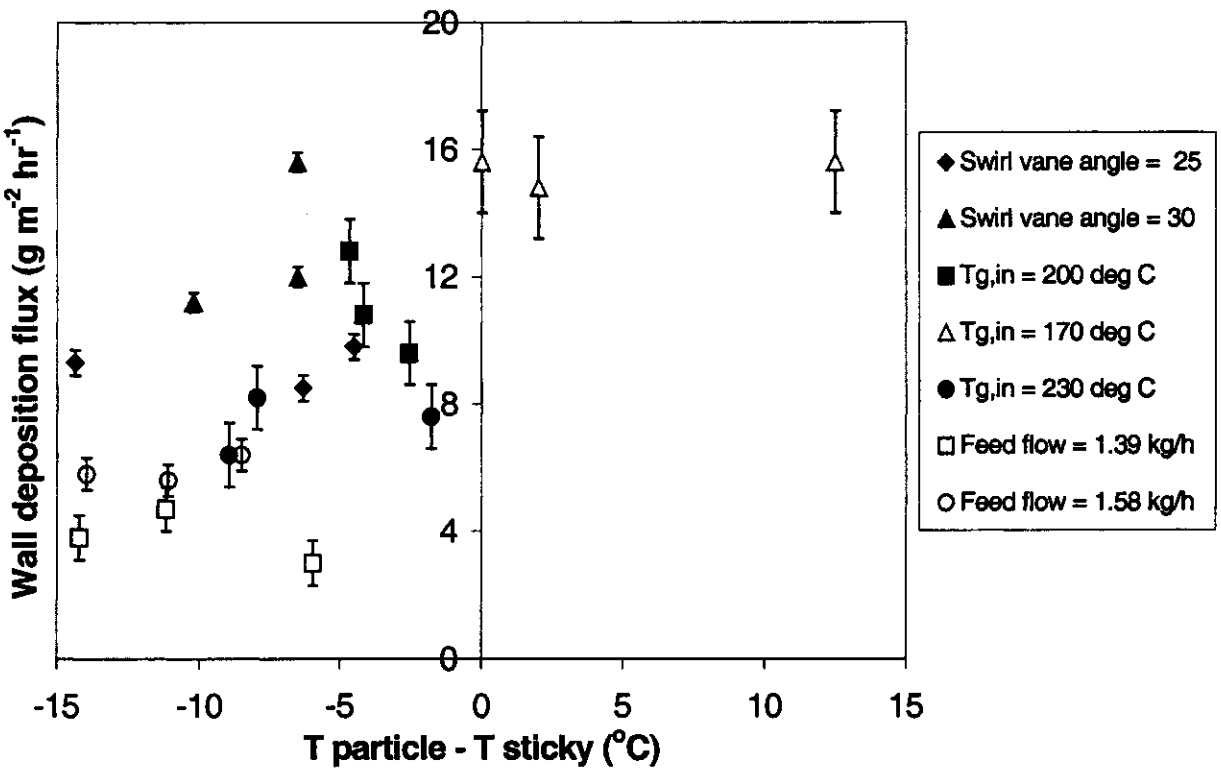

Figure 5.11 - Wall deposition flux as a function of the difference between the particle temperature and sticky-point temperature for different operating conditions.

The wall deposition flux does increase as the feed flowrate is increased. Earlier in this work, three reasons (increased spray impaction, increased stickiness, and increased number of particles or increased particle residence time) were suggested as reasons why the wall deposition flux increases with feed flowrate. The feed flowrate affects the stickiness of a

material being spray dried because it affects the humidity in the dryer, which in turn affects the equilibrium moisture content of the particles. It is also possible that the different feed flowrates interact with the air in different ways and thus affect the flow patterns in the spray dryer and consequently affect the wall deposition flux. Hence both increased stickiness and changes in air flow patterns may be important in increasing wall deposition fluxes when the feed flowrate is increased. In this work, the effect of the stickiness of the material on wall deposition flux has been partly quantified for areas of the spray dryer that are subject to spray impaction. One further step in future work will be to quantify the effect of flow patterns on the wall deposition flux in spray dryers using CFD. Another step is to assess the wall deposition flux experimentally throughout the drying chamber, for locations where direct spray impaction and turbulent deposition are important. Quantifying the effect of wall temperature will also be important, as will relating the wall deposition flux to both experimental and simulated air and particle flow patterns more closely. Then, a clear indication of which effects, particle stickiness or flow patterns, dominate in the wall deposition of skim milk powder can be determined.

Increasing the feed flowrate (with the same residence time) and decreasing the air flowrate (increasing the residence time) both increase the number of particles in the chamber and increase the air humidity, making the particles stickier. Figure 5.11 suggests that both stickiness and airflow patterns affect wall deposition fluxes significantly.

The concept of a product moisture locus is that the product moisture content is determined more by the equilibrium moisture content than the drying rate, particle size or surface area of the particles. The equilibrium moisture content is a thermodynamic aspect of drying that has no necessary connection with the drying rate, which is a kinetic aspect of the particle behaviour. If the product moisture locus is true, then by combining the mass and energy balances with the prediction of the equilibrium moisture content, the effects of increasing the inlet air temperature and increasing the feed flowrate on particle temperature and moisture content should be predictable relative to a sticky-point curve. Consequently, a range of operating conditions can be explored by the following iterative procedure:

1. Set the product moisture content to be initially 0%, to start the iterative procedure.
2. Find the absolute humidity of the air leaving the dryer, Y_o. As given in equation 5.5, the mass of water uptake by the drying air must be equal to the mass of water evaporated from the liquid feed which is sprayed into the spray dryer:

$$\dot{m}_a (Y_o - Y_n) = \dot{m}_p (X_i - X_o) \tag{5.5}$$

where m_a is the mass flowrate of the air (in kg s^{-1}), Y_i is the absolute humidity of the air entering the dryer (in kg water/kg dry air), m_p is the mass flowrate of the product entering the dryer (in kg solids per second), X_i is the moisture content of the product entering the dryer (in kg water/ kg dry powder), and X_o is the moisture content of the product leaving the dryer (in kg water/kg dry powder). From the mass and energy balances (section 4.3), there was a discrepancy in the water balance, where the mass of water entering the dryer was higher than the mass of water leaving the dryer. In section 4.3, a sensitivity analysis and propagation of error analysis was carried out, with the result that all but 33% of the discrepancy in the water balance was due to random error from measuring the outlet wet-bulb temperature and dry-bulb temperatures, which are used to determine the absolute humidity of the air. Furthermore, a systematic error of 2°C in the cold junction temperature can explain all the discrepancy in the water balance. To compensate for this discrepancy, the discrepancy between the mass of water entering the dryer and leaving the dryer (section 4.3.3, Table 4.6) is included in equation 5.5 (where it is added to the mass of water leaving the dryer) to give a new equation 5.6:

$$\dot{m}_a Y_i + \dot{m}_p X_{in} = \dot{m}_a Y_o + \dot{m}_p X_{out} + Z(\dot{m}_a Y_i + \dot{m}_p X_{in}) \tag{5.6}$$

where Z is the fractional discrepancy between the water entering and leaving the dryer, a number from 0 to 1. They physical significance of the parameter Z is that some moisture may leak out of the dryer and must be accounted for in a mass balance.

Rearranging equation 5.6 in terms of the outlet air humidity, and given the product moisture content, the outlet air humidity can be predicted from the water balance by using equation 5.7:

$$Y_o = (1 - Z)Y_i + \frac{\dot{m}_p}{\dot{m}_a}[(1 - Z)X_i - X_o] \tag{5.7}$$

Substituting the following data from run 10 (where the inlet air temperature was 170°C, the feed flowrate was 1.8 kg hr^{-1}, the compressed air pressure was 200 kPa and the swirl vane angle was 0°) into equation 5.7 gives the following results:

Y_{in} = 0.010 kg water/kg dry air
X_i = 9.12 kg water/kg dry product
X_o =0 kg water/kg dry product
m_a = 0.0158 kg air per second
Z = 0.14

If the total feed flowrate is 5.10×10^{-4} kg s^{-1} and the solids concentration is 8.8% w/v, m_p is calculated as follows:

$$m_p = 0.088 \times 5.10 \times 10^{-4} \text{ kg s}^{-1}$$
$$= 4.49 \times 10^{-5} \text{ kg solids s}^{-1}$$

$$Y_{out} = (1 - 0.14) \times 0.010 \text{ kg water/kg dry air} + \frac{4.49 \times 10^{-5} \text{ kg solids s}^{-1}}{0.0158 \text{ kg air per second}} [(1 - 0.14) \times (10.36 \text{ kg water/kg dry product} - 0)]$$
$$= 0.0339 \text{ kg water/kg dry air}$$

The next step is to find the temperature of the air leaving the dryer, T. On the assumption that the particle temperature equals the outlet air temperature (because the drying (mass-transfer) rate is likely to be low at the outlet if the particles are close to the equilibrium moisture content), then the outlet air temperature can be predicted from an energy balance given by equation 5.8:

$$H_{in} = H_{out} + H_{loss} \tag{5.8}$$

where H_{in} is the enthalpy entering the dryer (in kW), H_{out} is the enthalpy leaving the dryer (in kW) and H_{loss} is the heat loss from the dryer walls (in kW). The equation for the enthalpy entering the dryer H_{in}, when water is sprayed is given by equation 4.8 in section 4.3.5 of Chapter 4. Modifying this equation to include the spray drying of skim milk gives equation 5.9.

$$H_{in} = m_a C_{pa,i}(T_{hot\ air} - T_{ref}) + m_a Y_i[\lambda + C_{pw,v_{in}}(T_{hot\ air} - T_{ref})] + m_{skim\ milk} C_{p\ skim\ milk}(T_{skim\ milk} - T_{ref}) + m_{ca} C_{pca,i}(T_{ca} - T_{ref}) + m_{ca} Y_i[\lambda + C_{pw,v_{in}}(T_{ca} - T_{ref})] \quad (5.9)$$

where all the symbols are defined in section 4.3.5, except the symbols $m_{skim\ milk}$, which is the mass flowrate of skim milk (in kg s), $C_{p\ skim\ milk}$, which is the specific heat capacity of skim milk (in kJ (kg °C)$^{-1}$), and $T_{skim\ milk}$, which is the temperature of the skim milk fed into the spray dryer (in Kelvin).

As recommended by Pisecky (1997), the specific heat capacity of skim milk was calculated as a weight sum of heat capacity of the individual components using equation 5.10.

$$C_{p\ skim\ milk} = \frac{x_w C_{pw} + x_p C_{pp}}{x_w + x_p} \quad (5.10)$$

where x_w and x_p are the mass fractions of water and skim milk solids, respectively, and C_{pp} is the heat capacity of the milk solids, which was found to be 1.256 kJ (kg °C)$^{-1}$ (Pisecky (1997) p. 24).

So the heat capacity of skim milk is:

$$C_{p\ skim\ milk} = \frac{0.912 \times 4.18\ \text{kJ (kg°C)}^{-1} + 0.088 \times 1.256\ \text{kJ (kg°C)}^{-1}}{1}$$
$$= 3.92\ \text{kJ (kg °C)}^{-1}$$

The enthalpy of the air entering the spray dryer can be calculated as follows:

$m_a = 0.0158$ kg s^{-1}

$C_{pa,i} = 1$ kJ (kg °C)$^{-1}$

$T_{hot\ air} = 443$ K

$Y_i = 0.010$ kg kg^{-1}

$\lambda = 2500$ kJ kg^{-1}

$C_{pw,v\ in} = 1.9$ kJ (kg °C)$^{-1}$

$m_{skim\ milk} = 5.10 \times 10^{-4}$ kg s^{-1}

$T_{skim\ milk} = T_{ca} = 295$ K

$m_{ca} = 0.0004$ kg s^{-1} (Source: Delavan Manual)

$C_{pca,i} = 1$ kJ (kg °C)$^{-1}$

$T_{ref} = 273$ K

The specific heat capacity data and the latent heat of vapourisation of water were obtained from Perry's Chemical Engineers' Handbook (1997).

$$H_{in} = 0.0158\ \text{kg s}^{-1} \times 1\ \text{kJ (kg°C)}^{-1} \times (443\ \text{K} - 273\ \text{K}) + 0.0158\ \text{kg s}^{-1} \times 0.010\ \text{kg kg}^{-1} \times$$
$$[2500\ \text{kJ kg}^{-1} + 1.9\ \text{kJ (kg °C)}^{-1}(443 - 273)] + 5.10 \times 10^{-4}\ \text{kg s}^{-1} \times 3.92\ \text{kJ (kg °C)}^{-1} \times$$
$$(295\ \text{K} - 273\ \text{K}) + 0.0004\ \text{kg s}^{-1} \times 1\ \text{kJ(kg°C)}^{-1}(295\ \text{K} - 273\ \text{K}) + 0.0004\ \text{kg s}^{-1} \times$$
$$0.010\ \text{kg kg}^{-1}[2500\ \text{kJ kg}^{-1} + 1.9\ \text{kJ (kg °C)}^{-1}(295\ \text{K} - 273\ \text{K})]$$
$$= 3.20\ \text{kW}$$

The equation for the enthalpy of the air leaving the dryer was given by equation 5.11. If the enthalpy of the skim milk powder produced from spray drying skim milk is included in the enthalpy of air leaving the dryer (since the skim milk powder is carried with the air), then the enthalpy of air leaving the dryer is given by:

$$H_{out} = m_a C_{pa,o}(T - T_{ref}) + m_a Y_o(\lambda + C_{pw,v}(T - T_{ref})) + m_p C_{pp}(T - T_{ref}) \qquad (5.11)$$

where the above symbols were defined in section 4.3.6, except for m_p, which is mass flowrate of the milk solids leaving the spray dryer (in kg s^{-1}). T is the temperature of the air leaving the spray dryer (in K). The equation for the heat losses was given by equation 4.11 in section 4.3.5 of Chapter 4.

$$Q_{loss} = UA(T - T_{amb}) \qquad (5.12)$$

where A (in m^2) is constant and the overall heat transfer coefficient U (in W m^{-2} K^{-1}) does not change significantly with temperature. UA is an average of 0.039 kW K^{-1} when fitted to heat balance results found previously for run 10. T_{amb} is the ambient temperature, which can be taken as 298 K.

Combining equations 5.8, 5.11 and 5.12 and rearranging the equation so that T is a function of all the other parameters gives the following equation:

$$T = \frac{H_{in} + (UAT_{amb} + m_a C_{pa,o} T_{ref} - m_a Y_o \lambda + m_a Y_o C_{pw,v} T_{ref} + m_p C_{pp} T_{ref})}{(UA + m_a C_{pa,o} + m_a Y_o C_{pw,v} + m_p C_{pp})} \quad (5.13)$$

Substituting the following values from run 10 for the parameters in equation 5.11 gives:

H_{in} = 3.20 kW

UA = 0.039 kW K^{-1}

m_a = 0.0158 kg s^{-1}

m_p = 4.49 × 10^{-5} kg s^{-1}

Y_o = 0.0339 kg kg^{-1}

$C_{pa,o}$ = 1 kJ kg^{-1} K^{-1}

$C_{pw,v}$ = 1.9 kJ kg^{-1} K^{-1}

λ = 2500 kJ kg^{-1}

C_{pp} = 1.256 kJ kg^{-1} K^{-1} for skim milk powder (Pisecky, 1992, p. 24)

T_{amb} = 298 K

T_{ref} = 273 K

The specific heat capacity data and the latent heat of vapourisation of water were obtained from Perry's Chemical Engineers' Handbook (1997).

$$T = \frac{3.20\ \text{kW} + \left(\begin{array}{l} 0.039\ \text{kW K}^{-1} \times 298\ \text{K} + 0.0158\ \text{kg s}^{-1} \times 1\ \text{kJ kg}^{-1}\ \text{K}^{-1} \times 273\ \text{K} \\ -0.0158\ \text{kg s}^{-1} \times 0.0339\ \text{kg kg}^{-1} \times 2500\ \text{kJ kg}^{-1} + 0.0158\ \text{kg s}^{-1} \times \\ 0.0339\ \text{kg kg}^{-1} \times 1.9\ \text{kJ kg}^{-1}\ \text{K}^{-1} \times 273\ \text{K} + 4.49 \times 10^{-5}\ \text{kg s}^{-1} \times \\ 1.256\ \text{kJ kg}^{-1}\ \text{K}^{-1} \times 273\ \text{K} \end{array}\right)}{\left(\begin{array}{l} 0.039\ \text{kW K}^{-1} + 0.0158\ \text{kg s}^{-1} \times 1\ \text{kJ kg}^{-1}\ \text{K}^{-1} + \\ 0.0158\ \text{kg s}^{-1} \times 0.0339\ \text{kg kg}^{-1} \times 1.9\ \text{kJ kg}^{-1}\ \text{K}^{-1} \\ + 4.49 \times 10^{-5}\ \text{kg s}^{-1} \times 1.256\ \text{kJ kg}^{-1}\ \text{K}^{-1} \end{array}\right)}$$

$$= 324\ \text{K} = 51^{\circ}\text{C}$$

3. The relative humidity of the air leaving the spray dryer should be calculated next, before the new equilibrium moisture content, X_{eq} can be found. Using the outlet air humidity (Y_o) and the outlet air temperature (T), the saturation vapour pressure can be found using the

Antoine equation (equation 5.14), and then the relative humidity can be found using the saturation pressure and partial pressure of water in the atmosphere as follows:

$$P_{sat} = \exp\left(18.3036 - \frac{3816.44}{T - 46.13}\right) \tag{5.14}$$

where P_{sat} is the saturation vapour pressure of water (in mm Hg) and T is the outlet air temperature (in K). So,

$$\begin{aligned} P_{sat} &= \exp\left(18.3036 - \frac{3816.44}{51 + 273 - 46.13}\right) \\ &= 94.8 \text{ mm Hg} \\ &= 12\,640 \text{ Pa} \end{aligned}$$

Now the relative humidity (ψ) is given by equation (5.15):

$$\psi = \frac{P_v}{P_{sat}} \tag{5.15}$$

where P_v is the partial pressure of water (in Pa) in this system. The partial pressure of water was given by Keey (1978) as:

$$P_v = \frac{Y_o P \times MW_a / MW_w}{\left(1 + Y_o \times MW_a / MW_w\right)} \tag{5.16}$$

where MW_a and MW_w is the molecular weight of air and water (in g mol^{-1}), respectively, and P is the absolute pressure (in Pa). Substituting equation 5.14 into equation 5.13, the relative humidity is given by equation 5.17:

$$\psi = \frac{\dfrac{Y_o P \times MW_a / MW_w}{\left(1 + Y_o \times MW_a / MW_w\right)}}{P_{sat}} \tag{5.17}$$

Substituting the following values for the parameters in equation 5.17 gives:

$Y_o = 0.0339$ kg kg^{-1}

$P = 101\ 325$ Pa

$MW_a = 29$ g mol^{-1}

$MW_w = 18$ g mol^{-1}

$P_{sat} = 14\ 043$ Pa

$$\psi = \frac{\dfrac{0.0339\ \text{kg kg}^{-1} \times 101325\ \text{Pa} \times 29\ \text{g mol}^{-1} / 18\ \text{g mol}^{-1}}{\left(1 + 0.032\ \text{kg kg}^{-1} \times 29\ \text{g mol}^{-1} / 18\ \text{g mol}^{-1}\right)}}{14043\ \text{Pa}}$$

$$= 0.42$$

Thus, a new estimate of the product moisture content can be found from the sorption isotherm below:

$$X_{eq} = \frac{K_1 K_2 K_3 a_w}{(1 - K_2 a_w)(1 - K_2 a_w + K_2 K_3 a_w)} \tag{5.18}$$

where the symbols and the values for the empirical constants are given in section 3.2. Substituting the following values for the parameters in equation 5.18 gives:

$\psi = 0.42$

$T = 51°C = 324$ K

$$X_{eq} = \frac{(0.19662\ \text{kg kg}^{-1})(0.26244)(4.6167)0.42}{(1 - 0.26244 \times 0.42)(1 - 0.26244 \times 0.42 + 0.26244 \times 4.6167 \times 0.42)}$$

$$= 0.080 \text{kg kg}^{-1}$$

5. Returning to step 2, the calculation is repeated until the initial moisture content of the product (X_o) equals its final value (step 5). In this case, the solution converges very quickly (two iterations), so

$$X_{eq} = 0.080 \text{ kg water/kg dry powder}$$

with $Y_o = 0.0339$ kg kg^{-1} and $T = 51°C$.

Table 5.11 shows the predictions for the operating conditions, namely the outlet air temperature (T_{pred}) and equilibrium moisture content (X_{eq}); and the measured outlet air

temperature (T_{exp}) and moisture content, for different inlet conditions for the experimental work here. Some of these conditions, like the higher solids concentration, are not actual operating conditions. Appendix C.4. contains the spreadsheets used for finding the results in Table 5.11.

Table 5.11 – Comparison of the predictions of the outlet air temperature (T) and equilibrium moisture content (X_{eq}) with experimental values for different operating conditions.

Run	Inlet temperature (°C)	Feed flowrate ($\times 10^{-4}$ kg s^{-1})	Solids concentration in feed (%)	T_{exp} (°C) Experiment -al	T_{pred} (°C) Predict -ed	$X_{eq,}$ (kg kg^{-1}) Predict-ed	Measured moisture content (kg kg^{-1})
1	230	5.11	8.8	68	68	0.034	0.037
10	170	5.11	8.8	52	51	0.080	0.068
13	200	5.11	8.8	59	59	0.057	0.044
16	230	4.40	8.8	66	65	0.037	0.033
20	230	3.85	8.8	71	70	0.031	0.027
-	230	5.11	20	-	69	0.030	-
-	230	5.11	50	-	74	0.019	-

According to Pisecky (1997), when equilibrium is achieved between the drying air and a particle, the relative humidity at the surface of the particle is equal to the relative humidity of the surrounding air, the particle is unlikely to dry any further and its temperature will not change. Thus, the particle temperature is equal to the temperature of the surrounding air and the temperature of the particles leaving a co-current spray dryer is likely to approach the temperature of the air leaving the dryer. The predicted operating conditions (particle temperature and moisture content) in Table 5.11 can be plotted on the sticky-point curve (obtained from Hennigs *et al.*, 2001) with the measured operating conditions as shown in Figure 5.12, to show how closely these predictions compare with the experimental results. The absolute values of the particle temperature and moisture contents are slightly different for the predicted and experimental cases. The differences in the moisture content ranged from 0.005 kg kg^{-1} to 0.006 kg kg^{-1}, while the differences in the temperature ranged from 1°C to 3°C. However, the experimental and predicted operating conditions have a similar trend, and the predictions are "conservative" because they predict slightly stickier behaviour than that actually seen.

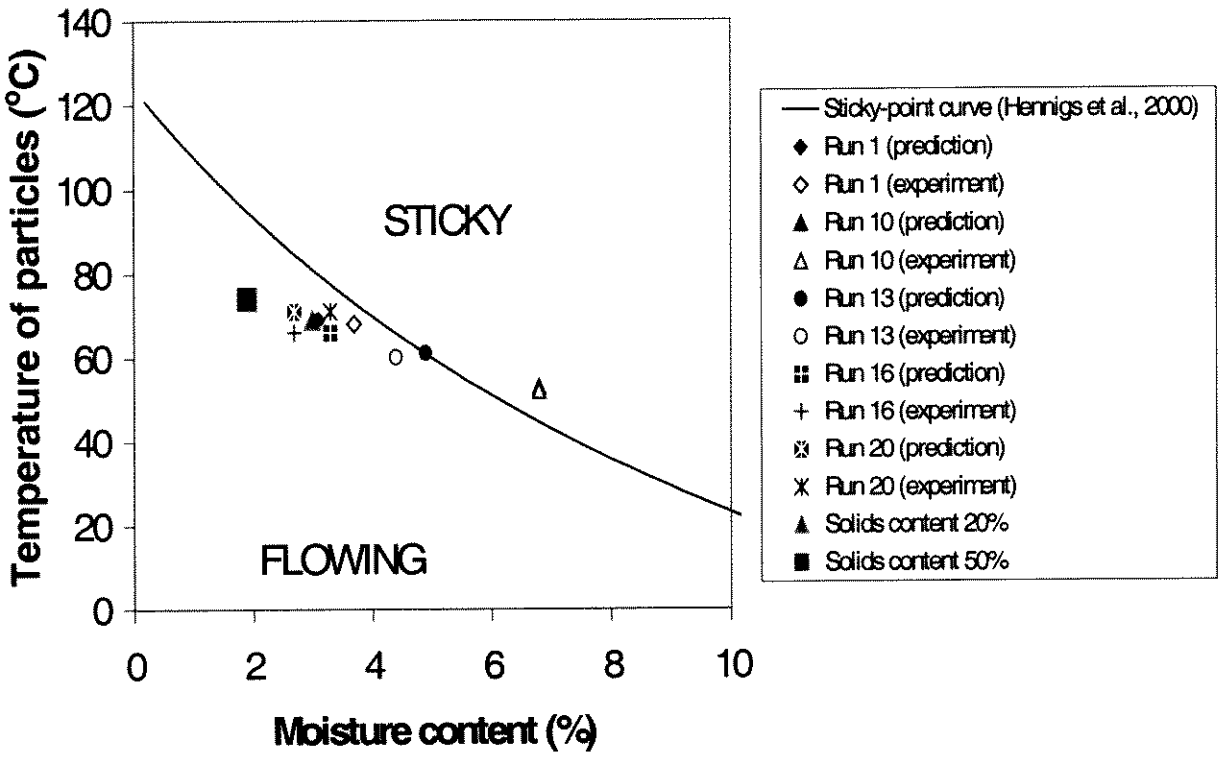

Figure 5.12 - Comparison between predicted and experimental operating points on sticky-point diagram for skim milk powder.

Figure 5.12 shows that, as the solids concentration of the skim milk is increased, the predicted operating points shift to the left hand side towards the non-sticky region. A higher concentration of 50% (w/w) solids of skim milk is spray dried in industry (Shallcross, 2000) compared with the concentration of 8.8% (w/v), which was used here. Pisecky (1997) recommended that a two-fluid nozzle (as used in this work), can handle process fluids with a solids concentration not much higher than 40% and therefore using a low solids concentration in this work is justified, since it allows the material to pass easily through the nozzle. Since the particles dry rapidly and approach their equilibrium moisture contents, it is possible that the different concentrations of materials used will affect the wall deposition fluxes significantly. A higher solids concentration will mean a lower total amount of evaporation, and hence a lower gas humidity in the dryer than with a lower solids concentration, as here. The lower gas humidity corresponding to a higher solids concentration may lead to lower outlet moisture contents (lower equilibrium moisture contents) and higher gas and particle outlet temperature. While lower moisture contents may make the particles less sticky, higher temperatures will have the opposite effect. Which effect dominates (lower moisture content or higher

temperature) will depend on the sticky-point curve and desorption isotherm for the material, and on the way in which the dryer is operated. The predictions in Figure 5.12 suggest that for skim milk powder, the effect that dominates is the lower moisture content rather than the higher temperature, giving rise to less stickiness and lower wall deposition fluxes with lower solids concentrations. A sample calculation showing how to find the impact of reducing the inlet air temperature on the productivity of the spray dryer (if this is necessary to reduce the stickiness of the particles and/or take into account the heat sensitivity of the material) is given next.

5.4.5 Estimation of Evaporative Capacity for Spray Dryer

In Chapter 3, the glass transition temperature of skim milk powder was found to be close to the sticky-point temperature. Thus, the glass transition temperature may be used to select the operating conditions of the spray dryer. The glass transition temperature has an uncertainty of about 20°C (White and Cakebread, 1966), and the sticky-point temperature has an uncertainty of at least 1°C (Hennigs *et al.*, 2001). The spray dryer should be run at lower chamber temperatures and thus lower air inlet temperatures to be certain that variations in the temperature due to control imperfections do not result in the chamber temperature exceeding the sticky-point temperature. Hence the inlet air temperature is limited by the uncertainty in the glass transition temperature. This in turn, means that the evaporative capacity of the dryer is limited by the uncertainty in the glass transition temperature; and the purpose of the following calculation is to quantify the limitations of the evaporative capacity due to an uncertainty in the glass transition temperature.

A diagram of a spray dryer showing the input and output streams given in Figure 5.13, where the symbols have been defined in section 5.4.4.

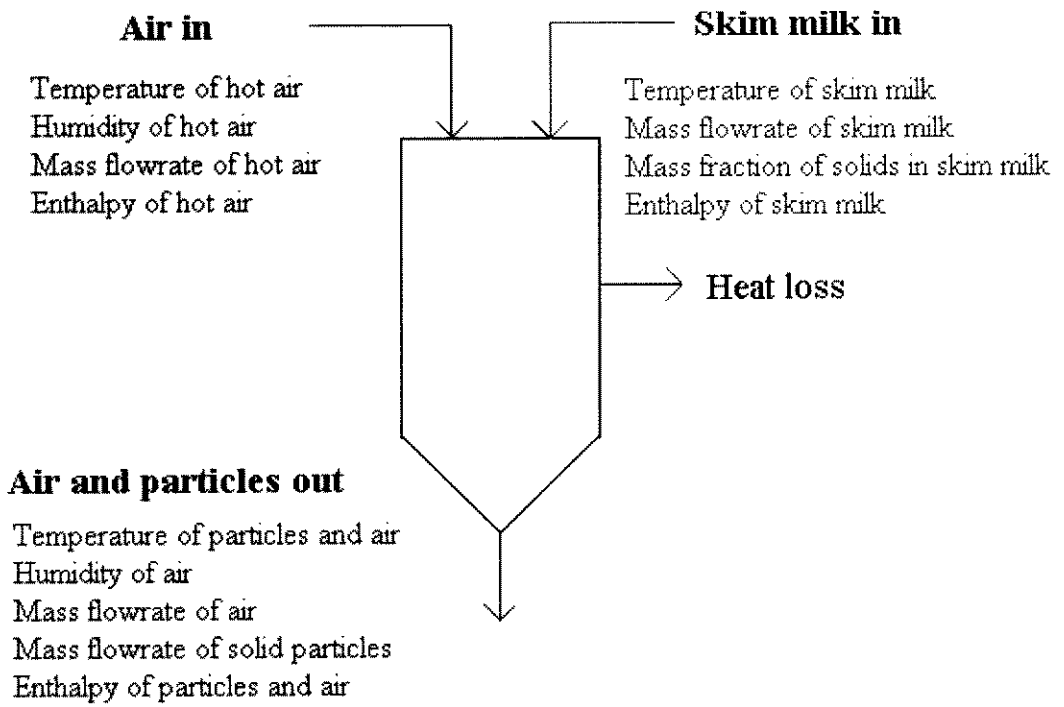

Figure 5.13– Schematic diagram showing input/output streams for the spray dryer, showing the parameters used to quantify the properties of the streams.

Suppose the maximum tolerable value of the skim milk flowrate, $m_{skim\ milk}$, which is also known as the evaporative capacity, is unknown. The maximum tolerable value of the skim milk flowrate occurs when the air leaving the spray dryer is saturated, that is, the air cannot hold any more water vapour. If the water flowrate is higher than this maximum value, the excess water will not evaporate, and wet product will deposit on the walls of the spray dryer.

The total enthalpy for the inlet streams, H_{in} (in kW) is given by equation 5.9. The unknown variable in this equation is the mass flowrate of the skim milk which can also be equated to:

$$\text{mass flowrate of skim milk} = \frac{\text{mass flowrate of water}}{\text{mass fraction of water in skim milk}} \tag{5.19}$$

The enthalpy of the outlet stream is given by equation 5.11 and the mass flowrate of the particles leaving the spray dryer may be expressed in terms of the mass flowrate of the water as given in equation 5.20.

$$\text{mass flowrate of solid particles} = \frac{\text{mass flowrate of water} \times \text{mass fraction of solids in feed}}{\text{mass fraction of water in feed}} \quad (5.20)$$

The unknown variable in equation 5.11 is the outlet air temperature, T and the outlet air humidity, Y_o.

The air leaving the dryer will only be saturated if the maximum amount of water is sprayed and is evaporated. Now Y_o can be found using equation 5.21 if the mass of water in the skim milk ($m_{water\ in}$) is known:

$$Y_o = \frac{m_{water\ in}}{m_{air\ in}} + Y_i \quad (5.21)$$

Keey (1978) gives an equation for the saturation humidity, Y_s on page 19 of his book:

$$Y_s = \left(\frac{M_w}{M_a}\right) \times \frac{p_w^o}{(P - p_w^o)} \quad (5.22)$$

where M_w and M_a were defined as the molecular weights of water and air, respectively; $p^o{}_w$ is the saturation vapour pressure of water and P is the total pressure of the system. The saturation vapour pressure can be found using equation 5.14, if T were known. The solver in Microsoft excel is used to find $m_{water\ in}$ and Y_o under the constraints that the heat entering the dryer is equal to the heat leaving the spray dryer, so that equation 5.23 holds; the outlet air humidity (equation 5.21) is equal the outlet air humidity if the air was saturated (equations 5.22) so that equation 5.24 holds. After find the $m_{water\ in}$, the mass flowrate of skim milk can be found using equation 5.19.

$$H_{in} - H_{out} = 0 \quad (5.23)$$

$$Y_o - Y_s = 0 \quad (5.24)$$

Appendix C4 provides a spreadsheet for the calculations carried out to find the evaporative capacity for an inlet air temperature of 170°C, 200°C and 230°C. Table 5.12 below provides the summary of the results for these calculations.

Table 5.12– Summary of evaporative capacity study for spray dryer for three different inlet air temperatures. The information required for the calculations were taken from Runs 1, 10 and 13 from this work, where skim milk was spray dried.

Inlet air temperature (°C)	Outlet air temperature (°C)	Water flowrate (Evaporative Capacity) ($kg\ s^{-1}$)
170 (Run 10)	41	7×10^{-4}
200 (Run 13)	44	8×10^{-4}
230 (Run 1)	45	9×10^{-4}

So decreasing the inlet air temperature by 30°C (from 230°C to 200°C) reduces the evaporative capacity by 10%, and decreasing the inlet air temperature by 60°C (from 230°C to 170°C) reduces the evaporative capacity by 25%.

5.5 A Preliminary Investigation of the Effect of Electrostatics Charges on the Wall Deposition Flux of Skim Milk Powder

An anti-static agent called Larostat 519 Antistat was added to the skim milk, at a concentration of 1% (w/w) in the skim milk. The anti-static agent did not dissolve in the skim milk, and a mill was used to disperse the material in the milk. The colour of the milk lightened, and a froth was formed at the surface of the milk. The milk was left in the fridge overnight to determine if the froth would settle. However, the milk had separated out into what appeared to be 'curds and whey'. Thus, this anti-static agent is unsuitable for addition to milk because it is probable that this anti-static agent breaks down the milk.

5.1.1 Grounding the Spray Dryer

The spray dryer was earthed by connecting the dryer to earth (water pipe) using conducting car booster cables, to make a preliminary assessment of whether or not electrostatic forces have an influence on the wall deposition flux in the spray dryer. According to AS/NZS 1020 (1995), a total resistance between object and earth not exceeding 1 MΩ is sufficient to prevent charge accumulation. Prior to earthing the spray dryer, the resistance between the earth and dryer was measured using a Multimeter as 0.5 Ω, so the equipment was virtually earthed. De-earthing the equipment could be very difficult and dangerous, in view of the potentially flammable nature of skim milk. Nevertheless, when two pairs of car booster cables were connected to the spray

dryer and water pipe, the resistance dropped to 0.1 Ω. The spray drying condition used was the one which gave the highest wall deposition flux, so as to determine if grounding can significantly alleviate the wall deposition problem. The inlet air temperature was 170°C, the feed flowrate was 1.84 kg hr^{-1}, the compressed air flowrate was 200 kPa and the swirl vane angle was set to 0°.

The average deposition flux when the spray dryer was grounded was 14.2 ± 1.2 g m^{-2} hr^{-1} compared with when the spray dryer was not grounded, 15.3 ± 1.6 g m^{-2} hr^{-1}. Statistical analysis in Appendix C3 shows that based on the standard deviations of 0.5 g m^{-2} hr^{-1} and 0.8 g m^{-2} hr^{-1}, the difference between the wall deposition fluxes for a grounded spray dryer and a non-grounded spray dryer is only slightly significant (with 75% confidence), suggesting that electrostatic effects have some influence on wall deposition. Nevertheless, there is little potential for grounding the equipment further than the 0.1 Ω resistance to ground found here. Even this excellent grounding (according to the AS/NZS1020 specification) has not eliminated wall deposition. In addition, if the uncertainty in the wall deposition flux is increased from 0.5 - 0.8 g m^{-2} hr^{-1} to 2 g m^{-2} hr^{-1}, as suggested earlier, the significance of the decrease in flux from an average of 15.3 g m^{-2} hr^{-1} (no grounding) to 14.2 g m^{-2} hr^{-1} (grounding) is much less clear.

5.6 The Effect of Changing the Wall Properties and Time on the Wall Deposition Fluxes

As shown in Figure 5.14, adhesive was placed on plate 5 and 6 to determine if this would have any influence on the wall deposition flux. It might be expected that more deposition of particles would occur with the presence of a adhesive if adhesion occurred at a different rate to cohesion for skim milk powder, because the chance of the particles sticking to the adhesive might be higher than to a clean stainless steel plate. Chen *et al.* (1993) observed that the milk particles were more likely to stick to each other than to a clean stainless steel section of the dryer, which might indicate that cohesion of particles to each other occurs more readily than adhesion of milk particles to stainless steel walls.

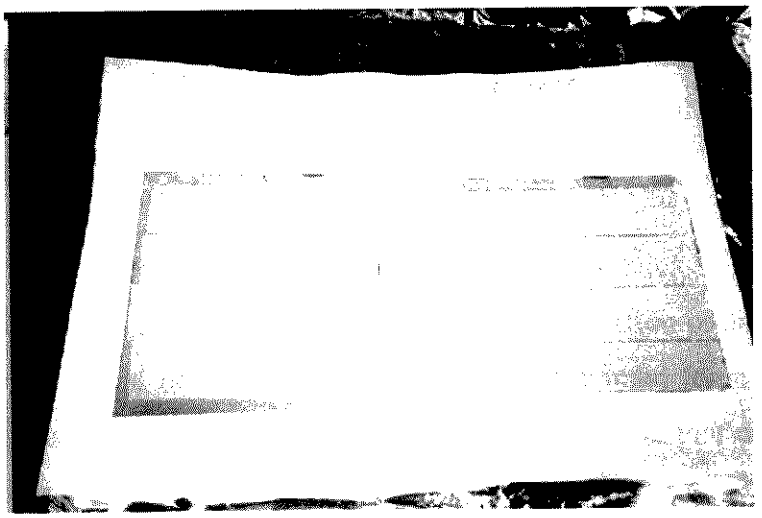

Figure 5.14 – Photograph of adhesive on plates 5 and 6 for experiments to test effect of adhesion and time on wall deposition flux of skim milk powder.

The spray drying conditions used here were a single inlet air temperature (170°C), compressed air pressure (200 kPa), swirl vane angle (0°) and feed flowrate (1.84 kg hr^{-1}). The spray dryer was run for 30 minutes, then 1 hour and finally for 2 hours. These experiments were repeated with the adhesive tape removed, and the plates were cleaned first before being placed back into the spray dryer. The wall deposition fluxes were measured for each case to assess whether or not the deposition process was time dependent. As shown in Figure 5.15, the amount of wall deposition increased as the duration of the experiment was increased, but the wall deposition flux (mass of powder/area of plate) was virtually constant. There was no significant difference between the wall deposition fluxes with and without adhesion for the spray impaction situation (plates 5 and 6). There was a maximum difference of 17% between the wall deposition fluxes for the case with adhesive and without adhesive, which occurred for the two hour runs. This difference is not very significant relative to the experimental uncertainties in measuring this flux (discussed in section 5.2). This figure shows that the amount of skim milk powder deposited increases linearly with time, and this may suggest that cohesion occurs at the same rate as adhesion for skim milk powder under the conditions in this spray dryer for the following two reasons, at least. First, increasing the adhesion tendency at the wall has no significant effect on the wall deposition flux (between a smooth stainless steel wall and a wall covered with double-sided adhesive tape). Second, if adhesion occurred at a different rate to cohesion, it might be expected that the initial deposition flux (when adhesion first occurs) might be different to subsequent fluxes when particles cohere to other adhered particles. Therefore the powder mass on the plate would not be expected to be a linear function of time if adhesion were an important process in wall deposition, rather a non-linear curve would be expected. The linear functions observed here are consistent with particles cohering to other particles that

are already adhered to walls. This is consistent with the observations that the plates were completely covered with a fine layer of particles after 30 minutes, and therefore that no further opportunities for adhesion were present after 30 minutes.

Agglomeration is a process by which wet particles are forced to stick to each other to form an agglomerate, and therefore liquid bridging forces cause the formation of an agglomerate. From section 2.6, while the liquid bridging force is likely to be the main force holding particles to each other (as long as a liquid bridge is formed), it is still possible that other mechanisms by which particles cohere to other particles on the walls of the spray dryer are van der Waals and electrostatic forces. In this work, it was observed when the skim milk powder in the product container, was shaken lightly, it clung lightly to each other and then detached when it was shaken again. Also, the skim milk powder adhered to a metal spoon when collected for tests to measure the moisture content of the sample, suggesting that electrostatic charges on particles might be significant. In any case, Since cohesion is the controlling process in wall deposition of skim milk powder, the sticky-point test, which measures the cohesive nature of particles is applicable to drying equipment, for skim milk powder, at least.

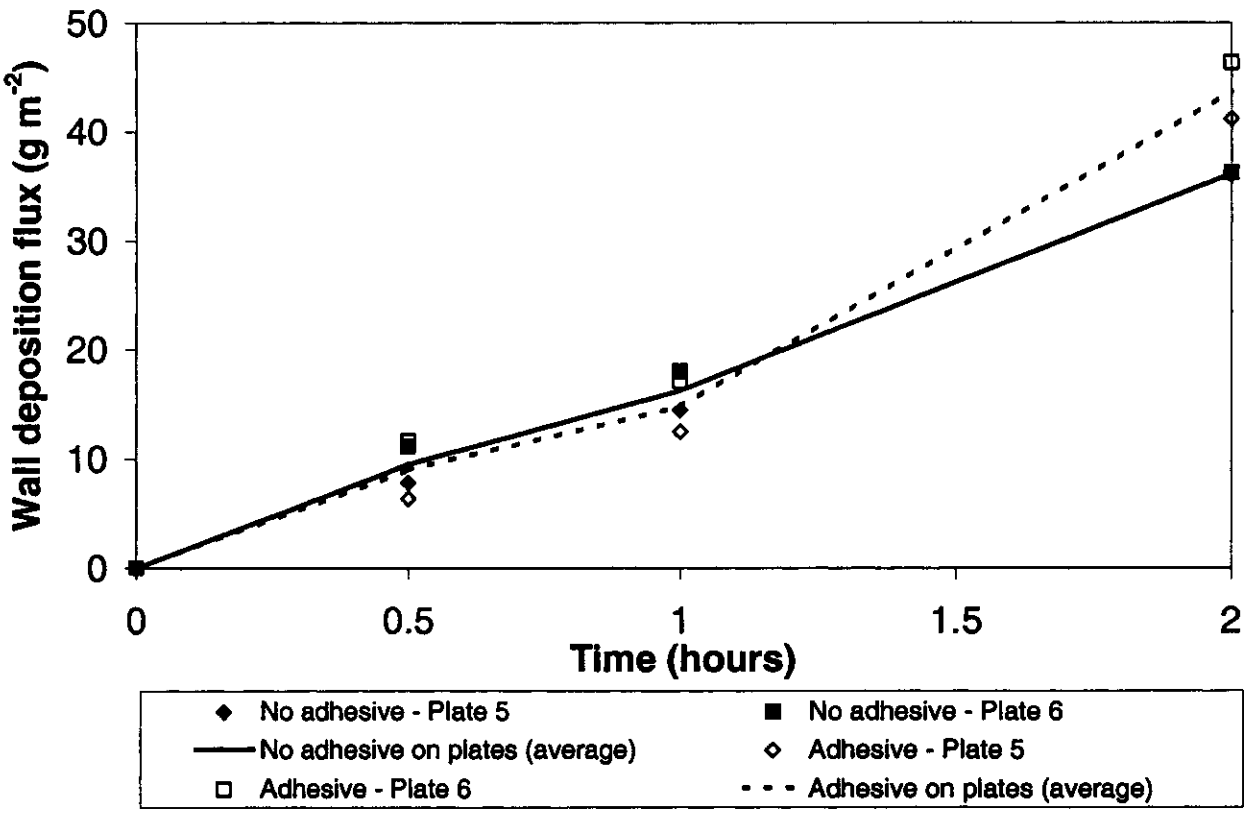

Figure 5.15 - The mass of powder collected on plates as a function of time for the cases of no adhesive and adhesive on plates 5 and 6.

To start to assess if agglomeration of particles occurs at the walls of the spray dryer, and thus whether or not cohesion occurs at the same rate as adhesion in wall deposition, small aluminium strips (sample plates) with dimensions 0.4 cm × 2 cm were connected to the wire holding plate 5 in place. These sample plates were left in the dryer for one hour to allow skim milk powder to collect on their surface. The sample plates were then coated with platinum and examined under a Philips XL30CP Scanning Electron Microscope operating at 10kV. Figure 5.16 shows agglomerates present on the surface, and agglomeration of particles to each other is a cohesion related process. However, it is uncertain whether agglomeration of particles occurs before or after the particles have adhered to the walls of the dryer. Furthermore, there is also a scattering of single particles that appear to be sitting on, possibly adhered to, the wall and on which other particles could cohere, so many opportunities for cohesion are present.

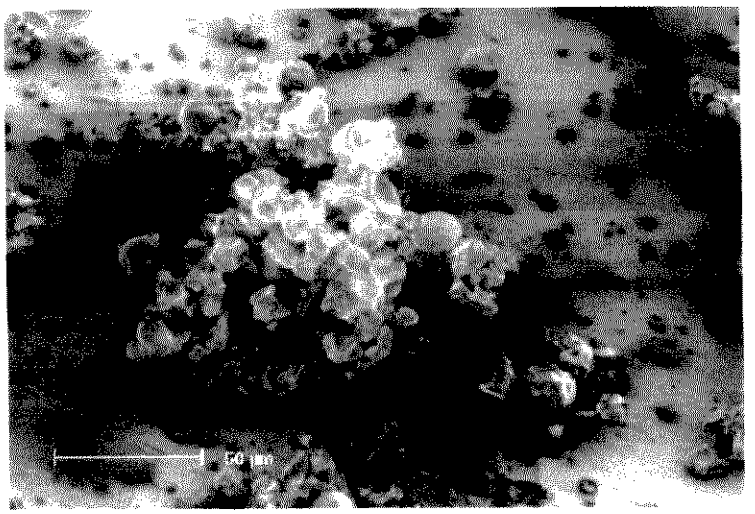

Figure 5.16 - Photograph of skim milk powder particles adhering to the aluminium sample plate placed in the spray dryer. Magnified ×1000 by Philips XL30CP Scanning Electron Microscope. Operating at 10kV. The bar shown in the photograph has a length of 50 microns.

To investigate further if agglomeration occurs before or during wall deposition, a sample of skim milk powder leaving the dryer was collected from the product container and placed onto a stub covered with a double sided conducting tab. The powder collected from the product container was observed to cling to other particles and also clung to the metal spoon used to remove it from the container. Therefore, it is possible that van der Waal forces and electrostatic forces were responsible for the skim milk powder behaving this way. The skim milk powder that was clinging to the powder in contact with the conducting tab was shaken off, by lightly tapping the stub. This action could have broken up agglomerates. The surface of the stub was coated with platinum and examined under a Scanning Electron Microscope (Figures

5.17). The particles were not agglomerated, and particle size analysis a Malvern Particle Size Analyser (Model 2600C) showed that 90% of the particles had a diameter less than 6 μm. In comparison with Figure 5.16, which showed agglomerated particles on walls, this suggests that primary particles cohere to already adhered particles on the walls to make agglomerates. However, it is also possible that agglomerates formed inside the dryer have deposited preferentially on the wall, so further study is required to assess this possibility further.

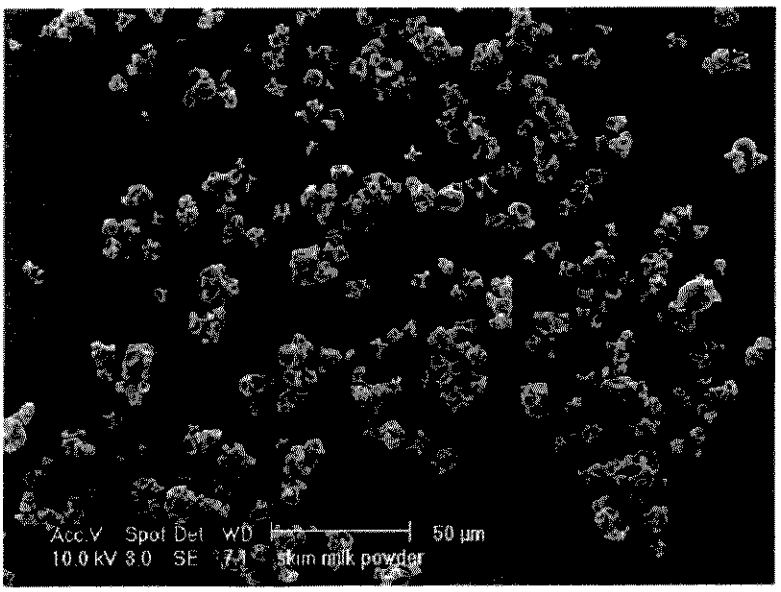

Figure 5.17 - Photograph of the skim milk powder particles that have left the spray dryer. Magnified ×1000 by Philips XL30CP Scanning Electron Microscope. Operating at 10kV. The bar in the photograph has a length of 50 microns.

The particle size distribution for the skim milk powder is given in Figure 5.18, showing the skim milk powder has a particle size distribution ranging from 0.6 microns to 20 microns. Appendix C7 contains more photographs of the skim milk powder taken using a Scanning Electron Microscope.

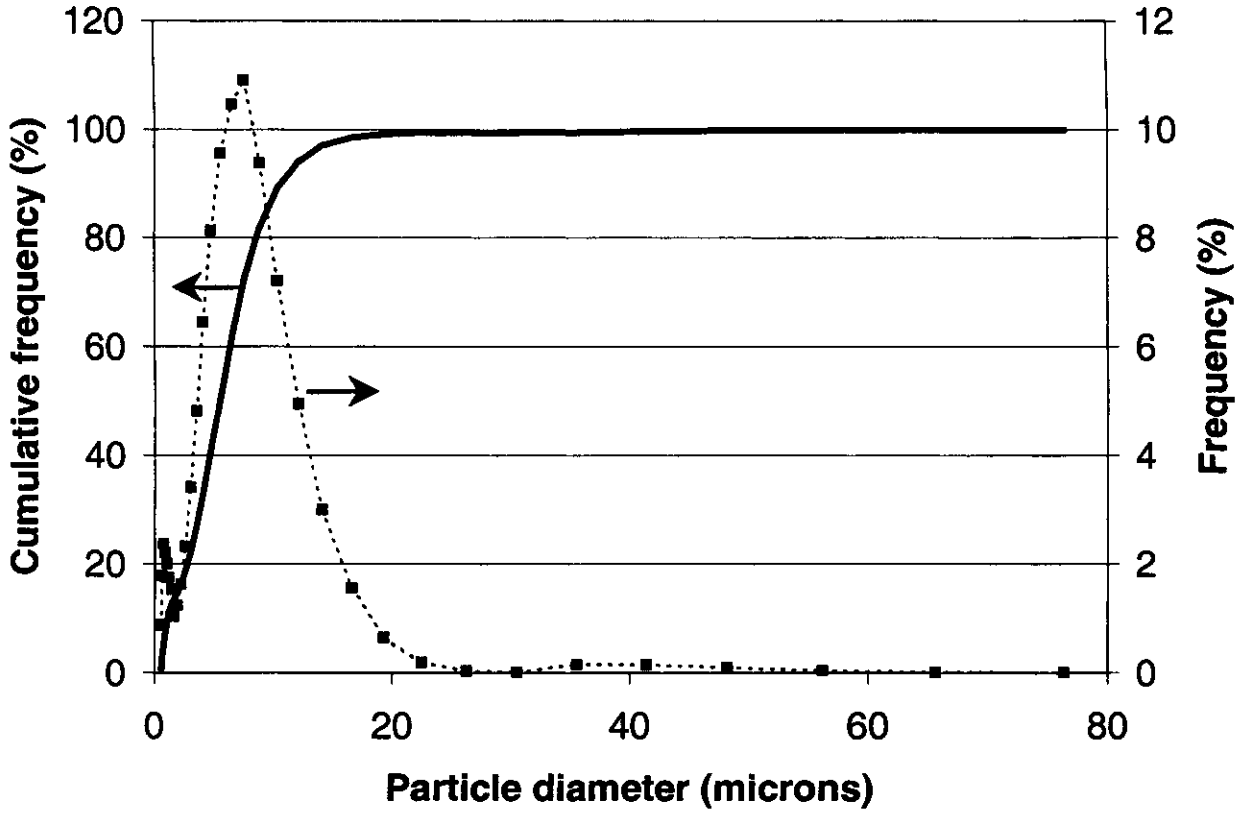

Figure 5.18 – Particle size distribution for the skim milk powder, showing the particle diameters ranged from 0.6 microns to 20 microns, and the median particle size was 6 microns.

So far, this section has investigated and discussed the effect of increasing the adhesiveness of the wall on the wall deposition flux. The use of a wall material that may reduce wall deposition was also investigated, since previous researchers such as Papadakis and Bahu, (1992), have pointed to the use of plastic film on surfaces as a possible means of reducing wall deposition (section 2.10). Plates 5 and 6 were coated with a food-grade non-stick nylon coat (run 32). The wall deposition flux for run 32 and run 20 (base case) were compared. The wall deposition flux did not decrease significantly by using a non-stick nylon coating on plates 5 and 6. The average wall deposition flux when using the nylon as a wall material was 4.7 ± 0.2 g m^{-2} h^{-1}, while the wall deposition flux was 4.8 ± 0.7 g m^{-2} h^{-1} for the case when the surface material was stainless steel. As discussed above, wall deposition by spray impaction seems to be a cohesion-related process for milk, at least, and changing the wall material does not appear to influence the wall deposition flux significantly here.

5.7 Overall Discussion and Conclusions

As pointed out in the introduction to this thesis, self-ignition of milk powder deposits are believed to be the most important cause of fires and explosions in milk powders. A sample calculation will be given now to provide an overall indication of the significance of these wall deposition fluxes with respect to fire hazards

Skim milk powder will self-ignite at a critical thickness layer of 13 mm at a temperature of 180°C (Chong *et al.*, 1999). To determine how long the spray dryer can operate before it has to be cleaned, to avoid self-ignition of the skim milk powder deposit, the rate at which the skim milk powder layer builds up, *rate* (in m hr^{-1}) is calculated by dividing the wall deposition flux (kg m^{-2} hr^{-1}) by the density of the skim milk powder (kg m^{-3}). The density of the skim milk powder can be calculated using the following equation from Pisecky, (1997) p. 23:

$$\rho = \frac{100}{\frac{m_1}{\rho_1} + \frac{m_2}{\rho_2} + \frac{m_3}{\rho_3}} \tag{5.25}$$

where m_1, m_2 and m_3 are the contents of the individual components of skim milk (in percent) and ρ_1, ρ_2 andρ_3 are their densities (in kg m^{-3}). Skim milk is a complex solution comprising of mainly protein, lactose and water. Table 5.13 shows the densities of these components (Source: Pisecky, 1997 p.23) and their concentration in skim milk powder (Singh and Newstead, 1992).

Table 5.13 – Densities and concentration of components of skim milk powder.

Component	Density at 20°C (kg m^{-3})	Concentration (% w/w)
Protein	1390	39
Lactose	1520	49
Water	1000	3.7

The concentration of the components of skim milk powder were given for the season of spring. The concentrations of protein and lactose vary from season to season, and in winter, the concentration of lactose is lower (45%) and protein is higher (43%). Since the fat content in skim milk is only 0.8%, which is negligible, and density data for ash, which makes up 7% of the skim milk powder, was not available, the density of skim milk powder was calculated using density and concentration data for protein, lactose and water.

$$\rho = \frac{100}{\frac{39}{1390} + \frac{49}{1520} + \frac{3.7}{1000}}$$
$$= 1563 \text{ kg m}^{-3}$$

Therefore, a high wall deposition flux of 15 g m^{-2} h^{-1} is equivalent to a rate of 15×10^{-3} kg m^{-2} h^{-1} /1563kg m^{-3} = 0.01×10^{-3} m hr^{-1}.

Apart from the hot spots around the air inlet, the temperature in the spray dryer seldom exceeds 100°C (Pisecky, 1997). However, if a skim milk powder layer with a thickness of 13 mm is located close to the air inlet region where the temperature is about 180°C, the spray dryer will require cleaning after the following number of days to prevent self-ignition of the skim milk powder and a fire:

$$\text{Number of days before critical thickness layer achieved} = \frac{0.013 \text{ m}}{0.01\times10^{-3} \text{ m hr}^{-1}}$$
$$= 1354 \text{ hours}$$
$$= 56 \text{ days}$$

If the wall deposition flux of skim milk powder was 4 g m^{-2} hr^{-1}, which was the lowest wall deposition flux found in this work, the number of days before the critical thickness layer is achieved increases to 270 days, which is almost five times as long as if the wall deposition flux was 15 g m^{-1} hr^{-1}.

Overall, this work directly supports the concept of a product moisture locus, as shown in Table 5.2, where the equilibrium moisture content is close to the measured moisture content of the skim milk powder. Furthermore, the concept of the product moisture locus has been supported by all the indirect evidence in section 5.3. For example, this concept suggests that a lower equilibrium moisture content means a lower product moisture content, so the decrease in the product moisture content at a higher temperature may be due more to the lower equilibrium moisture content than to the faster drying kinetics at higher tempreatures. It is true that the drying rate may be faster at higher particle temperatures, but this may not be the main reason for the trends that have been both predicted and observed experimentally, here. The work of Harvie *et al.* (2002) supports this concept, where they found the predicted (simulated) skim milk particle moisture contents predicted using CFD were similar to the equilibrium moisture

contents. Their spray dryer was large compared with the pilot spray dryer used here. In order to assess the research question of what process scale (size of dryer) causes the drying behaviour to be kineically limited, the next step from here would be to carry out tests using a spray dryer smaller than the one used in this work, such as a Buchi-191 spray dryer (width: 50 cm, depth: 60 cm, height: 100 cm) which is commonly used for spray drying pharmaceutical solutions, and meaure the outlet moisture contents of the particles, to determine if they are close to the equilibrium moisture contents. If the moisture contents (equilibrium and actual) are close, then it can be concluded that spray drying behaviour at most process scales is equilibrium limited rather than limited by kinetics.

The sticky-point curve helps to predict wall deposition, but stickiness does not appear to be a sudden process. Close approaches to the sticky-point curve appear to lead to more wall deposition for spray impaction, but wall deposition does not occur suddenly when the sticky-point curve is reached, nor does it stop suddenly when the product temperatures and moisture contents are below the curve. The sticky-point curve is not the only aspect that is important. Figure 5.3 shows that for the same inlet air temperature, feed flowrate and compressed air pressure, there is a signficant effect of swirl vane angle and hence the air flow pattern on the deposition flux. Electrostatics may affect wall deposition, but earthing the dryer well did not eliminate this problem. There was no significant increase in the amount of powder deposited on plates 5 and 6 (spray impaction) when an adhesive was placed on the plates. In addition, the wall deposition flux remained constant with time with or without an adhesive on the plates, suggesting that cohesion occurs at the same rate as adhesion in the wall deposition of skim milk particles in spray impaction.

Micrographic evidence suggests that significant agglomeration has occurred here at the wall itself, although it is also possible that agglomerates formed inside the dryer have deposited preferentially on the wall, so further study is required to assess this possibility further.

Chapter 6

Spray Drying of Concord Grape Skin Extract

In January 1999, two experiments were carried out at the Department of Chemical Engineering at the University of Sydney by Dr Tobias Kockel and David Southwell, to test the feasibility of spray drying concord grape skin extract, which from here onwards will be referred to grape skin extract. Their work will be referred to as Kockel and Southwell (1999) from here onwards. The grape skin extract was supplied by Food Ingredients Technologies Australia Pty Ltd (FITA), who removed the sugar from the grape skin extract by using a fermentation process (Private communication: Lang, 2001).

The operating conditions for the first experiment were a process fluid flowrate of 2.4 L hr^{-1} (for the first 2.5 hours of spray drying) and then 2.0 L hr^{-1} (for the last 1.5 hours of spray drying), and an inlet air temperature of 230°C. The reason the process fluid flowrate was reduced was so that the evaporative load imposed on the dryer could be reduced. They observed that this change allowed the cyclone to operate more effectively. The concentration of the solids in the process fluid was determined to be 20 % w/w (dry basis), after drying two samples of the process fluid for 48 hours at 105°C. The relative humidity of the air leaving the spray dryer was 47%. The operating conditions for the second experiment were a feed flowrate of 1.8 L hr^{-1}, an inlet air temperature of 200°C (for the first hour of operation) and then 210°C (for the remainder of the experiment). The concentration of the solids in the process fluid was determined to be 22%, after using the same spray drying method described above. The relative humidity of the air leaving the spray dryer was 47%.

The yield (defined as the total percentage recovery of solids minus the moisture content of the solids) of grape powder from their first experiment was 90.3%, and for their second experiment, was 89.0%. However, this yield was determined by collecting samples from the

cyclone, glass product container, the dryer cone, the pipe leaving the dryer, the pipe leaving the cyclone. They observed that in their first experiment, a relatively large quantity of material was recovered from the conical section of the spray dryer, and they suggested that this may have been the result of using a high feed flowrate for the first 2.5 hours of the experiment. Kockel and Southwell (1999) demonstrated that it is possible to spray dry grape skin extract to produce a powder. They stated that the operating conditions they used for spray drying the grape skin extract may not have been the optimum conditions. They also recommended that HPLC tests would be required to assess whether any change in composition and colour on the grape powder resulted from the drying process. The outcome of the HPLC tests carried out on the grape powder for this work is discussed in section 6.2.3.

The purpose of this work was to carry on from Kockel and Southwell's (1999) work and spray dry the grape skin extract using the optimum operating conditions found from spray drying skim milk. The optimum operating condition refers to the conditions which gave rise to the least spray deposition flux of the skim milk powder. A low wall deposition flux means that more product can be recovered from the spray drying process, and this is especially important when the material is expensive as it is here. The wall deposition flux of grape skin extract can then be compared with the wall deposition flux of skim milk, and this information is important, because it will provide quantitative information about the difference between drying different materials. HPLC tests were also carried out by CSIRO on the grape powder produced from spray drying the grape skin extract in this work.

Fermented grape skin extract with a solids content of 50% (w/w) on a total mass basis was supplied by FITA for this work. The sugar in the concord grape extract was removed by fermentation because, as suggested in section 2.9 of Chapter 2 of this thesis, the removal of components such as sugar that contribute to the stickiness of a mixture might reduce the stickiness of the material. If the material is less sticky, the particles produced by spray drying are less likely to stick to the walls of the dryer when they get there.

The operating parameters and feed conditions used for spray drying the grape skin extract will be described in section 6.1. The protocol for spray drying the grape extract was identical to the one for spray drying skim milk (section 4.2.9). The results for the moisture content, particle size and HPLC tests and observations for spray drying the grape skin extract will be discussed in section 6.2. This section will also include a comparison between the drying performance of

skim milk and grape skin extract. A sample calculation using equations and correlations for predicting the surface-volume diameter of droplets produced using a two-fluid nozzle will be given in section 6.3. This section will also include a comparison of predicted droplet sizes and actual particle sizes obtained in this work for grape powder and skim milk powder. Section 6.4 discusses the possibility of using apple fibre and orange fibre as additives for grape skin extract, to improve the drying performance of the grape skin extract by reducing the stickiness of the particles produced from the spray dryer, and thus minimise wall deposition. Finally, the conclusions are given in section 6.5.

6.1 Operating Conditions for Spray Drying Grape Skin Extract

6.1.1 Feed Conditions

The solids content of the grape skin extract supplied by FITA was determined as follows. Three samples of the grape skin extract, of approximately 35 g each, were weighed into glass petrie dishes and dried in a fan forced oven over a period of two days at 85°C as recommended by de Knegt and Van den Brink (1998) for milk powder. The material was not dried at 102°C to avoid the possibility of degrading the nutraceuticals present in the grape skin extract. The solids content was determined to be an average of 51% on a total mass basis.

Three process fluid samples of different solids concentrations were spray dried. The first sample of the process fluid had a solids concentration of 7% on a total mass basis, which was prepared by diluting a portion of the grape extract with water. This sample was used for finding the wall deposition flux of grape powder and comparing it with the wall deposition flux of skim milk powder, which was produced by spray drying skim milk with a solids concentration of 8.8% (w/v). The second sample of the process fluid had a solids concentration of 28.5% on a total mass basis and the third sample has a solids concentration of 16% on a total weight basis. These last two samples were used for obtaining grape powder for HPLC testing and particle sizing.

6.1.2 Spray Dryer Settings

The grape skin extract was spray dried using the optimum operating conditions for skim milk powder, which were the conditions that gave rise to the lowest wall deposition flux (4 g m^{-2} hr^{-1}) of skim milk powder (section 5.4). The grape skin extract contains valuable nutraceuticals (section 2.2.2), and it is desirable to recover as much of the powder as possible with minimal wall deposition. The dryer inlet air temperature was 230°C, the liquid feed flowrate was 1.4 kg hr^{-1}, the swirl vane angle was 0°, and the compressed air pressure was 200 kPa.

6.1.3 Comparison of Dryer Performance between Kockel and Southwell's (1999) Work and This Work

A comparison of the operating conditions used for spray drying grape extract, between Kockel and Southwell's (1999) first experiment and this work will now follow. The inlet air temperature (230°C) and outlet air temperature (70°C) were the same. The process fluid flowrate used by Kockel and Southwell (1999) was higher at 2.0 – 2.5 L hr^{-1}, compared to the process fluid flowrate used here, which was 1.4 kg hr^{-1}.

The relative humidity of the air leaving the dryer was different. In this work, the relative humidity of the air leaving the dryer was 12%, while in Kockel and Southwell's (1999) work the relative humidity was 47%. The relative humidity of the outlet air for this work was found to be 12%, which is the same as the relative humidity of the outlet air from spray drying skim milk. The mass and energy balances in this work have been checked carefully.

In Kockel and Southwell's (1999) second experiment, they used a lower inlet air temperature (20°C lower) compared with their first experiment. The process fluid flowrate was also lower by 0.2 L hr^{-1}. They found that in the second experiment, no build up of powder in the cyclone occurred.

Trace heating was used around the pipe leaving the spray dryer and around the cyclone to prevent condensation within the equipment for both spray drying grape extract and skim milk powder. The trace heating elements were set to a temperature of 45°C, which was previously found to be higher than the dew point temperature of water for the spray drying conditions used

in this work. This would prevent condensation within the container and caking of the powder. Kockel and Southwell (1999) also used trace-heating of the product container in their second experiment for the same reasons as mentioned above.

6.2 Results

6.2.1 Experimental Observations

Upon spray drying the concord grape extract with a solids concentration of 7% (w/w) on a total mass basis, a crimson to fuchsia coloured free-flowing powder was produced. Skim milk powder was white and also free-flowing. However, in contrast to skim milk powder, the grape powder became sticky and tacky and formed a viscous sticky liquid in less than an hour when it was left exposed to the atmosphere, suggesting that it was considerably more hygroscopic than skim milk powder. Kockel and Southwell (1999) also observed that when the grape powder was left exposed to the atmosphere, a skin was formed around the powder. They experienced problems in their first experiment with removing the powder deposits from the walls of the spray dryer because the powder was left exposed to the atmosphere for several weeks. In this work, it was found that the powder deposits could be easily removed from the walls of the spray dryer and the outlet pipes, if the spray dryer was cleaned immediately after the drying operation was stopped. Cleaning the spray dryer immediately would prevent the grape powder from absorbing moisture from the atmosphere, and transforming into a viscous sticky liquid, and therefore adhering to the walls of the spray dryer more strongly than the free flowing powder. These results may indicate the most appropriate conditions for storing grape powder produced from spray drying grape skin extract, since the powder was free flowing under the operating conditions for the spray dryer. The most important of these operating conditions was a relative humidity of 12%, since Keey (1992) indicates that the temperature does not affect the equilibrium moisture content significantly over a temperature range from ambient conditions (around 20°C) to the dryer outlet conditions of around 60°C. This reason for this is that changes in the equilibrium moisture content are typically related to changes in the absolute temperature (20°C, 293 K; 60°C, 343 K). The relative humidity in the dryer was 12%, giving free-flowing material, whereas the ambient relative humidity was 70%, giving sticky powder due to its absorption of atmospheric moisture. This outcome suggests that the grape powder certainly needs to be stored under a relative humidity of 70%, and also that a relative humidity of 12% will almost certainly be adequate to keep it free flowing.

6.2.2 Wall Deposition Flux of Grape Powder

The average wall deposition flux for the grape powder was 2.9 ± 0.2 g m^{-2} hr^{-1}, while that of skim milk powder was 3.8 ± 0.7 g m^{-2} hr^{-1} for the same operating conditions. The difference between the wall deposition fluxes is statistically significant with 95% confidence (refer to Appendix D.1 for calculation). The concentration of solids in the skim milk (8.8% w/v) was higher than that of the grape powder (7% w/w) by 1.8%. However, the difference in the concentration of solids in the skim milk and grape extract is not very high, and it is possible that the difference in the wall deposition of the material is due to the nature of the material being spray dried.

The work of Bhandari *et al.* (1993), Chen *et al.* (1993) and Mahony (2001) support the theory that the wall deposition depends on the nature of the material being spray dried. Bhandari *et al.* (1993) found that, depending on the type of sugar that was present in the fruit juice they were spray drying, the quantity of maltodextrin (additive used to raise the sticky-point temperature of the material) needed to be varied so as to obtain a satisfactory yield of product. Chen *et al.* (1993) and Mahony (2001) found that the wall deposition of whole milk powder was higher than that of skim milk powder. They both suggested that the difference in the wall deposition flux was due to the presence of fat in whole milk (absent in skim milk) which made the material (whole milk powder) more sticky, because it melts at temperatures inside the dryer, and thus more likely to stick to the walls of the dryer when the powder gets there.

6.2.3 Composition of Grape Powder

Spray drying the extract into a powder did not have any affect on the composition of nutraceuticals, colour or aroma when compared with the grape extract (Private communication: Lang, 2002).

6.2.4 Mass and Energy Balances

Appendix D.1 shows that the discrepancies in the water balance for spray drying grape skin extract (for measuring the wall deposition flux) ranged from –30% to –6%. In addition, as shown in Appendix D.1, the discrepancies in the energy balance ranged from –2.35 kW to

–1.99 kW. From section 5.1 of Chapter 5 in this thesis, the discrepancies in the water balance from spraying skim milk ranged from –38% to –2% and the discrepancy in the energy balance ranged from –1.01 kW to –2.39 kW. Thus, the water and energy balance discrepancies when spray drying grape skin extract appear to be reasonable, because they are consistent with the results for spraying skim milk.

6.2.5 Moisture Content of Grape Powder

The moisture content of the grape powder where the solids concentration of the feed was 16% (w/w) was determined as follows. Approximately 10 g of the grape powder was weighed out into three aluminium trays. The grape powder was dried for a period of 2 days at 85°C using a fan-forced oven according to de Knegt and Van den Brink (1998). The moisture content of the powder was 8.2% (w/w) on a dry basis. The moisture content of skim milk powder produced using the same spray dryer operating conditions here was 2.7% (w/w) on a dry basis. Once again, the higher moisture content for the grape powder could be due to the nature of the material and its ability to bind to water. The higher final moisture content of the grape powder (than skim milk powder) is consistent with the more hygroscopic nature of the grape powder (compared with skim milk), which has already been discussed in the context of the experimental observations. A further useful deduction can be made from the analysis in this thesis that the outlet moisture contents of the solids from this dryer are very close to being in equilibrium with the outlet gas. This finding suggests that the equilibrium moisture content of grape powder is around 8.2% at a relative humidity of 12%, which is a start to producing a desorption isotherm for grape powder. More information about this desorption isotherm could be obtained (more points on the equilibrium moisture content against relative humidity curve) by operating the spray dryer to give different outlet relative humidities, by using different feed flowrates to give different relative humidities. This procedure would take about 2.5 hours, including the time taken run to the spray dryer with just hot air first, for steady-state to be obtained. Hence, this procedure will taken less time than the static and dynamic procedures for obtaining sorption isotherms, as discussed in section 2.8. This procedure would also allow the wall deposition fluxes to be measured under different operating conditions. In any case, regardless of whether the wall deposition fluxes are acceptable or not, such a procedure is likely to give further equilibrium moisture content information. Different relative humidities could also be obtained at the same total feed flowrate by varying the water:solids ratio in the

feed (and hence the amount of water evaporated) over the range of water:solids ratios that can be atomised in the nozzle used here.

6.2.6 Particle Size Analysis

The size of the particles of grape powder leaving the spray dryer was assessed using a Malvern Particle Size Analyser (Model 2600C). A 1-2 mg sample of grape powder prepared using grape extract with a solids content of 28.5% was suspended in isopropanol (the dispersant), as recommended by Kockel and Southwell (1999), who observed no dissolution of the grape powder in the isopropanol when they carried out their particle sizing tests using the Malvern. The test was carried out as described in section 4.2.7 for skim milk powder. The median volume diameter of the particles was found to be 21.5 microns with a spread from d(v, 0.1) of 7.3 microns to d (v, 0.9) of 48 microns. The particle size distribution is given in Figure 6.1, showing a bimodal distribution, the main peak being at around 20 microns and a secondary peak (possibly corresponding to particles that had agglomerated during storage) at around 100 microns. The fact that the powder did not dissolve in isopropanol points to it consisting of polar compounds (soluble in water, not organic solvents).

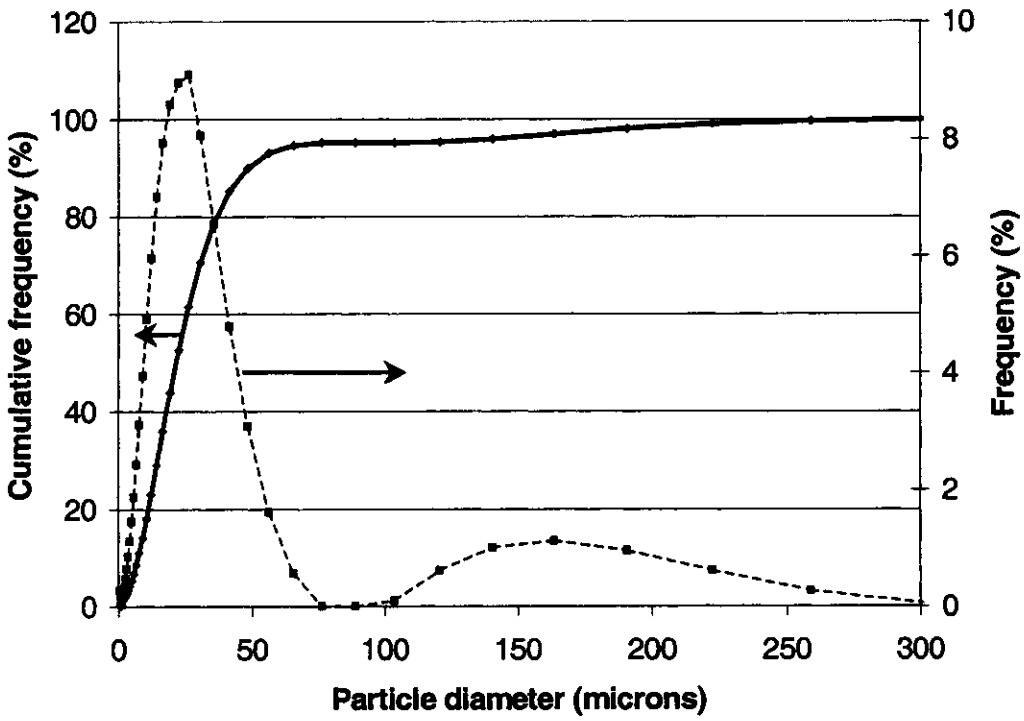

Figure 6.1 - Particle size distribution chart for grape powder, where the solids concentration of the grape extract feed was 28.5% on a total mass basis.

Kockel and Southwell's (1999) work with particle size analysis of grape powder produced the following results. For their first experiment, when the solids concentration of the process fluid was 20 % (w/w), the median volume diameter of the particles produced from spray drying was found to be 16.3 microns, with a spread from d(v, 0.1) of 6.2 microns to d (v, 0.9) of 28 microns. For their second experiment, when the solids concentration was 22 % (w/w), the median volume diameter of the particles produced by spray drying was found to be 32.2 microns, with a spread from d(v, 0.1) of 14.5 microns to d(v,0.9) of 53.8 microns. Thus, the particle size of the grape powder produced in this work is within the range found by Kockel and Southwell (1999).

In comparison to the grape powder particle size obtained in this work, the median volume diameter of skim milk powder was found to be 6.8 microns, with a spread from d(v,0.1) of 1.1 microns to d(v,0.9) of 13.3 microns. The spray drying conditions for skim milk and grape extract were the same, where the inlet air temperature was 230°C, the feed flowrate was 1.4 kg hr^{-1}, the compressed air pressure was 200 kPa and the swirl vane angle was 0°. However the solids concentration of the skim milk was more than half the solids concentration of the grape extract.

A discussion of the equations and correlations used for estimating the particle size of droplets produced by a two-fluid nozzle, including a sample calculation for a water droplet, skim milk droplet and grape extract droplet will be given next.

6.3 Estimating Particle Size for Two-Fluid Nozzle

According to Pazi and Prakhov (1971), the drop size of spray produced by a two-fluid nozzle, as used in this work, is influenced by the relative velocity between the gas and the liquid by the following equation:

$$D \sim \frac{1}{U_R^{4/3}} \tag{6.1}$$

According to equation 6.1, the diameter of the particles will increase if the relative velocity between the air and the liquid decreases. The relative velocity between the air and the liquid will decrease only when the liquid velocity is increased, since the velocity of the air is much higher than the velocity of the liquid. However, the operating conditions used for spray drying skim milk and grape extract were identical, so there must be another reason why the grape powder had a larger particle size than skim milk powder.

The break-up of bulk fluid is influenced by the following parameters, at least: a characteristic velocity U, a characteristic length of the spray L, and physical properties such as density ρ, viscosity μ and surface tension σ (Keey, 1992b). Lefebvre (1980) derived a fundamental equation using the conservation of momentum, where the diameter of a particle created using a two-fluid nozzle is given by equation 6.2:

$$D_{vs} = \left[0.073\left(\frac{\sigma}{\rho U_G^{\,2}}\right)^{0.6}\left(\frac{\rho}{\rho_G}\right)^{0.1} d_p^{\,0.4} + 0.015\left(\frac{\mu^2}{\sigma\rho d_p}\right)^{0.5}\right]\left(1+\frac{F}{G}\right) \qquad (6.2)$$

where D_{vs} is the volume-surface mean diameter of a spherical droplet (in m). This diameter is based on the assumption that the spherical droplet has the same surface area and volume as the actual droplet. F is the mass flowrate of the feed (in kg s^{-1}), G is the mass flowrate of the gas (in kg s^{-1}), σ is the surface tension of the feed (in N m^{-1}), ρ is the density of the feed (in kg m^{-3}), μ is the viscosity of the feed (in Pa s), ρ_G is the density of the gas (in kg m^{-3}), U_G is the velocity of the gas (in m s^{-1}) and d_p is the tip diameter (in m). The tip diameter is a characteristic dimension of the nozzle and corresponds to the diameter of the orifice through which the liquid exists the nozzle. The values 0.073 and 0.015 in the equation are used for a externally mixing two-fluid nozzle. Equation 6.2 was developed for fuel-oil spraying, however, the underlying physics should also make this equation applicable to the spraying of dryer feedstocks. The equation is valid for the following ranges of parameters:

$$784\ \text{kg m}^{-3} < \rho < 1000\ \text{kg m}^{-3}$$

$$0.001\ \text{Pa s} < \mu < 0.044\ \text{Pa s}$$

$$0.026\ \text{N m}^{-1} < \sigma < 0.074\ \text{N m}^{-1}$$

$$\frac{G}{F} = 0.5 - 5$$

On the other hand, Filkova and Cedik (1982) derived a correlation for an externally mixing two-fluid nozzle (equation 6.3), from dimensional analysis, using the square root of the outflow area A_G (in m) for the air as the characteristic dimension, on the grounds that this area governs the velocity of the air responsible for atomisation (Figure 6.2).

$$\frac{D_{vs}}{\sqrt{A_G}} = 0.016\left(\frac{We_s}{\mathrm{Re}_s}\right)^{-0.046}\left(\frac{F}{G}\right)^{0.73}\left(\frac{d_i}{\sqrt{A_G}}\right)^{0.4} \tag{6.3}$$

where the outflow area A_G is given by the following equation (6.4):

$$A_G = \pi\left(d_o^{\,2} - d_p^{\,2}\right)/4 \tag{6.4}$$

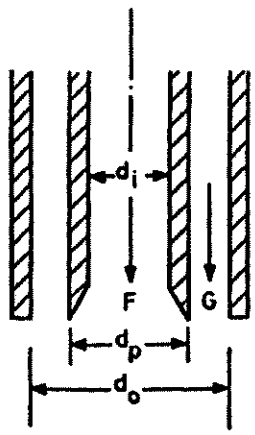

Figure 6.2 – An externally mixing two-fluid nozzle. Source: Filkova and Cedik (1982).

Figure 6.2 shows that d_o (in m) and d_p (in m) are characteristic dimensions of the nozzle. *We* (Weber number) and *Re* (Reynolds number) are dimensionless ratios that are used to characterise the physical properties of the feed. The dimensional equations We_s and Re_s are based on the characteristic dimension $\sqrt{A_G}$ and are defined by the following equations (6.5 and 6.6):

$$We_s = \frac{G^2}{A_G^{\,1.5}\rho\sigma} \tag{6.5}$$

$$\mathrm{Re}_s = \frac{G}{A_G^{0.5}\mu} \tag{6.6}$$

Filkova and Cedik (1982) claim that the average discrepancy between predicted and measured volume-surface diameters by droplet capture in oil is only 7%, with a maximum deviation of ± 20%.

The characterisic dimensions of the two-fluid nozzle used in this work were as follows:

$$d_i = 0.001 \text{ m}$$
$$d_p = 0.002 \text{ m}$$
$$d_o = 0.0025 \text{ m}$$

Both the Lefebvre (1980) equation and Filkova and Cedik (1982) correlations will now be used to calculate the diameter of a water droplet, a skim milk droplet and finally a grape extract droplet.

6.3.1 Water Droplet

In the case of using the Lefebvre (1980) equation for calculating the surface-volume diameter, the values of the parameters are:

Properties of water at 20°C (Source p. 6-3 CRC Handbook of Chemistry and Physics, 2000)

$\sigma = 0.07275$ N m^{-1}

$\rho = 998$ kg m^{-3}

$\mu = 0.001002$ Pa s

Properties of air at 27°C (Source p. 6-1 CRC Handbook of Chemistry and Physics, 2000)

$\rho_G = 1.161$ kg m^{-3}

The volumetric flowrate of the air (V in m^3 s^{-1}) was measured using a Metric 24 Type K air rotameter. The mass flowrate of the air (G in kg s^{-1}) was than calculated as follows:

$$G = \rho_G \times V$$
$$= 1.161\,\text{kg m}^{-3} \times 5.92\times10^{-3}\ \text{m}^3\,\text{s}^{-1}$$
$$= 6.87\times10^{-3}\ \text{kg air s}^{-1}$$

$d_p = 0.002$ m

$F = 3.89 \times 10^{-4}$ kg water s^{-1} (measured by recording the time taken to fill a 250 mL volumetric flask). The velocity of the air can be calculated by dividing the volumetric flowrate of the air (V in $m^3\ s^{-1}$), found using a rotameter, by the outflow area of the air from the nozzle (A_G). Thus,

$$U_G = \frac{V}{\pi\left(d_o^{\,2} - d_p^{\,2}\right)/4}$$
$$= \frac{5.92\times10^{-3}\ \text{m}^3\,\text{s}^{-1}}{\pi\left((0.0025\,\text{m})^2 - (0.002\,\text{m})^2\right)/4}$$

$$= 3350\ \text{m s}^{-1}$$

A value of 3350 m s^{-1} is virtually impossible, being approximately Mach 10, for the velocity of the air. An air pressure of 2.10 bars (30 psi) was used in this work for the two-fluid nozzle. Referring to the manufacturer's flow capacity specifications, this air pressure corresponds to an air flowrate of 0.025 $m^3\ min^{-1}$. Therefore, the air flowrate (in $m^3\ s^{-1}$) is:

$$V = \frac{0.025\,\text{m}^3\ \text{min}^{-1}}{60\,\text{s}}$$
$$= 4.17\times10^{-4}\ \text{m}^3\,\text{s}^{-1}$$

and the mass flowrate of the air (in kg s^{-1}) is:

$$G = 4.17\times10^{-4}\,\text{m}^3\,\text{s}^{-1} \times 1.161\,\text{kg m}^{-3}$$
$$= 4.84\times10^{-4}\ \text{kg s}^{-1}$$

and the velocity of the air (in m s^{-1}) is:

$$U_G = \frac{V}{\pi\left(d_o^{\,2} - d_p^{\,2}\right)/4}$$

$$= \frac{4.17\times10^{-4}\ \mathrm{m^3\,s^{-1}}}{\pi\left((0.0025\ \mathrm{m})^2 - (0.002\ \mathrm{m})^2\right)/4}$$

$$= 236\ \mathrm{m\,s^{-1}}$$

This value is more credible $\left(236\ \mathrm{m\,s^{-1}}/340\ \mathrm{m\,s^{-1}} = \text{Mach } 0.7\right)$ for a converging nozzle like this, which is only capable of subsonic flow (it is well known that supersonic flow cannot be generated by gas expansion except by a converging-diverging nozzle with a carefully designed diverger without violating the conversation equations for mass and energy).

Substituting these values for the parameters into equation (6.2) gives:

$$D_{vs} = \left[\begin{array}{l} 0.073\left(\dfrac{0.07275\ \mathrm{N\,m^{-1}}}{998\ \mathrm{kg\,m^{-3}}\times(236\ \mathrm{m\,s^{-1}})^2}\right)^{0.6}\left(\dfrac{998\ \mathrm{kg\,m^{-3}}}{1.161\ \mathrm{kg\,m^{-3}}}\right)^{0.1}(0.002\ \mathrm{m})^{0.4} \\ +\,0.015\left(\dfrac{(0.001002\ \mathrm{Pa\,s})^2}{0.07275\ \mathrm{N\,m^{-1}}\times998\ \mathrm{kg\,m^{-3}}\times0.002\ \mathrm{m}}\right)^{0.5} \end{array}\right]\left(1+\frac{0.000389\ \mathrm{kg\,s^{-1}}}{0.000484\mathrm{kg\,s^{-1}}}\right)$$

$$= 71\ \mu\mathrm{m}$$

The ratio *G/F* is 1.24, so the equation is valid for the conditions here.

In the case of using the Filkova and Cedik (1982) correlation for calculating the surface-volume diameter, the values of the parameters are:

$$A_G = \pi\left((0.0025\ \mathrm{m})^2 - (0.002\ \mathrm{m})^2\right)/4$$
$$= 1.77\times10^{-6}\ \mathrm{m^2}$$

$$We_s = \frac{(0.000484\ \mathrm{kg\,s^{-1}})^2}{(1.77\times10^{-6}\ \mathrm{m^2})^{1.5}\times998\ \mathrm{kg\,m^{-3}}\times0.07275\ \mathrm{N\,m^{-1}}}$$
$$= 1.37$$

$$\mathrm{Re}_s = \frac{(0.000484\ \mathrm{kg\,s^{-1}})^2}{(1.77\times10^{-6}\ \mathrm{m^2})^{0.5}\times0.001002\ \mathrm{Pa\,s}}$$
$$= 363$$

Substituting these values into equation 6.3 gives:

$$D_{vs} = (1.77\times10^{-6}\ \text{m})^{0.5}\times0.016\times\left(\frac{1.37}{363}\right)^{-0.046}\left(\frac{0.000389\ \text{kg s}^{-1}}{0.000484\ \text{kg s}^{-1}}\right)^{0.73}\left(\frac{0.001\ \text{m}}{\sqrt{(1.77\times10^{-6}\ \text{m})}}\right)^{0.4}$$

$$= 21\,\mu\text{m}$$

6.3.2 Skim Milk Droplet

The viscosity of skim milk was measured using a Brookfield DVIII Programmable Rheometer. The rheometer was operated using a program called "Rheocal V1.0 Brookfield Engineering Lab" using a Windows 3.11 operating system. The spindle used to carry out the test was a model LV SC4-18, which has the highest surface area compared with other spindles and is used for measuring the viscosity of low viscosity liquids. Approximately 20 mL of skim milk was added to a stainless steel cell and placed under the spindle, so that the level of the skim milk reached the level of the recess on the spindal. A temperature sensor was connected to the bottom of the cell to measure the temperature of the skim milk during the test. The speed of the spindle was increased gradually from 1 rpm to 150 rpm until the viscosity reading only fluctuated by ± 0.1 mPa s. Ten viscosity readings were taken at random time intervals and these readings were averaged to give a viscosity of 2.3 mPa s at a sample temperature of 19°C.

The surface tension of skim milk was measured using a KSV Sigma 70 Tensiometer equipped with a spring-loaded Du Noug ring probe with a radius of 9.545 mm. The program used to run the test was called "sigma 70". This equipment works by measuring the force required to pull a spring-load probe away from the liquid sample. Approximately 80 mL of skim milk was poured into a glass vessel. The glass diameter had a diameter of 66 mm and could hold a maximum volume of 110 mL. The milk was stirred at a speed of 100 % capacity using a magnetic stirrer. Care was taken that no bubbles were present between the milk and spring. When the spring was lowered, such that it touched the surface of the milk its location was tared as zero, and then the spring was programmed to sink into the milk to a depth of 5 mm. The spring was raised to 2 mm below the surface of the milk and then the probe was lifted from the milk at a speed of 3.0 mm min^{-1}. The program then calculated the surface tension, which is the force required to pull the spring from the milk just before the milk-ring interface is broken. For skim milk, the surface tension was found to be 48 mN m^{-1} at 20°C. This test was repeated and

the same result was obtained. The accuracy of the readings taken using this equipment is ± 0.5 mN m^{-1}. The skim milk had a solids concentration of 8.8% (w/v).

The density of skim milk at 20°C was found by using the following equation from Pisecky, 1997, page 23:

$$\rho = \frac{100}{\frac{m_1}{\rho_1} + \frac{m_2}{\rho_2} + \frac{m_3}{\rho_3}} \tag{6.7}$$

where the symbols are defined in section 5.7. Skim milk is a complex solution comprising of mainly protein, lactose and water. Table 6.1 shows the densities of these components (Source: Pisecky, 1997 p.23) and concentration (Source: Dairy Farmers Product Information) in skim milk.

Table 6.1 – Densities and concentration of components of skim milk.

Component	Density at 20°C (kg m^3)	Concentration (% w/v)
Protein	1390	3.5
Lactose	1520	4.9
Water	1000	91.2

Since the fat content in skim milk is only 0.1%, which is negligible, the density of skim milk was calculated using density and concentration data for protein, lactose and water.

Thus, using Pisecky's equation with the values from Table 6.1:

$$\rho = \frac{100}{\frac{3.5}{1390} + \frac{4.9}{1520} + \frac{91.2}{1000}}$$
$$= 1032 \text{ kg m}^{-3}$$

Substituting these values for the parameters into equation (6.1) gives:

$$D_{vs} = \left[\begin{array}{l} 0.073\left(\frac{0.048\ \text{N m}^{-1}}{1032\ \text{kg m}^{-3} \times (236\ \text{m s}^{-1})^2}\right)^{0.6}\left(\frac{1032\ \text{kg m}^{-3}}{1.161\ \text{kg m}^{-3}}\right)^{0.1}(0.002\ \text{m})^{0.4} \\ +0.015\left(\frac{(0.0023\ \text{Pa s})^2}{0.048\ \text{N m}^{-1} \times 1032\ \text{kg m}^{-3} \times 0.002\ \text{m}}\right)^{0.5} \end{array} \right]\left(1+\frac{0.000389\ \text{kg s}^{-1}}{0.000484\ \text{kg s}^{-1}}\right)$$

$$= 198\ \mu\text{m}$$

The ratio *G/F* is 1.24, so the equation is valid for the conditions here.

In the case of using the Filkova and Cedik (1982) correlation for calculating the surface-volume diameter, the values of the parameters are:

$$We_s = \frac{(0.00687\ \text{kg s}^{-1})^2}{(1.77\times10^{-6}\ \text{m}^2)^{1.5} \times 1033\ \text{kg m}^{-3} \times 0.048\ \text{N m}^{-1}}$$

$$= 2.01$$

$$\text{Re}_s = \frac{(0.00687\ \text{kg s}^{-1})}{(1.77\times10^{-6}\ \text{m}^2)^{0.5} \times 0.0023\ \text{Pa s}}$$

$$= 158$$

Substituting these values into equation 5.3 gives:

$$D_{vs} = (1.77\times10^{-6}\ \text{m})^{0.5} \times 0.016 \times \left(\frac{2.01}{158}\right)^{-0.046}\left(\frac{0.000389\ \text{kg s}^{-1}}{0.000484\ \text{kg s}^{-1}}\right)^{0.73}\left(\frac{0.001\ \text{m}}{\sqrt{(1.77\times10^{-6}\ \text{m})}}\right)^{0.4}$$

$$= 20\ \mu\text{m}$$

6.3.3 Grape Skin Extract Droplet

Mr Tim Lang from Food Ingredients Technologies Australia Pty Ltd supplied another sample of concord grape extract for the purpose of finding the surface tension, density and viscosity of the concord grape extract for estimating the particle size. The properties of the concord grape extract with a solids content of 32% (w/w) on a total mass basis are as follows:

σ= 44.3 mN m^{-1} (found by using tensiometer)

ρ= 1042 kg m^{-3} (found by using a measuring cylinder and scale)

μ= 0.0025 Pa s (found using Brookfield DV III Rheometer)

The solids concentration of the grape extract was found by weighing out two 70 g samples into a tray and drying the samples in the oven at 85°C for two days. The solids concentration was found to be 32%.

Substituting these values into equation 6.1:

$$D_{vs} = \left[\begin{array}{l} 0.073\left(\frac{0.044\ \text{N m}^{-1}}{1042\ \text{kg m}^{-3} \times (236\ \text{m s}^{-1})^2}\right)^{0.6}\left(\frac{1042\ \text{kg m}^{-3}}{1.161\ \text{kg m}^{-3}}\right)^{0.1}(0.002\ \text{m})^{0.4} \\ +0.015\left(\frac{(0.0025\ \text{Pa s})^2}{0.044\ \text{N m}^{-1} \times 1042\ \text{kg m}^{-3} \times 0.002\ \text{m}}\right)^{0.5} \end{array} \right]\left(1+\frac{0.000389\ \text{kg s}^{-1}}{0.000484\ \text{kg s}^{-1}}\right)$$

$$= 224\ \mu\text{m}$$

The ratio *G/F* is 1.24, so the equation is valid for the conditions here.

In the case of using the Filkova and Cedik (1982) correlation for calculating the surface-volume diameter, the values of the parameters are:

$$We_s = \frac{(0.000484\ \text{kg s}^{-1})^2}{(1.77\times10^{-6}\ \text{m}^2)^{1.5} \times 1042\ \text{kg m}^{-3} \times 0.044\ \text{N m}^{-1}}$$

$$= 2.18$$

$$\text{Re}_s = \frac{(0.000484\ \text{kg s}^{-1})^2}{(1.77\times10^{-6}\ \text{m}^2)^{0.5} \times 0.0025\ \text{Pa s}}$$

$$= 146$$

Substituting these values into equation 6.3 gives:

$$D_{vs} = (1.77\times10^{-6}\ \text{m})^{0.5} \times 0.016 \times \left(\frac{2.18}{146}\right)^{-0.046}\left(\frac{0.000389\ \text{kg s}^{-1}}{0.000484\ \text{kg s}^{-1}}\right)^{0.73}\left(\frac{0.001\ \text{m}}{\sqrt{(1.77\times10^{-6}\ \text{m})}}\right)^{0.4}$$

$$= 20\ \mu\text{m}$$

Table 6.2 and Table 6.3 provide summaries on the physical properties of the three different process fluids studied here, and the predicted drop sizes calculated using equations 6.2 and 6.3 and the actual particle size found using the Malvern, repectively.

Table 6.2 – Physical properties, namely surface tension, viscosity, density and solids concentration of the process fluids studied here.

Process fluid	σ (mN m^{-1})	μ (Pa s)	ρ (kg m^{-3})	Solids concentration
Water	72.75	0.0010	998	Nil
Skim milk	48	0.0023	1032	8.8% (w/v)
Concord grape extract	44.3	0.0025	1042	32 % (w/w)

Table 6.3 – Droplet sizes predicted using the Lebrevre (1980) equation and Filkova and Cedik (1982) correlation for a two-fluid nozzle, and actual particle sizes found using the Malvern.

Process fluid	Lebrevre (1980) particle size D_{vs} (microns)	Filkova and Cedik (1982) particle size D_{vs} (microns)	Volume diameter of particle $D_{(3,2)}$ (microns)
Water	71	21	Not determined
Skim milk	198	20	7.4
Concord grape extract	224	20	31

The volume diameter of the grape powder (for solids concentration of 28.5% which is close to 32%) was found to be 31 microns. Thus, the particle size of the grape powder found in this work is within the range found using the equations/correlations for predicting droplet size. The particle size of the skim milk powder is outside the range of predicted droplet sizes, but not by too much.

Table 6.2 and 6.3 show that the droplet size found using the Filkova and Cedik (1982) correlation did not vary, and thus, this correlation is not sensitive to changes in the density, viscosity and surface tension of the material being studied. However, the droplet size found using the Lefebvre (1980) equation shows that the droplet size is sensitive to changes in material density, viscosity and surface tension. More specifically, as the viscosity and density are increased, the droplet size also increases. Pisecky (1997) found a relationship between milk concentrate density and the concentration of solids in the milk. As concentration of the solids increases, the density of the concentrate also increases. Thus, it is likely that, since the concentration of solids in the grape extract was higher than that of the skim milk, this was the

reason why the grape extract had a higher density, and therefore, higher predicted droplet size and also actual particle size.

6.4 The Use of Fibre in Spray Drying Grape Skin Extract

FITA separated the nutraceuticals polymethoxylated flavones from the rest of the nutraceuticals present in citrus peel extract. When polymethoxylated flavones (in liquid form) were dried in an oven and then exposed to the atmosphere, they became very sticky (Private communication: Lang, 2002). However, when the polymethoxylated flavones were mixed with orange fibre and dried in the oven, a powder was produced which was free-flowing when left exposed to the atmosphere (Private communication: Lang, 2002). Thus, the fibre acted as an anti-caking agent. According to Aguilera *et al.* (1995), anti-caking agents are added to a hygroscopic material to inhibit caking and, therefore, stickiness, by a number of mechanisms:

(i) When left exposed to the atmosphere, the anti-caking agent in the mixture competes with the hygroscopic components of the mixture for available moisture, and absorbs large amounts of water vapour onto specific surface sites with high binding energy. Orange fibre has a moisture content of 9% at a relative humidity of 60% (Private communication: Lang, 2002), so orange fibre is hygroscopic, but not as hygroscopic as the polymethoxylated flavones.

(ii) Inhibit crystallisation growth, which later gives rise to caking.

(iii) By increasing the glass transition temperature of the mixture (Section 2.7).

Orange or apple fibre are natural constituents of fruit and therefore it is likely that using them as additive would not be objectionable, compared with using processed polysaccharides such as maltodextrins.

Orange and apple fibre in the form of a fine powder was supplied by Food Ingredients Technologies Australia Pty Ltd to test the possibility of reducing wall deposition by adding natural additive to the extract as suggested in section 2.9. The glass transition of the orange fibre and apple fibre were determined separately using DSC and a method similar to the one described in Chapter 3. It is expected that the fibre would raise the glass transition temperature of the mixture, and therefore the particles produced by spray drying would not be as sticky and attach to the walls of the spray dryer when they reach them. However, it was not possible to

test this idea because the two-fluid nozzle contained a liquid strainer which would have become blocked if a fibre/extract mixture was administered to the nozzle. It is recommended that a rotary atomiser be used in future to test the possibility of using fibre as an additive as a means of reducing wall deposition of grape powder. Such an atomiser would cost around $15 000.

6.5 Conclusions

Grape powder was found to give rise to less wall deposition (2.9 g m^{-2} hr^{-1}) than skim milk powder (4 g m^{-2} hr^{-1}), for the same spray dryer operating conditions and similar feed conditions. The difference is likely to be due to the inherent properties of the material. Thus, when drying other carbohydrate containing food material, it is important to characterise the stickiness of the material by carrying out glass transition measurements.

Since the grape powder was observed to be extremely hygroscopic, it is recommended that the powder be kept away from atmospheric moisture by storing it in watertight containers made of glass or metal (White and Cakebread, 1966) and thoroughly deaerating the container or storing the powder under vacuum (Karel and Nickerson, 1964). The reason why vacuum should be applied is that the relative humidity is directly proportional to the absolute pressure (Keey, 1992b, equation 6.18, page 120), and if vacuum is applied, the pressure of the gaseous environment falls, which in turn decreases the relative humidity of the gas and the equilibrium moisture content of the solid (sorption isotherm). In future, if the powder is to be processed, it is advised that the processing equipment are under vacuum, or kept under a nitrogen or low relative humidity atmosphere, such that atmospheric air cannot come into contact with the product.

The hypothesis made in Chapter 5 is that the further the operating point (particle temperature and moisture content) is above the sticky-point curve, the greater the spray deposition flux on the walls will be. Since the glass transition temperature is close to the sticky-point temperature (Chapter 3), the difference between the glass transition temperature and particle temperature at a given moisture content should indicate the spray deposition flux. Therefore, if the spray deposition flux for grape powder is measured, along with the outlet gas temperature of the air leaving the spray dryer (which should be close to the particle temperature), moisture content of the grape powder, and the glass transition temperature, then it will be possible to compare the

spray deposition fluxes for skim milk powder with the spray deposition fluxes of grape powder on a sticky-point diagram.

The conclusion and recommendations for future work are given next in Chapter 7.

Chapter 7

Conclusions and Recommendations

The main findings of the work covered in this thesis are summarised in section 7.1, followed by the recommendations for future work in this field of spray drying in section 7.2.

7.1 Conclusions

The glass transition temperature of skim milk powder with moisture contents ranging from 1.7% to 4.5% were determined using MDSC, and these results were compared with the sticky-point data obtained by Hennigs *et al.* (2001), and the predicted glass transition temperature, found using the Gordon-Taylor (1952) equation for skim milk powder. The skim milk powder was scanned at a rate of 2°C min^{-1}, from 0°C to 120°C and modulated at ± 0.5°C every 60 seconds. In addition, the glass transition temperature of skim milk powder with a moisture content of 4.77% was determined using two other scanning rates, namely, 5°C min^{-1} and 10°C min^{-1}, to assess if the scanning rate affects the glass transition temperature of skim milk powder.

The measured glass transition temperature decreased as the moisture content of the skim milk powder increased. The same trend was observed with the predicted glass transition temperature and the sticky-point data. The difference between the sticky-point temperature and measured glass transition temperature was 14°C-22°C. However, since the glass transition temperature is not a sharply located point and occurs over a temperature range of 10°C to 20°C, it might be considered that the glass transition and sticky-point temperatures are close. Thus, the glass transition test may be used to characterise the stickiness of food material containing carbohydrates, and used as a guide for selecting operating conditions for the spray dryer to minimise stickiness of the particles and thus, wall deposition. The measured glass transition temperature was 2°C to 10°C higher than the predicted glass transition temperature. When the

glass transition temperature of skim milk powder was predicted using the Gordon-Taylor equation, the proteins which are present in the skim milk powder were assumed to be inert. However, proteins denature, and this may be considered as a type of transition that may affect the glass transition temperature of skim milk powder. Since casein has a denaturation temperature of 200°C and makes up 79% of the proteins present in skim milk powder (39% of skim milk powder is protein), if this information was taken into account in predicting the glass transition temperature of skim milk powder, the glass transition temperature would be higher and the predicted and measured glass transition temperatures would be closer to each other. Thus, the Gordon-Taylor equation may be used to predict the stickiness of mixtures. The MDSC results for the glass transition temperature were found to be more accurate than the DSC results because MDSC has the advantage of disentangling overlapping phenomena, such as crystallisation, and is not significantly dependent on the scanning rate.

A pilot-scale spray dryer was modified in this work to enable the wall deposition flux of skim milk powder to be estimated. Four stainless steel plates (dimensions 110 mm by 120 mm) were inserted in place of the sightglasses, previously used as windows for the spray dryer, and two stainless steel plates with dimensions 110 mm by 110 mm; and 110 mm by 120 mmm, respectively, were placed on the conical section of the spray dryer, but at different circumferential locations. Mass and energy balances were carried out over the spray dryer for assessing the reliability of the humidity-temperature measurements. The findings from the water balance over the spray dryer were that all but 32% of the discrepancy found in the water balance can be attributed to random error. In addition, a systematic error of 2°C in the cold junction temperature can explain most of the discrepancy in the water balance, but has no large effect on the energy balance. A discrepancy of 1-2 kW in the energy balances were probably due to heat losses from the walls and pipes of the spray dryer.

This work has quantified the effect of the following parameters on the wall deposition flux of skim milk powder:

1. The swirl vane angle.
2. Inlet air temperature and process fluid flowrate.
3. Wall properties.
4. Electrostatics.
5. Combination of wall properties and time.

The highest wall deposition fluxes for all the runs carried out in this work were found to occur on the plates located on the conical section of the spray dryer due to spray impaction. Both the stickiness and flow patterns of particles in the spray dryer were found to be important in the wall deposition problem. The highest wall deposition flux of skim milk powder occurred at and above the sticky-point curve (in the sticky-region) for the tests where the feed flowrates and inlet air temperatures were varied. The wall deposition flux was also found to increase as the swirl vane angle was increased, and therefore as the flow patterns in the spray dryer became less stable. Cohesion was found to occur at the same rate as adhesion for skim milk powder under the conditions in this spray dryer, because there was no significant effect on the wall deposition flux between a smooth stainless steel wall, a wall covered with double-sided adhesive tape, and a wall coated with food grade nylon. In addition, if adhesion occurred at a different rate to cohesion, it might be expected that the initial deposition flux (when adhesion first occurs) would be different to subsequent fluxes when particles cohere to other adhered particles, and this was not observed here. Grounding the spray dryer did not have a significant effect on the wall deposition flux of skim milk powder. However, this test was only preliminary, and does not discount the effect of electrostatic and van der Waals' forces in wall deposition in spray dryers, since the milk powder produced from spray drying was found to cling loosely to each other and clung to a stainless steel spoon used for handling the powder. Furthermore, the drying behaviour of the spray dryer used in this work was found to be equilibrium limited, since the final particle moisture content was found to be close to the equilibrium moisture content.

Grape skin extract was spray dried using the optimum conditions found for spray drying skim milk, that is the conditions which gave rise to the least wall deposition flux. The inlet air temperature was 230°C, the feed flowrate was 1.4 kg hr^{-1}, the swirl vane angle was 0° and the compressed air pressure was 200 kPa. The spray deposition flux of grape powder was found to be less than that of skim milk powder, probably because the sugars present in the grape skin extract were removed, so the particles inside the spray dryer would be less sticky. However, even though the grape powder was less sticky than skim milk powder inside the spray dryer, the grape powder was found to be more hygroscopic than skim milk powder when it was left in the ambient environment. The grape powder adsorbed water until it become a viscous sticky liquid in less than one hour, while skim milk powder remained in a solid form. The possibility of adding natural fibre (as a fine powder) from apple or orange peels should be investigated on

the grounds that the presence of the fibre in the grape powder will give rise to the fibre competing with the grape powder for moisture in the atmosphere, and the fibre might raise the glass transition temperature of the grape powder, making the grape powder less sticky.

7.2 Recommendations for Future Work

Since Langrish and Kockel (2001) found that milk powder particles are dried in approximately one second, it should be possible to obtain particles close to the spray nozzle which are not semi-solid but completely dry. These particles should then be examined under a Scanning Electron Microscope to assess if agglomerates are formed inside the dryer first and then collect on the walls of the spray dryer.

Chen *et al.* (1993) found that the skim milk and whole milk particles collected from the ceiling of the industrial spray dryer had smaller particle sizes than the particles collected from the walls of the spray dryer. They suggested that these smaller particles were entrained in the turbulent mixing zone in the top of the dryer, and this led them to be deposited on the ceiling of the spray dryer. Thus, larger particles, which have a higher momentum than smaller particles, are more likely to travel down to the conical section of the spray dryer and impact on the conical section of the spray dryer. The particle size of the skim milk particles deposited on the walls of the spray dryer should be measured and compared with the particle size of the skim milk particles deposited on the cone section of the spray dryer. This will help to distinguish between spray impaction and turbulent deposition, for this dryer.

For turbulent deposition (plates 1 to 4), it is expected that adhesive forces between the particles and the surface would become significant in determining whether or not deposition will take place. Increasing the swirl vane angle to 30° would have allowed the particles to be closer to the walls of the spray dryer and electrostatic forces would be dominant if particles are more than one micron from the surface of the wall. However, the wall deposition flux data did not show any trend for increasing the swirl vane angle and thus changing the air flow patterns in the spray dryer on turbulent wall deposition (plates 1-4). This may have been caused by the particles being highly charged, since lactose in skim milk powder is an insulator and the charge on lactose is retained on its surface; and electrostatics would not have been significant (Hinds, 1999). However, increasing the swirl vane angle increased the wall deposition flux on plates 5 and 6 (spray impaction). Rennie *et al.* (1998) used measurements of centrifugal force to study

the effect of temperature on adhesive force of whole milk powder. Similarly, centrifugal force can be applied to wall plates to measure the upper diameter left behind after each level of centrifuging corresponding to 90% of the cumulative amount of particles. The larger the size of the particles that are left behind on the stainless steel plates, the higher the adhesive force. Particle size is important in adhesion, where the smaller the particles, the higher the adhesive force (Hinds, 1999). Hence it is important that the size of particles used in this test be comparable to the particles inside the spray dryer, so doing a centrifuging test on wall plates from the dryer itself may give some useful information about the particle sizes on the plates and the strength of particle-particle cohesion and wall-particle adhesion. Alternatively, the size of particles on the plates can be determined using Scanning Electron Microscopy.

In this work, it was found that increasing the feed flowrate increased the wall deposition flux of skim milk powder. Three possible reasons were suggested for this increase in wall deposition, namely, particle impaction on the conical section of the spray dryer; increased evaporation rates and therefore increased humidity in the spray dryer giving higher particle moisture contents, and stickier particles; larger number of particles in the spray dryer or higher residence time of the particles and hence a higher likelihood of particles impinging on the walls of the spray dryer. It is important to assess which of these three reasons is dominant because the feed flowrate is directly related to the production rate and spray dryer capacity. To test which of these three reasons is dominant, it is recommended that extensions should be added to the spray dryer height, so as to observe if spray impaction significantly influences the wall deposition flux. The particle residence time should be increased in the spray dryer by decreasing the air flowrate. However, to keep the outlet particle moisture content and temperature the same as when the air flowrate is not changed (control experiment), the inlet air temperature and air velocity should be adjusted together, so that the total enthalpy of the air entering the spray dryer is the same. The inlet air temperature and air velocity affect the volumetric flowrate and density of the air, which in turn affects the mass flowrate of the air. The air velocity should be controlled by restricting the diameter of the inlet air to the first blower using some sort of orifice plate. Care must be taken when doing this because if the pressure inside the dryer increases above atmospheric pressure, the particles and air inside the spray dryer will escape through small cracks and holes in the equipment.

A set of experiments should be carried out on a smaller spray dryer, like the Buchi-191 spray dryer (width 50 cm, depth 60 cm, height 100 cm) to assess if small spray dryers are

equilibirium limited or kinetically controlled by testing the moisture content of the spray dried material and comparing the result with the materials sorption isotherm. Then it will be possible to decide if spray drying behaviour at most process scales is equilibrium limited rather than limited by particle drying kinetics.

As previously explained in section 7.1, skim milk particles were observed to cling to each other and other surfaces, and this is likely to be due to electrostatic forces. To further investigate if cohesion of particles to particles already on the wall is significantly affected by electrostatic forces as well as liquid bridging forces, the air entering the spray dryer should be ionised. The ionised air may neutralise charged skim milk particles and this may reduce the wall deposition more significantly than grounding the spray dryer. Furthermore, since adhesion has to occur first before cohesion can take place, tests should be carried out where the wall of the spray dryer are exposed to ultrasound waves, which may vibrate the walls of the spray dryer and dislodge any particles adhering to the walls.

Finally, a network of temperature controlled plates should be installed in spray impaction zones (conical section) and turbulent deposition zones (walls) in the spray dryer to assess whether or not deposition mechanisms and processes are the same in both locations, and how and to what extent the wall temperature affects deposition for spray impaction and turbulent deposition.

References

Abbott, J.A.E., 1990, *Prevention of Fires and Explosions in Dryers - A User Guide*, 2nd edition, Institution of Chemical Engineers, Warwickshire, England.

Ade-John, A.D., Jeffreys, C.V., 1978, Flow Visualisation and Residence Time Studies in a Spray Drier, *Trans IChemE*, Vol. 56, pp. 36-42.

Aguilera, J.M., del Valle, J.M., Karel, M., 1995, Caking Phenomena in Amorphous Food Powders, *Trends in Food Science & Technology*, May 1995, Vol. 6, pp.149-155.

Arvanitoyannis, I., Blanshard, J.M.V., Ablett, S., Izzard, M.J., Lillford, P.J., 1993, Calorimetric Study of the Glass Transition Occuring in Aqueous Glucose:Fructose Solutions, *J. Sci Food Agric.*, Vol. 63, pp. 177-188.

AS/NZS 1020:1995, The Control of Undesirable Static Electricity, Standards Australia.

Bahu, R.E., 1992, Spray Drying - Maturity or Opportunities?, In *Drying 92*, Mujumdar, A.S (ed.), Elsevier, Amsterdam, pp. 74-91.

Bailey, A.G., 1993, Charging of Solids and Powders, *J. Electrostat*, Vol. 30, pp. 167-180.

Beever, P.F., 1985, Fire and Explosion Hazards in the Spray Drying of Milk, *Journal of Food Technology*, Vol. 20, pp. 637-645.

Beever, P., Crowhurst, D., 1989, Fire and Explosion Hazards Associated with Milk Spray Drying Operations, *Journal of the Society of Dairy Technology*, Vol. 42(3), pp. 65-70.

Belem, M.A.F., 1999, Application of Biotechnology in the Product Development of Nutraceuticals in Canada, *Trends in Food Science and Technology*, Vol 10, pp. 101-106.

BEP Engineering Products, Rydalmere, Australia.

Bhandari, B.R., Dumoulin, E.D., Richard, H.M.J., Noleau, I., Lebert, A.M., 1992, Flavour Encapsulation by Spray Drying : Application to Citral and Linalyl Acetate, *Journal of Food Science*, Vol 57 (1), pp. 217-221.

Bhandari, B. R., Senoussi, A., Dumoulin, E.D., Lebert, A., 1993, Spray Drying of Concentrated Fruit Juices, *Drying Technology*, Vol. 11(5), pp. 1081-1092.

Bhandari, B. R., Datta, N., Howes, T., 1997, Problems Associated with Spray Drying of Sugar-Rich Foods, *Drying Technology*, Vol. 15(2), pp. 671-684.

Bhandari, B. R., Howes, T., 1999, Implication of Glass Transition for the Drying and Stability of Dried Foods, *Journal of Food Engineering*, Vol. 40, pp. 71-79.

Bhandari, B. R., Howes,T., 2000, Glass Transition in Processing and Stability of Food, *Food Australia*, Vol. 52(12), pp. 579-585.

Birch, J., 1997, Australia's Largest Milk Powder Plant To Service East Gippsland, *Chemical Engineering in Australia* Vol. ChE22 No. 2, June-August 1997, pp. 9-12.

Bloore, C., 2001, Dairy Industry Trends, *6th World Congress of Chemical Engineering in Melbourne*, Melbourne, September 2001.

Bohm, C., Bornegg, C., 1931, Method of Drying Fruit Juices (U.S. Patent 1 800 501) (14 April 1931).

Boonyai, P., 2000, Comparative Evaluation of Soymilk Drying in a Spray Dryer and Spouted Bed of Inert Particles, MSc Thesis, Asian Institute of Technology, Bangkok, Thailand.

Boskovic, M. A., Vidal, S.M., Saleeb, F.Z, 1992, Spray-Dried Fixed Flavorants in a Carbohydrate Substrate and Process (U.S. Patent 5 124 162) (23 June 1992).

Breene, W. M., Coulter, S.T., 1967, Properties of Spray-Dried Combinations of Milk and Fruits and Vegetables, *Journal of Dairy Science*, Vol. 50, p. 1049.

Brennan, J. G., Herrera, J., Jowitt, R., 1971, A Study of Some of the Factors Affecting the Spray Drying of Concentrated Orange Juice, on a Laboratory Scale, *J. Food Technol.*, Vol. 6, pp. 295-307.

Campbell, W.I., Proctor, B.E., Sluder, J.G., 1944, Research Reports on Quartermaster Contract Projects. Massachusetts Institute of Technology, Food Technology Laboratories, Cambridge Mass. (July 1, 1944 – Oct. 31, 1945).

Canadian Dairy Information Centre Home Page. http://www.dairyinfo.agr.ca/mdisp.htm (accessed April 2002).

Channaud, R.C., 1965, *J. Fluid Mech.*, Vol. 21, Part 1, p. 111.

Chen, X. D., Lake, R., Jebson, S., 1993, Study of Milk Powder Deposition on a Large Industrial Dryer, *Trans. IChemE.*, Vol. 71(C3), pp. 180-186.

Chen, X. D., Rutherford, L., Lloyd, R.J., 1994, Preliminary Results of Milk Powder Deposition at Room Temperature on a Stainless Steel Surface Mimicking the Ceiling of a Spray Dryer, *Trans. IChemE.*, Vol. 72(C), pp. 170-175.

Cheng, A.F.C., 2002, A Study of Wall Deposition Rates in Spray Dryer, (Undergraduate Thesis), University of Sydney.

Chong, L.V., Chen, X.D., Mackereth, A.R., 1999, Effect of Ageing and Composition on the Ignition Tendency of Dairy Powders, *Journal of Food Engineering*, Vol. 39, pp. 269-276.

Chuy, L.E., Labuza, T.P., 1994, Caking and Stickiness of Dairy-Based Food Powders as Related to Glass Transition, *Journal of Food Science*, Vol..56(1), pp.43-46.

Clift, R., 1958, Particle-Particle Interactions in Gas-Particle Systems, In *Powdertech '85 Particle Technology*, IChemE Symposium Series No. 91, pp. 27- 43.

Couchman, P.R., Karasz, F.E., 1978, A Classical Thermodynamic Discussion of the Effect of Composition on Glass-Transition Temperatures, *Macromolecules*, Vol. 11(1), pp. 117-119.

Coulter, S. T., Breene, W.M., 1966, Spray Drying Fruits and Vegetables Using Skim milk as a Carrier, *Journal of Dairy Science*, Vol 49, p. 762.

CRC Handbook of Chemistry and Physics, 2000-2001, 81th Edition, Lide, D.R. (ed.), CRC Press LLC, London, New York.

Crowe, C. T., Sharma, M.P., Stock, D.E., 1977, The Particle-Source-in-Cell (PSI-Cell) Model for Gas-Droplet Flows, *J. Fluids Eng.*, Vol 99(2), pp. 325-332.

Crowe, C.T., 1980, Modelling Spray-Air Contact in Spray-Drying Systems, In *Advances in Drying*, Mujumdar, A.S. (ed.), Volume 1, Hemisphere, New York, pp. 63-99.

de Knegt, R.J., van den Brink, H., 1998, Improvement of the Drying Oven Method for the Determination of the Moisture Content of Milk Powder, *Int. Dairy Journal*, Vol. 8, pp. 733-738.

Delavan Industrial Nozzle and Accessories Manual. 2001.

Dellenback, P.S., Metzger, D.E. and Neitzel, G.P., 1988, Measurement in Turbulent Swirling Flow Through an Abrupt Axisymmetric Expansion, *AIAA Journal*, Vol. 26 (6), pp. 669-681.

Downton, G. E., Flores-Luna, J.L.,Judson King, C., 1982, Mechanism of Stickiness in Hygroscopic, Amorphous Powders, *Ind. Eng. Chem. Fundam.*, Vol. 21, pp. 447-451.

Eddy, C. W., 1950, Process of Drying Fruit or Vegetable Materials Containing Added Methyl Cellulose, (U.S. Patent 2 496 278) (February 7, 1950).

Filkova, I., Cedik, P., 1982, *Proceedings of the 3rd International Drying Symposium*, Vol. 1, pp. 516-527.

Fodor, I., Forgacs, A., 1991, I. Berta, Static Control of Charge Decay in Industry – Hazard and Risk, In *Inst. Phys. Conf. Ser.*, No.118: Section 4, pp. 191-196.

Freund, J.E., Simon, G.A., 1992, *Modern Elementary Statistics*, Prentice Hall, New Jersey.

Gardais, D., 1986, Le secheur haute temperature "Leaflash". Xleme Forum Electro-Industriel National "Industries Agro-Alimentaires" Angers, France, Juin 4-5.

Genskow, L. R., 1988, Considerations in Drying Consumer Products, *Proceedings of the Sixth International Drying Symposium (IDS'88)*, Versailles, France, pp. KL.39-K.L.46.

Gerbert, B.M., Davidson, M.R., Rudman, M.J., 1998, Computed Oscillations of a Confined Submerged Liquid Jet, *Applied Mathematical Modelling*, Vol. 22, pp. 843-850.

German Standard DIN 10321, 1973, *Bestimmung des Wassergehalts von Milchpulver. Deutsches Institut fur Normung*: Berlin.

Godijn, Z.M., Southwell, D.B., Kockel, T.K. and Langrish, T.A.G., 1999, Flow Visualisation in a Pilot-Scale Spray Dryer with Two-Fluid Atomisation, CHEMECA 99, Newcastle, Australia, pp. 265-270.

Goldberg, J. E., 1987, Prediction of Spray Dryer Performance (PhD Thesis), University of Oxford.

Goldstein, R.J., 1996, *Fluid Mechanics Measurements*, Goldstein R.J. (ed.), 2nd edition, Taylor and Francis, Washington, DC.

Gordon, M., Taylor, J.S., 1952, Ideal Copolymers and the Second-order Transitions of Synthetic Rubbers. I. Non-Crystalline Copolymers, *Journal of Applied Chemistry*, Vol. 2, pp. 493-500.

Grappin, R., Ribadeau-Dumas, B., 1992, Analytical Methods for Milk Proteins, In *Advanced Dairy Chemistry Volume 1 Proteins*, Fox, P.F. (ed.), Elsevier Science Publishers Ltd, England, Chapter 1.

Guo, B., Langrish, T.A.G. and Fletcher, D.F., 1998, Time-Dependent Simulation of Turbulent Flows in Axisymmetric Sudden Expansions, *13th Australasian Fluid Mechanics Conference*, Monash University, Melbourne, Australia, 13-18 December 1988, pp. 283-286.

Guo, B., 2001, CFD Simulation of Flow Instability in Axisymmetric Sudden Expansions (PhD Thesis), University of Sydney.

Guo, B., Langrish, T.A.G., Fletcher, D.F., 2001, Simulation of Turbulent Swirl Flow in an Axisymmetric Sudden Expansions, *Proceedings 13th Australasian Fluid Mechanics Conference*, Thompson, M.C., Hourigan, K. (eds.), Melbourne, Australia, Vol. 1, pp.283-286.

Gupta, A. S., 1978, Spray Drying of Orange Juice, (U.S. Patent 4 112 130) (5 September 1978).

Gupta, A.K., Lilley, D.G. and Syred, N., 1984, *Swirl flows*, Abacus, Turnbridge Wells, Kent, England.

Hallett, W.L.H. and Gunther, R., 1984, Flow and Mixing in Swirling Flow in a Sudden Expansion, *The Canadian Journal of Mechanical Engineering*, Vol. 62, pp. 149-155.

Hancock, B. C., Zografi, G., 1994, The Relationship Between the Glass Transition Temperature and the Water Content of Amorphous Pharmaceutical Solids, *Pharmaceutical Research*, Vol. 11(4), pp. 471-484.

Harvie, D.J.E., Langrish, T.A.G., Fletcher, D.F., 2002, A Computational Fluid Dynamics Study of a Tall-Form Spray Dryer, *Trans IChemE*, (accepted).

Harwalkar, V.R., Ma, C.Y., 1990, *Thermal Analysis of Foods*, Elsevier Applied Science, London.

Hennigs, C., 2000, Adhesion and Cohesion of Spray-dreid Skim Milk Powder on Stainless Steel Surfaces, (Masters Thesis), Technische Universitat, Hamburg.

Hennigs, C., Kockel, T.K., Langrish, T.A.G., 2001, New Measurements of the Sticky Behaviour of Skim Milk Powder, *Drying Technology - An International Journal*, Vol. 19(3), pp. 471-484.

Hill, S.J., Nathan, G.J. and Luxton, R.E., 1995, Precession in Axisymmetric Confined Jets, *Proceedings of 12th Australasian Fluid Mechanics Conference*, Bilger, T.W., Ed., The University of Sydney, Australia, December 10-15, pp. 135-138.

Hinds, W.C., 1999, *Aerosol Technology, Properties, Behavior, and Measurement of Airborne Particles*, 2nd Edition, John Wiley & Sons Inc., Canada.

Holmgren, F., 1993, *Health Issues. Wines and Vines*, Vol. 74(5), p. 42.

Holzcker, R., 1943, Two Methods for Dehydrating Citrus Juices, *Food Inds.*, Vol. 15, p. 62.

Honeyands, T.A. and Molloy, N.A., 1995, Oscillations of Submerged Jets in a Narrow Deep Rectangular Cavity, *Proceedings of 12th Australasian Fluid Mechanics Conference*, Bilger, T.W., The University of Sydney, Australia, December 10-15, pp. 493-496.

Hovenden, R.J. and Davidson, M.R., 1997, Turbulence Modelling of Single Phase Flow in a Spray Dryer, *International Conference on CFD in Mineral & Metal Processing and Power Generation*, CSIRO, 1997, pp.459-465.

International Dairy Federation (IDF), 1993, *Dried Milk and Cream Determination of Water Content*, Brussels.

Johari, G.P., Hallbrucker, A., Mayer, E., 1987, The Glass-Liquid Transition of Hyperquenched Water, *Nature*, 10 December, Vol. 330, pp. 552-553.

Jonassen, N, 1998, *Electrostatics*, Chapman & Hall, USA.

Jones, G.O., 1956, *Glass*, Methuen, London.

Jouppila, K., Roos, Y.H., 1994, Water Sorption and Time-dependent Phenomenon of Milk Powders, *Journal of Dairy Science*, Vol. 77(7), pp. 1799-1807.

Karatas, S., Esin, A., 1990, A Laboratory Scraped Surface Drying Chamber for Spray Drying of Tomato Paste, *Lebensm.-Wiss. u.-Technol.*, Vol. 23, pp. 354-357.
Karel, M., Nickerson, J.T.R., 1964, Effects of Relative Humidity, Air, and Vacuum on Browning of Dehydrated Orange Juice, *Food Technology*, August, Vol. 104, pp.104-108.
Katta, S. and Gauvin, W.H., 1975, Some Fundamental Aspects of Spray Drying, *AIChEJ*, Vol. 21 (1), pp. 143-152.
Kaul, T. N., Middleton, E.Jr.,Ogra,P.L., 1985, Antiviral Effects of Flavonoids on Human Viruses, *J. Med. Virol.*, Vol. 15, pp. 71-74.
Keey, R.B. and Pham, Q.T., 1976, Behaviour of Spray Dryers with Nozzle Atomizers, *The Chemical Engineer*, July 1976, pp. 516-521.
Keey, 1978, *Introduction to Industrial Drying Operations*, Pergamon, Oxford, New York.
Keey, R.B., 1992a, Characterisation of Feedstocks; In *Advances in Drying*, Mujumdar, A.S. (ed.), Volume 5, Hemisphere, Washington, pp. 11-76.
Keey, R.B., 1992b, *Drying of Loose and Particulate Materials*, Hemisphere, U.S.A.
Kieviet, F., Kerkhof, P.J.A.M., 1995, Measurements of Particle Residence Time Distributions in a Co-Current Spray Dryer, *Drying Technology*, Vol. 13(5-7), pp. 1241-1248.
Kieviet, F.G., Kerkhof, P.J.A.M., 1997, Air Flow, Temperature and Humidity Patterns in a Co-Current Spray Dryer: Modelling and Measurements, *Drying Technology*, Vol. 15(6-8), pp. 1763-1773.
Kieviet, F.G., Van Raaij, J., De Moor, P.P.E.A., Kerkhof, P.J.A.M, 1997, Measurement and Modelling of the Air Flow Pattern in a Pilot-Plant Spray Dryer, *Trans. IChemE*, Vol 75, Part A, March 1997, pp.321-328.
King, C.J., 1990, Spray Drying Food Liquids and the Retention of Volatiles, *Chemical Engineering Progress*, June, pp. 33-39.
Kirchmeier, O., 1962, The Physicochemical Causes of Heat Stability of Milk Proteins, Vol.17, p.408-412 (accessed using in June 2002 using SciFinder Scholar).
Kirkup, L., 1994, *Experimental Methods. An Introduction to the Analysis and Presentation of Data*, John Wiley & Son, Brisbane.
Kliafas, Y., Holt, M., 1987, LDV Measurements of a Turbulent Air-Solid Two-Phase Flow in a 90° Bend, *Exp. Fluids*, Vol. 5, p.73.
Kockel, T.K., Allen, S., Hennigs, C., Langrish, T.A.G., 2002, An Experimental Study of the Equilibrium for Skim Milk Powder at Elevated Temperatures, *Journal of Food Engineering*, Vol. 51, pp. 291-297.
Kockel, T.K., Southwell, D.B., 1999, FITA Concord Grape Colour Spray Drying Experiment – 7 and 19 January 1999.
Kuprianoff, J., 1958, "Bound water" in foods, In *Fundamental Aspects of the Dehydration of Foodstuffs.*", Soc. Chem. Ind., London, p. 14.
Labuza, T.P., 1968, Sorption Phenomena in Foods, *Food Technology*, Vol. 22, pp. 263-272.
Labuza, T.P., 1984, Moisture Sorption: Practical Aspects of Isotherm Measurement and Use, American Association of Cereal Chemists, St. Paul, MN.
Labuza, T. P., Kaanane, A., Chen, J.Y., 1985, Effect of Temperature on the Moisture Sorption Isotherms and Water Activity Shift of Two Dehydrated Foods, *Journal of Food Science*, Vol. 50, pp. 385-391.
Labuza, T.P., 1995, Properties of Sorption Isotherms of Foods, in Water Activity Theory, Management and Application, Course Workbook, August 21-24 1995, University of Queensland, Department of Food Science and Technology Gatton College and Shanaglen Technology, Brisbane, Australia, pp.13.
Lafuente, B., Welti, J.S., 1984, Quality of Spray-Dried Comminuted Orange Products as Influenced by Process Variables. *Advances in theFruit and Vegetable Juice Industry, Processes, Quality Evaluation, Product Development*, Tel Aviv, pp. 239-260.
Lam, L. K. T., Zhang,J., Hasegawa,S., Schut, H.A.J., 1993, Inhibition of Chemically Induced Carcinogenesis by Citrus Limonoids. Food Phytochemicals for Cancer Prevention 1: Fruit & Vegetables, Haung, M.T., Osawa, O., Ho, C.T., Rosen,R., (eds.), American Chemical Society, Washington,DC, pp. 209-219.
Lang, T. (Private communication, 2000-2002).
Langrish, T.A.G., Oakley, D.E., Keey, R.B., Bahu, R.E. and Hutchinson, C.A, 1993, Time-Dependent Flow Patterns in Spray Dryers., *Trans. IChemE*, Vol. 71(A), pp. 355-360.
Langrish, T.A.G. and Zbicinski, I., 1994, The Effects of Air Inlet Geometry and Spray Cone Angle on the Wall Deposition Rate in Spray Dryers, *Trans. IChemE*, Vol. 72(A), pp. 420-430.
Langrish, T.A.G., 1996, Flowsheet Simulation and the Use of CFD in Drying Technology, *Drying 96, Proceedings of the 10th Internaltional Drying Symposium (IDS '96)*, Krakow, Poland, 30 July-2 August 1996, Vol. A, pp. 40-51.
Langrish, T.A.G., Fletcher, D., 2001, Prospects for the Modelling and Design of Spray Dryers in the 21st Century, *Proc. The Sixth World Congress of Chemical Engineering*, Melbourne,September 2001, CD-ROM, paper 362.
Langrish, T.A.G., Kockel, T.K., 2001, The Assessment of a Characteristic Drying Curve for Milk Powder for Use in Computational Fluid Dynamics Modelling, *Chemical Engineering Journal*, Vol. 84, pp. 69-74.
Lazar, M. E., Brown, A.H., Smith, G.S., Wong, F.F., Linquist, F.E., 1956, Experimental Production of Tomato Powder by Spray Drying, *Food Technology*, March, pp.129-134.
LeBarbier, C., Kockel, T.K., Fletcher, D.F., Langrish, T.A.G., 2001, Experimental Measurement and Numerical Simulation of the Effect of Swirl Flow on Flow Stability in Spray Dryers, *Trans IChemE.*, Vol. 79, Part A., pp. 260-268.
Lefebvre, A.H., 1980, Airblast Atomisation, *Progr. Energy Combust. Sci.*, Vol. 6, pp. 233-261.
Lee, C. Y., 2000, Phenolic Compounds, *Nature*, June, pp. 2055-2061.
Lemetais, C., 2000, A Sticky Problem, *The Chemical Engineer*, 14 December, pp. 14-15.
Lomauro, C.J., Bakshi, A.S., Labuza, T.P., 1985, Evaluation of Food Moisture Sorption Isotherm Equations. Part I: Fruit, Vegetables and Meat Products, *Lebensmittel Wissenschaft und- Technologie*, Vol. 18, pp. 111-117.
Luikov, A.V., 1966, *Heat and Mass Transfer in Capillary Porous Bodies*, Pergamon, Oxford, p. 199.
Machowski, W., Balachandran, W., 1998, Dispersion and Transport of Cohesive Lactose Powder using Travelling Wave Field Technique, *Powder Technology*, pp. 251-256.

Mahony, G. S, 2001, Wall Deposition Rates in Spray Dryers, (Undergraduate Thesis), Department of Chemical Engineering, University of Sydney.

Main, J. H., Clydesdale,F.M., Francis,F.J., 1978, Spray Drying Anthocyanin Concentrates for Use as Food Colorants, *Journal of Food Science*, Vol. 43, pp. 1693-1694, p. 1697.

Malvern Instruments Ltd, *Malvern User Manual*, 1997, Worcestershire, U.K.

Mangiapane, H., Thomson,J., Salter,A.,Brown,S.,Duncan Bell,G.,White,D.A., 1992, The Inhibition of the Oxidation of Low Density Lipoprotein by (+)-Catechin, A Naturally Occuring Flavonoid, *Biochemical Pharmacology*, Vol. 43(3), pp. 445-450.

Manners, G. D., Hasegawa,S., 1999, Squeezing More from Citrus Fruits, *Chemistry & Industry*, pp. 542-545.

Masters, K., 1991, *Spray Drying Handbook*, 5th Edition, Longman Group, U.K.

Masters, K., 1996, Deposit-Free Spray Drying: Dream or Reality?, *Drying 96, Proceedings of the 10th Internaltional Drying Symposium (IDS '96)*, Krakow, Poland, 30 July-2 August 1996, Vol. A, pp. 52-60.

Montanari, A., Widmer,W., Nagy, S., 1997, Health Promoting Phytochemicals in Citrus Fruit and Juice Products, *The Thirty-Sixth Annual Meeting of the Phytochemical Society of North America on Functionality of Food Phytochemicals: Flavors, Stimulants, and Health Promoters*, New Orleans, Louisiana.

Montgomery, D.C., 1991, *Design and Analysis of Experiments*, Third Edition, John Wiley & Sons, Canada.

Nathan, G.J., Hill, S.J. and Luxton, R.E., 1998, An Axisymmetric 'Fluidic' Nozzle to Generate Jet Precession, *Journal of Fluid Mechanics*, Vol. 370, pp. 347-380.

Niro Atomisers, as cited in Masters, K., 1991, Spray Drying Handbook, 5th Edition, Longman Group, U.K.

Noel, T.R., Ring, S.G., Whittam, M.A., 1991, Kinetic Aspects of the Glass-transition Behaviour of Maltose-Water Mixtures, *Carbohydrate Research*, Vol.212, pp.109-117.

Notter, G. K., Taylor, D.H., Downes, N.J., 1959, *Food Technology*. Vol. 13, p. 113.

Oakley, D.E., Bahu, R.E. and Reay, D., 1988, The Aerodynamics of Co-Current Spray Dryers, *Sixth International Drying Symposium IDS '88*, Versailles, Sept 5-8 1988, pp. OP.373-378.

Oakley, D.E., Bahu, R.E., 1991, Spray/Gas Mixing Behaviour Within Spray Dryers; In *Drying 91*, Mujumdar, A.S. and Filkova, I. (eds.), Elsevier, Amsterdam, pp. 303-313.

Ozmen, L., Langrish, T.A.G., Comparison of Glass Transition Temperature and Sticky Point Temperature for Skim Milk Powder, In *Drying Technology*, Vol. 20, pp. 1177-1192.

Papadakis, S. E., Bahu, R.E., 1992, The Sticky Issues of Drying, *Drying Technology*, Vol. 10(4), pp. 817-837.

Papadakis, S.E., Bahu, R.E., McKenzie, K.A., Kemp, I.C., 1993, Correlations for the Equilibrium Moisture Content of Solids, *Drying Technology An International Journal*, Vol. 11(3), pp. 543-553.

Papadakis, S. E., King, C., 1988, Factors Governing Temperature and Humidity Fields in Spray Drying. *6th International Drying Symposium*, Versailles, France, pp. OP.345-OP.352.

Paris, J.R., Ross, P.N., Dastur, S.P. and Morris, R.L., 1971, Modelling of the Air Flow Pattern in a Countercurrent Spray-Drying Tower, *Ind Eng Chem Proc Des Dev*, Vol. 10(2), pp. 157-164.

Patankar, S.V., 1980, *Numerical Heat Transfer and Fluid Flow*, Hemisphere, New York.

Pazi, D.G., Prakhov, A.M., 1971, Forsunky v khimicheskoj promyslenosti, *Khim. M*oskva [cited by Filkova and Cedki, 1984).

Percy, S.R., 1872, Improvements in Drying and Concentrating Liquid Substances by Atomising, (U.S. Patent 125 406) (9 April).

Perech, R., 1946, Vegetable Concentrates and Method of Preparing Same, (U.S. Patent 2 393 561) (22 January 1946).

Perry, R.H. and Chilton, C.H. eds., 1997, *Chemical Engineers' Handbook, 7th Edition*, McGraw Hill International.

Pineau, J. P., 1984, *Protection Against Fire and Explosion in Milk Powder Plants*, Antwerp: Europex.

Pisceky, J., 1968, Priciny explose suseneho mleka (Cause of explosions in Dried Milk), Prumysl Potravin 19, 7, 1.

Pisecky, J., 1972, *Causes of Explosions in Dried Milk*, Prague: Milk Research Institute (translation Niro Atomiser, Denmark).

Pisecky, J., 1997, *Handbook of Milk Powder Manufacture*, Niro A/S, Copenhagen, Denmark.

Place, G., Ridgway, K., Danckwerts, P.V., 1959, Investigation of Air-Flow in a Spray Drier by Tracer and Model Techniques. *Trans. IChemE.*, Vol. 37, pp. 268-276.

Prudhon, F., 1979, Atomiseur Leflash, *Informations Chimie*, Vol. 189, p. 1.

Raemy, A., Hurrell, R.F., Loliger, J., 1983, Thermal Behaviour of Milk Powders Studied by Differential Thermal Analysis and Heat Flow Calorimetry, *Thermochimica Acta*, Vol. 65, pp. 81-92.

Reading, M., Luget, A., Wilson, R., 1994, Modulated Differential Scanning Calorimetry, *Thermochimica Acta*, Vol. 238, pp. 295-307.

Reay, D., 1988, Fluid Flow, Residence Time Simulation and Energy Efficiency in Industrial Dryers, *6th International Drying Symposium*, Versailles, France, pp. KL.1-KL.8.

Renaud, S., De Lorgeril, M., 1992, Wine, Alcohol, Platelets and the French Paradox for Coronary Heart Disease, *Lancet*, Vol. 339, p. 1523.

Rennie, P. R., Chen, X.D., Mackereth, A.R., 1998, Adhesion Characteristics of Whole Milk Powder to a Stainless Steel Surface, *Powder Technology*, Vol. 97, pp. 191-199.

Rennie, P. R., Chen, X.D.,Hargreaves, C.,Mackereth, A.R., 1999, A Study of the Cohesion of Dairy Powders, *Journal of Food Engineering*, pp. 277-284.

Robe, K., Malvick, A., Heid, J.L., 1968, First US Installation is Applicable to Spray Drying Other Heat-sensitive, Hygroscopic Food Products, *FOOD Processing-Marketing*, p. 48.

Roger, L.N., Reed, J., 1984, The Adhesion of Particles Undergoing an Elastic-Plastic Impact with a Surface, *J. Phys. D:Appl. Phys.*, Vol. 17, pp. 677-689.

Roos, Y., 1993, Melting and Glass Transitions of Low Molecular Weight Carbohydrates, *Carbohydrate Research*, Vol. 238: pp.39-48.

Roos, Y., Karel, M., 1990, Differential Scanning Calorimetry Study of Phase Transitions Affecting the Quality of Dehydrated Materials, *Biotechnology Progress*, Vol. 6, pp. 159-163.

Roos, Y., Karel, M., 1991a, Phase Transitions of Mixtures of Amorphous Polysaccharides and Sugars, *Biotechnology Progress*, Vol. 7, pp. 49-53.
Roos, Y., Karel, M., 1991b, Phase Transitions of Amorphous Sucrose and Frozen Sucrose Solutions, *Journal of Food Science*, Vol. 56(1), pp. 266-267.
Roos, Y., Karel, M., 1991c, Plasticizing Effect of Water on Thermal Behaviour and Crystallisation of Amorphous Food Models, *Journal of Food Science*, Vol. 56(1), pp. 38-43.
Roos, Y., Karel, M., 1991d, Amorphous State and Delayed Ice Formation in Sucrose Solutions, *International Journal of Food Science and Technology*, Vol. 26, pp. 553-566.
Roos, Y., Karel, M., 1991e, Water and Molecular Weight Effects on Glass Transitions in Amorphous Carbohydrates and Carbohydrate Solutions, *Journal of Food Science*, Vol. 56(6), pp. 1676-1681.
Ross, R., Harker, L., 1976, Hyperlipidaemia and Atherosclerosis, *Science*, Vol. 193, pp. 1094-1100.
Ruegg, M., Moor, U., Blanc, B., 1977, A Calorimetric Study of the Thermal Denaturation of Whey Proteins in Simulated Milk Ultrafiltrate, *Journal of Dairy Research*, Vol. 44, pp. 509-520.
Rumpf, H., 1975, *Particle Technology*, Powder Technology Series, Chapman and Hall, London.
Sapryngin, G., Kiselejev, J.A., 1966, Inflammation spontanee du lait en poudre, La technique laitiere, XI, Vol. 537, pp.15-18.
Sauerbrunn, S.R., Crowe, B.S., Reading, M., 1992, Modulated Differential Scanning Calorimetry, *Proceedings of the 21st NATAS Conference*, pp. 137-144.
Schuh, M.J., Schuler, C.A., Humphrey, J.A.C., 1989, Numerical Calculation of Particle-Laden Gas Flows Past Tubes, *AIChE Journal*, March 1989, Vol. 35(3), pp.466-480.
Shallcross, D., 2000, Module 4-3 Process Overview - Skim milk powder, *Dairy Engineering Modules*, Dairy Process Engineering Centre, Melbourne, Australia (Feb 3 issue, 2000), (with input from Prvcic,L.; Nicol, R.).
Singh, H., Newstead, D.F., 1992, Aspects of Proteins in Milk Powder Manufacture, In *Advanced Dairy Chemistry Volume : Proteins*, Fox, P.F. (ed.) Essex: Elsevier Science Publishers Ltd, England, Chapter 18.
Singleton, V.L., 1982, In *Proceedings University California, Davis, Wine Grape Centennial Symposium*, Webb, A.D., (ed.), Department of Viticulture and Enology, University of California.
Slade, L., Levine, H., 1991, A Polymer Science Approach to Structure/Property Relationships in Aqueous Food Systems: Non-Equilibrium Behaviour of Carbohydrate-Water Systems, In *Water Relationships in Foods*, Levine H, Slade L., (eds), Plenum Press, New York, USA, pp. 29-101.
So, F. V., Guthrie,N.,Chambers, A.F., Moussa, M, Carroll, K.K., 1996, Inhibition of Human Breast Cancer Cell Proliferation and Delay of Mammary Tumorigenesis by Flavonoids and Citrus Juices, *Nutrition and Cancer*, Vol. 26(2), pp. 167-181.
Sommerfeld, M., 1992, Modelling of Particle-Wall Collisions in Confined Gas-Particle Flows, *Int. J. Multiphase Flow*, Vol. 18(6), pp. 905-926.
Southwell, D.B., 2000, *Operability and Performance Assessment of Spray Dryers*, PhD Thesis, University of Sydney.
Southwell, D.B., Langrish, T.A.G., 2000, Observation of Flow Patterns in a Spray Dryer, *Drying Technology*, Vol 18(3), pp. 661-686.
Southwell, D. B., Langrish, T.A.G., 2001, The Effect of Swirl on Flow Stability in Spray Dryers, *Trans IChemE*, Vol. 76, Part A, April 2002, pp. 222-234.
Stafford, R.A., Fauroux, O. And Glass, D.H., 1996 Flow Visualisation and Instantaneous Velocity Measurements of Spray Dryer Gas and Spray Flows Using Particle Image Velocimetry , In *Drying 96, Proceedings of the 10th International Drying Symposium (IDS '96)*, Krakow, Poland, 30 July-2 August 1996, Vol. A, pp. 555-562.
Stern, R.M., Storrs, A.B., 1969, Method of Drying Sugar-Containing Materials, (U.S. Patent 3 483 032) (9 December 1969).
Straatsma, J., Van Houwelingen, G., Steenbergen, A.E., De Jong, P., 1999, Spray Drying of Food Products: 1. Simulation Model, *Journal of Food Engineering*, Vol. 42, pp. 67-72.
Strashun, S.I., 1951, The Drying of Fruit and Vegetable Products, (U.S. Patent 2 557 155) (19 June 1951).
Strashun, S.I., Talburt, W.F., 1954, Stabilized Orange Juice Powder. I. Preparation and Packaging, *Food Technology*, January, pp. 40-45.
Strashun, S.I., Cerrito, E., Talburt, W.F.,1960, Dehydration of Fruit and Vegetable Juices, (U.S. Patent 2 959 486).
TA Instruments, 1995, DSC 2920 Differential Scanning Calorimeter Manual.
TA Instruments, 1998, Characterisation of the Glass Transition Temperature of Lactose by MDSC®, Thermal Solutions TS-43 (http://www.tainst.com/support/TS45.PDF, accessed September, 2000).
TA Instruments, 1998, Characterisation of the Glass Transition Temperature of Lactose by MDSC®, Thermal Solutions TS-45 (http://www.tainst.com/support/TS45.PDF, accessed September, 2000).
Tu, J.Y., 2000, Numerical Investigation of Particulate Flow Behaviour in Particle-Wall Impaction, *Aerosol Science and Technology*, Vol. 32, pp. 509-526.
Tu, J.Y., Fletcher, C.A.J., 1995, Numerical Computation of Turbulent Gas-Solid Particle Flow in a 90° Bend, *AIChE Journal*, October 1995, Vol. 41 (10), pp. 2187-2197.
Turi, E.A., 1981, *Thermal Characterization of Polymeric Mateirals*, Academic Press, Orlando, FL.
Wallack, D. A., King, C., 1988, Sticking and Agglomeration of Hygroscopic, Amorphous Carbohydrate and Food Powders, *Biotechnology Progress*, Vol. 4(1), pp. 31-35.
Welty, J.R., 1978, *Engineering Heat Transfer*, John Wiley & Sons Inc., New York.
White, G. W., Cakebread, S.H., 1966, The Glassy State in Certain Sugar-Containing Food Products, *J. Food Technol.*, Vol. 1, pp. 73-82.
Williams, J. C., 1990, Mixing and Segregation in Powders, *Principles of Powder Technology*, Rhodes, M., (ed.), pp. 71-90.
Wilcox, D.C., 1998, *Turbulence Modelling for CFD*, 2nd edition, DCW Industries, California, U.S.A.
Wunderlich, B., 1990, *Thermal Analysis*, Academic Press, Boston, MA, USA.
Yang, W., Siebermorgen, T.J., Jia, C.-C.,Howell, T.A., Cnossen, A.G., 2000, Cross-Flow Drying of Rough Rice as Mapped on its Glass Transition State Diagram, *Proceeding of the 12th International Drying Symposium IDS2000*, Noorwijkerhout, The Netherlands.

Young, J.F., 1967, Humidity Control in the Laboratory using Salt Solutions – A Review, *J. Appl. Chem.*, September, Vol. 17, pp.241-245.

Zhang, Y.F., Yang, Y., Arastoopour, H., 1996, Electrostatic Effect on the Flow Behavior of Dilute Gas/Cohesive Particle Flow System, *AIChE Journal*, Vol. 42(6), pp. 1590-1599.

Zimon, A.D., 1969, *Adhesion of Dust and Powder*, Plenum Press, N.Y.

Zumdahl, S.S., 1989, *Chemistry*, 2nd Edition, D.C. Health and Company, U.S.A.

Appendix A

A1. Experimental Set-Up for Calibrating Analogue to Digital Converter Card (PC-74)

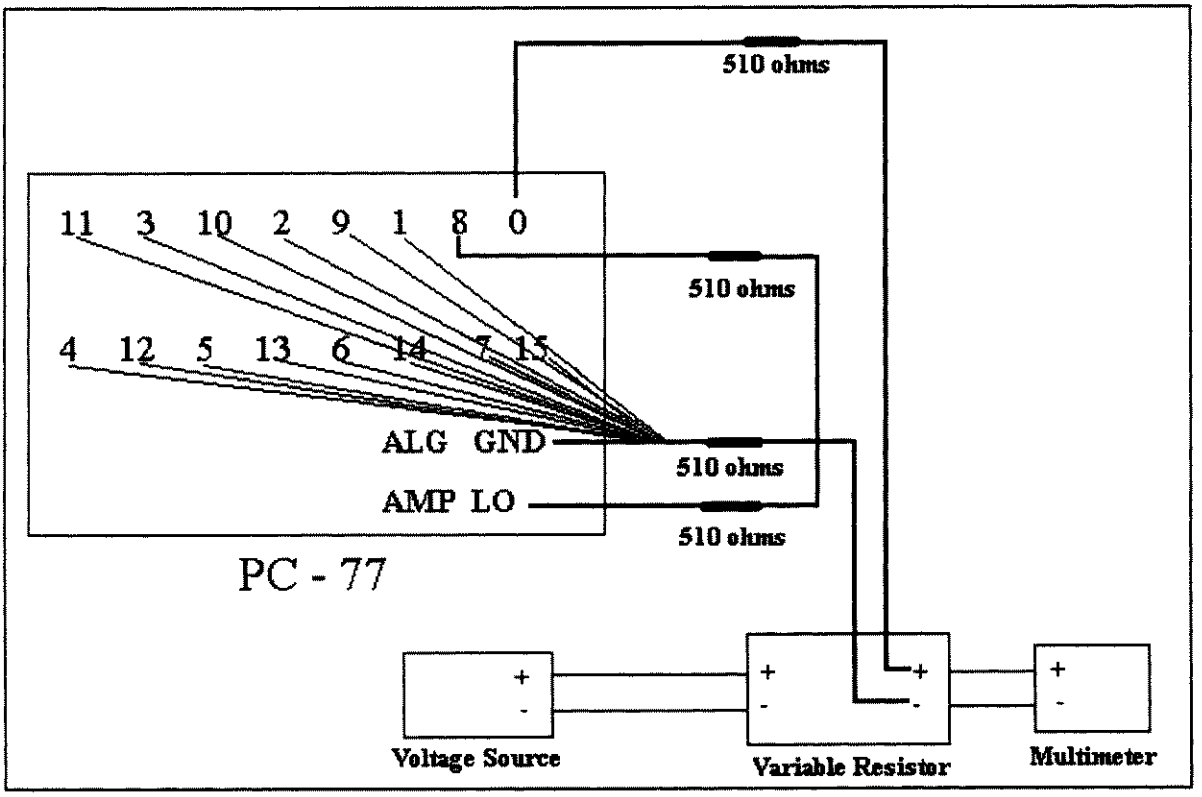

Figure A1 – The experimental set-up for the connections between the screw terminal board, PC-77, and voltage source, variable resistor and multimeter, for calibrating the Analogue to Digital converter card, PC-74, located inside the computer for controlling the drying process.

A2. Procedure for Specifying Values for the Conversion Between Digital and Analogue Values for the Thermocouples

Two pairs of values for the conversion between digital and analogue values for the thermocouples were specified as follows:

1. The low digital output signal was specified for a low temperature of 0°C by placing the thermocouples in ice-water (0°C) and the digital output signal corresponding to this

temperature was recorded from the computer for each thermocouple (Table A1). A glass mercury thermometer was used to measure the temperature of the ice-water bath.

2. The high digital output signal was specified for a high temperature of 100°C by placing the thermocouples in boiling water (100°C), and the digital output signal corresponding to this temperature was recorded from the computer for each thermocouple. Once again, a glass mercury thermometer was used to measure the temperature of the boiling water.

3. The low pair and high pair digital and analogue values for the thermocouples were entered and saved in the computer program CEDRIER under "Parameters" as a new case called loz1.dat. For example, the low pair for the inlet dry-bulb thermocouple is (0, 2037), and the high pair is (100, 2216).

Table A1 - Low pair and high pair digital and analogue values for the thermocouples.

Thermocouple	Digital output at 0°C (low pair)	Digital output at 100°C (high pair)
Dry-bulb in ($T_{d\,in}$)	2037	2216
Wet-bulb in ($T_{w\,in}$)	2039	2217
Dry-bulb out ($T_{d\,out}$)	2037	2217
Wet-bulb out ($T_{w\,out}$)	2039	2222
Hot air ($T_{hot\,air}$)	2039	2217
Dryer exit ($T_{dryer\,exit}$)	2038	2215
Dryer (T_{dryer})	2038	2215

loz1.dat was used to control and monitor the dryer's operation during the runs for both spraying water and spray drying skim milk and then spray drying grape extract. loz1.dat was modified such that the heaters would heat the air entering the dryer to the required temperature.

A3. Calibration Curves for the Thermocouples

The calibration graphs for the thermocouples are shown in Figures A2 to A8.

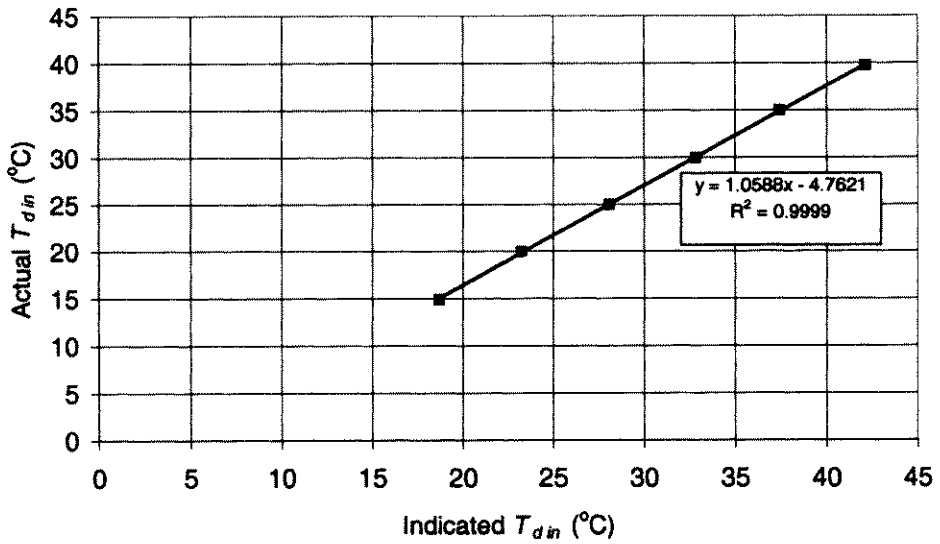

Figure A2 - Calibration of inlet dry-bulb thermocouple for assessing mass and energy balances.

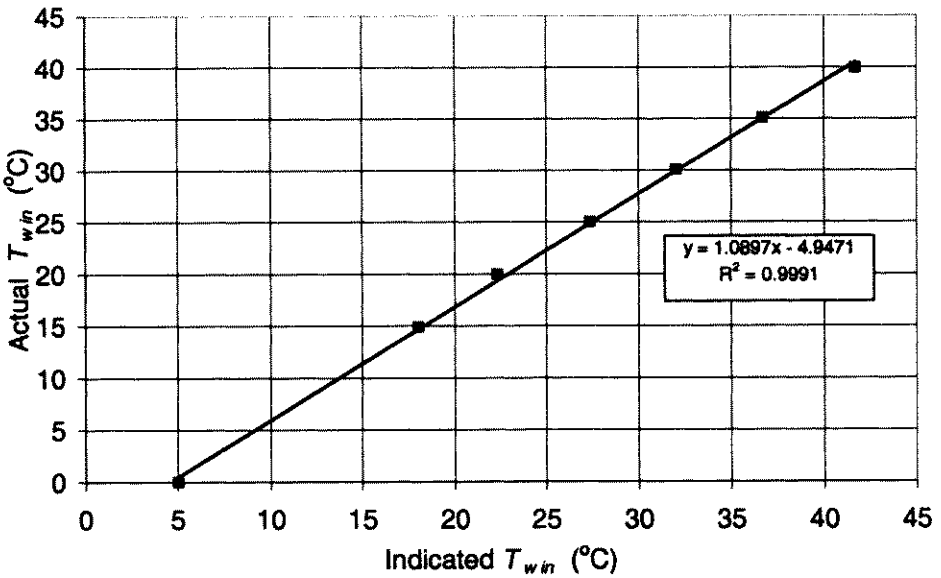

Figure A3 - Calibration of inlet wet-bulb thermocouple for assessing mass and energy balances.

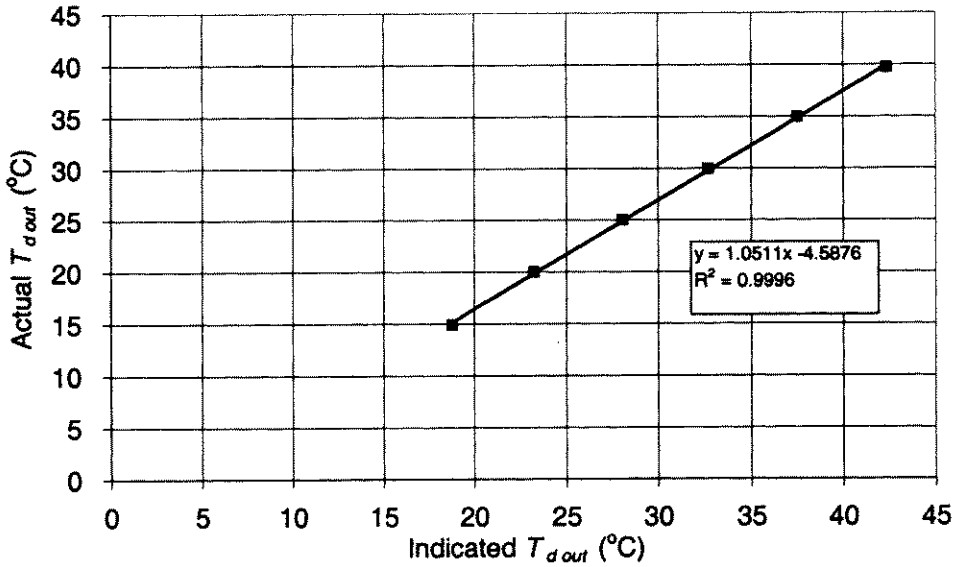

Figure A4 - Calibration of outlet dry-bulb thermocouple for assessing mass and energy balances.

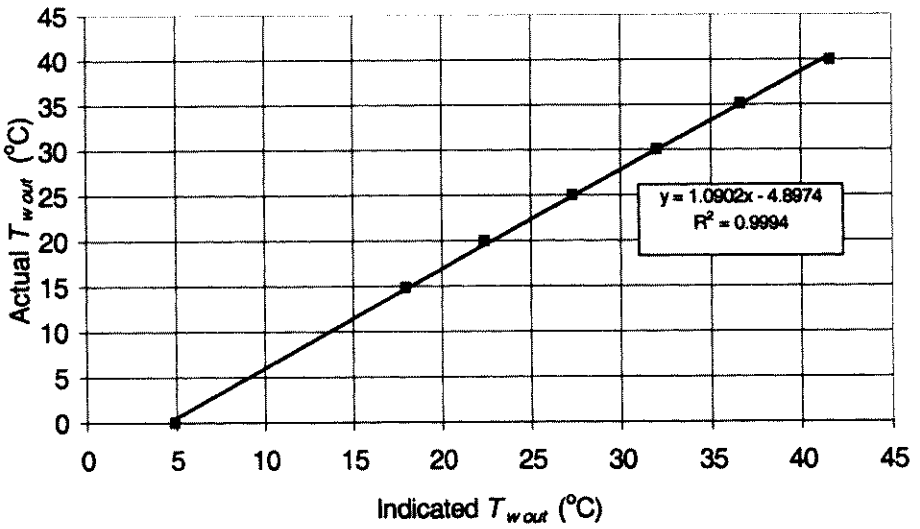

Figure A5 - Calibration of outlet wet-bulb thermocouple for assessing mass and energy balances.

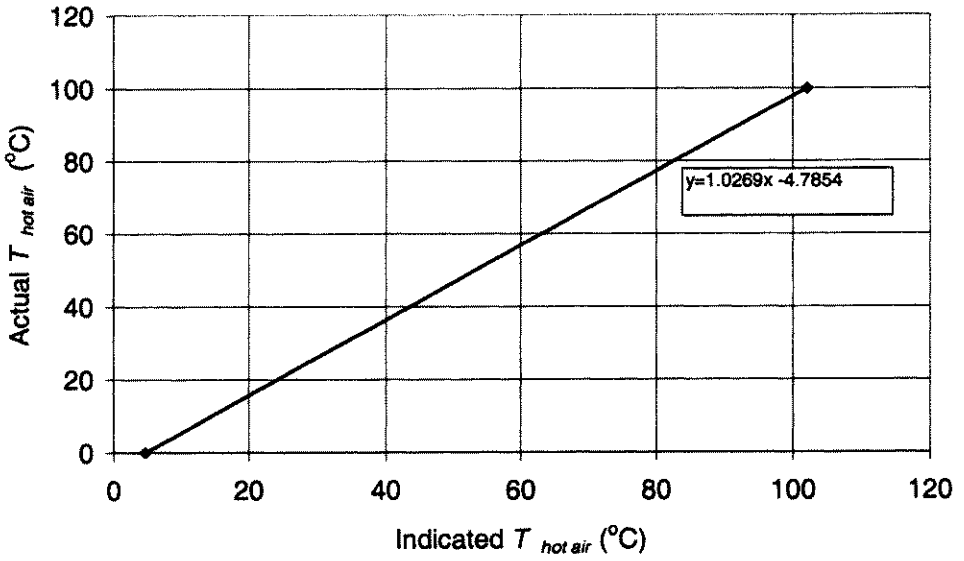

Figure A6 - Calibration of inlet air (hot air) thermocouple for assessing mass and energy balances.

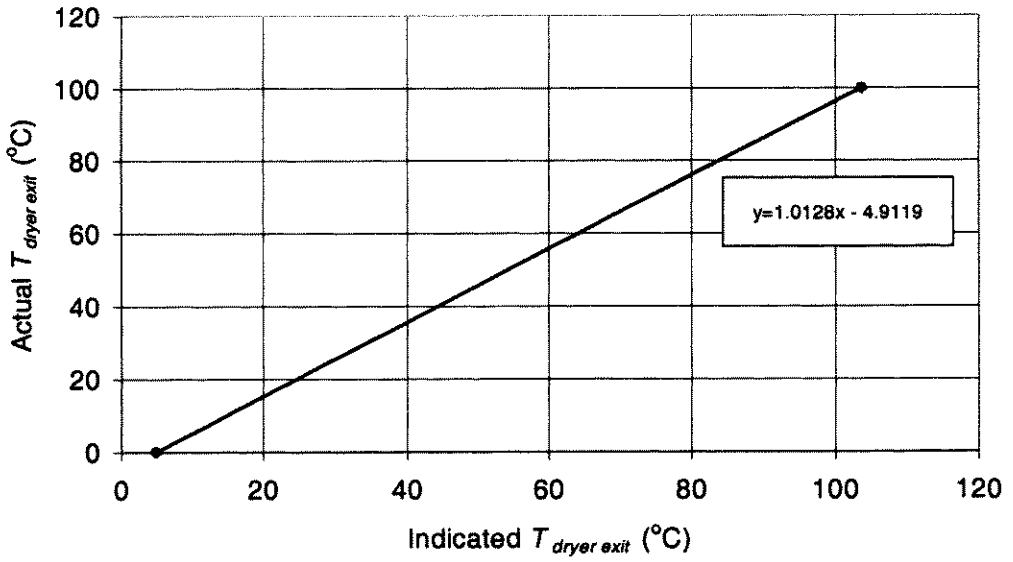

Figure A7 - Calibration of dryer exit thermocouple for assessing mass and energy balances.

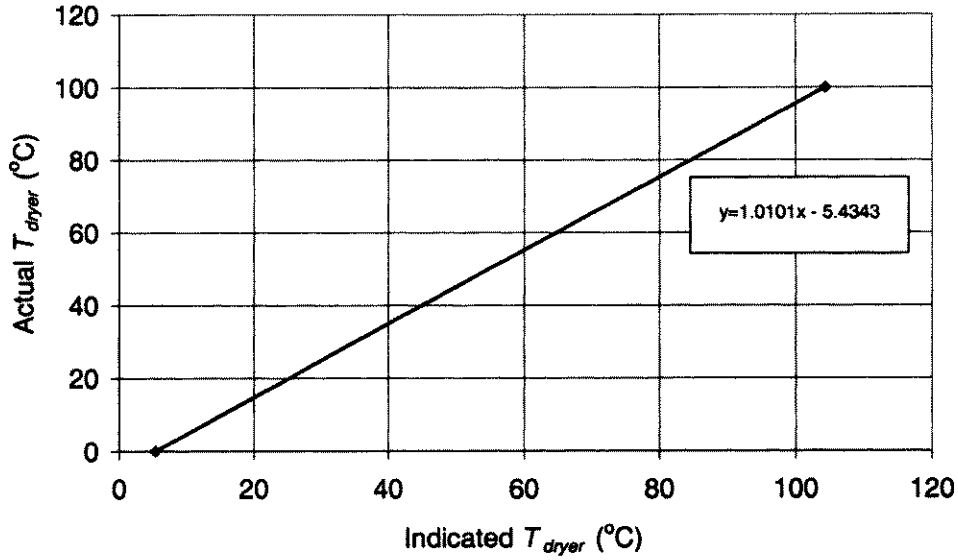

Figure A8 - Calibration of dryer thermocouple for assessing mass and energy balances.

Appendix B

B1. Calibration of Peristaltic Pump

A peristaltic pump was used to pump water to the spray nozzle. The pump was calibrated at the three pump settings (1.0, 1.5 and 2.0) by recording the time it took to fill a 250 mL volumetric flask. This was repeated three times at each pump setting, and the results averaged to quantify the variability. The variation between the highest and the lowest recorded times was less than 2.2%. Therefore, a typical amount of variation in the water flowrate will be assumed to be 2%. The flowrates of water pumped to the spray nozzle and corresponding pump settings are shown in Table B.1.

Table B.1 - Water flowrates at each pump setting for experiments assessing mass and energy balances.

Pump setting	Average time to fill 250 mL (s)	Average flowrate ($L\ h^{-1}$)	Average flowrate ($kg\ s^{-1}$)	Maximum deviation from average (%)
1.0	648.9	1.39	3.85×10^{-4}	2.2
1.5	568.1	1.58	4.40×10^{-4}	1.0
2.0	490.0	1.84	5.10×10^{-4}	0.3

Appendix B

B1.1 Material Safety Data Sheet for Larostat 519

BASF Corporation

Material Safety Data Sheet

Page : 1

Original Date: 02/27/1998
Revision Date: 05/19/2001

BASF CORPORATION
PERFORMANCE CHEMICALS
3000 CONTINENTAL DRIVE NORTH
MOUNT OLIVE, NJ 07828
(800) 443-6460

EMERGENCY TELEPHONE: (800) 424-9300 CHEMTREC
(800) 832-HELP (BASF Hotline)
BOTH NUMBERS ARE AVAILABLE DAYS, NIGHTS, WEEKENDS, & HOLIDAYS.

SECTION 1 - PRODUCT INFORMATION

LAROSTAT® 519 ANTISTAT
Product ID: NCS 558116
Common Chemical Name:
ANTISTATIC AGENT
Synonyms:
NONE
Molecular Formula:

Chemical Family: Not Applicable
Molecular Wt.: NOT APPLICABLE

SECTION 2 - INGREDIENTS

Chemical Name:	CAS	Amount
QUATERNARY AMMONIUM COMPO	68308-67-8	60.0 %
PEL/TLV NOT ESTABLISHED		
SILICA	7631-86-9	40.0 %
ACGIH TLV	TWA 10 MG/CU. M	

SECTION 3 - PHYSICAL PROPERTIES

Color: Clear Yellow
Form/Appearance: Powder
Odor: Sweet

	Typical	Low/High	U.O.M.
Specific Gravity:	NOT AVAILABLE		
Bulk Density:	0.52		KILOGRAMS
pH:	NOT AVAILABLE		

	Typical	Low/High	Deg.	@	Pressure
Boiling Pt:	> 200		F	1	ATMOSPHERES
Freezing Pt:	NOT AVAILABLE				
Decomp. Tmp:	NOT AVAILABLE				

Solubility in Water Description: Dispersible

Vapor Pressure:	< 1	MM HG	X	25	DEG. C	XX
Evaporation Rate Std.:	>1					
Volatile by Vol. %:	< 2					

SECTION 4 - FIRE AND EXPLOSION DATA

	Typical	Low/High	Deg.	Method
Flash Point:	> 200		F	PENSKY-MARTENS CLOSED C
Autoignition:	NOT AVAILABLE			

Extinguishing Media:
Use CO2 or dry chemical extinguishing media.
Fire Fighting Procedures:
Firefighters should be equipped with self-contained breathing apparatus and turn out gear.
Unusual Hazards:
There are no known unusual fire or explosion hazards.

SECTION 5 - HEALTH EFFECTS

Routes of entry for solids and liquids include eye and skin contact, ingestion and inhalation. Routes of entry for gases include inhalation and eye contact. Skin contact may be a route of entry for liquified gases.

Acute Overexposure Effects:
Eye contact may cause severe irritation, redness, swelling, discharge or corneal clouding. Skin contact may cause severe damage on prolonged contact.
Inhalation may result in respiratory irritation.
Chronic Overexposure Effects:
There are no known chronic effects associated with this material.
First Aid Procedures - Skin:
Wash affected areas with soap and water. Remove and launder contaminated clothing before reuse. If irritation develops, get medical attention.
First Aid Procedures - Eyes:
Immediately rinse eyes with running water for 15 minutes. Get immediate medical attention.
First Aid Procedures - Ingestion:
If swallowed, dilute with water and immediately induce vomiting. Never give fluids or induce vomiting if the victim is unconscious or having convulsions. Get immediate medical attention.
First Aid Procedures - Inhalation:
Move to fresh air. Aid in breathing, if necessary, and get immediate medical attention.
First Aid Procedures - Notes to Physicians:
None known.
First Aid Procedures - Aggravated Medical Conditions:
No data is available which addresses medical conditions that are generally recognized as being aggravated by exposure to this product. Please refer to the effects of overexposure section for effects observed in animals.
First Aid Procedures - Special Precautions:
None

SECTION 6 - REACTIVITY DATA

Stability Data:
Stable
Incompatability:
Strong oxidizers.
Conditions/Hazards to Avoid:
None known.
Hazardous Decomposition/Polymerization:
Hazardous Decomposition Products: No Data Available.
Corrosive Properties:
Corrosive.
Oxidizer Properties:
Not an oxidizer

SECTION 7 - PERSONAL PROTECTION

Clothing:
Gloves, coveralls, apron, and boots as necessary to prevent contact.
Eyes:
Chemical goggles; also wear a face shield if splashing hazard exists.
Respiration:
If vapors or mists are generated, wear a NIOSH/MSHA approved organic vapor/mist respirator or an air-supplied respirator as appropriate.
Ventilation:
Use local exhaust to control vapors/mists.
Explosion Proofing:
See Section 4 - Fire and Explosion Data.
Other Personal Protection Data:
Eyewash fountains and safety showers must be easily accessible.
Shower after handling.

SECTION 8 - SPILL-LEAK/ENVIRONMENTAL

General:
Spills should be contained, solidified and placed in suitable containers for disposal in a RCRA licensed facility. This material is RCRA hazardous due to its properties.
Waste Disposal:
Incinerate or bury in a RCRA licensed facility. Do not discharge into waterways or sewer systems without proper authority.
Container Disposal:
Empty containers with less than 1 inch of residue may be landfilled at a licensed facility. Recommend crushing or other means to prevent unauthorized reuse. Other containers must be disposed of in a RCRA licensed facility.

SECTION 9 - STORAGE AND HANDLING

General:
Store in tightly closed containers.
STORE IN WELL VENTILATED AREA BELOW 120F.

SECTION 10 - REGULATORY INFORMATION

TSCA Inventory Status
Listed on Inventory: YES

RCRA Haz. Waste No .: D002
CERCLA: NO Reportable Qty.: (If YES)
State Regulatory Information: (By Component) NJ/PA/MA RTK
CAS: 7631-86-9 NO
NAME: SILICA
CAS: 68308-67-8 NO
NAME: QUATERNARY AMMONIUM COMPO
Hazard Ratings:

	Health:	Fire:	Reactivity:	Special:
HMIS	3	1	0	NA

SECTION 11 - TRANSPORTATION INFORMATION

DOT Proper Shipping Name:
SEE BELOW
DOT Technical Name:
SEE BELOW
DOT Primary Hazard Class:
SEE BELOW
DOT Secondary Hazard Class:
SEE BELOW
DOT Label Required:
SEE BELOW
DOT Placard Required:
SEE BELOW
DOT Poison Constituent:
SEE BELOW
BASF Commodity Codes: UN/NA Code: E/R Guide: N/A
Bill of Lading Description:
CORROSIVE SOLID, NOS, (QUATERNARY AMMONIUM),
8, UN1759, PGIII
"IMPORTANT: WHILE THE DESCRIPTIONS, DESIGNS, DATA AND INFORMATION CONTAINED HEREIN ARE PRESENTED IN GOOD FAITH AND BELIEVED TO BE ACCURATE, IT IS PROVIDED FOR YOUR GUIDANCE ONLY. BECAUSE MANY FACTORS MAY AFFECT PROCESSING OR APPLICATION/USE, WE RECOMMEND THAT YOU MAKE TESTS TO DETERMINE THE SUITABILITY OF A PRODUCT FOR YOUR PARTICULAR PURPOSE PRIOR TO USE. NO WARRANTIES OF ANY KIND, EITHER EXPRESSED OR IMPLIED, INCLUDING WARRANTIES OF MERCHANTABILITY OR FITNESS FOR A PARTICULAR PURPOSE, ARE MADE REGARDING PRODUCTS DESCRIBED OR DESIGNS, DATA OR INFORMATION SET FORTH, OR THAT THE PRODUCTS, DESIGNS, DATA OR INFORMATION MAY BE USED WITHOUT INFRINGING THE INTELLECTUAL PROPERTY RIGHTS OF OTHERS. IN NO CASE SHALL THE DESCRIPTIONS, INFORMATION, DATA OR DESIGNS PROVIDED BE CONSIDERED A PART OF OUR TERMS AND CONDITIONS OF SALE. FURTHER, YOU EXPRESSLY UNDERSTAND AND AGREE THAT THE DESCRIPTIONS, DESIGNS, DATA, AND INFORMATION FURNISHED BY BASF HEREUNDER ARE GIVEN GRATIS AND BASF ASSUMES NO OBLIGATION OR LIABILITY FOR THE DESCRIPTION, DESIGNS, DATA AND INFORMATION GIVEN

SECTION 11 - TRANSPORTATION INFORMATION (cont)

OR RESULTS OBTAINED, ALL SUCH BEING GIVEN AND ACCEPTED AT YOUR RISK".

END OF DATA SHEET

Appendix B

B2. Mass Balance Air – Spraying of Water

Table B.2 – Measured air velocities and calculated air mass flowrates and uncertainties (run 1), for assessing mass and energy balances.

RUN 1	Air Flowrate (Inlet)				Air Flowrate (Outlet)			
Air only	Pipe Radius =	0.03	Radius^2 =	0.0009	Pipe Radius =	0.03	Radius^2 =	0.0009
Point	Velocity (m/s)	Error	Radius (m)	Radius^2 (m^2)	Velocity (m/s)	Error	Radius (m)	Radius^2 (m^2)
1	4.5	0.5	0.02	0.0004	3.5	0.5	0.025	0.000625
2	4	0.5	0.01	0.0001	6.5	0.5	0.0125	0.00015625
3	5	0.5	0	0	8	0.5	0	0
4	4.5	0.5	0.01	0.0001	9.5	0.5	0.0125	0.00015625
5	4.5	0.5	0.02	0.0004	10.2	0.5	0.025	0.000625
u(r)d(r^2)	0.004025	0.000115921			0.0066	0.00013		
Vol. Flowrate (m3/s)	0.01264	0.000364176			0.02078	0.000399		
Temp. Air (°C)	19.9				22.7			
ρ_{air} (kg/m3)	1.1936				1.1823			
Mass Flowrate (kg/s)	0.0151	0.0004			0.0246	0.0005		

Table B.3 – Measured air velocities and calculated air mass flowrates and uncertainties (run 3), for assessing mass and energy balances.

RUN 3	Air Flowrate (Inlet)				Air Flowrate (Outlet)			
Pump:1; Air: 200°C	Pipe Radius =	0.03	Radius^2 =	0.0009	Pipe Radius =	0.0375	Radius^2 =	0.00140625
Point	Velocity (m/s)	Error	Radius (m)	Radius^2 (m^2)	Velocity (m/s)	Error	Radius (m)	Radius^2 (m^2)
1	6	0.5	0.02	0.0004	0.8	0.2	0.025	0.000625
2	4	0.5	0.01	0.0001	2.2	0.2	0.0125	0.00015625
3	4	0.5	0	0	3.4	0.1	0	0
4	3.5	0.5	0.01	0.0001	4	0.1	0.0125	0.00015625
5	4	0.5	0.02	0.0004	4.5	0.1	0.025	0.000625
u(r)d(r^2)	0.0042	0.000115921			0.0039	0.00006		
Vol. Flowrate (m3/s)	0.01319	0.000364176			0.01233	0.00018		
Temp. Air In (°C)	22.2				56.3			
ρ_{air} (kg/m3)	1.1843				1.0617			
Mass Flowrate (kg/s)	0.0156	0.0004			0.0131	0.0002		

Table B.4 – Measured air velocities and calculated air mass flowrates and uncertainties (run 5), for assessing mass and energy balances.

RUN 5	Air Flowrate (Inlet)				Air Flowrate (Outlet)			
Pump:1.5; Air: 230°C	Pipe Radius =	0.03	Radius^2 =	0.0009	Pipe Radius =	0.0375	Radius^2 =	0.00140625
Point	Velocity (m/s)	Error	Radius (m)	Radius^2 (m^2)	Velocity (m/s)	Error	Radius (m)	Radius^2 (m^2)
1	4.7	0.5	0.02	0.0004	0.8	0.5	0.025	0.000625
2	5.2	0.5	0.01	0.0001	2.2	0.5	0.0125	0.00015625
3	5	0.5	0	0	3.4	0.5	0	0
4	4.5	0.5	0.01	0.0001	4	0.5	0.0125	0.00015625
5	4.6	0.5	0.02	0.0004	4.5	0.5	0.025	0.000625
u(r)d(r^2)	0.0042425	0.00012			0.0039	0.00018		
Vol. Flowrate (m3/s)	0.01333	0.000364176			0.01233	0.000569		
Temp. Air In (°C)	21.6				62.9			
ρ_{air} (kg/m3)	1.1867				1.0408			
Mass Flowrate (kg/s)	0.0158	0.0004			0.0128	0.0006		

Appendix B

B3. Temperature Readings for Assessing Mass and Energy Balances

Table B.5 – Temperature readings, measured by thermocouples, for assessing mass and energy balances – Spraying of water

		RUN					
Thermocouple (°C)		**1**	**2**	**3**	**4**	**5**	**6**
Indicated reading	$T_{d\ in}$	23.46	23.46	22.35	21.79	22.35	21.79
"as above"	$T_{w\ in}$	19.66	19.66	19.10	17.98	18.54	17.98
"as above"	$T_{d\ out}$	26.67	55.00	62.22	70.56	68.89	65.56
"as above"	$T_{w\ out}$	21.35	37.67	38.00	40.00	39.33	39.33
"as above"	$T_{hot\ air}$	25.84	168.50	197.00	231.5	232.5	232.5
"as above"	T_{dryer}	24.86	48.02	54.80	59.89	59.32	57.06
"as above"	$T_{dryer\ exit}$	24.86	56.50	64.97	74.01	72.32	68.36
Mercury reading (°C)	T_{room}	20.50	20.50	21.50	22.10	21.60	21.60
"as above"	$T_{cold\ junction}$	19.60			22.20		
"as above"	$T_{d\ in}$	19.90	21.10	22.20		21.6	
"as above"	$T_{d\ out}$	22.70	49.20	56.30		62.9	
Compressed air	P_{air} (psi)	-	17.00	17.00	17.00	17.00	17.00
Water flowrate	Q_{water} ($L\ hr^{-1}$)	-	1.40	1.40	1.40	1.60	1.80

The equations used for adjusting the temperature readings measured by the thermocouples are given below:

Calibration adjustment for mercury thermometer (°C)

$$T_{actual} = \frac{T_{indicated} - 0.2}{0.996}$$

Calibration adjustment for hot air thermocouple ($T_{hot\ air}$) (°C)

$$T_{actual} = 1.0269 \times T_{indicated} - 4.7854$$

Calibration adjustment for inlet dry-bulb thermocouple ($T_{d\ in}$) (°C)

$$T_{actual} = 1.0588 \times T_{indicated} - 4.7621$$

Calibration adjustment for dryer thermocouple (T_{dryer}) (°C)

$$T_{actual} = 1.0101 \times T_{indicated} - 5.4343$$

Calibration adjustment for inlet wet-bulb thermocouple ($T_{w\ in}$) (°C)

$$T_{actual} = 1.0897 \times T_{indicated} - 4.9471$$

Calibration adjustment for dryer thermocouple ($T_{dryer\ exit}$) (°C)

$$T_{actual} = 1.0128 \times T_{indicated} - 4.9119$$

Calibration adjustment for outlet wet-bulb thermocouple ($T_{w\ out}$) (°C)

$$T_{actual} = 1.0902 \times T_{indicated} - 4.8974$$

Calibration adjustment for outlet dry-bulb thermocouple ($T_{d\ out}$) (°C)

$$T_{actual} = 1.0511 \times T_{indicated} - 4.5876$$

Table B.6 – Adjusted thermocouple readings for runs in Table B.5 (in °C).

		RUN					
Thermocouple (°C)		**1**	**2**	**3**	**4**	**5**	**6**
Indicated reading	$T_{d\ in}$	20.08	20.08	18.90	18.31	18.90	18.31
"as above"	$T_{w\ in}$	16.48	16.48	15.87	14.65	15.26	14.65
"as above"	$T_{d\ out}$	23.45	53.22	60.81	69.58	67.82	64.32
"as above"	$T_{w\ out}$	18.38	36.17	36.53	38.71	37.98	37.98
"as above"	$T_{hot\ air}$	21.75	168.25	197.51	232.94	233.97	233.97
"as above"	T_{dryer}	19.68	43.07	49.92	55.06	54.48	52.20
"as above"	$T_{dryer\ exit}$	20.27	52.31	60.89	70.05	68.33	64.32
Mercury reading (°C)	T_{room}	20.50	20.50	21.50	22.10	21.60	21.60

Table B.7 – Adjusted thermocouple readings for runs in TableB.5 (in °F).

		RUN					
Thermocouple (°C)		**1**	**2**	**3**	**4**	**5**	**6**
Indicated reading	$T_{d\ in}$	68	68	66	65	66	65
"as above"	$T_{w\ in}$	62	62	61	58	59	58
"as above"	$T_{d\ out}$	74	128	141	157	154	148
"as above"	$T_{w\ out}$	65	97	98	102	100	100
"as above"	$T_{hot\ air}$	71	335	388	451	453	453
"as above"	T_{dryer}	67	110	122	131	130	126
"as above"	$T_{dryer\ exit}$	68	126	142	158	155	148

Appendix B

B4. Mass Balance Water – Spraying of Water

Table B8 – Inlet and outlet air flowrates for each run, used to carry out water balances.

Run	Air In $m_{a\ in}$ (kg s^{-1})	Air Out $m_{a\ out\ 1}$ (kg s^{-1})	Air Out $m_{a\ out\ 2}$ (kg s^{-1})
1	0.0158	0.0158	0.0258
2	0.0158	0.0158	
3	0.0158	0.0158	0.0131
4	0.0158	0.0158	
5	0.0158	0.0158	0.0128
6	0.0158	0.0158	

Table B.9 – Water balances, where mass flowrate of air in ($m_{air\ in}$) = mass flowrate of air out ($m_{air\ out\ 1}$).

Run	Y_{in} (kg kg^{-1})	Y_{out} (kg kg^{-1})	H_2O in inlet air (kg s^{-1})	H_2O sprayed (kg s^{-1})	Total H_2O in (kg s^{-1})	H_2O in outlet air (kg s^{-1}) using $m_{a\ out\ 1}$	Discrepancy (kg s^{-1})	Discrepancy (%)
1	0.0110	0.0115	1.74E-04	0	1.74E-04	1.82E-04	7.90E-06	4.5
2	0.0110	0.0315	1.74E-04	3.85E-04	5.59E-04	4.98E-04	-6.14E-05	-11.0
3	0.0105	0.0300	1.66E-04	4.40E-04	6.06E-04	4.74E-04	-1.32E-04	-21.8
4	0.0090	0.0325	1.42E-04	5.10E-04	6.52E-04	5.14E-04	-1.39E-04	-21.3
5	0.0095	0.0300	1.50E-04	4.40E-04	5.90E-04	4.74E-04	-1.16E-04	-19.7
6	0.0090	0.0315	1.42E-04	5.10E-04	6.52E-04	4.98E-04	-1.55E-04	-23.7

Table B.10 - Water balances with mass flowrate of air out ($m_{air\ out\ 2}$).

Run	H_2O in outlet air (kg s^{-1})	Discrepancy (kg s^{-1})	Discrepancy (%)
1	2.97E-04	1.23E-04	70.7
2		-5.59E-04	
3	3.93E-04	-2.13E-04	-35.1
4		-6.52E-04	
5	3.84E-04	-2.06E-04	-34.9
6		-6.52E-04	

Appendix B

B5. Sensitivity Analysis and Propagation of Errors and Uncertainties for Run 1 and 2

SENSITIVITY ANALYSIS FOR RUN 1

For run 1, the inlet air temperature was at ambient conditions and no water was sprayed. Thus, it is expected that the humidity of the air entering the dryer will equal the humidity of the air leaving the dryer.

Run 1 – Air was not heated and no water was sprayed

Typical Air Inlet Conditions

$T_{d\,in} = 20.1\ ^{\circ}C$

$T_{w\,in} = 16.5\ ^{\circ}C$

Using a psychometric chart, the humidity of the air is determined to be:

$Y_i = 0.011$ kg water/kg dry air

Sensitivity of the air humidity to uncertainties in the dry-bulb temperature:

If there is a 1.0 °C error in the dry-bulb temperature, then the air inlet conditions could actually be:

$T_{d\,in} = 21.1\ ^{\circ}C$

$T_{w\,in} = 16.5\ ^{\circ}C$

This leads to a humidity of:

Y_i = 0.0105 kg water/kg dry air

Expressing the sensitivity of the inlet air humidity to the dry-bulb temperature, the equation used is $\frac{0.011-0.0105}{0.011}\times 100 = 4.5\%$. Therefore, the sensitivity of Y_i to an error in the dry-bulb inlet temperature of 1.0°C is 5%.

Sensitivity of the air humidity to uncertainties in the wet-bulb temperature :

If there is a 1.0 °C error in the wet-bulb temperature, then the air inlet conditions could actually be:

$T_{d\,in}$ = 20.1 °C
$T_{w\,in}$ = 17.5 °C

This leads to a humidity of:

Y_i = 0.012 kg water/kg dry air

Expressing the sensitivity of the inlet air humidity to the wet-bulb temperature, the equation used is $\frac{0.012-0.011}{0.011}\times 100 = 9\%$. Therefore, the sensitivity of Y_i to an error in the wet-bulb inlet temperature of 1.0°C is 9%.

Typical Air Outlet Conditions

$T_{d\,out}$ = 23.5 °C
$T_{w\,out}$ = 18.4 °C

This leads to a humidity of:

Y_o = 0.012 kg water/kg dry air

Sensitivity of the air humidity to uncertainties in the dry-bulb temperature :

If there is a 1.0 °C error in the dry-bulb temperature, then the air inlet conditions could actually be:

$T_{d\,out}$ = 24.5 °C
$T_{w\,out}$ = 18.4 °C

This leads to a humidity of:

Y_o = 0.0115 kg water/kg dry air

Expressing the sensitivity of the outlet air humidity to the dry-bulb temperature, the equation used is $\frac{0.012-0.0115}{0.012}\times 100 = 4\%$. Therefore, the sensitivity of Y_o to an error in the dry-bulb outlet temperature of 1.0°C is 4%.

Sensitivity of the air humidity to uncertainties in the wet-bulb temperature :

If there is a 1.0 °C error in the wet-bulb temperature, then the air inlet conditions could actually be:

$T_{d\,out}$ = 23.5 °C
$T_{w\,out}$ = 19.4 °C

This leads to a humidity of:

Y_o = 0.0127 kg water/kg dry air

Expressing the sensitivity of the outlet air humidity to the wet-bulb temperature, the equation used is $\frac{0.013-0.012}{0.012}\times 100 = 8\%$. Therefore, the sensitivity of Y_o to an error in the outlet wet-bulb temperature of 1.0°C is 8%.

This sensitivity analysis shows that the calculation of the absolute humidity of the air is more sensitive to the wet-bulb temperatures than to the dry-bulb temperatures. Observation of a psychometric chart shows that, as the dry-bulb temperature increases, the estimated humidity of the air (absolute humidity) becomes increasingly sensitive to changes in the wet-bulb temperature, due to the increasing wet-bulb temperature scale. Figure B.1 shows this behaviour on a psychometric chart.

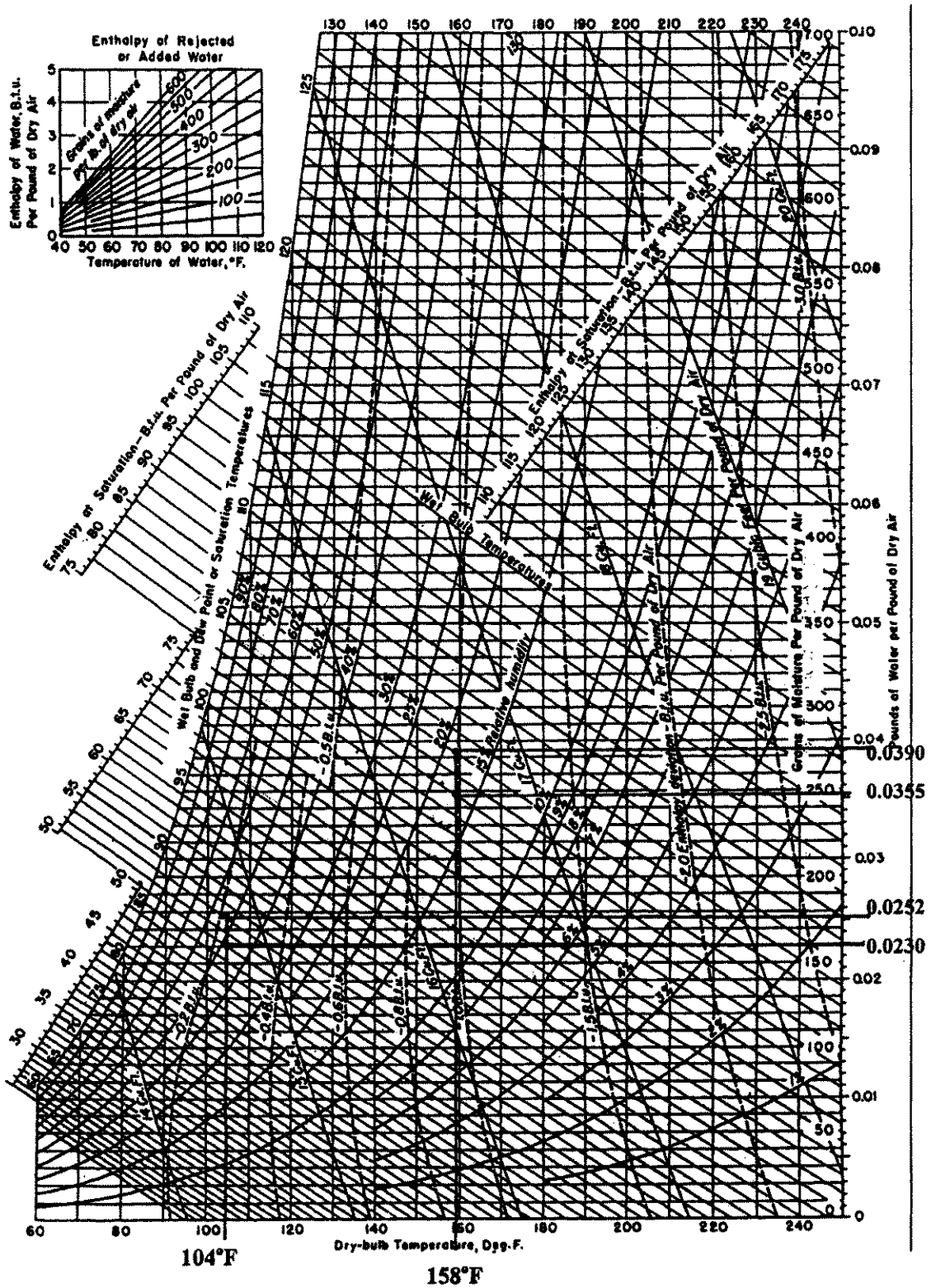

Figure B.1 – Psychometric chart for high temperatures. Barometric pressure, 29.92 in Hg. Source : Perry's Chemical Engineering Handbook (1997).

Figure B.1 shows that, at a high dry-bulb temperature of 70°C (e.g. 158°F), if the wet-bulb temperature increases by 1°C from 40°C (104°F) to 41°C (100°F), the absolute humidity increases from 0.0353 kg water per kg of dry air to 0.0390 kg kg^{-1}, a change of 0.0037 kg kg^{-1}. This contrasts with a 1°C wet-bulb temperature change at lower dry-bulb temperatures. For example, when the dry-bulb temperature is 40°C (104°F), a change in the wet-bulb temperature from 30°C (86°F) to 31°C (88°F) only results in a change in the humidity of 0.0022 kg kg^{-1}. Observations of the psychometric chart shows that as the wet-bulb temperature increases, the distance between the lines on the chart increases, leading to an increased sensitivity of the humidity to temperature changes.

The sensitivity of the inlet absolute humidity to the wet-bulb temperature can be more clearly shown by considering the partial derivatives of the inlet moisture content with respect to the dry-bulb and wet-bulb temperatures in the case of the dry-bulb, wet-bulb temperature combination of (20.1, 16.5):

***Sensitivity of Y_i to temperature uncertainties*:**

$$\frac{\partial Y_i}{\partial T_{d\,in}} = \frac{(0.011 - 0.0105)\,\text{kg kg}^{-1}}{+1\,\text{K}} \qquad \text{(B.1)}$$

$$= 0.0005\,\text{kg water/kg dry air K}$$

$$\frac{\partial Y_i}{\partial T_{w\,in}} = \frac{(0.012 - 0.011)\,kg\ kg^{-1}}{+1K} \qquad \text{(B.2)}$$

$$= 0.0010\text{kg water/kg dry air K}$$

Thus, the absolute humidity is twice as sensitive to the wet-bulb temperature as to the dry-bulb temperature. This sensitivity study demonstrates how important correct wet-bulb measurement is for accurate results. Even with a random uncertainty in the wet-bulb temperature of ±0.6 K, the uncertainty of Y_i is:

$$\frac{\partial Y_i}{\partial T_{w\,out}} \times \partial T_{w\,out} = 0.0010\ \text{kg kg}^{-1}\ \text{K}^{-1} \times 0.6\ \text{K}$$

$$= 0.0006\ \text{kg water/kg dry air}$$

Thus, even if systematic error is eliminated and considering that the outlet humidity is 0.011 kg water/kg dry air, an uncertainty of 5% will still exist for Y_i under these conditions. Since the absolute humidity is used to calculate further results for mass and energy balances, it is important to take several wet-bulb temperatures and to average them in order to reduce the random uncertainty in the results. The propagation of error in the water balances from random uncertainty in the experimental measurements will be considered next.

PROPAGATION OF ERRORS AND UNCERTAINTIES FOR RUN 1

The variance or standard error in the absolute humidity (δY), is related to the standard error in the dry-bulb temperature δT_d and the wet-bulb temperature δT_w, respectively, by the following equation B.6 (provided that the uncertainties in the wet-bulb and dry-bulb temperature are independent of each other):

$$\delta Y^2 = \left(\frac{\delta Y}{\delta T_d}\right)^2 \delta T_d{}^2 + \left(\frac{\delta Y}{\delta T_w}\right)^2 \delta T_w{}^2 \qquad \text{(B.3)}$$

$$\delta Y = \sqrt{\left(\frac{\delta Y}{\delta T_d} \times \delta T_d\right)^2 + \left(\frac{\delta Y}{\delta T_w} \times \delta T_w\right)^2} \qquad \text{(B.4)}$$

The uncertainties associated with the dry-bulb and wet-bulb temperatures need to be incorporated into the balances, by calculating the standard error in the absolute humidity. The data from run 1, where $\frac{\delta Y}{\delta T_d} = 0.0005\ \text{kg kg}^{-1}$, $\frac{\delta Y}{\delta T_w} = 0.0010\ \text{kg kg}^{-1}$ and $\delta T_d = \delta T_w = 0.6$ K, have been used for the calculations outlined here.

Applying equation B.4 to the inlet conditions,

$$\pm \delta Y = \sqrt{\left(0.0005\ \text{kg kg}^{-1} \times 0.6\text{K}\right)^2 + \left(0.0010\ \text{kg kg}^{-1} \times 0.6\text{K}\right)^2}$$
$$= 0.0007\ \text{kg kg}^{-1}$$

Therefore, $Y_i = 0.011 \pm 0.001$ kg water/kg dry air

Assuming a 5% uncertainty in the inlet air flowrate measurement, where m_a is 0.016 kg s^{-1},

$$\delta m_a = 0.0008\ \text{kg/s}$$

Therefore,

$$m_a = 0.016 \pm 0.001\ \text{kg s}^{-1}$$

Now, the equation for the mass of water entering the dryer with the air is:

$$m_{w\,air\,in} = m_a \times Y_i \tag{B.5}$$

where Y_i is the absolute humidity of the air entering the dryer. The propagation of these uncertainties can be calculated using equation B.6 and/or equation B.7:

For addition/subtraction (use absolute errors) (Kirkup, 1994):

$$(A \pm \delta A) \pm (B \pm \delta B) = A \pm B \pm \sqrt{\delta A^2 + \delta B^2} \tag{B.6}$$

For multiplication/division (use relative errors) (Kirkup, 1994):

$$(A \pm \delta A)(B \pm \delta B) = AB \pm AB\sqrt{\left(\frac{\delta A}{A}\right)^2 + \left(\frac{\delta B}{B}\right)^2} \tag{B.7}$$

Thus, the mass of water entering the dryer with the air is:

$$m_{w\,air\,in} = (0.016 \pm 0.001)\ \text{kg air s}^{-1} \times (0.011 \pm 0.001)\ \text{kg water/kg dry air}$$
$$= 1.76 \times 10^{-4}\ \text{kg water s}^{-1}$$

The relative uncertainty is $= \sqrt{\left(\frac{0.001}{0.016}\right)^2 + \left(\frac{0.001}{0.011}\right)^2}$

$= 0.11 \approx \frac{0.001}{0.011}$

so most of the uncertainty is contributed by the uncertainty in the absolute humidity of the air.

The absolute uncertainty = 1.76×10^{-4} kg water $s^{-1} \times 0.11 = 1.94 \times 10^{-5}$ kg water s^{-1}, so

$m_{w\ air\ in} = 0.00018 \pm 0.00002$ kg water s^{-1}

Now considering the water leaving the dryer, the absolute humidity and the outlet air flowrate (with errors), calculated as for the inlet conditions (See Appendix A2.1), are as follows:

$$Y_o = 0.012 \pm 0.001 \text{ kg water/kg dry air}$$

$$m_a = 0.016 \pm 0.001 \text{ kg/s}$$

Now, the mass of water leaving the dryer with the air is,

$$m_{w\ air\ out} = m_a \times Y_o \tag{B.8}$$

Thus, the mass of water leaving the dryer with the air is:

$$m_{w\ air\ out} = 1.92 \times 10^{-4} \text{ kg water } s^{-1}$$

The relative uncertainty is = $0.10 \approx \frac{0.001}{0.012}$

and most of the uncertainty is contributed by the uncertainty in the absolute humidity of the air.

The absolute uncertainty = 1.92×10^{-4} kg water $s^{-1} \times 0.10 = 1.92 \times 10^{-5}$ kg water s^{-1}, so

$$m_{w\ air\ out} = 0.00019 \pm 0.00002 \text{ kg water } s^{-1}$$

Now, the actual discrepancy for the water balance is given by equation B.9:

$$\text{Discrepancy} = m_{w\ air\ out} - m_{w\ air\ in} \qquad \text{(B.9)}$$
$$= 0.00019 \pm 0.00002\ \text{kg water s}^{-1} - 0.00018 \pm 0.00002\ \text{kg water s}^{-1}$$
$$= 1.0 \times 10^{-5}\ \text{kg water s}^{-1}$$

where the uncertainty in the discrepancy is $\sqrt{0.00002^2 + 0.00002^2} = 3.0 \times 10^{-5}$ kg water s^{-1}.

Since the uncertainty in the discrepancy (3.0×10^{-5} kg water s^{-1}) is greater than the discrepancy itself (1.0×10^{-5} kg water s^{-1}), the discrepancy could possibly be zero within the uncertainties in the measurements. This result supports the expectation that the absolute humidity of the air should not change when no water is sprayed into the drying chamber.

An analysis of the sensitivity of the absolute humidity of the air entering the dryer (Y_i) and leaving the dryer (Y_o) to the dry bulb and wet bulb temperature readings will now be outlined using experimental values from run 2. For run 2, the air was heated to 170°C before it entered the dryer and the flowrate of the water was 1.4 L hr^{-1}.

SENSITIVITY ANALYSIS FOR RUN 2

Typical Air Inlet Conditions

$T_{d\ in}$ = 20.1 °C (three significant figures)
$T_{w\ in}$ = 16.5 °C

Since the inlet air conditions ($T_{d\ in}$ and $T_{w\ in}$) are the same as those of run 1,the sensitivity of Y_i to an error in the dry-bulb inlet temperature of 1.0°C is 5% and the sensitivity of Y_i to an error in the wet-bulb inlet temperature of 1.0°C is 9%.

Typical Air Outlet Conditions

$T_{d\ out}$ = 53.2°C
$T_{w\ out}$ = 36.2 °C

This leads to a humidity of:

Y_o = 0.0315 kg water/kg dry air

Sensitivity of the air humidity to uncertainties in the dry-bulb temperature :

If there is a 1.0 °C error in the dry-bulb temperature, then the air inlet conditions could actually be:

$T_{d\,out}$ = 54.2 °C

$T_{w\,out}$ = 36.2°C

This leads to a humidity of:

Y_o= 0.031 kg water/kg dry air

Expressing the sensitivity of the outlet air humidity to the dry-bulb temperature, the equation used is $\frac{0.0315-0.031}{0.0315}\times 100 = 1.5\%$. Therefore, the sensitivity of Y_o to an error in the dry-bulb inlet temperature of 1.0°C is 2%.

Sensitivity of the air humidity to uncertainties in the wet-bulb temperature :

If there is a 1.0 °C error in the wet bulb temperature, then the air inlet conditions could actually be:

$T_{d\,out}$ = 53.2 °C

$T_{w\,out}$ = 37.2 °C

This leads to a humidity of:

Y_i = 0.034 kg water/kg dry air

Expressing the sensitivity of the outlet air humidity to the wet-bulb temperature, the equation used is $\frac{0.034-0.0315}{0.0315}\times 100 = 7.9\%$. Therefore, the sensitivity of Y_o to an error in the wet-bulb inlet temperature of 1.0°C is 8%. This result confirms, as found previously for the case where no water was sprayed, that the calculation of the absolute humidity of the air is more sensitive to the wet-bulb temperatures than to the dry-bulb temperatures. The inlet absolute humidity (Y_i) is 2 times as sensitive to the wet-bulb temperature ($T_{w\,in}$) as the dry-bulb temperature ($T_{d\,in}$).

The sensitivity of the outlet absolute humidity to the wet-bulb temperature can be more clearly shown by considering the partial differentials of the outlet moisture content with respect to the dry-bulb and wet-bulb temperatures in the case of the dry-bulb, wet-bulb temperature combination of (53.2, 36.2).

Sensitivity of Y_o to thermocouples:

$$\frac{\partial Y_o}{\partial T_{d\,out}} = \frac{(0.0315-0.031)\,\text{kg kg}^{-1}}{+1\text{K}}$$

$$= 0.0005 \text{ kg water/kg dry air K}$$

$$\frac{\partial Y_o}{\partial T_{w\,out}} = \frac{(0.034-0.0315)\,\text{kg kg}^{-1}}{+1\text{K}}$$

$$= 0.0025 \text{ kg water/kg dry air K}$$

The outlet absolute humidity (Y_o) is 5 times as sensitive to the wet-bulb temperature ($T_{w\,out}$) as the dry- bulb temperature ($T_{d\,out}$). For run 1, the outlet wet-bulb temperature was low at 16.5°C compared to run 2, where the outlet wet-bulb temperature was 36.2°C. The outlet absolute humidity is 2.5 times more sensitive to the wet-bulb temperature when the wet-bulb temperature is high.

These sensitivity studies demonstrate how important correct wet-bulb measurement is for accurate results , especially if the outlet wet-bulb temperature is high. Even with a random uncertainty in the wet-bulb temperature of ±0.6 K, the uncertainty of Y_o *is*:

$$\frac{\partial Y_o}{\partial T_{w\,out}} \times \partial T_{w\,out} = 0.0025\ \text{kg kg}^{-1}\text{K}^{-1} \times 0.6\ \text{K}$$

$$= 0.0015\ \text{kg water/kg dry air}$$

Thus, even if systematic error is eliminated and considering that the outlet humidity is 0.0315 kg water/kg dry air, an uncertainty of 5% will still exist for Y_o under these conditions. A propagation of error and uncertainties analysis for run 2 is discussed next.

PROPAGATION OF ERRORS AND UNCERTAINTIES FOR RUN 2

The data from run 2 have been used for the calculations outlined below. The uncertainty in the inlet absolute humidity is:

$$\pm \delta Y = \sqrt{\left(0.0005\ \text{kg kg}^{-1} \times 0.6\ \text{K}\right)^2 + \left(0.0010\ \text{kg.kg}^{-1} \times 0.6\ \text{K}\right)^2}$$

$$\pm \delta Y = 0.0007\ \text{kg kg}^{-1}$$

Therefore,

$$Y_i = 0.011 \pm 0.001\ \text{kg water/kg dry air}$$

The mass flowrate of the air is:

$$m_a = 0.016 \pm 0.001\ \text{kg s}^{-1}$$

Now, the equation for the mass of water entering the dryer with the air is:

$$m_{w\,air\,in} = m_a \times Y_i + m_{w\,spray}$$

where

$$m_{w\,air\,in} = (0.016 \pm 0.001)\ \text{kg air s}^{-1} \times (0.011 \pm 0.001)\ \text{kg water/kg dry air} +$$

$$(3.9 \times 10^{-4} \pm 8.5 \times 10^{-6})\ \text{kg water s}^{-1}$$

$$= (0.00018 \pm 0.00002)\ \text{kg water s}^{-1} + (3.9 \times 10^{-4} \pm 8.5 \times 10^{-6})\ \text{kg water s}^{-1}$$
$$= 5.6 \times 10^{-4}\ \text{kg water s}^{-1}$$

The absolute uncertainty is $= \sqrt{0.00002^2 + 0.0000085^2} = 2.2 \times 10^{-5}\ \text{kg water s}^{-1}$

So, $m_{w\,air\,in} = 5.6 \times 10^{-4} \pm 2.2 \times 10^{-5}\ \text{kg water s}^{-1}$.

Now considering the water leaving the dryer, the uncertainty in the inlet absolute humidity is:

$$\pm \delta Y = \sqrt{\left(0.0005\ \text{kg kg}^{-1} \times 0.6\text{K}\right)^2 + \left(0.0025\ \text{kg kg}^{-1} \times 0.6\text{K}\right)^2}$$
$$= 0.0015$$

so the absolute humidity for the outlet air (with errors) calculated as for the outlet conditions are as follows:

$$Y_o = 0.0315 \pm 0.0015\ \text{kg water/kg dry air}$$

$$m_a = 0.016 \pm 0.001\ \text{kg s}^{-1}$$

Now, the mass of water leaving the dryer with the air is,

$$m_{w\,air\,out} = m_a \times Y_o$$

Thus, the mass of water leaving the dryer with the air is:

$$m_{w\,air\,out} = (0.016 \pm 0.001)\ \text{kg air s}^{-1} \times (0.0315 \pm 0.0015)\ \text{kg water/kg dry air}$$
$$= 5.0 \times 10^{-4}\ \text{kg water s}^{-1}$$

The relative uncertainty is $= \sqrt{\left(\frac{0.001}{0.016}\right)^2 + \left(\frac{0.0015}{0.0315}\right)^2}$

$$= 0.08 \approx \frac{0.001}{0.016}$$

The absolute uncertainty = 5.0×10^{-4} kg water $s^{-1} \times 0.08 = 4.0 \times 10^{-5}$, so

$$m_{w\,air\,out} = 5.0 \times 10^{-4} \pm 4.0 \times 10^{-5} \text{ kg water s}^{-1}$$

Now, the actual discrepancy for the water balance is given by:

$$\text{Discrepancy} = (5.0 \times 10^{-4} \pm 4.0 \times 10^{-5}) \text{ kg water s}^{-1} - (5.6 \times 10^{-4} \pm 2.2 \times 10^{-5}) \text{ kg water s}^{-1}.$$

$$= -6 \times 10^{-5} \text{ kg water s}^{-1}$$

where the uncertainty in the discrepancy is $\sqrt{0.00004^2 + 0.00002^2} = 4 \times 10^{-5}$ kg water s^{-1}. The uncertainty in the discrepancy accounts for 67% of the discrepancy. Thus, if we have a discrepancy of 20% in the water balance, than all but 6% of the discrepancy can be attributed to random uncertainty.

In summary, the sensitivity of Y_i to an error in the inlet dry-bulb temperature of 1.0°C is 5% and the sensitivity of Y_i to an error in the inlet wet-bulb temperature of 1.0°C is 9%. This result confirms, as found previously for the case where no water was sprayed, that the calculation of the absolute humidity of the air is more sensitive to the wet-bulb temperatures than to the dry-bulb temperatures. The inlet absolute humidity (Y_i) is twice as sensitive to the wet-bulb temperature ($T_{w\,in}$) as to the dry-bulb temperature ($T_{d\,in}$), and the outlet absolute humidity (Y_o) is four times as sensitive to the wet-bulb temperature as to the dry-bulb temperature.

The uncertainty in the inlet absolute humidity δY is 0.0007 kg kg^{-1}, so Y_i = (0.011 ± 0.001) kg water/kg dry air. Now, the equation for the mass of water entering the dryer with the air is:

$$m_{w\,air\,in} = m_a \times Y_i + m_{w\,spray} \qquad \text{(B.10)}$$

where $m_{w\,spray}$ is $(3.9 \times 10^{-4} \pm 8.5 \times 10^{-6})$ kg water s^{-1}, so $m_{w\,air\,in}$ is $(5.6 \times 10^{-4} \pm 2.2 \times 10^{-5})$ kg water s^{-1}.

The absolute humidity for the outlet air calculated as for the outlet conditions was Y_o = (0.0315 ± 0.0015) kg water/kg dry air.

The mass of water leaving the dryer with the air is $m_{w\,air\,out} = (5.0 \times 10^{-4} \pm 4.0 \times 10^{-5})$ kg water s^{-1}, so the actual discrepancy for the water balance is:

$$\text{Discrepancy} = (5.0 \times 10^{-4} \pm 4.0 \times 10^{-5}) \text{ kg water s}^{-1} - (5.6 \times 10^{-4} \pm 2.2 \times 10^{-5}) \text{ kg water s}^{-1}.$$

$$= -6 \times 10^{-5} \text{ kg water s}^{-1}$$

where the uncertainty in the discrepancy is $\sqrt{0.00004^2 + 0.00002^2} = 4 \times 10^{-5}$ kg water s^{-1}. The uncertainty in the discrepancy accounts for 67% of the discrepancy. A number of temperature readings were recorded for each thermocouple per run, and these readings were averaged to reduce the uncertainty from random error. A propagation of error analysis will now be carried out for the energy balances over the dryer.

PROPAGATION OF ERROR ANALYSIS FOR ENERGY BALANCES FOR RUN 1

From equation 4.5 in Chapter 4, the energy balance is given by equation B.11.

$$H_{in} = H_{out} + H_{loss} \tag{B.11}$$

where

$$H_{in} = m_a C_{pa,i}(T_{hot\,air} - T_{ref}) + m_a Y_i(\lambda + C_{pw,v\,in}(T_{hot\,air} - T_{ref})) \tag{B.12}$$

$$H_{out} = m_a C_{pa,o}(T_{d\,out} - T_{ref}) + m_a Y_o(\lambda + C_{pw,v\,out}(T_{d\,out} - T_{ref})) \tag{B.13}$$

Here H_{in} is the enthalpy rate entering the dryer, and H_{out} is the enthalpy rate leaving the dryer (in kW). $C_{pa,i}$ and $C_{pa,o}$ are the heat capacities of the air entering the dryer and leaving the dryer, and $C_{pw,v\,in}$ and $C_{pw,v\,out}$ are the heat capacities of the water vapour entering and leaving the dryer in (kJ kg^{-1} K^{-1}). λ is the latent heat of vaporisation of water in (kJ kg^{-1}). $T_{hot\,air}$ and $T_{d\,out}$ are the temperature of the air entering (after heating) and leaving the dryer (in K) and T_{ref} is the reference temperature, which was taken as 273 K.

So,

$$H_{in} = (0.016 \pm 0.001)\ \text{kg air s}^{-1} \times 1.001\ \text{kJ kg}^{-1}\text{K}^{-1} \times (294.9 \pm 0.6 - 273)\text{K} +$$
$$(0.016 \pm 0.001)\ \text{kg air s}^{-1} \times (0.011 \pm 0.001)\ \text{kg water/kg dry air} \times$$
$$(2500\text{kJ kg}^{-1} + 1.863\ \text{kJ kg}^{-1}\text{K}^{-1} \times (294.9 \pm 0.6 - 273))$$
$$= 0.81\ \text{kW}$$

Uncertainty in first term

$$= 1.001\ \text{kJ kg}^{-1}\text{K}^{-1} \times 0.016\ \text{kg air s}^{-1} \times 21.75\ \text{K} \times \sqrt{\left(\frac{0.001}{0.016}\right)^2 + \left(\frac{0.6}{21.75}\right)^2}$$
$$= 0.0237\ \text{kW}$$

Uncertainty in second term

$$= (1.76 \times 10^{-4} \pm 1.94 \times 10^{-5})\text{kg water s}^{-1} \times$$
$$(2540\text{kJ kg}^{-1} \pm 1.12)\ \text{kJ kg}^{-1}$$
$$= 0.45\ \text{kW} \pm 0.45 \times \sqrt{\left(\frac{1.94 \times 10^{-5}}{1.76 \times 10^{-4}}\right)^2 + \left(\frac{1.118}{2540}\right)^2}$$
$$= 0.049\ \text{kW}$$

The absolute uncertainty is $= \sqrt{(0.0237^2) + (0.049)^2}$
$= 0.05\ \text{kW}$

So, $H_{in} = 0.81 \pm 0.05$ kW

Likewise, calculating H_{out}

$$H_{out} = (0.016 \pm 0.001)\ \text{kg air s}^{-1} \times 1.001\ \text{kJ kg}^{-1}\ \text{K}^{-1} \times (296.6 \pm 0.6 - 273)\text{K} +$$
$$(0.016 \pm 0.001)\ \text{kg air s}^{-1} \times (0.012 \pm 0.001)\ \text{kg water/kg dry air} \times$$
$$(2500\ \text{kJ kg}^{-1} + 1.863\ \text{kJ kg K}^{-1}) \times (296.6 \pm 0.6 - 273)\text{K}$$
$$= 0.84\ \text{kW}$$

Uncertainty in first term:

$$= 1.001\ \text{kJ kg}^{-1}\ \text{K}^{-1} \times 0.016\ \text{kg air s}^{-1} \times 23.6\ \text{K} \times \sqrt{\left(\frac{0.001}{0.016}\right)^2 + \left(\frac{0.6}{23.6}\right)^2}$$

= 0.024 kW

Uncertainty in second term

$$= 0.016 \text{ kg air s}^{-1} \times 0.012 \text{ kg water/kg dry air} \times 2544 \text{ kJ kg}^{-1} \times \sqrt{\left(\frac{0.001}{0.016}\right)^2 + \left(\frac{0.001}{0.012}\right)^2 + \left(\frac{1.118}{2544}\right)}$$

= 0.051 kW

$$\text{Absolute uncertainty} = \sqrt{(0.024^2) + (0.051)^2}$$
$$= 0.06 \text{ kW}$$

So, $H_{out} = 0.84 \pm 0.06$ kW

$$\text{The discrepancy in the heat balance is} = 0.84 \pm 0.06 \text{ kW} - 0.81 \pm 0.05 \text{ kW}$$
$$= 0.03 \pm 0.08 \text{ kW}$$

Since the uncertainty in the discrepancy is greater than the discrepancy itself, the discrepancy could possibly be zero within the uncertainties in the measurements. Thus, there may well be no real increase in energy across the spray dryer when the air is not heated.

A propagation of error analysis will now be carried for the case where water is sprayed and the air entering the dryer is heated. The experimental results from run 2 will be used here. The energy entering the dryer is the sum of the enthalpy from the hot air, water and compressed air entering through the nozzle.

From Chapter 4:

$$H_{in} = H_{in\ air} + H_{in\ water} + H_{in\ comp\ air} \tag{4.8}$$

$$H_{in} = m_a C_{pa,i}(T_{hot\ air} - T_{ref}) + m_a Y_i[\lambda + C_{pw,v_{in}}(T_{hot\ air} - T_{ref})] + m_w C_{pw}(T_{water} - T_{ref}) + m_{ca} C_{pca,i}(T_{ca} - T_{ref}) + m_{ca} Y_i[\lambda + C_{pw,v_{in}}(T_{ca} - T_{ref})] \tag{4.9}$$

where $C_{pca,i}$ and C_{pw} are the heat capacities of the compressed air entering the dryer and the water sprayed into the dryer, respectively (in kJ kg^{-1} K^{-1}), m_w is the mass flowrate of the water sprayed into the dryer (in kg s^{-1}), T_{water} is the temperature of the water (in K) and T_{ca} is the temperature of the compressed air (in K), which were both taken as ambient, and m_{ca} is the mass flowrate of compressed air entering the dryer (in kg s^{-1}).

So,

H_{in}= (0.016 ± 0.001) kg air s^{-1} × 1.019 kJ kg^{-1} K^{-1} × (441.4 ± 0.6–273)K +
(0.016 ± 0.001) kg air s^{-1} × (0.011 ± 0.001) kg water/kg dry air ×
(2500 kJ kg^{-1} + 1.938 kJ kg^{-1} K^{-1} × (441.4 ± 0.6 –273 K)) +
(3.9 × 10^{-4} ± 8.5 × 10^{-6}) kg water s^{-1}× 4.188 kJ kg^{-1} K^{-1} × (293.7 ± 0.6 -273) K +
0.0004 kg compressed air s^{-1} × 1.004 kJ kg^{-1} K^{-1} × (293.7 ± 0.6 –273) K +
0.0004 kg compressed air s^{-1} × (0.011 ± 0.001) kg water/kg dry air ×
(2500 kJ kg^{-1} + 1.863 kJ kg^{-1} K^{-1} × (293.7 ± 0.6 –273 K))

= 3.26 kW

Uncertainty in first term = $1.019 \times 0.016 \times 168.4 \times \sqrt{\left(\frac{0.6}{168.4}\right)^2 + \left(\frac{0.001}{0.016}\right)^2}$ kJ kg^{-1} K^{-1} × kg air s^{-1} × K

= 0.172 kW

Uncertainty in second term

$= 1.76 \times 10^{-4} \times 2826.35 \sqrt{\left(\frac{1.67\times10^{-5}}{1.76\times10^{-4}}\right)^2 + \left(\frac{1.16}{2826.35}\right)^2}$ kg water s^{-1}× kJ kg^{-1}

= 0.05 kW

Uncertainty in the third term = $4.188 \times 3.9 \times 10^{-4} \times 20.7 \times \sqrt{\left(\frac{8.5\times10^{-6}}{3.9\times10^{-4}}\right)^2 + \left(\frac{0.6}{20.7}\right)^2}$ kJ kg^{-1} K^{-1} × kg water s^{-1} × K

= 0.0012 kW

Uncertainty in fourth term = 0.0004 kg compressed air $s^{-1} \times 1.004$ kJ kg^{-1} $K^{-1} \times 0.6$ K

$= 2.41 \times 10^{-4}$ kW

Uncertainty in the fifth term = 0.0004 kg compressed air $s^{-1} \times 0.011$ kg water/kg dry air $\times$

$$2538.56 \text{ kJ kg}^{-1} \times \sqrt{\left(\frac{0.001}{0.011}\right)^2 + \left(\frac{1.118}{2538.56}\right)^2}$$

$= 0.001$ kW

$$\text{Absolute uncertainty} = \sqrt{(0.172^2) + (0.05)^2 + (0.0012)^2 + (0.00024)^2 + (0.001)^2}$$

$= 0.18$ kW

The uncertainty in the enthalpy of the air entering the spray dryer contributes most to the uncertainty of the total enthalpy entering the spray dryer. This uncertainty in the enthalpy of the air can be reduced by measuring the air temperature and humidity more accurately.

So, $H_{in} = 3.3 \pm 0.2$ kW

Likewise, calculating H_{out} using equation B.13:

H_{out}= (0.016 ± 0.001) kg air $s^{-1} \times 1.003$ kJ kg^{-1} $K^{-1} \times$ (326.4 ± 0.6–273)K +

(0.016 ± 0.001) kg air $s^{-1} \times$ (0.0315 ± 0.0015) kg water/kg dry air $\times$

(2500 kJ kg^{-1} + 1.875 kJ kg^{-1} $K^{-1} \times$ (326.4 –273 K))

= 2.14 kW

Uncertainty in first term = 0.054 kW

Uncertainty in second term = 0.10 kW

$= 0.085$ kW

$$\text{Absolute uncertainty} = \sqrt{(0.054^2) + (0.1)^2}$$

$= 0.10$ kW

So, $H_{out} = 2.1 \pm 0.1$ kW

The heat loss is given by equation 4.10 from Chapter 4:

$$\begin{aligned} H_{loss} &= H_{in} - H_{out} \\ &= 1.1 \pm 0.1\,\text{kW} \end{aligned} \tag{4.10}$$

The uncertainty in the discrepancy in the energy entering and leaving the dryer accounts for 18% of the discrepancy. The most likely cause of the difference between the inlet and outlet energy is heat losses from the spray dryer and connecting pipework.

Appendix B

B6. Heat Balance – Spraying of Water

Table B.11 – Data used for calculating heat balances where only water was sprayed into the spray dryer. Heat capacity data taken from Perry's Chemical Engineers' Handbook, 7th Edition (1997), McGraw Hill, New York.

Cp (water) =	4.180	kJ/(kg °C)	at 25°C
Cp (air) =	1.001	kJ/(kg °C)	at 25°C
Cp (air) =	1.003	kJ/(kg °C)	at 65°C
Cp (air) =	1.019	kJ/(kg °C)	at 200°C
Cp (air) =	1.026	kJ/(kg °C)	at 230°C
Cp (comp. air) =	1.004	kJ/(kg °C)	at 20 psi, 25°C
Cp (comp. air) =	0.681	kJ/(kg °C)	at 40 psi, 25°C
Cp (water vapour) =	1.863	kJ/(kg °C)	at 25°C
Cp (water vapour) =	1.875	kJ/(kg °C)	at 65°C
Cp (water vapour) =	1.938	kJ/(kg °C)	at 200°C
Cp (water vapour) =	1.959	kJ/(kg °C)	at 230°C
T_{ref} =	0	°C	
λ =	2500	kJ kg^{-1}	

Table B.12 –Inlet air temperatures, outlet air temperatures, absolute humidities and water flowrates used to calculate heat balances.

Run	$T_{hot\ air}$ (K)	$T_{d\ out}$ (K)	Y_1(kg H2O/kg air)	Y_o (kg H2O/kg air)	m_w (kg/s)
1	294.90	296.60	0.0110	0.0115	0.00E+00
2	441.40	326.37	0.0110	0.0315	3.85E-04
3	470.66	333.96	0.0105	0.0300	4.40E-04
4	506.09	342.73	0.0090	0.0325	5.10E-04
5	507.12	340.97	0.0095	0.0300	4.40E-04
6	507.12	337.47	0.0090	0.0315	5.10E-04

Table B.13 – Calculated enthalpies over spray dryer where water was sprayed.

Run	Heat In (Air) (kW)	Heat In (H_2O) (kW)	Heat In (Comp. air) (kW)	Heat In (kW)	Heat Out (kW)	Heat Losses (kW)
1	0.79	0.00E+00	0.019	0.81	0.84	0.03
2	3.20	3.31E-02	0.019	3.26	2.14	-1.12
3	3.66	3.96E-02	0.019	3.72	2.21	-1.52
4	4.20	4.72E-02	0.018	4.26	2.46	-1.81
5	4.24	3.98E-02	0.018	4.30	2.32	-1.97
6	4.22	4.62E-02	0.018	4.28	2.33	-1.95

Table B.14 – Summary of heat balances where water was sprayed.

Run	Heat In (kW)	Heat Out (kW)	Heat Loss (kW)
1	0.808	0.84	0.03
2	3.256	2.14	-1.12
3	3.721	2.21	-1.52
4	4.264	2.46	-1.81
5	4.298	2.32	-1.97
6	4.280	2.33	-1.95

Appendix C

C1. Skim Milk Powder Wall Deposition Fluxes and Moisture Content of Particles

Table C.1 – Wall deposition fluxes and moisture contents of skim milk powder, where the swirl vane angle was varied and a single feed flowrate (1.8 kg hr^{-1}), inlet air temperature (230°C), and compressed air pressure (200 kPa) was used.

Run	Swirl vane angle	Plate 5 deposit (g)	Plate 6 deposit (g)	Plate 5 flux (g m^{-2} hr^{-1})	Plate 6 flux (g m^{-2} hr^{-1})	Average flux (g m^2 hr^{-1})	Flux uncertainty (g m^2 hr^{-1})	Moisture content (%dry)	Deviation of moisture content from mean
1	0°	0.10	no plate 6	7.58	-	7.6	0.2	3.7	-0.4
2	0°	0.09	no plate 6	6.44	-	6.4	1.0	3.1	0.2
3	0°	0.11	no plate 6	8.18	-	8.2	0.8	3.1	0.2
4	25°	0.12	no plate 6	9.32	-	9.3	0.1	2.6	0.5
5	25°	0.11	no plate 6	8.48	-	8.5	0.7	3.4	-0.3
6	25°	0.13	no plate 6	9.85	-	9.8	0.6	3.3	-0.2
7	30°	0.15	0.13	11.52	10.92	11.2	0.3	3.0	0.2
8	30°	0.20	0.19	15.15	16.08	15.6	0.5	3.3	-0.1
9	30°	0.16	0.15	11.74	12.25	12.0	0.3	3.3	-0.1

Table C.2 – Average wall deposition fluxes and moisture contents of skim milk powder for different swirl vane angle (obtained from data in Table C.1).

Swirl vane angle	Average deposition flux (g m^2 hr^{-1})	Uncertainty (g m^2 hr^{-1})	Moisure content (kg kg^{-1})	Uncertainty (kg kg^{-1})
0	7.4	0.6	0.033	0.002
25	9.2	0.4	0.031	0.003
30	12.9	0.3	0.032	0.001

Table C.3 – Wall deposition fluxes and moisture contents of skim milk powder, where the inlet air temperature was varied and a single feed flowrate (1.8 kg hr^{-1}), swirl vane angle (0°), and compressed air pressure (200 kPa) was used.

Run	Inlet Air T (°C)	Plate 5 deposit (g)	Plate 6 deposit (g)	Plate 5 flux (g m^{-2} hr^{-1})	Plate 6 flux (g m^{-2} hr^{-1})	Average flux (g m^2 hr^{-1})	Flux uncertainty (g m^2 hr^{-1})	Moisture content (%dry)	Deviation of moisture content from mean
10	170	0.17	0.22	12.9	18.3	15.6	2.7	6.80	-0.9
11	170	0.18	0.21	13.6	17.5	15.6	1.9	5.50	0.4
12	170	0.17	0.20	12.9	16.7	14.8	1.9	5.50	0.4
13	200	0.11	0.13	8.3	10.8	9.6	1.3	4.35	-0.05
14	200	0.15	0.17	11.4	14.2	12.8	1.4	4.34	-0.04
15	200	0.12	0.15	9.1	12.5	10.8	1.7	4.20	0.10

Table C.4 – Average wall deposition fluxes and moisture contents of skim milk powder for different inlet air temperatures (obtained from data in Table C.3).

Inlet air temp (°C)	Average deposition flux (g m^2 hr^{-1})	Uncertainty (g m^2 hr^{-1})	Moisure content (kg kg^{-1})	Uncertainty (kg kg^{-1})
170	15.3	1.6	0.059	0.005
200	11.0	1.0	0.043	0.001
230	7.4	1.0	0.032	0.001

Table C.5 – Wall deposition fluxes and moisture contents of skim milk powder, where the feed flowrate was varied and a single inlet air temperature (230°C), swirl vane angle (0°), and compressed air pressure (200 kPa) was used.

Run	Feed flowrate (kg/hr)	Plate 5 deposit (g)	Plate 6 deposit (g)	Plate 5 flux ($g\ m^{-2}\ hr^{-1}$)	Plate 6 flux ($g\ m^{-2}\ hr^{-1}$)	Average flux ($g\ m^{2}\ hr^{-1}$)	Flux uncertainty ($g\ m^{2}\ hr^{-1}$)	Moisture content (%dry)	Deviation of moisture content from mean
16	1.58	0.073	0.086	5.530	7.167	6.35	0.82	3.30	-0.3
17	1.58	0.072	0.068	5.455	5.667	5.56	0.11	2.93	0.1
18	1.58	0.079	0.068	5.985	5.667	5.83	0.16	2.63	0.4
19	1.39	0.053	0.043	4.015	3.583	3.80	0.22	2.46	0.24
20	1.39	0.065	0.054	4.924	4.500	4.71	0.21	2.68	0.02
21	1.39	0.056	0.020	4.242	1.667	2.95	1.29	2.94	-0.24

Table C.6 – Average wall deposition fluxes and moisture contents of skim milk powder for different feed flowrates (obtained from Table C.5).

Feed flowrate ($kg\ hr^{-1}$)	Average deposition flux ($g\ m^{2}\ hr^{-1}$)	Uncertainty ($g\ m^{2}\ hr^{-1}$)	Moisure content ($kg\ kg^{-1}$)	Uncertainty ($kg\ kg^{-1}$)
1.39	3.8	0.7	0.027	0.001
1.58	5.9	0.5	0.030	0.002
1.84	7.4	1.0	0.032	0.001

Table C.7 – Wall deposition fluxes and moisture contents of skim milk powder, where spray dryer was grounded and a single inlet air temperature (170°C), feed flowrate (1.8 kg hr^{-1}), swirl vane angle (0°) and compressed air pressure (200 kPa) were used.

Run	Plate 5 deposit (g)	Plate 6 deposit (g)	Plate 5 flux ($g\ m^{-2}\ hr^{-1}$)	Plate 6 flux ($g\ m^{-2}\ hr^{-1}$)	Average flux ($g\ m^{-2}\ hr^{-1}$)	Flux uncertainty ($g\ m^{-2}\ hr^{-1}$)	Moisture content (%dry)
22	0.166	0.184	12.6	15.3	14.0	-1.4	6.67
23	0.144	0.189	10.9	15.8	13.3	-2.4	7.49
24	0.211	0.194	16.0	16.2	16.1	-0.1	7.33
25	0.162	0.18	12.3	15.0	13.6	-1.4	5.06

Table C.8 – Average wall deposition fluxes of skim milk powder, where spray dryer was grounded (obtained from Table C.7).

Ave. deposition flux ($g\ m^2\ hr^{-1}$)	Uncertainty ($g\ m^2\ hr^{-1}$)
14.2	1.2

Table C.9 – Wall deposition fluxes ($g\ m^{-2}$) of skim milk powder, where adhesive was placed on plates 5 and 6, and a single inlet air temperature (170°C), feed flowrate ($1.8\ kg\ hr^{-1}$), swirl vane angle (0°) and compressed air pressure (200 kPa) were used..

Run	Time (hr)	No adhesive					
		Plate 5 deposit (g)	Plate 6 deposit (g)	Plate 5 flux ($g\ m^{-2}$)	Plate 6 flux ($g\ m^{-2}$)	Average flux ($g\ m^{-2}$)	Uncertainty in flux ($g\ m^{-2}$)
27	0.5	0.103	0.135	7.8	11.3	9.5	-1.7
28	1	0.191	0.218	14.5	18.2	16.3	-1.8
29	2	0.476	0.439	36.1	36.6	36.3	-0.3

Table C.10 – Wall deposition fluxes ($g\ m^{-2}$) of skim milk powder, where no adhesive was placed on plates 5 and 6 (obtained from Table C.9).

Run	Time (hr)	Adhesive					
		Plate 5 deposit (g)	Plate 6 deposit (g)	Plate 5 flux ($g\ m^{-2}$)	Plate 6 flux ($g\ m^{-2}$)	Average flux ($g\ m^{-2}$)	Uncertainty in flux ($g\ m^{-2}$)
26	0.5	0.084	0.141	6.4	11.8	9.1	-2.7
30	1	0.165	0.207	12.5	17.3	14.9	-2.4
31	2	0.544	0.561	41.2	46.8	44.0	-2.8

Table C.11 – Comparison of wall deposition fluxes of skim milk powder between run 32 (plate 5 and 6 were coated with food grade nylon) and run 1 (plates 5 and 6 had stainless steel surface). A single inlet air temperature (230°C), feed flowrate (1.8 kg hr^{-1}), swirl vane angle (0°) and compressed air pressure (200 kPa) were used..

Run	Plate 5 deposit (g)	Plate 6 deposit (g)	Plate 5 flux (g m^{-2} hr^{-1})	Plate 6 flux (g m^{-2} hr^{-1})	Average flux (g m^{-2} hr^{-1})	Flux uncertainty (g m^{-2} hr^{-1})	Moisture content (%dry)
1	0.06	0.07	4.17	5.50	4.8	0.7	5.5
32	0.055	0.066	4.92	4.5	4.7	0.2	2.7

Table C.12 – Wall deposition fluxes of skim milk powder on plates 1 to 4 after insulation was placed behind these plates. A single inlet air temperature (230°C), feed flowrate (1.8 kg hr^{-1}), swirl vane angle (0°) and compressed air pressure (200 kPa) were used..

Plate	Area of plate (m^2)	Deposit (g)	Flux (g m^{-2} hr^{-1})
1	0.0132	0.005	0.4
2	0.0128	0.009	0.7
3	0.0128	0.002	0.2
4	0.0125	0.006	0.5

Table C.13 – Wall deposition fluxes and moisture contents of skim milk powder when increasing the residence time of the particles inside the spray dryer by decreasing the air flowrate. A single inlet air temperature (230°C), feed flowrate (1.8 kg hr^{-1}), swirl vane angle (0°) and compressed air pressure (200 kPa) were used.

Run	Plate 5 deposit (g)	Plate 6 deposit (g)	Plate 5 flux (g m^{-2} hr^{-1})	Plate 6 flux (g m^{-2} hr^{-1})	Average flux (g m^{-2} hr^{-1})	Flux uncertainty (g m^{-2} hr^{-1})	Moisture content (%dry)
33	0.11	0.14	9.0	14.0	11.5	2.5	7.35
34	0.141	0.147	11.7	14.7	13.2	1.5	7.50

Table C.14 – Average wall deposition fluxes and moisture contents of skim milk powder when increasing the residence time of the particles inside the spray dryer by decreasing the air flowrate.

Ave. deposition flux (g m^2 hr^{-1})	Uncertainty (g m^2 hr^{-1})	Average Moisture content (% dry)	Uncertainty in moisture content (%)
12.3	1.8	7.43	0.05

Table C.15 – Deposits of skim milk powder (g) and wall deposition fluxes (g m-2 hr-1) for plates 1 to 4. "NR" means no measurement was made.

Run	Plate 1 deposit (g)	Plate 2 deposit (g)	Plate 3 deposit (g)	Plate 4 deposit (g)	Plate 1 flux ($g\ m^{-2}\ hr^{-1}$)	Plate 2 flux ($g\ m^{-2}\ hr^{-1}$)	Plate 3 flux ($g\ m^{-2}\ hr^{-1}$)	Plate 4 flux ($g\ m^{-2}\ hr^{-1}$)
1	0.000	0.003	0.001	0.015	0.00	0.23	0.08	1.14
2	0.001	0.003	0.002	0.015	0.08	0.23	0.15	1.14
3	0.000	0.001	0.000	0.003	0.00	0.08	0.00	0.23
4	0.001	0.003	0.000	0.005	0.08	0.23	0.00	0.38
5	0.002	0.001	0.000	0.010	0.15	0.08	0.00	0.76
6	0.000	0.002	0.000	0.002	0.00	0.15	0.00	0.15
7	0.000	0.000	0.002	0.009	0.00	0.00	0.15	0.68
8	0.000	0.001	0.000	0.013	0.00	0.08	0.00	0.98
9	0.000	0.000	0.002	0.013	0.00	0.00	0.15	0.98
10	0.001	0.002	0.003	0.014	0.08	0.15	0.23	1.06
11	0.000	0.002	0.002	0.010	0.00	0.15	0.15	0.76
12	0.001	0.002	0.003	0.009	0.08	0.15	0.23	0.68
13	0.000	0.002	0.003	0.010	0.00	0.15	0.23	0.76
14	0.000	0.002	0.002	0.012	0.00	0.15	0.15	0.91
15	0.000	0.002	0.002	0.012	0.00	0.15	0.15	0.91
16	0.000	0.000	0.000	0.005	0.00	0.00	0.00	0.38
17	0.000	0.000	0.000	0.004	0.00	0.00	0.00	0.30
18	0.000	0.000	0.000	0.003	0.00	0.00	0.00	0.23
19	0.000	0.001	0.001	0.003	0.00	0.08	0.08	0.23
20	0.000	0.000	0.001	0.004	0.00	0.00	0.08	0.30
21	0.007	0.000	0.000	0.002	0.53	0.00	0.00	0.15
22	0.002	0.003	0.005	0.017	0.15	0.23	0.38	1.29
23	0.001	0.002	0.002	0.017	0.08	0.15	0.15	1.29
24	0.001	0.004	0.003	0.013	0.08	0.30	0.23	0.98
25	0.001	0.001	0.001	0.009	0.08	0.08	0.08	0.68
26	NR	NR	NR	NR	NR	NR	NR	NR
27	0.001	0.000	0.000	0.004	0.08	0.00	0.00	0.30
28	0.000	0.002	0.001	0.010	0.00	0.15	0.08	0.76
29	0.005	0.011	0.005	0.026	0.38	0.83	0.38	1.97
30	NR	NR	NR	NR	NR	NR	NR	NR
31	NR	NR	NR	NR	NR	NR	NR	NR
32	0.005	0.009	0.002	0.006	0.38	0.68	0.15	0.45
33	NR	NR	NR	NR	NR	NR	NR	NR
34	NR	NR	NR	NR	NR	NR	NR	NR

Appendix C

C2 – Mass and Energy Balances – Spray Drying of Skim Milk

Table C.16 – Concentration of components in skim milk (Source – *Product Information on Dairy Farmers skim milk carton) and density of components in skim milk (Source - **Source - Pisecky (1997) p.23). The total solids content in skim milk is 8.8% (w/v).

Skim milk composition	Concentration* (g/100 mL)	Density** (kg m^{-3})
Protein	3.5	1390
Fat	0.1	940
Lactose	4.9	1520
Sodium	0.051	
Potassium	0.156	
Calcium	0.120	
Water	91.173	1000

Table C.17 – Concentration and density of skim milk powder components (calculated using data in Table C.16 and taking a moisture contents of 5% for skim milk powder). The density of the skim milk powder was calculated using equation 3-14 from Pisecky (1997), p.23 and was found to be 1421 kg m^{-3}.

Skim milk powder composition	Concentration of components (%)
Protein	39
Fat	1
Lactose	55
Sodium	negligible
Potassium	negligible
Calcium	negligible
Water	5

Table C.18 – Raw experimental data for runs where the swirl vane angle was varied and a single feed flowrate (1.8 kg hr^{-1}), inlet air temperature (230°C), and compressed air pressure (200 kPa) was used.

	Date done	4/9/01	4/9/01	6/9/01	6/9/01	12/9/01	13/9/01	8/10/01	9/10/01	9/10/01
Thermocouple (°C)	Run	1	2	3	4	5	6	7	8	9
Indicated reading	$T_{d\ in}$	24.58	24.58	24.58	24.58	24.02	25.14	25.14	24.58	24.58
"as above"	$T_{w\ in}$	16.29	16.85	17.98	17.98	19.10	18.00	18.54	17.98	16.85
"as above"	$T_{d\ out}$	69.44	69.44	70.00	70.00	68.33	70.56	68.89	68.89	69.44
"as above"	$T_{w\ out}$	37.70	37.70	40.98	40.98	38.80	39.34	37.70	38.80	38.80
"as above"	$T_{hot\ air}$	230.00	233.71	233.15	236.52	238.76	239.89	232.02	230.34	233.15
"as above"	T_{dryer}	55.93	56.20	60.45	60.45	57.63	57.63	57.62	56.50	55.37
"as above"	$T_{dryer\ exit}$	73.45	74.01	74.58	74.58	75.14	77.40	75.71	74.02	73.45
Mercury reading (°C)	T_{room}	21.20	21.20	21.40	21.40	22.10	22.90	22.00	22.20	22.30
Compressed air	P_{air} (psi)	30	30	30	30	30	30	30	30	30
Swirl vane angle	SV (°)	0	0	25	25	0	25	30	30	30
Skim milk flowrate	Q (kg hr^{-1})	1.84	1.84	1.84	1.84	1.84	1.84	1.84	1.84	1.84

Table C.19 – Adjusted thermocouple readings for Table C.18 above.

Thermocouple (°C)	Run	1	2	3	4	5	6	7	8	9
Indicated reading	$T_{d\ in}$	21.3	21.3	21.3	21.3	20.7	21.9	21.9	21.3	21.3
"as above"	$T_{w\ in}$	12.8	13.4	14.6	14.6	15.9	14.7	15.3	14.6	13.4
"as above"	$T_{d\ out}$	68.4	68.4	69.0	69.0	67.2	69.6	67.8	67.8	68.4
"as above"	$T_{w\ out}$	36.2	36.2	39.8	39.8	37.4	38.0	36.2	37.4	37.4
"as above"	$T_{hot\ air}$	231.4	235.2	234.6	238.1	240.4	241.6	233.5	231.8	234.6
"as above"	T_{dryer}	51.1	51.3	55.6	55.6	52.8	52.8	52.8	51.6	50.5
"as above"	$T_{dryer\ exit}$	69.5	70.0	70.6	70.6	71.2	73.5	71.8	70.1	69.5
Mercury reading (°C)	T_{room}	21.2	21.20	21.40	21.40	22.10	22.90	22.00	22.20	22.30

Table C.20 – Moisture content of skim milk powder (kg water/kg dry solid) for runs where the swirl vane angle was varied and a single feed flowrate (1.8 kg hr^{-1}), inlet air temperature (230°C), and compressed air pressure (200 kPa) was used.

Run	Swirl vane angle (°)	X_o (kg water/kg dry solid)
1	0	0.0373
2	0	0.0311
3	25	0.0257
4	25	0.0339
5	0	0.0313
6	25	0.0313
7	30	0.0295
8	30	0.0327
9	30	0.0329

Table C.21 – Water balances for runs where the swirl vane angle was varied and a single feed flowrate (1.8 kg hr^{-1}), inlet air temperature (230°C), and compressed air pressure (200 kPa) was used.

Run	1	2	3	4	5	6	7	8	9
Swirl vane angle (°)	0	0	25	25	0	25	30	30	30
Y_{in} (kg water/kg dry air)	0.006	0.0065	0.008	0.008	0.010	0.008	0.009	0.008	0.007
Y_{out} (kg water/kg dry air)	0.026	0.026	0.036	0.036	0.029	0.030	0.026	0.028	0.028
$M_{water\ in}$ (kg s^{-1})	5.05E-04	5.13E-04	5.37E-04	5.37E-04	5.61E-04	5.29E-04	5.45E-04	5.37E-04	5.13E-04
$M_{water\ in}$ (kg hr^{-1})	1.82	1.85	1.93	1.93	2.02	1.90	1.96	1.93	1.85
$M_{water\ out}$ (kg s^{-1})	4.05E-04	4.04E-04	5.70E-04	5.70E-04	4.60E-04	4.68E-04	4.04E-04	4.44E-04	4.44E-04
$M_{water\ out}$ (kg hr^{-1})	1.456	1.455	2.052	2.053	1.655	1.683	1.455	1.598	1.598
Difference (kg hr^{-1})	-0.362	-0.392	0.119	0.121	-0.363	-0.221	-0.506	-0.335	-0.249
Difference (%)	-20	-21	6	6	-18	-12	-26	-17	-13

Table C.22 – Data used for calculating heat balances when skim milk was spray dried, for all conditions unless otherwise specified. Heat capacity data taken from Perry's Chemical Engineers' Handbook, 7th Edition (1997), McGraw Hill, New York, unless otherwise stated in the Table.

Cp (water) =	4.185	kJ/(kg °C)	at 25°C
Cp (air) =	1.025	kJ/(kg °C)	at 25°C
Cp (air) =	1.015	kJ/(kg °C)	at 230°C
Cp (air) =	1.020	kJ/(kg °C)	at 200°C
Cp (air) =	1.015	kJ/(kg °C)	at 170°C
Cp (air) =	1.003	kJ/(kg °C)	at 60°C
Cp (comp. air) =	1.004	kJ/(kg °C)	at 20 psi, 25°C
Cp (comp. air) =	0.690	kJ/(kg °C)	at 40 psi, 25°C
Cp (water vapour) =	1.864	kJ/(kg °C)	at 25°C
Cp (water vapour) =	1.874	kJ/(kg °C)	at 60°C
Cp (water vapour) =	1.923	kJ/(kg °C)	at 170°C
Cp (water vapour) =	1.940	kJ/(kg °C)	at 200°C
Cp (water vapour) =	1.957	kJ/(kg °C)	at 230°C
Cp (milk solids)=	1.256	kJ/(kg °C)	Pisecky 1997 p.24
Solids flowrate (P1)=	3.40E-05	kg/s	
Liquid flowrate (P1)=	3.85E-04	kg/s	
Solids flowrate (P1.5)=	3.88E-05	kg/s	
Liquid flowrate (P1.5)=	4.40E-04	kg/s	
Solids flowrate (P2)=	4.50E-05	kg/s	
Liquid flowrate (P2)=	4.65E-04	kg/s	
Compressed air flow =	0.0004	kg/s	Delavan Manual
T_{ref}	0	°C	
λ =	2500	kJ/kg	

Table C.23 –Inlet air temperatures, outlet air temperatures, absolute humidities and water flowrates used to calculate heat balances for runs where the swirl vane angle was varied and a single feed flowrate (1.8 kg hr^{-1}), inlet air temperature (230°C), and compressed air pressure (200 kPa) was used.

Run	T air in (K)	T air out (K)	Y_{in} (kg water/kg air)	Y_{out} (kg water/kg air)
1	504.6	341.6	0.006	0.026
2	508.4	341.6	0.007	0.026
3	507.8	342.1	0.008	0.036
4	511.2	342.1	0.008	0.036
5	513.5	340.4	0.010	0.029
6	514.7	342.7	0.008	0.030
7	506.6	341.0	0.009	0.026
8	504.9	341.0	0.008	0.028
9	507.8	341.6	0.007	0.028

Table C.24 – Calculated enthalpies over spray dryer, and heat balances for runs where the swirl vane angle was varied and a single feed flowrate (1.8 kg hr^{-1}), inlet air temperature (230°C), and compressed air pressure (200 kPa) was used.

Run	Heat In (kW)	Heat Out (kW)	Heat Losses (kW)	Discrepancy (%)
1	4.50	2.20	-2.31	-51
2	4.59	2.20	-2.39	-52
3	4.66	2.63	-2.03	-44
4	4.71	2.63	-2.09	-44
5	4.86	2.30	-2.56	-53
6	4.80	2.39	-2.42	-50
7	4.70	2.19	-2.51	-53
8	4.63	2.27	-2.36	-51
9	4.63	2.28	-2.35	-51

Table C.25 – Raw experimental data for conditions where the inlet air temperature was varied and a single feed flowrate (1.8 kg hr^{-1}), swirl vane angle (0°), and compressed air pressure (200 kPa) was used.

	Date done	21/11/2001	22/11/2001	22/11/2001	22/11/2001	23/11/2001	23/11/2001
Thermocouple (°C)	Run	**10**	**11**	**12**	**13**	**14**	**15**
Indicated reading	$T_{d\,in}$	25.46	25.56	24.98	24.58	25.14	24.99
"as above"	$T_{w\,in}$	20.25	19.52	18.62	18.63	20.04	19.91
"as above"	$T_{d\,out}$	53.89	53.12	54.29	60.97	59.88	61.16
"as above"	$T_{w\,out}$	37.13	34.63	36.01	37.10	38.25	37.51
"as above"	$T_{hot\,air}$	169.85	169.45	170.06	198.72	198.06	198.19
"as above"	T_{dryer}	47.38	45.90	46.84	53.16	49.53	52.32
"as above"	$T_{dryer\,exit}$	55.50	54.94	55.10	63.84	62.15	63.06
Mercury reading (°C)	T_{room}	21.40	22.00	22.00	22.00	NR	NR
Compressed air	P_{air} (psi)	30	30	30	30	30	30
Swirl vane angle	SV (°)	0	0	0	0	0	0
Skim milk flowrate	Q (kg hr^{-1})	1.84	1.84	1.84	1.84	1.84	1.84

Table C.26 – Adjusted thermocouple readings for Table C.25 above.

Thermocouple (°C)	Run	**10**	**11**	**12**	**13**	**14**	**15**
Indicated reading	$T_{d\,in}$	22.2	22.3	21.7	21.3	21.9	21.7
"as above"	$T_{w\,in}$	17.1	16.3	15.3	15.4	16.9	16.7
"as above"	$T_{d\,out}$	52.1	51.2	52.5	59.5	58.4	59.7
"as above"	$T_{w\,out}$	35.6	32.9	34.4	35.5	36.8	36.0
"as above"	$T_{hot\,air}$	169.6	169.2	169.8	199.3	198.6	198.7
"as above"	T_{dryer}	42.4	40.9	41.9	48.3	44.6	47.4
"as above"	$T_{dryer\,exit}$	51.3	50.7	50.9	59.7	58.0	59.0
Mercury reading (°C)	T_{room}	21.40	22.00	22.00	22.00	NR	NR

Table C.27 – Moisture content of skim milk powder (kg water/kg dry solid) where the inlet air temperature was varied and a single feed flowrate (1.8 kg hr^{-1}), swirl vane angle (0°), and compressed air pressure (200 kPa) was used.

Run	T in (°C)	X_o (kg water/kg solids)
10	170	0.068
11	170	0.055
12	170	0.055
13	200	0.044
14	200	0.043
15	200	0.042

Table C.28 – Water balances for runs where the inlet air temperature was varied and a single feed flowrate (1.8 kg hr^{-1}), swirl vane angle (0°), and compressed air pressure (200 kPa) was used.

Run	10	11	12	13	14	15
T in (°C)	170	170	170	200	200	200
Y_{in} (kg water/kg dry air)	0.010	0.010	0.008	0.009	0.010	0.010
Y_{out} (kg water/kg dry air)	0.032	0.026	0.028	0.029	0.032	0.029
$M_{water\ in}$ (kg s^{-1})	5.69E-04	5.69E-04	5.37E-04	5.53E-04	5.69E-04	5.69E-04
$M_{water\ in}$ (kg hr^{-1})	2.05	2.05	1.93	1.99	2.05	2.05
$M_{water\ out}$ (kg s^{-1})	5.09E-04	4.13E-04	4.45E-04	4.60E-04	5.08E-04	4.52E-04
$M_{water\ out}$ (kg hr^{-1})	1.83	1.49	1.60	1.66	1.83	1.63
Difference (kg hr^{-1})	-0.216	-0.559	-0.332	-0.333	-0.220	-0.419
Difference (%)	-11	-27	-17	-17	-11	-20

Table C.29 - Inlet air temperatures, outlet air temperatures, absolute humidities and water flowrates used to calculate heat balances where the inlet air temperature was varied and a single feed flowrate (1.8 kg hr^{-1}), swirl vane angle (0°), and compressed air pressure (200 kPa) was used.

Run	T air in (K)	T air out (K)	Y_{in} (kg water/kg dry air)	Y_{out} (kg water/kg dry air)
10	442.78	325.21	0.010	0.032
11	442.37	324.40	0.010	0.026
12	443.00	325.63	0.008	0.028
13	472.43	332.65	0.009	0.029
14	471.75	331.50	0.010	0.032
15	471.89	332.85	0.010	0.029

Table C.30 - Calculated enthalpies over spray dryer, and heat balances for condition where the inlet air temperature was varied and a single feed flowrate (1.8 kg hr^{-1}), swirl vane angle (0°), and compressed air pressure (200 kPa) was used.

Run	Heat In (kW)	Heat Out (kW)	Heat Losses (kW)	Discrepancy (%)
10	3.23	2.14	-1.09	-34
11	3.22	1.88	-1.34	-42
12	3.14	1.99	-1.16	-37
13	3.68	2.15	-1.54	-42
14	3.72	2.25	-1.47	-40
15	3.72	2.15	-1.57	-42

Table C.31 – Raw experimental data for conditions where the feed flowrate was varied and a single inlet air temperature (230°C), swirl vane angle (0°), and compressed air pressure (200 kPa) was used.

	Date done	27/11/2001	28/11/2001	28/11/2001	28/11/2001	29/11/2001	29/11/2001
Thermocouple (°C)	Run	**16**	**17**	**18**	**19**	**20**	**21**
Indicated reading	$T_{d\,in}$	24.88	24.55	24.61	24.29	24.78	24.51
"as above"	$T_{w\,in}$	18.39	19.00	18.12	17.18	19.10	19.10
"as above"	$T_{d\,out}$	67.19	69.25	69.53	71.81	71.72	73.33
"as above"	$T_{w\,out}$	37.01	37.16	37.24	36.58	37.70	37.91
"as above"	$T_{hot\,air}$	233.00	231.13	230.45	230.46	233.55	233.64
"as above"	T_{dryer}	61.24	59.72	61.67	64.08	62.15	63.77
"as above"	$T_{dryer\,exit}$	74.39	73.78	76.02	79.45	77.56	79.59
Mercury reading (°C)	T_{room}	23.90	23.70	23.70	23.70	24.90	24.90
Compressed air	P_{air} (psi)	30	30	30	30	30	30
Swirl vane angle	Swirl vane angle (°)	0	0	0	0	0	0
Skim milk flowrate	Q_{water} (L/h)	1.58	1.58	1.58	1.39	1.39	1.39

Table C.32– Adjusted thermocouple readings for Table C.31 above.

Thermocouple (°C)	Run	**16**	**17**	**18**	**19**	**20**	**21**
Indicated reading	$T_{d\,in}$	21.6	21.2	21.3	21.0	21.5	21.2
"as above"	$T_{w\,in}$	15.1	15.8	14.8	13.8	15.9	15.9
"as above"	$T_{d\,out}$	66.0	68.2	68.5	70.9	70.8	72.5
"as above"	$T_{w\,out}$	35.5	35.6	35.7	35.0	36.2	36.4
"as above"	$T_{hot\,air}$	234.5	232.6	231.9	231.9	235.0	235.1
"as above"	T_{dryer}	56.4	54.9	56.9	59.3	57.3	59.0
"as above"	$T_{dryer\,exit}$	70.4	69.8	72.1	75.6	73.6	75.7
Mercury reading (°C)	T_{room}	23.90	23.70	23.70	23.70	24.90	24.90

Table C.33 – Moisture content of skim milk powder (kg water/kg dry solid) for runs where the feed flowrate was varied and a single inlet air temperature (230°C), swirl vane angle (0°), and compressed air pressure (200 kPa) was used.

Run	Feed flowrate (kg hr^{-1})	X_o (kg water/kg solids)
16	1.58	0.033
17	1.58	0.0293
18	1.58	0.0263
19	1.39	0.0246
20	1.39	0.0268
21	1.39	0.0294

Table C.34 - Water balances for runs where the inlet air temperature was varied and a single inlet air temperature (230°C), swirl vane angle (0°), and compressed air pressure (200 kPa) was used.

Run	16	17	18	19	20	21
Feed flowrate (kg hr^{-1})	1.6	1.6	1.6	1.4	1.4	1.4
Y_{in} (kg water/kg dry air)	0.008	0.010	0.009	0.009	0.010	0.010
Y_{out} (kg water/kg dry air)	0.024	0.026	0.026	0.021	0.024	0.024
$M_{water\ in}$ (kg s^{-1})	4.81E-04	5.12E-04	4.96E-04	4.52E-04	4.68E-04	4.68E-04
$M_{water\ in}$ (kg hr^{-1})	1.730	1.844	1.787	1.628	1.685	1.685
$M_{water\ out}$ (kg s^{-1})	3.80E-04	4.12E-04	4.12E-04	3.33E-04	3.80E-04	3.80E-04
$M_{water\ out}$ (kg hr^{-1})	1.370	1.483	1.483	1.197	1.368	1.369
Difference (kg hr^{-1})	-0.360	-0.361	-0.305	-0.430	-0.316	-0.316
Difference (%)	-21	-20	-17	-26	-19	-19

Table C.35 – The solid and liquid flowrates used for run where the feed flowrate was varied and a single inlet air temperature (230°C), swirl vane angle (0°), and compressed air pressure (200 kPa) was used.

Phase	Flowrate (kg s^{-1})
Solids (Runs 16-18)	3.88E-05
Liquid (Runs 16-18)	4.40E-04
Solids (Runs 19-21)	3.40E-05
Liquid (Runs 19-21)	3.85E-04

Table C.36 – Inlet air temperatures, outlet air temperatures, absolute humidities and water flowrates used to calculate heat balances where the feed flowrate was varied and a single inlet air temperature (230°C), swirl vane angle (0°), and compressed air pressure (200 kPa) was used.

Run	T air in (K)	T air out (K)	Y_{in} (kg water/kg dry air)	Y_{out} (kg water/kg dry air)
16	507.63	339.19	0.008	0.024
17	505.71	341.35	0.010	0.026
18	505.01	341.65	0.009	0.026
19	505.02	344.04	0.009	0.021
20	508.20	343.95	0.010	0.024
21	508.29	345.64	0.010	0.024

Table C.37 – Calculated enthalpies over spray dryer, and heat balances for condition where the feed flowrate was varied and a single inlet air temperature (230°C), swirl vane angle (0°), and compressed air pressure (200 kPa) was used.

Run	Heat In (kW)	Heat Out (kW)	Heat Losses (kW)	Discrepancy (%)
16	4.20	2.05	-2.15	-51
17	4.26	2.17	-2.10	-49
18	4.20	2.17	-2.03	-48
19	4.20	2.00	-2.19	-52
20	4.28	2.13	-2.15	-50
21	4.28	2.15	-2.13	-50

Table C.38 – Raw experimental data for runs where spray dryer was grounded and a single inlet air temperature (170°C), feed flowrate (1.8 kg hr^{-1}), swirl vane angle (0°) and compressed air pressure (200 kPa) were used.

	Date done	4/12/01	6/12/01	6/12/01	10/12/01
Thermocouple (°C)	Run	**22**	**23**	**24**	**25**
Indicated reading	$T_{d\,in}$	24.99	24.80	25.11	25.30
"as above"	$T_{w\,in}$	19.04	19.03	19.22	15.94
"as above"	$T_{d\,out}$	51.95	50.92	51.54	50.85
"as above"	$T_{w\,out}$	33.43	35.40	35.64	34.01
"as above"	$T_{hot\,air}$	170.00	170.22	170.10	170.04
"as above"	T_{dryer}	44.67	44.71	46.33	43.72
"as above"	$T_{dryer\,exit}$	54.86	50.63	51.07	50.90
Mercury reading (°C)	T_{room}	24.50	23.90	23.90	24.20
Compressed air	P_{air} (psi)	30	30	30	30
Swirl vane angle	SV (°)	0	0	0	0
Skim milk flowrate	Q (kg hr^{-1})	1.84	1.84	1.84	1.84

Table C.39 – Adjusted thermocouple temperature for Table C.38.

	Date done	4/12/01	6/12/01	6/12/01	10/12/01
Thermocouple (°C)	Run	**22**	**23**	**24**	**25**
Indicated reading	$T_{d\,in}$	21.70	21.50	21.82	22.03
"as above"	$T_{w\,in}$	15.80	15.79	16.00	12.42
"as above"	$T_{d\,out}$	50.02	48.93	49.59	48.86
"as above"	$T_{w\,out}$	31.55	33.70	33.96	32.18
"as above"	$T_{hot\,air}$	169.79	170.01	169.89	169.83
"as above"	T_{dryer}	39.69	39.73	41.36	38.73
"as above"	$T_{dryer\,exit}$	50.65	46.37	46.81	46.64
Mercury reading (°C)	T_{room}	24.50	23.90	23.90	24.20

Table C.40 – Moisture content of skim milk powder (kg water/kg dry solid) for runs where the spray dryer was grounded and a single inlet air temperature (170°C), feed flowrate (1.8 kg hr^{-1}), swirl vane angle (0°) and compressed air pressure (200 kPa) were used.

Run	X_o (kg water/kg solids)
22	0.07
23	0.079
24	0.077
25	0.054

Table C.41 - Water balances for runs where the spray dryer was grounded and a single inlet air temperature (170°C), feed flowrate (1.8 kg hr^{-1}), swirl vane angle (0°) and compressed air pressure (200 kPa) were used.

Run	22	23	24	25
Y_{in} (kg water/kg dry air)	0.009	0.009	0.009	0.006
Y_{out} (kg water/kg dry air)	0.024	0.028	0.028	0.024
$M_{water\ in}$ (kg s^{-1})	5.53E-04	5.53E-04	5.53E-04	4.97E-04
$M_{water\ in}$ (kg hr^{-1})	1.990	1.990	1.990	1.791
$M_{water\ out}$ (kg s^{-1})	3.82E-04	4.46E-04	4.46E-04	3.82E-04
$M_{water\ out}$ (kg hr^{-1})	1.376	1.605	1.605	1.374
Difference (kg hr^{-1})	-0.613	-0.384	-0.385	-0.417
Difference (%)	-31	-19	-19	-23

Table C.42 - Raw experimental data where adhesive was place on plates 5 and 6. A single inlet air temperature (170°C), feed flowrate (1.8 kg hr^{-1}), swirl vane angle (0°) and compressed air pressure (200 kPa) were used.

	Date done	10/12/01	13/12/2001	13/12/2001
Thermocouple (°C)	Run	**26**	**30**	**31**
Indicated reading	$T_{d\,in}$	25.02	24.73	24.80
"as above"	$T_{w\,in}$	19.14	19.55	20.51
"as above"	$T_{hot\,air}$	170.16	170.49	170.44
"as above"	$T_{d\,out}$	50.68	54.00	50.96
"as above"	$T_{w\,out}$	37.81	37.46	37.48
"as above"	T_{dryer}	45.51	45.35	41.34
"as above"	$T_{dryer\,exit}$	50.72	54.05	51.41
Mercury reading (°C)	T_{room}	NR	24.90	NR
Time	hour	1.00	0.50	2.00
Compressed air	P_{air} (psi)	30	30	30
Swirl vane angle	SV (°)	0	0	0
Skim milk flowrate	Q (kg hr^{-1})	1.8	1.8	1.8

Table C.43 – Adjusted thermocouple temperature for Table C.42.

	Date done	10/12/01	13/12/2001	13/12/2001
Thermocouple (°C)	Run	**26**	**30**	**31**
Indicated reading	$T_{d\,in}$	21.73	21.42	21.50
"as above"	$T_{w\,in}$	15.91	16.36	17.40
"as above"	$T_{hot\,air}$	169.95	170.29	170.24
"as above"	$T_{d\,out}$	48.68	52.17	48.98
"as above"	$T_{w\,out}$	36.32	35.94	35.96
"as above"	T_{dryer}	40.54	40.37	36.32
"as above"	$T_{dryer\,exit}$	46.46	49.83	47.16
Mercury reading (°C)	T_{room}	NR	24.90	24.90

Table C.44 - Raw experimental data where no adhesive was place on plates 5 and 6 and looking at the effect of time on wall deposition. A single inlet air temperature (170°C), feed flowrate (1.8 kg hr^{-1}), swirl vane angle (0°) and compressed air pressure (200 kPa) were used.

Thermocouple (°C)	Date done	12/12/01	12/12/01	12/12/01
Indicated reading	Run	**27**	**28**	**29**
"as above"	$T_{d\ in}$	25.38	25.06	25.25
"as above"	$T_{w\ in}$	19.14	18.85	18.94
"as above"	$T_{hot\ air}$	169.87	169.94	169.90
"as above"	$T_{d\ out}$	53.12	53.13	51.35
"as above"	$T_{w\ out}$	36.84	37.46	37.48
"as above"	T_{dryer}	46.12	45.48	43.31
"as above"	$T_{dryer\ exit}$	54.38	53.80	52.52
Mercury reading (°C)	T_{room}	23.70	NR	24.00
Time	hour	0.50	1.00	2.00
Compressed air	P_{air} (psi)	30	30	30
Swirl vane angle	SV (°)	0	0	0
Skim milk flowrate	Q (kg hr^{-1})	1.80	1.80	1.80

Table C.45 – Adjusted thermocouple readings for Table C.44.

	Date done	12/12/01	12/12/01	12/12/01
Thermocouple (°C)	Run	**26**	**30**	**31**
Indicated reading	$T_{d\ in}$	22.11	21.77	21.97
"as above"	$T_{w\ in}$	15.91	15.59	15.69
"as above"	$T_{hot\ air}$	169.65	169.73	169.68
"as above"	$T_{d\ out}$	51.25	51.26	49.39
"as above"	$T_{w\ out}$	35.27	35.94	35.96
"as above"	T_{dryer}	41.15	40.51	38.31
"as above"	$T_{dryer\ exit}$	50.16	49.58	48.28
Mercury reading (°C)	T_{room}	NR	24.90	24.90

Table C.46 – Raw experimental data where plates 5 and 6 were coated with nylon and insulation was placed behind plates 1 – 4. A single inlet air temperature (230°C), feed flowrate (1.8 kg hr^{-1}), swirl vane angle (0°) and compressed air pressure (200 kPa) were used.

Thermocouple (°C)	Date done	20-2-02
Indicated reading	Run	32
"as above"	$T_{d\ in}$	24.25
"as above"	$T_{w\ in}$	20.28
"as above"	$T_{hot\ air}$	231.38
"as above"	$T_{d\ out}$	73.61
"as above"	$T_{w\ out}$	37.49
"as above"	T_{dryer}	58.35
"as above"	$T_{dryer\ exit}$	75.22
Mercury reading (°C)	T_{room}	26.40
Time	hour	1.00
Compressed air	P_{air} (psi)	30
Swirl vane angle	SV (°)	0
Skim milk flowrate	Q (kg hr^{-1})	1.39

Table C.47 – Adjusted thermocouple readings for Table C.46.

	Date done	20-2-02
Thermocouple (°C)	Run	32
Indicated reading	$T_{d\ in}$	20.91
"as above"	$T_{w\ in}$	17.15
"as above"	$T_{hot\ air}$	232.82
"as above"	$T_{d\ out}$	72.78
"as above"	$T_{w\ out}$	35.97
"as above"	T_{dryer}	53.51
"as above"	$T_{dryer\ exit}$	71.27
Mercury reading (°C)	T_{room}	NR

Table C.48 – Raw experimental data when increasing the residence time of the particles inside the spray dryer by decreasing the air flowrate. A single inlet air temperature (230°C), feed flowrate (1.8 kg hr^{-1}), swirl vane angle (0°) and compressed air pressure (200 kPa) were used.

Thermocouple (°C)	Date done	15/2/02	1/3/02
Indicated reading	Run	**33**	**34**
"as above"	$T_{d\ in}$	25.01	24.43
"as above"	$T_{w\ in}$	18.89	17.57
"as above"	$T_{hot\ air}$	248.31	255.43
"as above"	$T_{d\ out}$	55.6	59.35
"as above"	$T_{w\ out}$	38.84	39.42
"as above"	T_{dryer}	65.93	60.36
"as above"	$T_{dryer\ exit}$	58.15	66.73
Mercury reading (°C)	T_{room}	25.8	25.40
Compressed air	P_{air} (psi)	30	30
Swirl vane angle	SV (°)	0	0
Skim milk flowrate	Q (kg hr^{-1})	1.8	1.8

Table C.49 – Adjusted thermocouple readings for Table C.48.

	Date done	15/2/02	1/3/02
Thermocouple (°C)	Run	**33**	**34**
Indicated reading	$T_{d\ in}$	21.72	21.10
"as above"	$T_{w\ in}$	15.64	14.20
"as above"	$T_{hot\ air}$	250.20	257.52
"as above"	$T_{d\ out}$	53.85	57.80
"as above"	$T_{w\ out}$	37.45	38.08
"as above"	T_{dryer}	61.16	55.54
"as above"	$T_{dryer\ exit}$	53.98	62.67
"as above"	T_{room}	25.8	25.40
Mercury reading (°C)	NR	25.8	25.4

Table C.50 – Moisture content of skim milk powder (kg water/kg dry solid) for runs where adhesive was placed on plates 5 and 6. A single inlet air temperature (170°C), feed flowrate (1.8 kg hr^{-1}), swirl vane angle (0°) and compressed air pressure (200 kPa) were used.

Run	X_o (kg water/kg solids)
26	0.044
30	0.044
31	0.070

Table C.51 - Water balances for runs where adhesive was placed on plates 5 and 6. A single inlet air temperature (170°C), feed flowrate (1.8 kg hr^{-1}), swirl vane angle (0°) and compressed air pressure (200 kPa) were used.

Run	26	30	31
Y_{in} (kg water/kg dry air)	0.01	0.01	0.011
Y_{out} (kg water/kg dry air)	0.034	0.032	0.033
$M_{water\ in}$ (kg s^{-1})	5.69E-04	5.69E-04	5.84E-04
$M_{water\ in}$ (kg hr^{-1})	2.047	2.047	2.104
$M_{water\ out}$ (kg s^{-1})	5.39E-04	5.08E-04	5.25E-04
$M_{water\ out}$ (kg hr^{-1})	1.941	1.827	1.888
Difference (kg hr^{-1})	-0.106	-0.220	-0.215
Difference (%)	-5	-11	-10

Table C.52 – Moisture content of skim milk powder (kg water/kg dry solid) for runs where no adhesive was place on plates 5 and 6 and looking at the effect of time on wall deposition. A single inlet air temperature (170°C), feed flowrate (1.8 kg hr^{-1}), swirl vane angle (0°) and compressed air pressure (200 kPa) were used.

Run	X_o (kg water/kg solids)
27	0.072
28	0.0655
29	0.066

Table C.53 - Water balances for runs where no adhesive was placed on plates 5 and 6 and the effect of time on wall deposition was studied. A single inlet air temperature (170°C), feed flowrate (1.8 kg hr^{-1}), swirl vane angle (0°) and compressed air pressure (200 kPa) were used.

Run	27	28	29
Y_{in} (kg water/kg dry air)	0.009	0.009	0.0090
Y_{out} (kg water/kg dry air)	0.030	0.033	0.034
$M_{water\ in}$ (kg s^{-1})	5.53E-04	5.53E-04	5.53E-04
$M_{water\ in}$ (kg hr^{-1})	1.990	1.990	1.990
$M_{water\ out}$ (kg s^{-1})	4.77E-04	5.24E-04	5.40E-04
$M_{water\ out}$ (kg hr^{-1})	1.72E+00	1.89E+00	1.94E+00
Difference (kg hr^{-1})	-0.272	-0.102	-0.045
Difference (%)	-14	-5	-2

Table C.54 – Moisture content of skim milk powder (kg water/kg dry solid) for run where plates 5 and 6 were coated with nylon and insulation was placed behind plates 1 – 4. A single inlet air temperature (230°C), feed flowrate (1.8 kg hr^{-1}), swirl vane angle (0°) and compressed air pressure (200 kPa) were used.

Run	X_o (kg water/kg solids)
32	0.027

Table C.55 –Water balances for run where plates 5 and 6 were coated with nylon and insulation was placed behind plates 1-4 (run 32). A single inlet air temperature (230°C), feed flowrate (1.8 kg hr^{-1}), swirl vane angle (0°) and compressed air pressure (200 kPa) were used.

Run	32
Y_{in} (kg water/kg dry air)	0.011
Y_{out} (kg water/kg dry air)	0.023
$M_{water\ in}$ (kg s^{-1})	5.84E-04
$M_{water\ in}$ (kg hr^{-1})	2.104
$M_{water\ out}$ (kg s^{-1})	3.65E-04
$M_{water\ out}$ (kg hr^{-1})	1.31
Difference (kg hr^{-1})	-0.791
Difference (%)	-38

Table C.56 – Moisture content of skim milk powder (kg water/kg dry solid) for runs where the residence time of the particles inside the spray dryer was increased by decreasing the air flowrate. A single inlet air temperature (230°C), feed flowrate (1.8 kg hr^{-1}), swirl vane angle (0°) and compressed air pressure (200 kPa) were used.
air flowrate was reduced (runs 33-34).

Run	X_o (kg water/kg solids)
33	0.074
34	0.075

Table C.57 – Water balances for runs where the residence time of the particles inside the spray dryer was increased by decreasing the air flowrate. A single inlet air temperature (230°C), feed flowrate (1.8 kg hr^{-1}), swirl vane angle (0°) and compressed air pressure (200 kPa) were used.
air flowrate was reduced (runs 33-34).

Run	33	34
Y_{in} (kg water/kg dry air)	0.0115	0.0115
Y_{out} (kg water/kg dry air)	0.034	0.035
$M_{water\ in}$ (kg s^{-1})	5.92E-04	5.92E-04
$M_{water\ in}$ (kg hr^{-1})	2.132	2.132
$M_{water\ out}$ (kg s^{-1})	5.33E-04	5.53E-04
$M_{water\ out}$ (kg hr^{-1})	1.92E+00	1.99E+00
Difference (kg hr^{-1})	-0.215	-0.141
Difference (%)	-10	-7

Table C.58 – Inlet air temperatures, outlet air temperatures, absolute humidities and water flowrates used to calculate heat balances for runs 22-34 .

Run	T air in (K)	T air out (K)	Y_{in} (kg water/kg dry air)	Y_{out} (kg water/kg dry air)
Grounding runs				
22	442.94	323.17	0.009	0.024
23	443.16	322.08	0.009	0.028
24	443.04	322.74	0.009	0.028
25	442.98	322.01	0.0055	0.024
Adhesive runs				
26	443.10	321.83	0.010	0.034
30	443.44	325.32	0.010	0.032
31	443.39	322.13	0.011	0.033
Non adhesive runs				
27	442.80	324.40	0.009	0.03
28	442.88	324.41	0.009	0.033
29	442.83	322.54	0.009	0.034
Nylon plates runs				
32	505.97	345.93	0.011	0.023
Studying kinetics runs				
33	523.35	327.00	0.0115	0.0335
34	530.67	330.95	0.0115	0.035

Table C.59 – Energy balance results for runs 22-34.

Run	Heat In (kW)	Heat out (kW)	Heat Losses (kW)	Discrepancy (%)
Grounding runs				
22	3.19	1.78	-1.41	-44
23	3.20	1.93	-1.27	-40
24	3.19	1.94	-1.26	-39
25	3.03	1.76	-1.27	-42
Adhesive runs				
26	3.24	2.17	-1.07	-33
30	3.25	2.15	-1.10	-34
31	3.29	2.13	-1.16	-35
Non adhesive runs				
27	3.19	2.05	-1.14	-36
28	3.19	2.17	-1.02	-32
29	3.19	2.18	-1.01	-32
Nylon plates runs				
32	4.32	2.12	-2.20	-51
Studying kinetics runs				
33	4.63	2.24	-2.39	-52
34	4.75	2.36	-2.38	-50

Appendix C

C3. Statistical Analysis of the Difference in the Wall Deposition Fluxes and Moisture Contents of Skim Milk Powder Obtained for Different Operating Conditions (From Chapter 5).

C.3.1 –Swirl Vane Angle 0° and 30°.

Wall Deposition Fluxes

The null hypothesis that there is no difference between the wall deposition fluxes of skim milk powder when the swirl vane angles are 0° and 30° can be tested as follows. The mean and the variance of the two samples is $\overline{x_1}$ =7.4 g m^{-2} hr^{-1}, $\overline{x_2}$ = 12.9 g m^{-2} hr^{-1}, s_1=0.6 g m^{-2} hr^{-1}, and s_2 = 0.3 g m^{-2} hr^{-1}, respectively. n_1=3 and n_2=3, so there are 4 degrees of freedom. The null hypothesis can be rejected with 99.5% confidence if $t < -4.604$ or $t \geq 4.604$, where 4.604 is the value of t at 0.005 level of significance ($t_{0.005}$, 4). t is calculated by using equation 5.1 (Chapter 5) to be –14.2. Thus, the null hypothesis can be rejected with 99.5% confidence and we can conclude that the difference between the wall deposition fluxes for a swirl vane angle of 0° and 30° is significant.

The null hypothesis that there is no difference between the wall deposition fluxes of skim milk powder when the swirl vane angles are 25° and 30° can be tested as follows. The mean and the variance of the two samples is $\overline{x_1}$ =9.2 g m^{-2} hr^{-1}, $\overline{x_2}$ = 12.9 g m^{-2} hr^{-1}, s_1=0.4 g m^{-2} hr^{-1}, and s_2 = 0.3 g m^{-2} hr^{-1}, respectively. n_1=3 and n_2=3, so there are 4 degrees of freedom. The null hypothesis can be rejected with 99.5% confidence if $t < -4.604$ or $t \geq 4.604$, where 4.604 is the value of t at 0.005 level of significance ($t_{0.005}$, 4). t is calculated by using equation 5.1 (Chapter 5) to be –12.8. Thus, the null hypothesis can be rejected with 99.5% confidence and we can conclude that the difference between the wall deposition fluxes for a swirl vane angle of 25° and 30° is significant.

C.3.2 – Inlet Air Temperatures 170°C and 200°C.

Wall Deposition Fluxes

The null hypothesis that there is no difference between the wall deposition fluxes of the skim milk powder when the inlet air temperatures are 170°C and 200°C, can be tested as follows. The mean and the variance of the two samples is $\overline{x_1}$ = 15.3 g m^{-2} hr^{-1}, $\overline{x_2}$ = 11.0 g m^{-2} hr^{-1}, s_1 =1.6 g m^{-2} hr^{-1} and s_2 = 1.0 g m^{-2} hr^{-1}, respectively. n_1=3 and n_2=3, so there are 4 degrees of freedom. The null hypothesis can be rejected with 99% confidence if $t < -3.747$ or $t \geq 3.747$, where 3.747 is the value of t at 0.01 level of significance ($t_{0.01}$, 4). t is calculated by using equation 5.1 (Chapter 5) to be 3.9. Thus, the null hypothesis can be rejected with 99% confidence and we can conclude that the difference between the wall deposition fluxes for inlet air temperatures of 170°C and 200°C is significant.

Moisture Contents

The null hypothesis that there is no difference between the moisture content of the particles when the inlet air temperatures are 170°C and 200°C can be tested as follows. The mean and the variance of the two samples is $\overline{x_1}$ = 5.9 g m^{-2} hr^{-1}, $\overline{x_2}$ = 4.3 g m^{-2} hr^{-1}, s_1 =0.5 g m^{-2} hr^{-1} and s_2 = 0.1 g m^{-2} hr^{-1}, respectively. n_1=3 and n_2=3, so there are 4 degrees of freedom. The null hypothesis can be rejected with 99% confidence if $t < -4.604$ or $t \geq 4.604$, where 4.604 is the value of t at 0.005 level of significance ($t_{0.005}$, 4). t is calculated by using equation 5.1 to be 5.4. Thus, the null hypothesis can be rejected with 99.5% confidence and we can conclude that the difference between the moisture contents of skim milk powder for inlet air temperatures of 170°C and 200°C is significant.

C.3.3 – Inlet Air Temperatures 200°C and 230°C

Wall Deposition Fluxes

The null hypothesis that there is no difference between the wall deposition fluxes of the skim milk powder when the inlet air temperatures are 200°C and 230°C, can be tested as follows. The mean and the variance of the two samples is $\overline{x_1}$ = 11.0 g m^{-2} hr^{-1}, $\overline{x_2}$ = 7.4 g m^{-2} hr^{-1}, s_1 =1.0 g m^{-2} hr^{-1}and s_2 = 1.0 g m^{-2} hr^{-1}, respectively. n_1=3 and n_2=3, so there are 4 degrees of freedom. The null hypothesis can be rejected with 99% confidence if $t < -3.747$ or $t \geq 3.747$, where 3.747 is the value of t at 0.01 level of significance ($t_{0.01}$, 4). t is calculated by using equation 5.1 to be 4.4. Thus, the null hypothesis can be rejected with 99% confidence and we can conclude that the difference between the wall deposition fluxes for inlet air temperatures of 200°C and 230°C is significant.

Moisture Contents

The null hypothesis that there is no difference between the moisture content of the particles when the inlet air temperatures are 200°C and 230°C can be tested as follows.The mean and the variance of the two samples is $\overline{x_1}$ = 5.9 g m^{-2} hr^{-1}, $\overline{x_2}$ = 4.3 g m^{-2} hr^{-1}, s_1 =0.5 g m^{-2} hr^{-1}and s_2 = 0.1 g m^{-2} hr^{-1}, respectively. n_1=3 and n_2=3, so there are 4 degrees of freedom. The null hypothesis can be rejected with 99% confidence if $t < -4.604$ or $t \geq 4.604$, where 4.604 is the value of t at 0.005 level of significance ($t_{0.005}$, 4). t is calculated by using equation 5.1 to be 4.4. Thus, the null hypothesis can be rejected with 99.5% confidence and we can conclude that the difference between the moisture contents of skim milk powder for inlet air temperatures of 200°C and 230°C is significant.

C.3.4 – Feed Flowrate 1.6 kg hr^{-1} and 1.8 kg hr^{-1}

Wall Deposition Fluxes

The null hypothesis that there is no difference between the wall deposition fluxes when the feed flowrates are 1.6 kg hr^{-1} and 1.8 kg hr^{-1} can be tested as follows. The mean and the variance of the two samples is $\overline{x_1}$ = 5.9 g m^{-2} hr^{-1},$\overline{x_2}$ =7.4 g m^{-2} hr^{-1}, s_1 =0.5 g m^{-2} hr^{-1}

and s_2=1.0 g m^{-2} hr^{-1}, and, respectively. n_1=3 and n_2=3, so there are 4 degrees of freedom. The null hypothesis can be rejected with 95% confidence if $t < -2.312$ or $t \geq 2.132$, where 2.132 is the value of t at 0.05 level of significance ($t_{0.05}$, 4). t is calculated by using equation 5.1 to be -2.3. Thus, the null hypothesis can be rejected with 95% confidence and we can conclude that the difference between the wall deposition fluxes for feed flowrates of 1.6 kg hr^{-1} and 1.8 kg hr^{-1} is significant.

Moisture Contents

The null hypothesis that there is no difference between the moisture contents of the skim milk powder samples when the feed flowrates are 1.6 kg hr^{-1} and 1.8 kg h^{-1} can be tested as follows. The mean and the variance of the two samples is $\overline{x_1}$=3.0%, $\overline{x_2}$ = 3.2%, s_1=0.5%, and s_2=1.0%, respectively. n_1=3 and n_2=3, so there are 4 degrees of freedom. t is found to be - 0.31. However, we can reject the null hypothesis with 60% level of confidence since $t_{0.40,4}$ (Montgomery, 1991) = 0.271.

C.3.4 – Feed Flowrate 1.4 kg hr^{-1} and 1.6 kg hr^{-1}

Wall Deposition Fluxes

The null hypothesis that there is no difference between the wall deposition fluxes when the feed flowrates are 1.6 kg hr^{-1} and 1.4 kg hr^{-1} can be tested as follows. The mean and the variance of the two samples is $\overline{x_1}$ = 5.9 g m^{-2} hr^{-1}, $\overline{x_2}$ = 3.8 g m^{-2} hr^{-1}, s_1=0.5 g m^{-2} hr^{-1}, and s_2= 0.7 g m^{-2} h^{-1}, respectively. n_1=3, n_2=3, so there are 4 degrees of freedom. The null hypothesis can be rejected with 99% confidence if $t < -3.747$ or $t \geq 3.747$, where3.747 is the value of t at 0.01 level of significance ($t_{0.01,4}$). t is calculated by using equation 5.1 to be 4.2. Thus, the null hypothesis can be rejected with 99% confidence and we can conclude that the difference between the wall deposition rate at feed flowrates of 1.4 kg hr^{-1} and 1.6 kg hr^{-1} is significant.

Moisture Contents

The null hypothesis that there is no difference between the moisture contents of the skim milk powder samples when the feed flowrates are 1.6 kg hr^{-1} and 1.4 kg hr^{-1} can be tested as follows.

The mean and the variance of the two samples is $\overline{x_1}$ = 3.0%, $\overline{x_2}$ = 2.7%, s_1=0.2%, and s_2 = 0.1%, respectively. n_1= 3, n_2= 3, so there are 4 degrees of freedom. The null hypothesis can be rejected with 95% confidence if $t < -2.132$ or $t \geq 2.132$, where 2.132 is the value of t at 0.05 level of significance ($t_{0.05,}$ 6). t is calculated by using equation 5.1 to be 2.3. Thus, the null hypothesis cannot be rejected and we can conclude that the difference between the moisture contents of particles when feed flowrates of 1.4 kg hr^{-1} and 1.6 kg hr^{-1} is significant.

C.3.4 –Grounding the Spray Dryer

Wall Deposition Fluxes

The null hypothesis that there is no difference between the wall deposition fluxes of the skim milk powder when the spray dryer was grounded and when it was not grounded, can be tested as follows. The mean and the variance of the two samples is $\overline{x_1}$ = 14.2 g m^{-2} hr^{-1}, $\overline{x_2}$ = 15.3 g m^{-2} hr^{-1}, s_1=1.2 g m^{-2} hr^{-1}, and s_2=1.6 g m^{-2} hr^{-1} respectively. n_1=4, n_2=3, so we have 5 degrees of freedom. The null hypothesis can be rejected with 75% confidence if $t < -0.727$ or $t \geq 0.727$, where 0.727 is the value of t at 0.25 level of significance ($t_{0.25,5}$). t is calculated by using equation 4.1 to be -1. The null hypothesis can be rejected with 75% confidence. Thus, it can conclude that the difference between the wall deposition fluxes for a grounded spray dryer and a non-grounded spray dryer is only slightly significant.

Appendix C

C4. Iterations for Linking Operating Points with Sticky-Point Curve for Skim Milk Powder

Table C.60 - Case 1, where inlet air temperature 170°C, feed flowrate 1.8 kg hr^{-1}, swirl vane angle 0° and compressed air pressure 200 kPa. (Data taken from Run 10)

Finding absolute air humidity leaving dryer		
X_o	0.069	kg water/kg dry powder
X_i	9.12	kg water/kg dry powder
Y_{in}	0.01	kg water/kg dry air
m_a	0.0158	kg/s
m_p	4.51E-05	kg/s
Y_o	0.032	kg water/kg dry air
Z	0.14	Discrepancy in water balance
Tamb	298.15	
Tref	273	
Finding temperature of air leaving dryer		
Look at case where inlet air temperature is 170°C		
Hin	3.23	kW from equation 5.9
lambda	2500	kJ/kg
Cp w,v	1.9	kJ/kg K
Cp a	1	kJ/kg K
UA	0.039	kW/K
numerator	18.185	
denominator	0.056	
T	**326.53**	K from equation 5.13
	53	°C
Heat loss	1.08	kW from equation 5.12
Heat out	2.15	kW from equation 5.11
From outlet temperature, find the saturation vapour pressure using the Antoine equation		
Psat	14043	Pa from equation 5.14
RH	0.35	
Now find the equilibrium moisture content		
Papadakis *et al.* (1993) equation		
A	0.1499	kg /kg
B	2.306E-03	K^{-1}
RH	0.35	
T	326	K
X eq	0.0686	kg/kg from equation 5.18

Table C.61 - Case 2, where inlet air temperature 200°C, feed flowrate 1.8 kg hr^{-1}, swirl vane angle 0° and compressed air pressure 200 kPa. (Data taken from Run 13).

Finding absolute air humidity leaving dryer			
X_o	0.0489	kg water/kg dry powder	
X_i	9.12	kg water/kg dry powder	
Y_{in}	0.012	kg water/kg dry air	
m_a	0.0158	kg s^{-1}	
m_p	4.50E-05	kg s-1	
Y_o	0.031	kg water/kg dry air	
Z	0.17		
Tamb	298	K	
Tref	273	K	
Finding temperature of air leaving dryer			
Look at case where inlet air temperature is 200°C			
Hin	3.82	kW	
lambda	2500	kJ/kg	
Cp w,v	1.9	kJ/(kg°C)	
Cp a	1	kJ/(kg°C)	
UA	0.043	kW/K	
numerator	19.98025		
denominator	0.059799		
T	**334**	K	
	61	C	
From outlet temperature, find the saturation vapour pressure using the Antoine equation			
Psat	20839.09	Pa	
RH	0.233894		
Papadakis *et al.* (1993) equation			
A	0.1499		
B	2.306E-03		
RH	0.233894		
T	334	K	same as gas temperature at equilibrium
X eq	0.0489	kg/kg	

Table C.62 - Case 3, where inlet air temperature 230°C, feed flowrate 1.8 kg hr^{-1}, swirl vane angle 0° and compressed air pressure 200 kPa. (Data taken from Run 1).

Finding absolute air humidity leaving dryer			
X_o	0.0306	kg water/kg dry powder	
X_i	9.12	kg water/kg dry powder	
Y_{in}	0.006	kg water/kg dry air	
m_a	0.0158	kg s^{-1}	
m_p	4.50E-05	kg s-1	
Y_o	0.026	kg water/kg dry air	
Z	0.20		
Tamb	298	K	
Tref	273	K	
Finding temperature of air leaving dryer			
Look at case where inlet air temperature is 230°C			
Hin	4.5	kW	
lambda	2500	kJ/kg	
Cp w,v	1.9	kJ/(kg°C)	
Cp a	1	kJ/(kg°C)	
UA	0.053	kW/K	
numerator	23.82455		
denominator	0.069622		
T	**342**	K	
	69	C	
From outlet temperature, find the saturation vapour pressure using the Antoine equation			
Psat	29910.38	Pa	
RH	0.133598		
Papadakis *et al.* (1993) equation			
A	0.1499		
B	2.306E-03		
RH	0.133598		
T	342	K	same as gas temperature at equilibrium
X eq	0.0306	kg/kg	

Table C.63 - Case 4, where inlet air temperature 230°C, feed flowrate 1.4 kg hr^{-1}, swirl vane angle 0° and compressed air pressure 200 kPa. (Data taken from Run 20).

Finding absolute air humidity leaving dryer

X_o	0.0271	kg water/kg dry powder	
X_i	9.12	kg water/kg dry powder	
Y_{in}	0.01	kg water/kg dry air	
m_a	0.0158	kg s^{-1}	
m_p	3.40E-05	kg s-1	
Y_o	0.024	kg water/kg dry air	
Z	0.19		
Tamb	298.15	K	
Tref	273	K	

Finding temperature of air leaving dryer

Look at case where feed flowrate = 1.38 kg/hr

Hin	4.28	kW	
lambda	2500	kJ/kg	
Cp w,v	1.9	kJ/(kg °C)	
Cp a	1	kJ/(kg °C)	
UA	0.047	kW/K	
numerator	21.87		
denominator	0.063561		
T	**344**	K	
	71	C	

From outlet temperature, find the saturation vapour pressure using the Antoine equation

Psat	32434	Pa	
RH	0.11584		

Papadakis *et al.* (1993) equation

A	0.1499		
B	2.306E-03		
RH	0.11584		
T	344	K	same as gas temperature at equilibrium
X eq	0.0271	kg/kg	

Table C.64 - Case 5, where inlet air temperature 230°C, feed flowrate 1.6 kg hr^{-1}, swirl vane angle 0° and compressed air pressure 200 kPa. (Data taken from Run 26).

Finding absolute air humidity leaving dryer			
X_o	0.0000	kg water/kg dry powder	
X_i	9.12	kg water/kg dry powder	
Y_{in}	0.008	kg water/kg dry air	
m_a	0.0158	kg s^{-1}	
m_p	3.88E-05	kg s^{-1}	
Y_o	0.024	kg water/kg dry air	
Z	0.21		
Tamb	298	K	
Tref	273	K	
Finding temperature of air leaving dryer			
Look at case where inlet air temperature is 200°C			
Hin	4.2	kW	
lambda	2500	kJ/kg	
Cp w,v	1.9	kJ/(kg°C)	
Cp a	1	kJ/(kg°C)	
UA	0.052	kW/K	
numerator	23.27088		
denominator	0.06857		
T	**339**	K	
	66	C	
From outlet temperature, find the saturation vapour pressure using the Antoine equation			
Psat	26420.17	Pa	
RH	0.142771		
Papadakis *et al.* (1993) equation			
A	0.1499		
B	2.306E-03		
RH	0.142771		
T	339	K	same as gas temperature at equilibrium
X eq	0.0327	kg/kg	

Table C.65 - Case 6, where solids concentration 20% (w/w) inlet air temperature 230°C, feed flowrate 1.8 kg hr^{-1}, swirl vane angle 0° and compressed air pressure 200 kPa.

Finding absolute air humidity leaving dryer			
X_o	0.0303	kg water/kg dry powder	
X_i	4	kg water/kg dry powder	
Y_{in}	0.006	kg water/kg dry air	
m_a	0.0158	kg s^{-1}	
m_p	1.02E-04	kg s^{-1}	
Y_o	0.025	kg water/kg dry air	
Z	0.20		
Tamb	298	K	
Tref	273	K	
Finding temperature of air leaving dryer			
Look at case where inlet air temperature is 230°C			
Hin	4.5	kW	
lambda	2500	kJ/kg	
Cp w,v	1.9	kJ/(kg °C)	
Cp a	1	kJ/(kg °C)	
UA	0.053	kW/K	
numerator	23.85154		
denominator	0.069686		
T	**342**	K	
	69	°C	
From outlet temperature, find the saturation vapour pressure using the Antoine equation			
Psat	30002.96	Pa	
RH	0.13199		
Papadakis *et al.* (1993) equation			
A	0.1499		
B	2.306E-03		
RH	0.13199		
T	342	K	same as gas temperature at equilibrium
X eq	0.0303	kg/kg	

Table C.66 - Case 6, where solids concentration 50% (w/w) inlet air temperature 230°C, feed flowrate 1.8 kg hr^{-1}, swirl vane angle 0° and compressed air pressure 200 kPa.

Finding absolute air humidity leaving dryer

X_o	0.0191	kg water/kg dry powder
X_i	1	kg water/kg dry powder
Y_{in}	0.006	kg water/kg dry air
m_a	0.0158	kg s^{-1}
m_p	2.55E-04	kg s^{-1}
Y_o	0.017	kg water/kg dry air
Z	0.20	
Tamb	298	K
Tref	273	K

Finding temperature of air leaving dryer

Look at case where inlet air temperature is 230°C

Hin	4.5	kW
lambda	2500	kJ/kg
Cp w,v	1.9	kJ/(kg °C)
Cp a	1	kJ/(kg °C)
UA	0.053	kW/K
numerator	24.15004	
denominator	0.069643	
T	**347**	K
	74	°C

From outlet temperature, find the saturation vapour pressure using the Antoine equation

Psat	36388.35	Pa
RH	0.075894	

Papadakis *et al.* (1993) equation

A	0.1499	
B	2.306E-03	
RH	0.075894	
T	347 K	same as gas temperature at equilibrium

X eq 0.0191 kg/kg

Appendix C

C5. Evaporative Capacity of the Spray Dryer

Table C.67 – Spreadsheet used for finding evaporative capacity of the spray dryer used in this work using data from run 10, where the inlet air temperature was 170°C, the feed flowrate was 1.8 kg hr^{-1}, the swirl vane angle was 0°, and the compressed air pressure was 200 kPa.

Basic Data				
Cp_a	1.0 kJ kg^{-1} K^{-1}			
$Cp_{w,v}$	1.9 kJ kg^{-1} K^{-1}			
Cp_w	4.2 kJ kg^{-1} K^{-1}			
lamda	2500 kJ kg^{-1}			
T_{amb}	25 °C			
P_{atm}	101325 Pa			
Inlet Conditions				
Air		***Water***		
$T_{air\ in}$	170 °C	$T_{water\ in}$	25 °C	
$Y_{air\ in}$	0.014 kg kg^{-1}	$m_{water\ in}$	0.000591 kg/s	must be adjusted
$m_{air\ in}$	0.0158 kg s^{-1}			
Heat loss				
UA	40 W K^{-1}			
Mass balance				
$Y_{air\ out}$	0.051376 kg kg^{-1}	From equation 5.7		
Assumes that all water entering is evaporated, not that outlet air is saturated				
Total inlet flowrate of enthalpy				
H_{in}	3.39 kW	From equation 5.9		
Must guess $T_{air\ out}$				
$T_{air\ out}$	41 oC	From equation 5.13		
Outlet flowrate of enthalpy				
Q_{loss}	0.64 kW	From equation 5.12		
$H_{air\ out}$	2.75 kW	From equation 5.11		
Total outlet flowrate of enthalpy				
H_{out}	3.4 kW			
Heat imbalance				
	0.00 kW			
This tells us what outlet temperature is likely for this liquid flowrate, but not what liquid flowrate is the maximum one.				
Let us now look at what the saturation humidity would be at this outlet air temperature.				
P_{sat}	7740.814 Pa	From equation 5.14		
Y_{sat}	0.051376 kg/kg			
Y_{sat}-$Y_{air\ out}$	-2.1E-07 kg/kg			
Using solver Set the Target Cell (Ysat -Yair out) to equal 0				
By changing the Tair out and mwater in				
Subject to the constraint that				
Heat imbalance (Heat in -Heat out) is equal to 0				

Appendix C

C6. Sticky-Point Data for Skim Milk Powder (Source : Hennigs *et al.* 2001)

Moisture content (%)	Sticky-point temperature (°C)
0.2	120.83
0.4	117.46
0.6	114.18
0.8	111.00
1	107.90
1.2	104.89
1.4	101.96
1.6	99.10
1.8	96.32
2	93.62
2.2	90.98
2.4	88.41
2.6	85.90
2.8	83.45
3	81.06
3.2	78.73
3.4	76.46
3.6	74.23
3.8	72.06
4	69.94
4.2	67.87
4.4	65.84
4.6	63.86
4.8	61.92
5	60.02
5.2	58.17
5.4	56.35
5.6	54.57
5.8	52.83
6	51.12
6.2	49.45
6.4	47.81
6.6	46.20
6.8	44.63
7	43.09
7.2	41.57
7.4	40.09
7.6	38.63
7.8	37.20
8	35.80
8.2	34.42
8.4	33.07
8.6	31.74
8.8	30.44
9	29.16
9.2	27.90
9.4	26.66
9.6	25.45
9.8	24.26
10	23.08

Appendix C

C7. Scanning Electron Microscope Photos of Skim Milk Powder

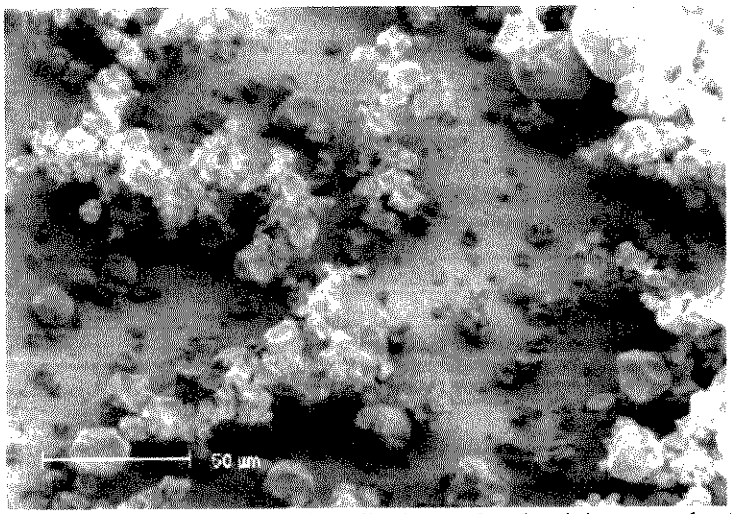

Figure C.1 - Photograph of skim milk powder particles adhering to the aluminium sample plate placed in the spray dryer. Magnified ×1000 by Philips XL30CP Scanning Electron Microscope. Operating at 10kV. The bar shown in the photograph has a length of 50 microns.

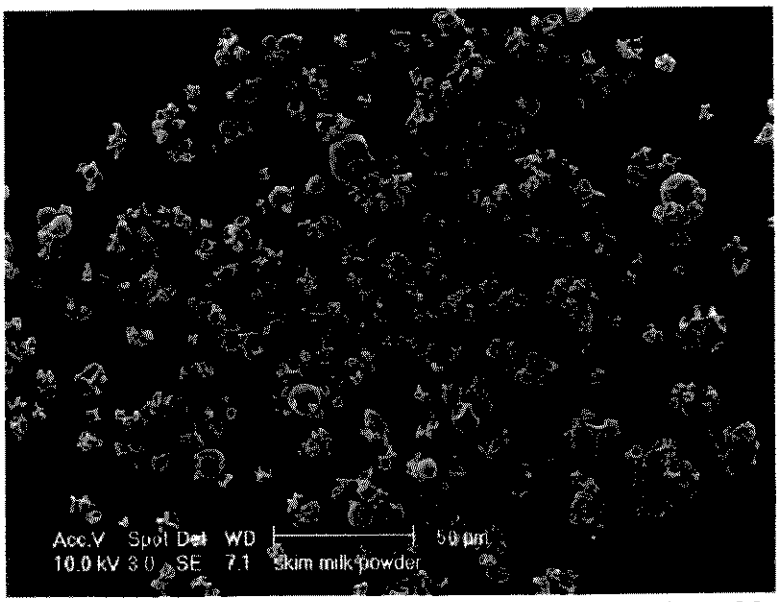

Figure C.2 - Photograph of the skim milk powder particles that have left the spray dryer. Magnified ×1000 by Philips XL30CP Scanning Electron Microscope. Operating at 10kV. The bar in the photograph has a length of 50 microns.

Appendix D

D1. Wall Deposition Fluxes and Heat and Mass Balances – Spray Drying Grape Skin Extract

Table D.1 – Wall deposition flux data for spray drying grape extract (solids concentration 7%) using inlet air temperature 230°C, feed flowrate 1.4 kg hr^{-1}, swirl vane angle 0°, and compressed air pressure 200 kPa.

Run	Plate 5 flux ($g\ m^{-2}\ hr^{-1}$)	Plate 6 flux ($g\ m^{-2}\ hr^{-1}$)	Average Flux ($g\ m^{-2}\ hr^{-1}$)	Discrepancy ($g\ m^{-2}\ hr^{-1}$)	Moisture content (%dry)
1	1.7	0.6	1.1	0.5	15.3
2	2.6	3.4	3.0	0.4	11.8
3	2.7	3.2	2.9	0.3	9.8
4	2.7	2.9	2.8	0.1	10.7
		Average (overall)	2.9	0.2	

TableD.2 – Raw experimental data used for calculating mass and energy balances from spray drying grape extract using inlet air temperature 230°C, feed flowrate 1.4 kg hr^{-1}, swirl vane angle 0°, and compressed air pressure 200 kPa..

Thermocouple (°C)	Run	1	2	3	4
Indicated reading	$T_{d\ in}$	24.66	24.33	24.23	23.78
"as above"	$T_{w\ in}$	19.66	19.66	19.66	19.15
"as above"	$T_{d\ out}$	69.44	69.95	71.25	70.98
"as above"	$T_{w\ out}$	37.65	39.36	37.64	35.87
"as above"	$T_{hot\ air}$	230.02	234.27	236.80	237.16
"as above"	T_{dryer}	57.79	59.22	58.33	61.58
"as above"	$T_{dryer\ exit}$	74.41	76.89	76.69	77.59
Mercury reading (°C)	T_{room}	NR	NR	NR	NR
Compressed air	P_{air} (psi)	30	30	30	30
Swirl vane angle	SV (°)	0	0	25	25
Grape extract flowrate	Q (kg hr^{-1})	1.4	1.4	1.4	1.4

Table D.3 – Adjusted temperature readings for Table D.2.

Thermocouple (°C)	Run	1	2	3	4
Indicated reading	$T_{d\ in}$	21.3	21.0	20.9	20.4
"as above"	$T_{w\ in}$	16.5	16.5	16.5	15.9
"as above"	$T_{d\ out}$	68.4	68.9	70.3	70.0
"as above"	$T_{w\ out}$	36.1	38.0	36.1	34.2
"as above"	$T_{hot\ air}$	231.4	235.8	238.4	238.8
"as above"	T_{dryer}	52.9	54.4	53.5	56.8
"as above"	$T_{dryer\ exit}$	70.5	73.0	72.8	73.7

Table D.4 – Data about grape skin extract feed material used for calculating mass and energy balances.

Mass flowrate of solids (kg hr^{-1})	2.72E-05
Water concentration in solids (kg water/kg dry solid)	13.00

Table D.5 – Moisture content of grape powder (kg water/kg dry solid) obtained from spray drying grape skin extract using inlet air temperature 230°C, feed flowrate 1.4 kg hr^{-1}, swirl vane angle 0°, and compressed air pressure 200 kPa.

Run	X_o (kg water/kg solids)
1	0.16
2	0.12
3	0.1
4	0.11

Table D.6 – Water balances from spray drying grape extract using inlet air temperature 230°C, feed flowrate 1.4 kg hr^{-1}, swirl vane angle 0°, and compressed air pressure 200 kPa.

Run	1	2	3	4
Y_{in} (kg water/kg dry air)	0.012	0.012	0.012	0.012
Y_{out} (kg water/kg dry air)	0.030	0.032	0.029	0.024
$M_{water\ in}$ (kg s^{-1})	5.43E-04	5.43E-04	5.43E-04	5.43E-04
$M_{water\ in}$ (kg hr^{-1})	1.96	1.96	1.96	1.96
$M_{water\ out}$ (kg s^{-1})	4.78E-04	5.09E-04	4.61E-04	3.82E-04
$M_{water\ out}$ (kg hr^{-1})	1.722	1.832	1.659	1.376
Difference (kg hr^{-1})	-0.234	-0.125	-0.297	-0.581
Difference (%)	-12	-6	-15	-30

Table D.7 – Data used for calculating heat balances when grape extract was spray dried . Heat capacity data taken from Perry's Chemical Engineers' Handbook, 7th Edition (1997), McGraw Hill, New York. The specific heat capacity of grape extract was not available so the specific heat capacity of the milk solids was used here.

Cp (water) =	4.18	kJ/(kg °C)	at 25°C
Cp (air) =	1.026	kJ/(kg °C)	at 25°C
Cp (air) =	1.027	kJ/(kg °C)	at 230°C
Cp (comp. air) =	1.004	kJ/(kg °C)	at 20 psi, 25°C
Cp (comp. air) =	0.698	kJ/(kg °C)	at 40 psi, 25°C
Cp (water vapour) =	1.958	kJ/(kg °C)	at 25°C
Cp (water vapour) =	1.962	kJ/(kg °C)	at 230°C
Cp (milk solids)=	1.256	kJ/(kg °C)	Pisecky (1992)p24
Compressed air flow	0.0004	kg s^{-1}	Delavan Manual
solids flowrate=	2.72E-05	kg s^{-1}	
water flowrate=	3.62E-04	kg s^{-1}	
T_{ref}	0	°C	
λ =	2500	kJ/kg	

Table D.8 –Inlet air temperatures, outlet air temperatures and absolute humidities used to calculate heat balances for spray drying grape skin extract using inlet air temperature 230°C, feed flowrate 1.4 kg hr^{-1}, swirl vane angle 0°, and compressed air pressure 200 kPa.

Run	T air in (K)	T air out (K)	Y_{in} (kg water/kg air)	Y_{out} (kg water/kg air)
1	504.6	341.6	0.012	0.030
2	508.9	342.1	0.012	0.032
3	511.5	343.5	0.012	0.029
4	511.9	343.2	0.012	0.024

Table D.9 – Summary of heat balances from spray drying grape skin extract using inlet air temperature 230°C, feed flowrate 1.4 kg hr^{-1}, swirl vane angle 0°, and compressed air pressure 200 kPa.

Run	Heat In (kW)	Heat Out (kW)	Heat Losses (kW)	Discrepancy (%)
1	4.37	2.36	-2.01	-46
2	4.44	2.46	-1.99	-45
3	4.49	2.35	-2.13	-48
4	4.49	2.14	-2.35	-52

D2. Statistical Analysis of Difference between Wall Deposition Fluxes for Skim Milk Powder and Grape Skin Extract

The null hypothesis that there is no difference between the wall deposition fluxes of the skim milk powder and grape skin extract, can be tested as follows. The mean and the variance of the two samples is $\overline{x_1}$ = 3.8 g m^{-2} hr^{-1}, $\overline{x_2}$ = 2.9 g m^{-2} hr^{-1}, s_1 =0.7 g m^{-2} hr^{-1}, and s_2=0.2 g m^{-2} hr^{-1} respectively. n_1=3, n_2= 4, so we have 5 degrees of freedom. The null hypothesis can be rejected with 95% confidence if $t < -2.015$ or $t \geq 2.015$, where 2.015 is the value of t at 0.05 level of significance ($t_{0.05,5}$). t is calculated by using equation 5.1 to be 2.51. The null hypothesis can be rejected with 95% confidence.

Appendix D

D3. Calculating the Diameter of Droplets using the Lefebvre Equation and Filkova and Cedik Correlation

Table D.10 – Spread sheet used to calculate diameter of water droplet.

Lefebvre equation

Value of parameters to be used in Lefebvre (1980) equation:

F	0.000389	kg water hr^{-1}	Mass flowrate of water
Properties of water at 20°C			
surface tension	0.07275	Nm^{-1}	
density	998	kg m^{-3}	
viscosity	0.001002	Pa s	
Properties of air at 300 K			
density air	1.161	kg m^{-3}	
V	0.025	m^3 min^{-1}	
V	4.167E-04	m^3 s^{-1}	Volumetric flowrate of air
G	4.838E-04	kg s^{-1}	Mass flowrate of air
d_o	2.500E-03	m	
d_p	2.000E-03	m	
d_i	1.000E-03	m	
A_G	1.766E-06	m^2 from equation 6.4	
U_G	235.90	m s^{-1}	
Dvs	7.126E-05	m from equation 6.2	71 microns
G/F	1.24		

Filkova and Cedik correlation

$A_G^{0.5}$	1.329E-03		
We_s	1.373E+00	from equation 6.5	
Re_s	3.633E+02	from equation 6.6	
Dvs	2.092E-05	m from equation 6.3	20 microns

Table D.11 – Spreadsheet used to calculate diameter of skim milk droplet.

Lefebvre equation

Value of parameters to be used in Lefebvre (1980) equation:

F	0.000389	kg water hr^{-1}	Mass flowrate of skim milk
Properties of water at 20°C			
surface tension	0.048	Nm^{-1}	at 20°C
density	1032	kg m^{-3}	(Pisecky, 1997)
viscosity	0.0023	Pa s	
Properties of air at 300 K			
density air	1.161	kg m^{-3}	
V	4.17E-04	m^3 s^{-1}	Volumetric flowrate of air
G	4.84E-04	kg s^{-1}	Mass flowrate of air
d_o	2.500E-03	m	
d_p	2.000E-03	m	
d_i	1.000E-03	m	
A_G	1.766E-06	m^2	
U_G	236.00	m s^{-1}	
Dvs	1.978E-04	m	198 microns
G/F	1.24		

Filkova and Cedik correlation

$A_G^{0.5}$	1.329E-03	
We_s	2.013E+00	
Re_s	1.583E+02	
Dvs	1.978E-05 m	20 microns

Table D.12 – Spreadsheet used to calculate diameter of grape skin extract droplet.

Lefebvre equation

Value of parameters to be used in Lefebvre (1980) equation:

F	0.000389 kg water hr^{-1}	Mass flowrate of skim milk
Properties of water at 20°C		
surface tension	0.044 Nm^{-1}	
density	1042 kg m^{-3}	
viscosity	0.0025 Pa s	
Properties of air at 300 K		
density air	1.161 kg m^{-3}	
V	4.168E-04 m^3 s^{-1}	Volumetric flowrate of air
G	4.839E-04 kg s^{-1}	Mass flowrate of air
d_o	2.500E-03 m	
d_p	2.000E-03 m	
d_i	1.000E-03 m	
A_G	1.766E-06 m^2	
U_G	236.00 m s^{-1}	
Dvs	2.235E-04 m	224 microns
G/F	1.24	

Filkova and Cedik correlation

$A_G^{0.5}$	1.329E-03	
We_s	2.176E+00	
Re_s	1.457E+02	
Dvs	1.963E-05	20 microns